# An Experimental and Numerical Study of the Effects of Surrounding Disturbances on Vortex Rings

# An Experimental and Numerical Study
# of the Effects of Surrounding Disturbances
# on Vortex Rings

by

Siu Kin, HO. B. Eng.

A Thesis Submitted to the Faculty of Graduate Studies
in Partial Fulfilment of the Requirements
for the Degree
Master of Engineering

McMaster University

October 25, 1991.

Master of Engineering (1991) McMaster University

(Mechanical Engineering) Hamilton, Ontario

TITLE: An Experimental and Numerical Study of the Effects of Surrounding Disturbances on Vortex Rings

AUTHOR: Siu Kin, HO. B. Eng.

SUPERVISOR: Dr. Brian Latto

NUMBER OF PAGES: 201

Abstract:

In this thesis, the effect of the following three aspects related to the generation and efficient transport of vortex rings were studied. They included:

1) the initial boundary condition where the vortex ring is generated. A comparison between previous results and the data obtained in this study showed that vortex rings generated at a tube orifice were both slower in velocity and larger in size than vortex rings generated at a plate orifice under similar conditions.

2) the presence of a stratified layer of fluid in a vessel. Flow visualization experiments showed that after a vortex ring penetrated through the interface of the stratified layer, it was able to mix the fluid inside the ring with the surrounding fluid. The amount of mixing depended on the depth of penetration of the ring into the stratified layer. An empirical relationship was obtained to predict the maximum penetration depth of a vortex ring into a stratified layer. It is:

$$\frac{Xp}{Rm} = -29.7\log_{10}Ri - 22.7$$

3) the proximity of a wall or another vortex ring to the path of the primary ring. Through numerical simulation, it was shown that the primary ring would slow down and turn away from its original path. Eventually, this ring would either crash into the wall or collide with another ring. In order to prevent this turning of a vortex ring from happening, the centre of the generation orifice should be 7.5 times the radius of the injection orifice (Rm) from the wall or 15Rm between two generation orifices.

These results can be used to optimize the design and positioning of vortex ring mixers for various mixing vessel geometries and mixing processes.

General Introduction:

The mixing of liquids is one of the most common processes in industries. Some of these processes may involve destratification of liquids, such as the destratification of lakes, and the mixing of liquid with solid suspension, for example keeping the particles in suspension in slurries in a sewage treatment plant. Rotation and oscillation impeller mixers are generally used for this type of application, but these type of mixers use a lot of energy. Latto (1987) has developed a novel group of mixers that utilized vortex rings as the mechanism for agitating and mixing fluids, see Figure 1. These group of mixers are much more energy efficient and convenient to install than conventional impeller type mixers. The mixers agitate a fluid by generating a series of vortex rings, each vortex ring carries a volume of fluid, that is entrained into the ring during the formation period, to a distant location and mixes this fluid with the surrounding fluid as it is travelling across the tank. Latto (1989) showed that these type of mixers were especially useful and quick in the destratification of two layers of fluid with a relatively sharp density gradient located in the tanks. Although these mixers have been proven to be effective and efficient for various mixing processes, there are still other factors that will affect the operation of these mixers.

These factors include; the initial boundary condition, the shape of the generating orifice, where the vortex ring is generated, the distance between the boundary of the vessel and the centre line of the mixer or the distance between two generating orifices and the presence of a stratified layer of fluid in the vessel, etc. In the research reported in this thesis, the three factors described above were studied. The results from this research will assist in the selection, positioning and operation characteristic of these type of mixers for the destratification and mixing of fluids.

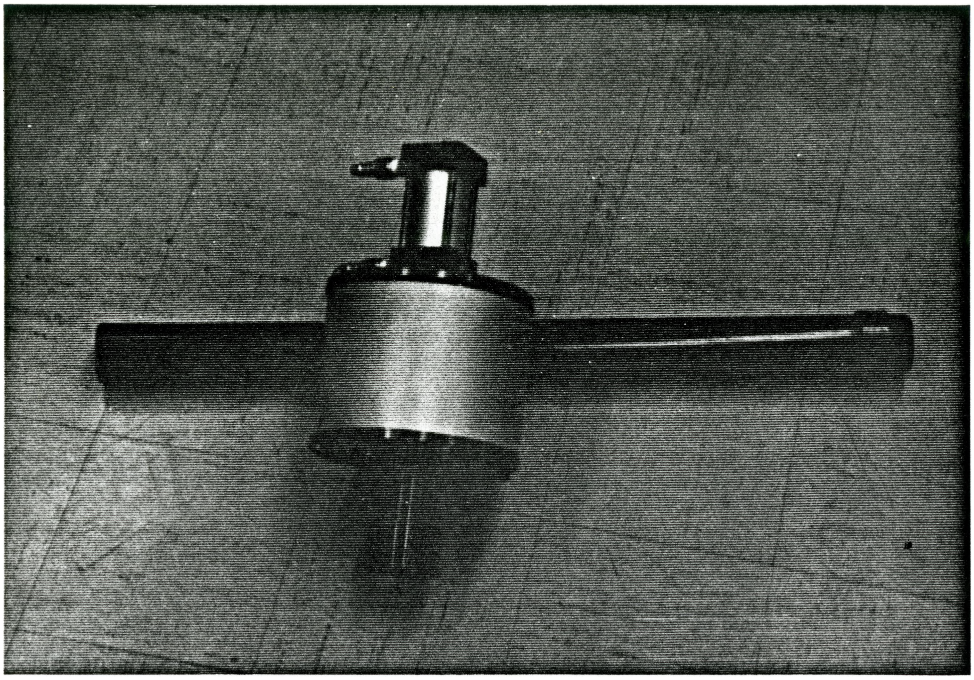

a) tube type mixer

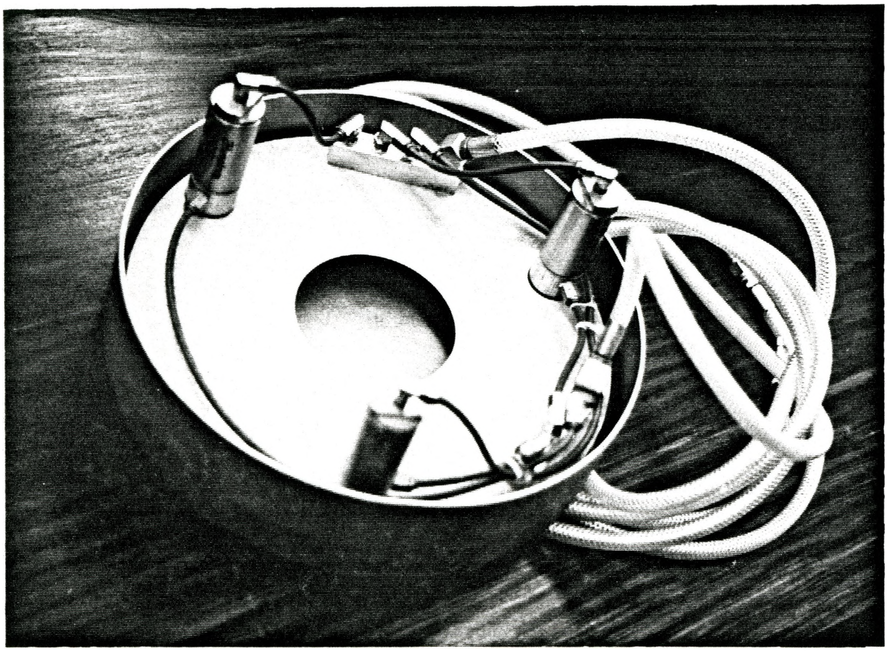

b) plate type mixer

Figure 1. Photographs of the various type of vortex ring mixers; a) tube type mixer, b) plate type mixer. Courtesy of MIXIS Corp.

## Acknowledgement

I would like to thank you Dr. Latto for giving me this opportunity to work on this project and all the helpful assistance that I received throughout this project. I would also like to thank the technicians in the Department of Mechanical Engineering for valuable information and help they gave me during the modification of the ejection mechanism. I would like to thank the late Mr. Ken Chow for all the helpful discussions at the initial stage of this project. Finally, thank you to my colleagues, Chi Tran, Aneesh Chopra and Greg Kopp, for valuable discussions.

# Table of Contents:

List of figures:

Figure Titles

## List of Tables

**Table** **Titles**

Nomenclature:

| | |
|---|---|
| A - | Cross sectional area of each segment used in the calculation of the volume of the jet |
| Ap - | Cross sectional area of injection plate |
| D ,d - | Core diameter of the vortex ring |
| Dm - | Orifice diameter |
| Dv - | Diameter of the vortex ring |
| $g\Delta\rho$ - | Gravitational acceleration multiply by the density gradient between the two fluids of the stratified layer |
| Li - | Distance of the interface from the opening of the orifice |
| Lm - | Plug length of the jet (Volume of jet/Area of orifice) |
| R - | Core radius of the vortex ring |
| $r_{2}, r_{1}$ - | Outer and inner radius of each segment used for the calculation of the measured volume of the jet |
| Rv - | Radius of the vortex ring |
| $\Delta t$ - | Time increment between each velocity measurement obtained by the hot film anemometer |
| Tp - | Injection period (time) |
| $U_j$ - | Theoretical jet velocity; $Uj = 4 * Ap * U_{plate} / (\pi * Dm^2)$ |
| $U_{javg}$ - | Averaged measured jet velocity |

$U_{plate}$ - Velocity of the injection plate

$U_{radial}$ - Radial velocity of the jet

$U_{measured}$ - Jet velocity measured using hot film anemometer

U, Uv - Traverse velocity of the vortex ring

V - Volume of the vortex ring

$V_o$ - Initial volume of the vortex ring after the generation period

Xm - Maximum penetration depth of a vortex ring into a stratified layer

$X_{wall}$ - Distance of the walls of the tank from the centre of the orifice

Greek Variables:

$\rho$ - Density of water or density of fluid which the vortex ring was generated in

$\sigma$ - Density of the other fluid of the stratified layer

$\mu$ - Viscosity of fluid

$\alpha$ - Entrainment rate, dR/dX

$\alpha_d$ - Detrainment rate

$\eta$ - $R/R_o$

$\Gamma$ - circulation $= \oint U \cdot ds$

Dimensionless variables:

$Re_m$ - Orifice Reynolds number ($\rho * U_j * Dm / \mu$)

$Re_R$ - Ring Reynolds number ($\rho * U * Dv / \mu$)

$Ri$ - Richardson number $\{(g * \Delta\rho * Rm) / (\rho * U_{javg}^{2)}\}$

$C_D'$ - Drag coefficient

Subscript:

$_o$ - Initial conditions

# Chapter 1

# Literature Review on General Properties of Vortex Rings

## 1.1 Introduction:

Various aspects of vortex rings have been investigated by many researchers for over a hundred years. During this period, studies on vortex rings concentrated in two particular areas: (1) the general characteristics of the rings which include the necessary conditions for the successful formation of a ring and the path of the ring after it is generated; and (2) the effect of surrounding disturbances on the path of the ring, for example, the proximity of a solid boundary or the existance of two layers of stratified fluid with either a sharp or linear change in density gradient or a stratified layer.

In this chapter, prior research on the general characteristics of a vortex ring is reviewed, this includes the generation parameters and the path of the ring after generation. Also various types of entrainment processes for different types of vortex rings are reviewed. This permits the selection of a particular type of vortex ring that is the most suitable for mixing purposes. A literature review on studies that deal with the effect of a stratified layer on a ring is given in Chapter 4.

## 1.2 Generation Parameters:

A vortex ring can be generated by ejecting a volume of fluid through an orifice. As the jet of fluid passes through the orifice, vorticity begins to accumulate in the boundary layer of the jet. When this jet of fluid leaves the orifice, the vorticity in the boundary layer causes the fluid to roll up to form a vortex ring that has a toroidal core and the overall shape of an oblate spheroid. A diagram of the rolling up process is shown in Figure 1.1.

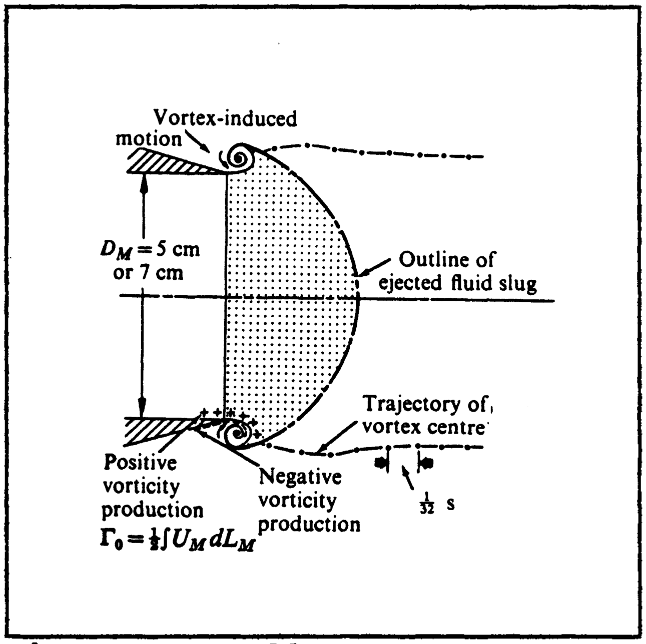


Figure 1.1 Roll up process of a vortex ring during the generation process. Maxworthy(1977)

The duration of this jet plays an important role in the successful formation of a vortex ring. If the volume of fluid ejected is not enough, the vortex ring does not accumulate enough vorticity in its core and is unable to form properly and travel away from the orifice. On the other hand, if the jet of fluid ejected is too long, the ring will eventually be destroyed because the translational velocity of the ring is only a fraction of the jet velocity and the jet continues to impinge onto the ring after it is formed and may destroy the ring. It has also been shown that under certain conditions a secondary smaller ring is created which is ingested by the primary ring and is subsequently destroyed. However, many researchers failed to recognise the effect of the initial volume of the jet or the duration of the jet on the formation of the ring. This makes comparisons between current and previous experimental data very difficult. Maxworthy (1977) through experimental studies observed that the core diameter and the size of a vortex ring are directly proportional to the volume of the jet that is injected into the ring during its formation. The volume of this jet can be related to the plug length of the fluid injected, Lm, which is calculated from,

$$Lm = 4 * \text{Volume of jet} / \pi * Dm^2$$

The relation between the plug length or the volume of the jet and the core diameter of the ring is given in Figure 1.2.

After this paper, Baird et al (1979) and Latto (1987) published data on generation criteria, and recommended a ratio of Lm/Dm for the generation of the most efficient vortex ring for mixing purposes. Baird et al (1979) suggested that for vortex rings generated at an orifice, the Lm/Dm ratio should be between the range of 0.7 to 2.8. Within this range, the linear momentum of the jet is conserved. This means the linear momentum in the jet is equal to the linear momentum in the fully formed ring. The velocity of the vortex ring, that is generated within this range of Lm/Dm at an orifice, is equal to:

Uv = 0.5 * Uj

or the velocity of the ring is approximately 50% of the jet velocity. Later, Latto (1987) suggested that this range should be 1.5 < Lm/Dm < 3.5 and recommended an Lm/Dm ratio of 2.8 for the optimum condition. The translational velocity of vortex rings generated at an orifice observed by Latto (1987) was,

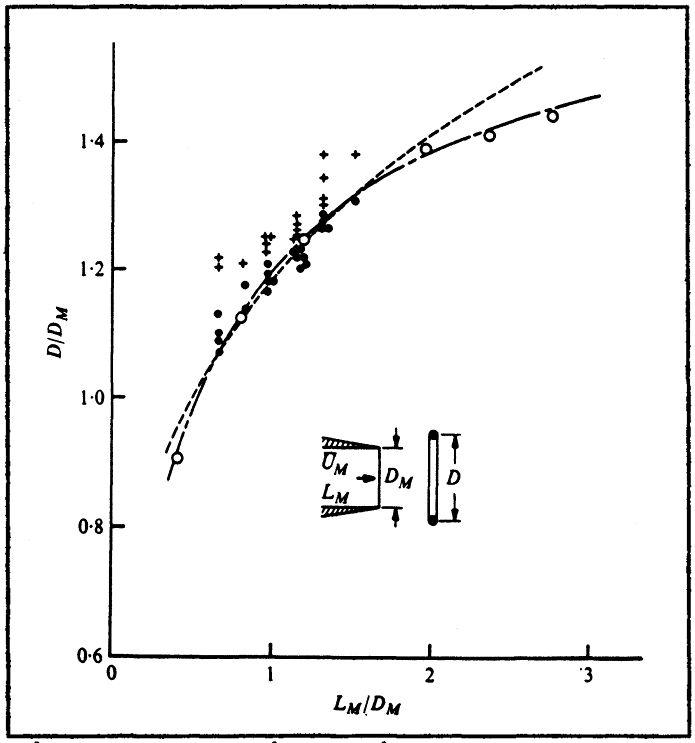


**Figure 1.2** Ring diameter D/Dm at 2.5Dm downstream vs. length of ejected fluid slug Lm/Dm. Maxworthy (1977)

Uv = 0.6 * Uj

The relation between the velocity of the jet and the velocity of the ring for the given range of Lm/Dm was only true for vortex rings generated at an orifice. No results were presented concerning vortex rings that were generated by ejecting a volume of fluid through a tube. Irdumsa et al (1983) used the balance of linear momentum equation to obtain the following generalized relationship for vortex rings that were generated at either an orifice or a tube:

$$U^* = 2.4711 D^{*-2}$$

where,

$$U^* = \frac{D_v U}{U_j^2 T_p} \quad and \quad D^* = \frac{D_v}{D_m}$$

and $U^*$ is a ratio between the translational speed and the rotational speed of the vortex ring after it was formed. Irdumsa et al (1983) explained that a ring generated at a tube is able to entrain more ambient fluid into itself during the formation period, due to the absence of a solid boundary at the back of the vortex ring. Since the vortex ring is bigger and must contain the same amount of energy from the jet as one generated at a plane orifice, rings generated at a tube have a slower translational velocity. The opposite is true for the rings generated at an orifice. The boundary of the orifice plate reduces the amount of entrained fluid in the ring during its formation, resulting in a smaller and faster ring. Irdumsa et al (1983) performed some experiments with vortex rings generated with air to verify their derived equation, and these results are shown in Figure 1.3. The data showed that the dimensionless vortex speed for the tube type generator is always less than unity, which means this type of generator will generate rings that have a higher rotational speed than translational speed.

Another factor that will affect the characteristics of a vortex ring is the translational velocity of the vortex ring or the ring Reynolds number. For a relatively small ring Reynolds number, $Re_R < 2000$, the ring generated will be completely laminar. Brasseur (1983) showed these type of laminar vortex rings are affected by the viscosity of the fluid and the velocity of the ring continues to decrease after it is generated. See Figure 1.4.

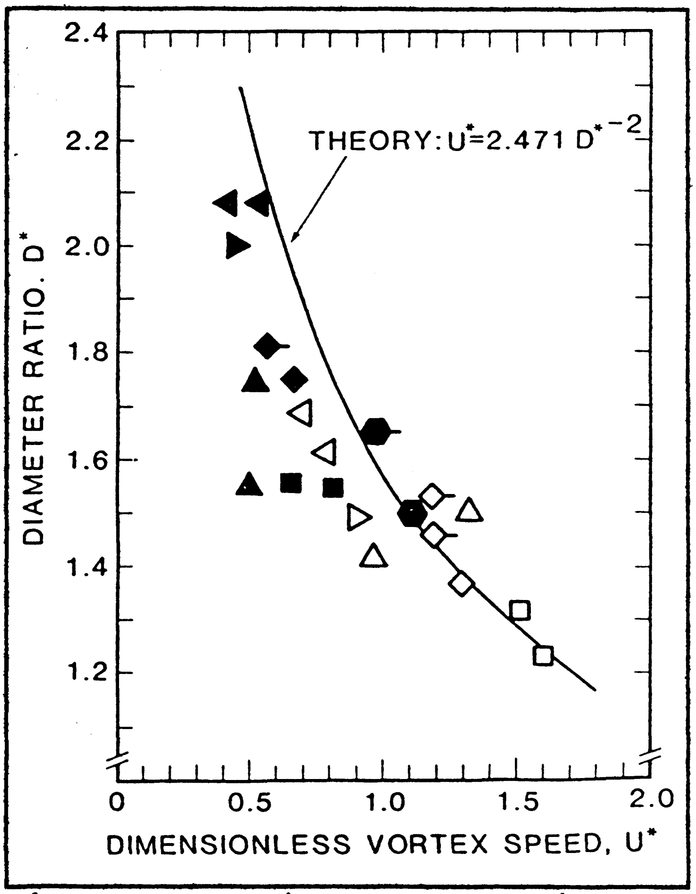


**Figure 1.3** Ratio of vortex diameter to exit diameter vs. dimensionless vortex speed, $U^*$. The filled symbols are for tube type generator and the unfilled symbols are for orifice type generator. Irdumsa (1983)

For rings with Reynolds numbers in the range, $Re_R \approx 2000$ to 20000, see Figure 1.5, Brasseur (1983) observed the translational velocity of the ring remains fairly constant after it is generated. Then after the ring has travelled some distance, its velocity suddenly changes.

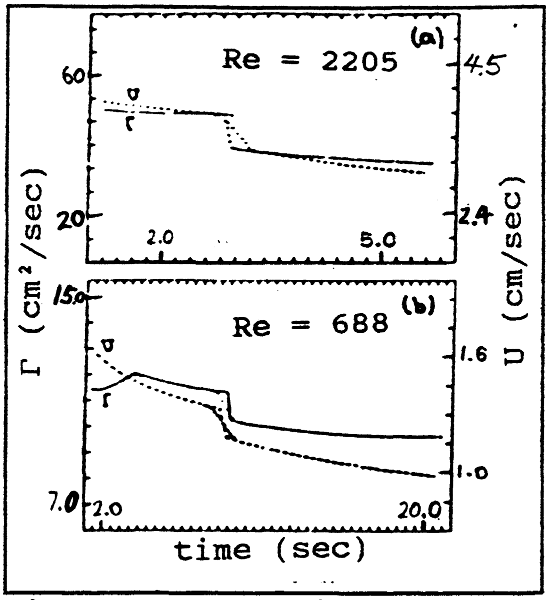


Figure 1.4 Transient changes in velocity for vortex rings at low Reynolds numbers. Brasseur (1986)

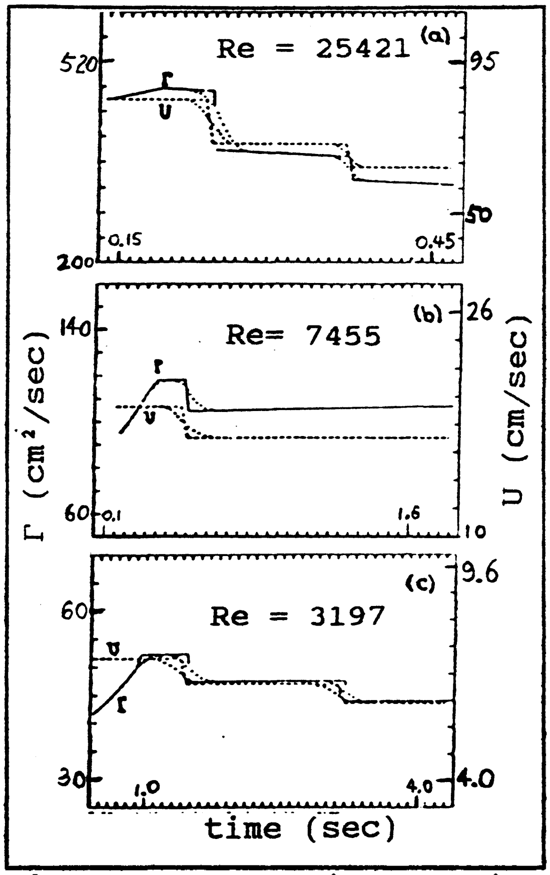


Figure 1.5 Velocity of ring vs. time at intermediate Reynolds no. Brasseur (1986)

**The same type of phenomena was observed by Maxworthy (1974), he attributed this transition to the formation of waves in the core of the ring. As the ring travels in a fluid, waves begin to form along the core[1] of the ring and the amplitude of these waves gradually increase. Eventually these waves break up and the ring converts into a turbulent vortex ring resulting in a decrease in the translational velocity of the ring.**

**Maxworthy (1977) showed that the core diameter was a function**

[1] core in this case refers to the centre of rotation of a vortex ring where a linear velocity profile occurs

of the Reynolds number at the orifice, where $Re_M = Uj * \rho * Dm / \mu$ The relationship between these two variables is shown in Figure 1.6.

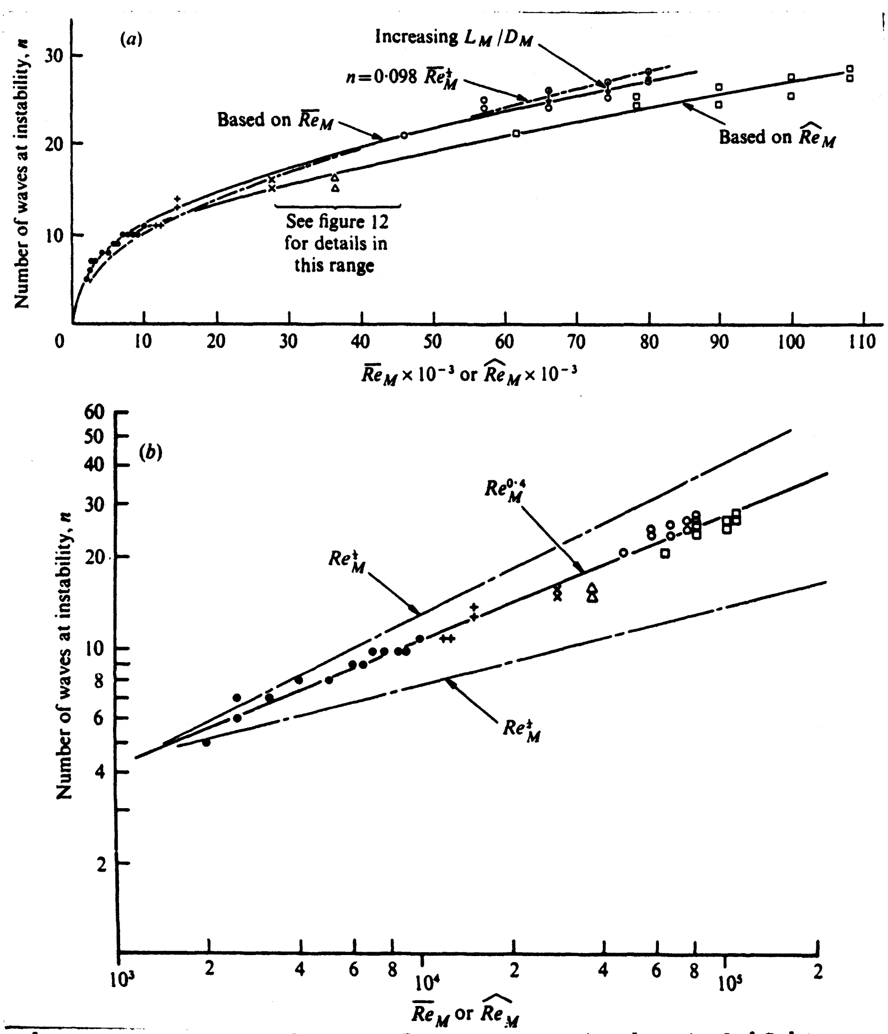


Figure 1.6 Number of waves at instability n vs. $Re_M$. Maxworthy(1977)

It was found that the number of waves in the core was inversely proportional to the core diameter of the ring or $n \propto (1/d)$

Two other formation parameters that are of importance are; 1) the velocity of the jet during the formation of the vortex ring; and 2) the proximity of solid boundary to the path of the ring.

1.2.1 The velocity profile of the jet during the injection period;

Sallet et al (1974) noticed that a ring formed by the injection of a constant velocity jet of air from an orifice, with an orifice Reynolds number of $Re_M \approx$ 11000, was laminar. However, if the jet had a constant acceleration period followed by a constant deceleration period, a turbulent vortex ring was formed. The difference between a laminar and a turbulent vortex ring was indicated by the output from a hot wire anemometer, located along the path of a vortex ring, as shown in Figure 1.7. The signal from a turbulent vortex ring has a lot of fluctuation while the signal from a laminar vortex ring is very smooth.

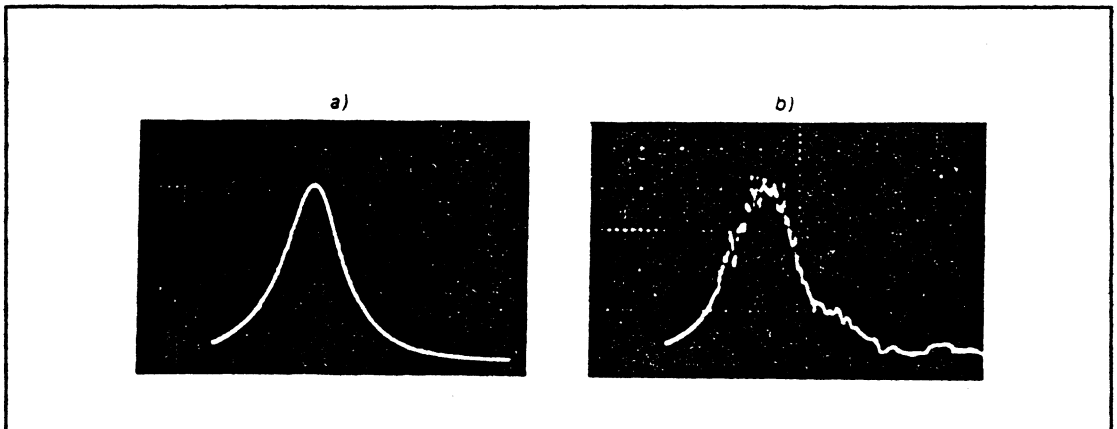


Figure 1.7 Typical hot wire trace for a) laminar and b) turbulent vortex ring. Sallet (1974)

Sallet et al (1974) also measured the rate of decay of circulation in the core of the two types of rings as shown in Figure 1.8. He showed that the circulation in the turbulent ring formed with a non-uniform velocity jet decreased much faster than that of a laminar ring formed with a constant velocity jet. Maxworthy (1977) showed that, for rings generated with the constant velocity jet, the circulation inside the core of the ring was 50% of the total circulation of the ring immediately after the formation of the ring. At a distance of

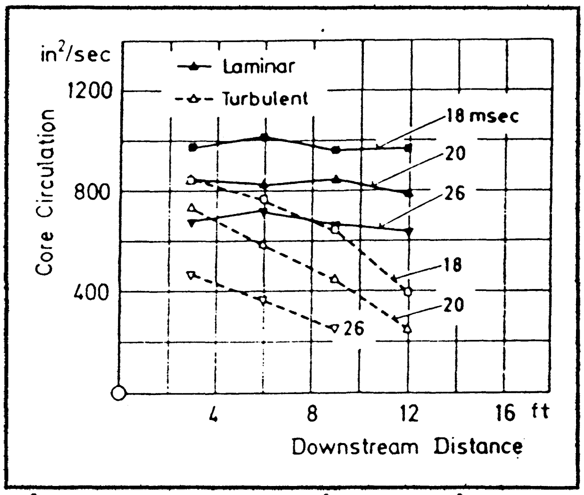


**Figure 1.8** Core circulation vs. downstream distance for laminar and turbulent ring. Sallet (1974)

14Dm downstream from the orifice, the total circulation of the vortex ring was 84% of the total circulation of the ring immediately after its formation. The range of $Re_M$ was between 2 to 6 * $10^4$. These results are presented in Figures 1.9, 1.10 and 1.11. The data obtained by Sallat et al (1983) and Maxworthy (1977) showed that it is better to use a constant velocity jet for the formation of vortex rings because these rings are able to retain much of their circulation for a longer period. Since the self induced velocity or translational velocity of the ring is proportional to the circulation in the ring, rings that are generated with a constant velocity jet will travel further than those that are generated with a non-uniform velocity jet.

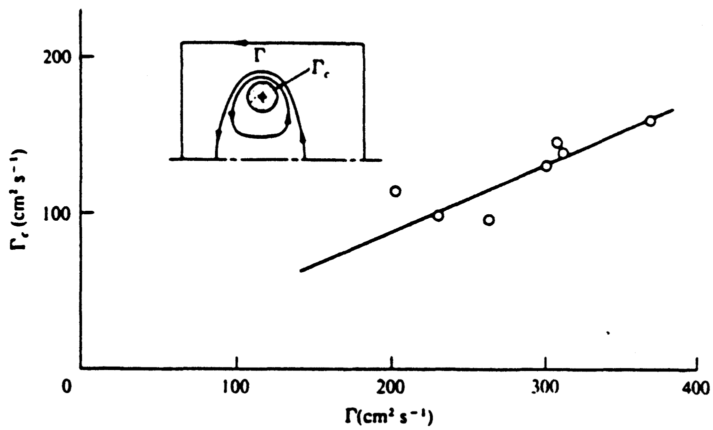


**Figure 1.9** Core circulation $\Gamma_c$ as a function of total circulation at 2.5Dm. Maxworthy (1977)

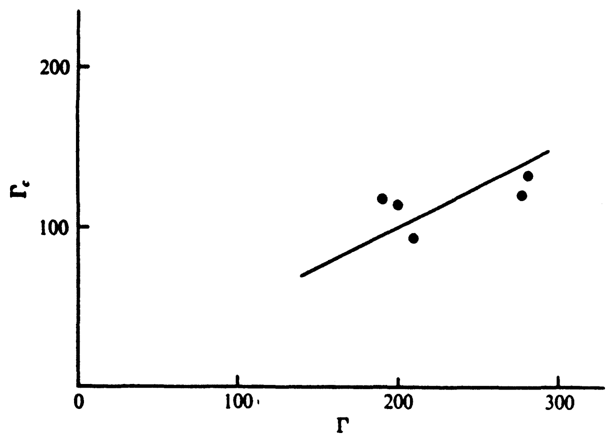


**Figure 1.10** Amount of circulation $\Gamma_c$ contained within the core compared with total circulation $\Gamma$ for turbulent ring at 14Dm. Maxworthy (1977)

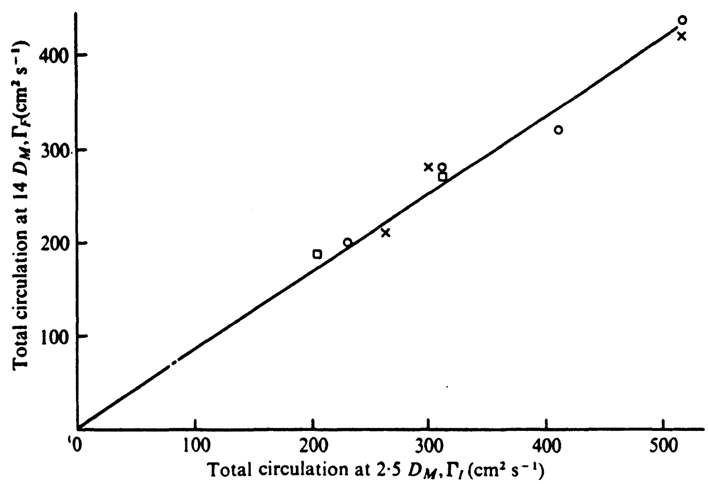


**Figure 1.11** Change $\Delta\Gamma$ in total circulation, showing the small decrease induced by instability and wave breaking. Maxworthy(1977)

### 1.2.2 The proximity of the vortex ring to the wall of the vessel:

All the experimental studies previously discussed assumed that the rings were generated in a semi-infinite media and the walls of the vessel were very far away from the ring such that it had little or no effect on the properties and the path of the ring as it travelled in a vessel. As a ring comes closer to a solid boundary, wall effects on the ring can no longer be ignored. Brasseur (1986) analyzed the effect on the translational velocity of a ring travelling axially in a circular container where the wall was close to the path of the ring and deduced that wall effect could not be ignored. In his calculations, he used potential flow theory to determine the translational velocity of an inviscid vortex filament. The induced velocity on the filament due to the proximity of the boundary of the vessel was then superimposed onto the initial velocity of the filament to determine the net effect on the translational velocity of the filament due to the proximity of the wall. His results are presented in Figure 1.12, where a/R = core radius divided by radius of the ring; $\epsilon$ = radius of the ring over radius of the tank, $\rho_o$; $U_i$ - induced velocity on the ring due to the wall that surrounded the ring; and $U_o$ - self induced velocity of the filament.

As $\epsilon$ increases, the ratio of Ui/Uo approached unity very rapidly. This means that as the ring comes close to the boundary of the vessel, the induced velocity on the ring due to the proximity of the boundary will increase rapidly to a point where the ring will stop travelling forward. This is when $U_i/U_o = 1$. In order to minimize the effect of the wall on the translational velocity of the ring, where $Ui/Uo \approx 0$, the value of $\epsilon$ should not be larger than 0.2 or the ring should be approximately five times the radius of the ring, 5R, from the surrounding wall of any circular tank.

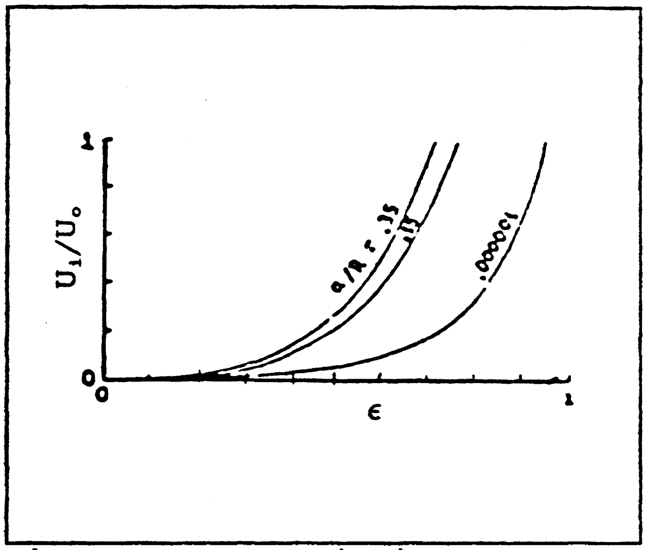

Figure 1.12 Variation of wall induced velocity vs. $\epsilon$. Brasseur (1986)

The above discussion indicated the importance of the generation parameters: Lm/Dm, $Re_R$, the velocity of the jet during the formation and the type of generator geometry. These parameters have a direct effect on the size, the translational velocity and the state of the ring after it is generated.

Another factor which will affect the ring after it is formed is the proximity of the wall to the path of the ring. If the walls are too close to a ring, the translational velocity of the ring will decrease more rapidly than a ring travelling in a semi infinite media. This information is essential for the successful generation of a vortex ring that will travel the furthest distance while achieving the mixing of the fluid in the ring with its surrounding. In the next section, the entrainment mechanism and the entrainment rate of both the laminar and turbulent vortex ring will be discussed.

## 1.3 Entrainment rate of vortex ring:

The entrainment rate of a vortex ring was defined by Maxworthy (1974) as the growth rate of the core radius of the ring R with respect to the distance travelled by the ring x, or dR/dx. Perrakis (1988) gathered data from various researchers, on the entrainment rate for both laminar and turbulent vortex rings. His results, shown in Figure 1.13, showed that the entrainment rate was related to the ring Reynolds number $Re_R$. It also showed that laminar rings with $Re_R < 1000$ had a larger entrainment coefficient than turbulent rings with $Re_R \approx 10{,}000 - 100{,}000$. Perrakis (1988) explained that although laminar rings entrained a smaller amount of fluid into the core of the ring than turbulent rings, they retained most of the fluid after it was entrained. On the other hand, turbulent rings entrained fluid through the side and the rear of the ring, but some of this entrained fluid lost its momentum and was unable to follow the rotational motion of the ring and was eventually deposited into the

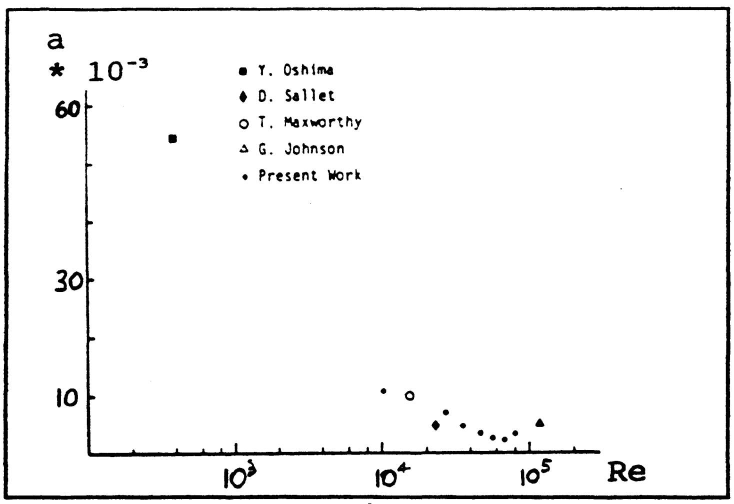


Figure 1.13 Entrainment rate a vs. $Re_R$. Perrakis (1988)

wake. Consequently, turbulent vortex rings have a lower entrainment rate than laminar rings since a portion of this fluid entrainment does not enter into the ring.

Wooller et al (1974) proposed a model for the entrainment mechanism for laminar vortex rings. He assumed that the vorticity in the ring spreaded to the edge of the ring, with no concentrated core of vorticity. Even if such a core existed, the surrounding fluid was so thin that it would not show up in the measurements. Sallet et al (1974) had similar observations for very slow laminar rings. He observed that for rings with very small Reynolds numbers, a ring with a thick core was formed which did not travel very far. Wooller et al (1974) assumed the entrainment was controlled by a diffusive mechanism that was similar to that of a boundary layer. He assumed that the thickness of the diffusive layer was given by;

$$\delta = k(\nu\tau)^{\frac{1}{2}}$$

where

$\delta$ - thickness of a layer of fluid around the ring;

k - a numerical constant;

$\nu$ - kinematic viscosity of the fluid; and

$\tau$ - characteristic time interval.

Assuming the laminar ring had the shape of an oblate spheroid and the linear momentum of the ring remained constant, Wooller et al (1974) were able to show the velocity of a laminar vortex ring was proportional to

$$U \propto t_1^{-1}$$

and the growth of the diameter of a laminar ring could be described by

$$D \propto t_1^{\frac{1}{3}}$$

where $t_1$ was the time that was shifted in origin or

$$t_1 = t + t_0 = 0 \qquad when \qquad D = 0$$

and

$t_0$ - time added to the actual measured time and,

$t$ - actual time of travel of the ring.

These results were in agreement with the experimental results obtained by Maxworthy (1972) shown in Figure 1.14.

Since U = dx/dt, by integrating U he determined that $U \alpha t^{-1}$. This result supported the theory of Wooller et al (1974), that the vorticity in a laminar ring was distributed throughout the entire ring and the entrainment mechanism was controlled by diffusion at the boundary of the ring.

For turbulent vortex rings, the entrainment mechanism is different from that of laminar vortex rings. Maxworthy (1974) suggested that the entrainment mechanism for a turbulent vortex ring was controlled by the turbulent fluctuations in the vortex ring. In the core of the ring where vorticity is highly concentrated, turbulent fluctuation perpendicular to the axis of rotation in the core is suppressed. Therefore, the entrainment into the core is slow. This results in a lower entrainment rate than that for laminar vortex rings, as shown in Figure 1.13.

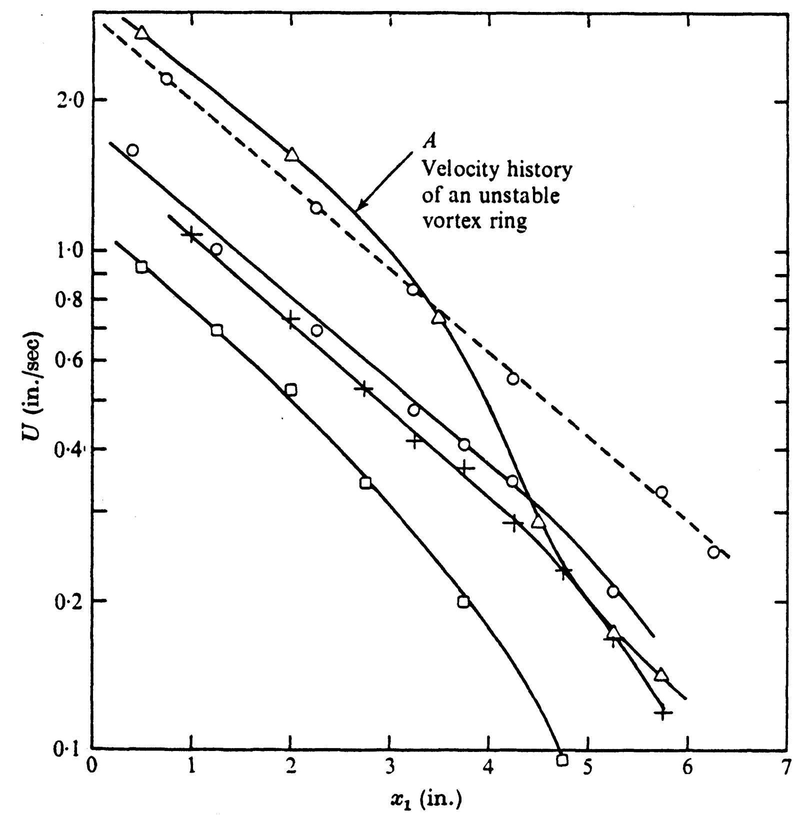


Figure 1.14 Velocity of translation of the ring U vs. distance from the hole at which it was formed. $Re_R \approx 600$. Maxworthy (1972)

Glezer (1990) showed in his experiments that a turbulent vortex ring has a thin core of concentrated vorticity, as shown in Figure 1.15, when compared with the size of the ring showed in Figure 1.16. This area of concentrated vorticity has minimized the intermittency in the core of the ring. Figure 1.17 shows that the core of the vortex ring is surrounded by a shaded area where the intermittency is higher than

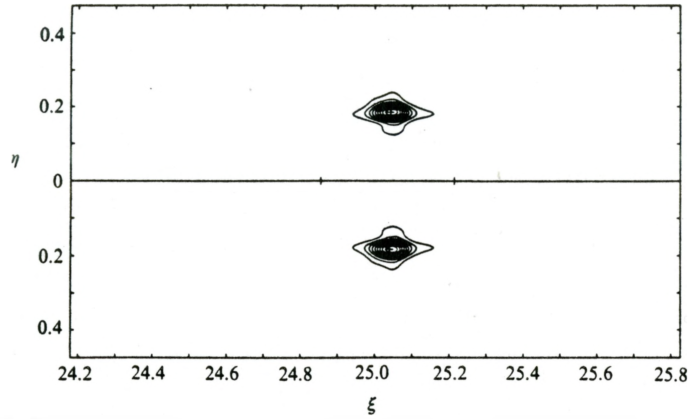


Figure 1.15 Vorticity contour around the core of a vortex ring, "+" is the centre of the core. Glezer(1990)

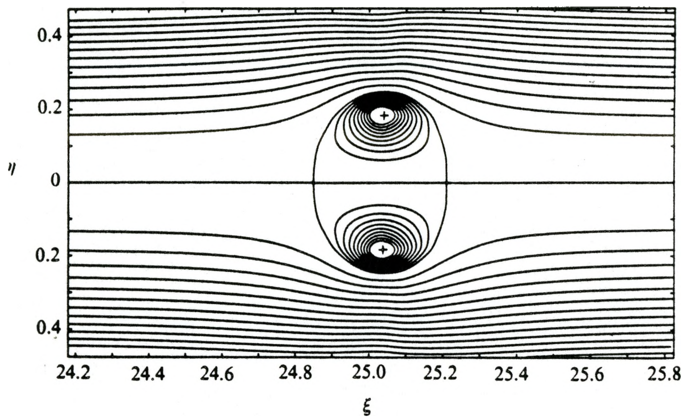


Figure 1.16 Streamlines of a vortex ring, "+" is the centre of the core. Glezer(1990)

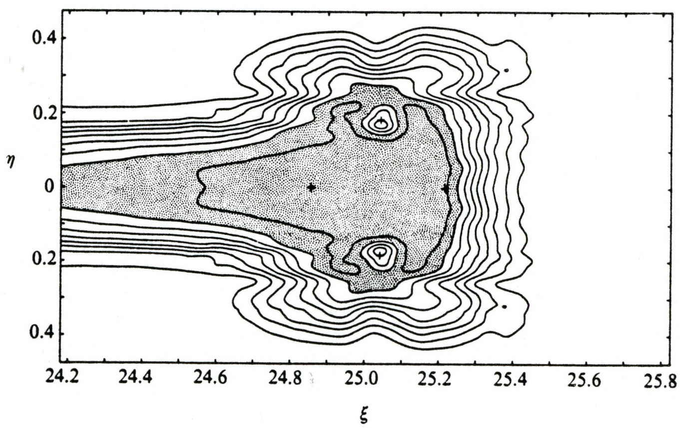


Figure 1.17 Intermittency around a vortex ring, "+" is the centre of the core. Glezer(1990)

that in the core of the ring. This means that turbulence production in the core of the ring is limited, as noticed by Maxworthy (1974). Glezer (1990) plotted the turbulence production in a vortex ring, see Figure 1.18. This figure shows that the production of turbulence is largest at the front part of the ring just outside of the core where vortex stretching is important and this is where the entrainment of surrounding fluid takes place. These results are in good agreement with Maxworthy's (1974) observation.

Maxworthy (1977) noted that as the turbulence in the outer body of the vortex ring flows over the inner core of the ring, it tears off some of the fluid along with the vorticity from the core. This fluid which is torn off is then deposited into the wake of the ring. This loss of vorticity from the core of the ring results in the decrease of linear momentum and translational velocity of the vortex ring. Figure 1.19 shows the decrease in total circulation, which is proportional to the vorticity, of the ring at a distance of 14Dm downstream from the orifice when compares with the total circulation of the ring at a distance of 2.5Dm from the orifice.

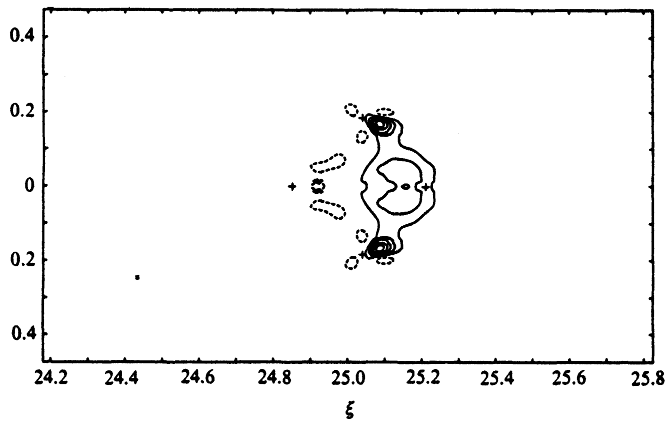


**Figure 1.18 Estimated turbulence production around a vortex ring, "+" is the centre of the core. Glezer(1990)**

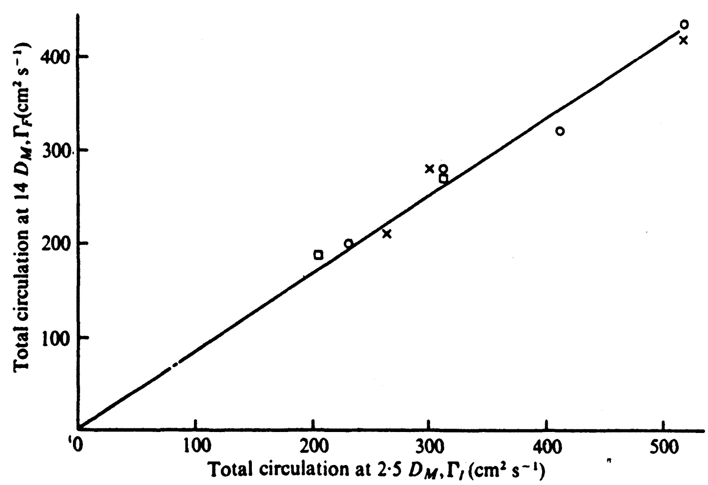


**Figure 1.19 Change $\Delta\Gamma$ in total circulation, showing the small decrease induced by instability and wave breaking. Maxworthy(1977)**

In conclusion, the entrainment of surrounding fluid into a laminar vortex ring is controlled by a diffusion mechanism, once this fluid enters the ring, it will remain in the ring. Hence very little mixing occurs along the path of a laminar vortex ring. On the other hand, the entrainment of fluid into a turbulent vortex ring is controlled by turbulence production at the edge of the core. After this fluid is entrained into the ring, some of it will enter the core of the ring and remain there, while most of this entrained fluid will be detrained into a wake behind the ring. This mixes the fluid inside the ring with the surrounding fluid. Hence turbulent vortex rings are more suitable for the majority of mixing processes as they can cause more mixing between the fluid in the ring and its surrounding as they travel through a fluid.

## 1.4 Other characteristic of turbulent vortex ring:

Lastly, Maxworthy (1974) showed a special feature of turbulent vortex rings that makes them so desirable for mixing process. Turbulent vortex rings have a low drag coefficient and are able to travel much longer distance than turbulent eddies. In his paper, he described the growth of the ring by an entrainment coefficient and the loss of linear momentum by a drag force acting on the ring. By equating these two quantities and eliminating the dependence on time, he obtained the following relationships;

$$R = \alpha x + 1$$

and $$U = \{\alpha x + 1\}^{-(Cd+3)}$$

From the measurements of the core radius of the ring R and the displacement of the ring x the entrainment rate of the ring, $\alpha$, can be determined. The drag coefficient Cd can be evaluated by substituting the entrainment rate into the velocity equation. He found that for a turbulent vortex ring with the same cross sectional area as a solid sphere, the drag coefficient for the ring was 0.04 as compare to 0.23 for the sphere.

With a thin core of highly concentrated vorticity and a relatively low drag coefficient, turbulent vortex rings are able to travel a much longer distance than other types of turbulent eddies.

## 1.5 Conclusion:

In this chapter, both the characteristics of laminar and turbulent vortex rings were reviewed. It showed that the effect of the volume of fluid injected during the formation of a vortex ring, the velocity of the jet, the shape of the orifice and the proximity of the wall have considerable effects on the successful generation of a vortex ring. These parameters must be carefully controlled in any vortex ring experiments in order to allow for a better comparison between different experimental results.

It has also been shown that the entrainment of a laminar vortex ring is controlled by a diffusion mechanism, and a laminar ring retains most of the fluid that it has entrained. The entrainment mechanism of turbulent vortex rings is controlled by turbulence production at the edge of the core of the ring. As the turbulent ring travels, it entrains the surrounding fluid and then deposits most of it into the wake. This means that turbulent rings are good for mixing the surrounding fluid with the fluid in the ring.

A general deduction for the parameters that will generate vortex rings most suitable for mixing are:

- $1 < Lm/Dm < 3$,
- $2{,}000 < Re_R$ for turbulent ring,
- constant jet velocity during formation, and
- wall boundary should be at least 5R from the centre of the ring.

# Chapter 2

## Initial Set up of the Apparatus for the Experiments

### 2.1 Introduction:

Part of the research involved the modification of an existing equipment and the setting up of a new apparatus. The modifications involved some changes to the injection mechanism for the production of vortex rings. These modifications were necessary in order to eliminate the unknown factors that might affect the formation of a vortex ring. These factors included:

1) the effect of the motion of the injection tube on the formation of vortex rings, and
2) the exact amount of fluid that was ejected through the orifice during the injection period.

By making the proper changes to the injection mechanism, the effect of these factors were either eliminated or minimized.

In order to increase the accuracy of the measurements of the size and location of the vortex ring, a video camera was used to record the generation and traverse of the vortex ring in a rectangular tank. A video frame grabber was used to analyse the video images to obtain the required data.

The following sections will discuss the modifications to the injection mechanism while the procedures for operating the frame grabber will be given in Appendix A.

## 2.2 Experimental Apparatus:

The schematic of the experimental apparatus is shown in Figure 2.1, it consisted of a 1.52m deep .305m square cross section tank. Two adjacent sides of this tank were made of plexiglass so that the generation process and the traverse of a vortex ring could be viewed and recorded using a video camera. The other two sides of the tank were made out of aluminum plate. The initial injection mechanism consisted of a .305m square plexiglass plate with a .051m diameter by .178m long tube centrally placed with its axis perpendicular to the plate as shown in Figure 2.2. The motion of this plate was controlled by a cam which was driven by a D.C. motor. As the cam pushed the plate down at a constant velocity, a constant velocity jet was ejected through the tube and a vortex ring was formed. The displacement and velocity of the plate was measured using a displacement transducer which was connected to an oscilloscope, where the displacement of the plate versus time was recorded.

A video camera was used to record the process of generation and the path of the vortex ring until it reached the liquid surface or disintegrated. The camera sat on a stand which could be raised using a pulley system driven by a variable D.C. motor, to follow and record the displacement of the vortex ring with respect to the opening of the tube. The approximate location and arrangement of this camera stand is showed in Figure 2.1.

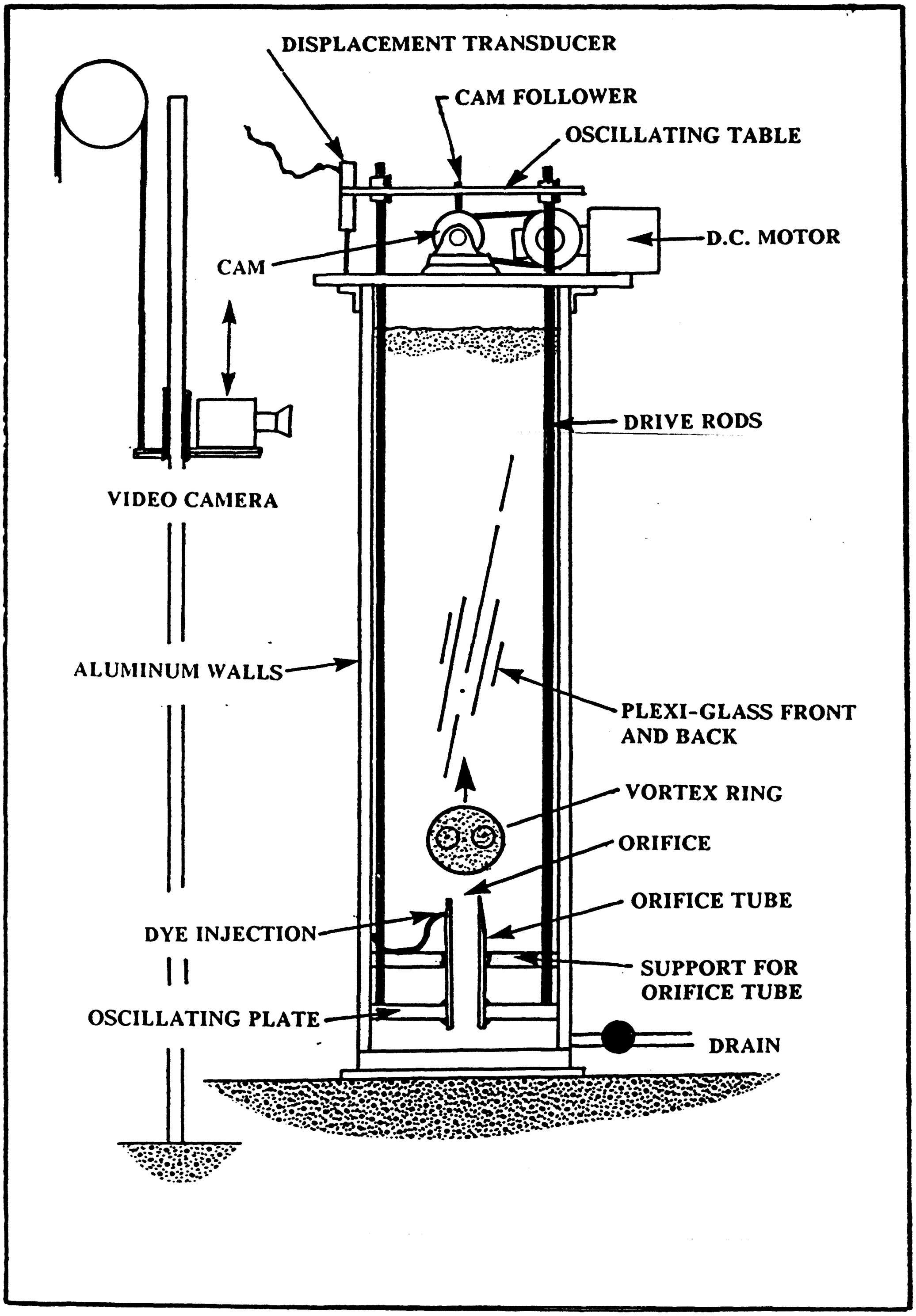


Figure 2.1 Schematic of the whole experimental set up.

## 2.2.1 Modifications to the injection mechanism:

In the original design of the tube type vortex ring generator, the orifice was attached to the movable injection plate. During the injection period, the injection plate was pushed down to eject a volume of fluid from the under side of the plate through the orifice. As the volume of fluid was ejected from the tube, a vortex ring was formed. A diagram of the earliest version of this vortex generator is shown in Figure 2.2.

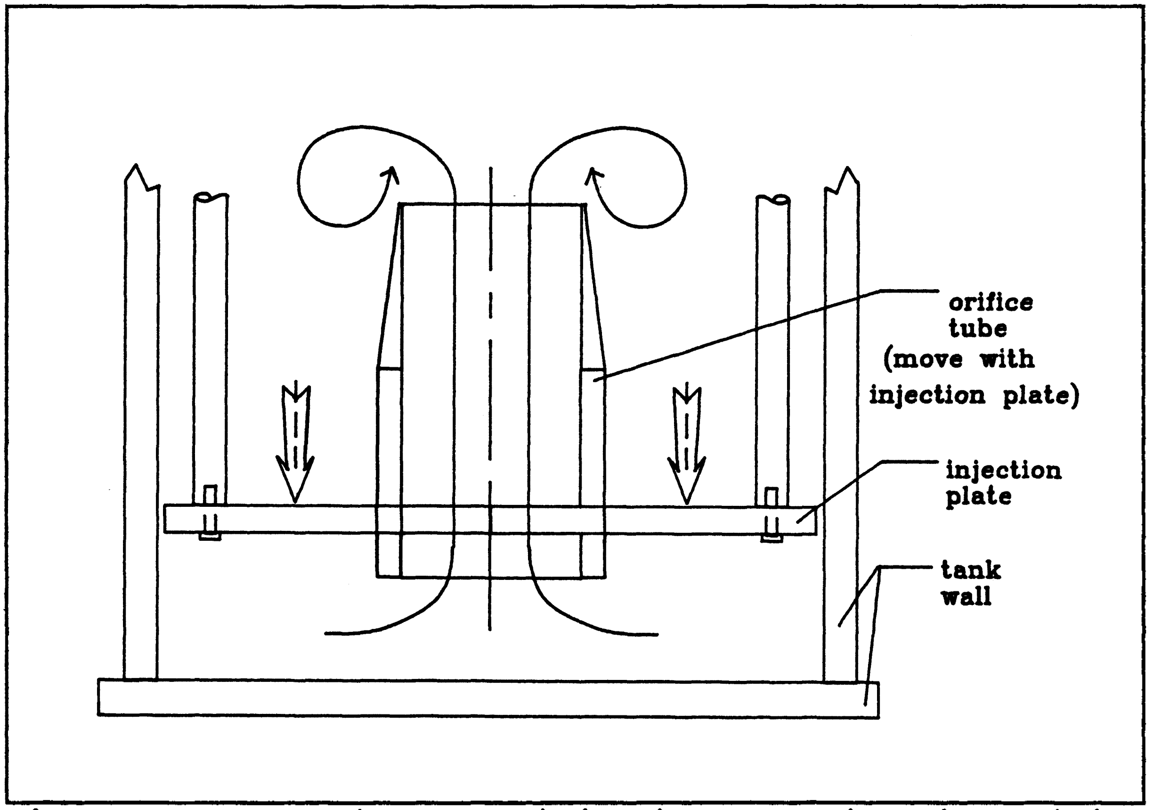


**Figure 2.2** Schematic of the injection mechanism with orifice tube fixed onto the injection plate

Vortex rings were successfully produced by this injection mechanism. However, the orifice tube moved with the injection plate during the injection. Since the effect of the relative motion of the orifice tube on the vortex rings was uncertain, in order the minimized any uncertainty that may affect the production of a vortex ring this injection mechanism was modified. Instead of attaching the orifice tube onto the injection plate, the orifice was supported by another plate which was attached onto the wall of the tank, see Figure 2.3.

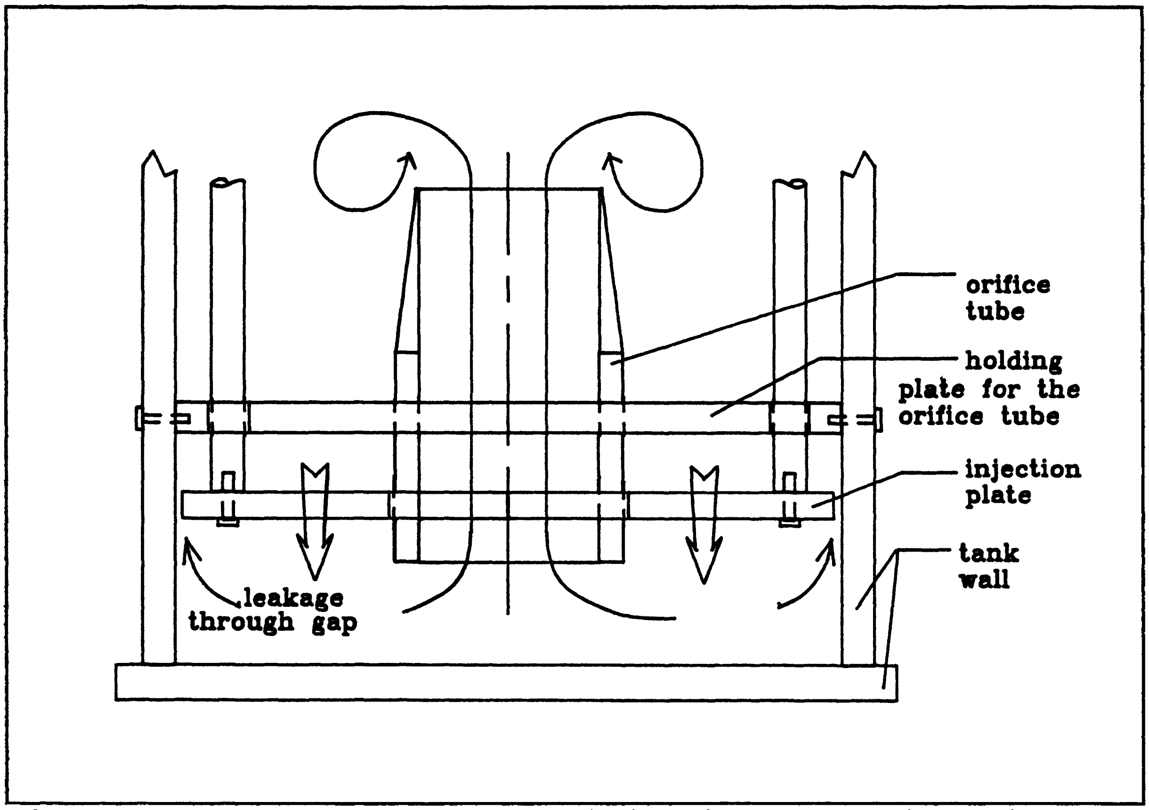


**Figure 2.3** Schematic of the injection mechanism with the orifice tube separated from the injection plate

In this way the orifice tube did not move during the injection period and the effect of the relative motion of the orifice tube on the formation of the vortex ring was eliminated. This particular apparatus was then used for the study of vortex rings travelling in a stratified fluid with a sharp density gradient. However there was some inconsistency in the results obtained, and the velocity profile of the jet was suspected to have caused this problem. Hence, the actual velocity profile and the volume of the jet was measured using hot film anemometry. These results are described in detail in Chapter3. The measurements showed that the actual velocity and volume coming out from the orifice was very different from what was expected based on the displacement of the injection plate. It was assumed that this was due to the leakage through the gaps around the edge of the injection plate. Hence the injection mechanism was modified again to minimized this leakage. This was done by the addition of plastic flaps onto the upper surface around the periphery of the injection plate. The location of these plastic flaps is shown in Figure 2.4.

After this modification, the velocity profiles of the jet was measured again using hot film anemometry. The results indicated that the addition of the plastic flaps onto the injection plate were able to minimize leakage through the gap of the injection plate. All the results from the hot film anemometry measurements are described in detail in

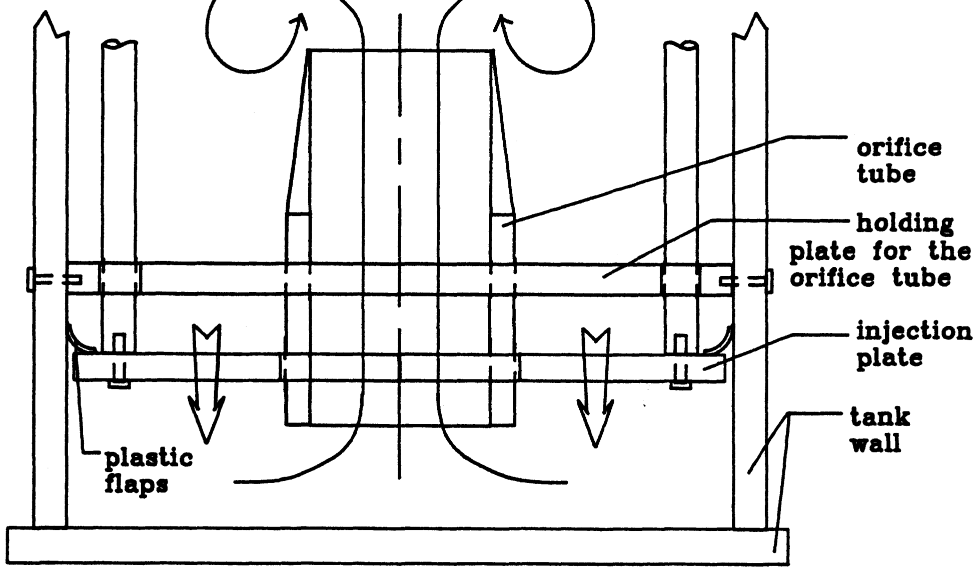


Figure 2.4 Schematic of the injection mechanism with the plastic flaps on the edge of the injection plate to minimize leakage

Chapter 3. In the next section, the use of the video frame grabber for the measurements of the experimental data is described.

## 2.3 Description of the video frame grabber:

After an experimental run was recorded using a video recorder, a digital video frame grabber was used to analysis these images and obtain information about the location and core diameter of the vortex ring after it was generated. The advantages of a frame grabber are:

1) it minimizes the time required to analyse the properties (e.g.

location and core diameter) of the vortex ring from the beginning of the injection period to the final decay of the ring; and

2) it gives an accurate measurement of the location of the ring and its diameter, because the horizontal and vertical distances are digitized.

A digital video frame grabber system, HRT 512-8, was chosen for this application. The set up for this system is discussed in the Appendix A which includes:

1) hardware set up on a computer,
2) set up and operation of the data collection software, and
3) analysing the data stored in the data file.

## 2.4 Conclusion:

This chapter described the modifications that was done on the experimental apparatus during the course of this research project. These modifications were performed on the injection mechanism to eliminate the factors that might affect the generation of a vortex ring. A digital video frame grabber was used for more accurate and quick measurements of the location and diameter of the ring while it travelled along the tank. A description of the hardware and software for this system is included in Appendix A.

# Chapter3

# Measurements of the Velocity Profile Coming Out From the Injection Tube During the Formation of a Vortex Ring Using Hot Film Anemometer

## 3.1 Introduction:

One of the purposes of this research was to determine the criteria for vortex rings to penetrate a stratified layer. A model was developed to predict the maximum distance a vortex ring can penetrate through a stratified layer. This model relied on the knowledge of the initial velocity of the jet forming the vortex ring. A precise knowledge of the velocity profile of the jet at the orifice was required in order to calculate the energy and volume of the jet. Hot film anemometry was used to measure the velocity profile of the jet leaving the orifice. The following discusses the result of this study.

3.2.1 Description of the hot film equipment:

A TSI hot film anemometer was used to perform the velocity measurements. The unit consists of the following items:

1) Constant temperature anemometer (model no. 1053B);
2) Variable decade resistance (model no. 1056);
3) Monitor and power supply (model no. 1051-2);
4) TRI axial cable for connection between the probe and the anemometer(model no. 10110-20ft); this is of particular importance for the operation of this system because it has the correct impedance that matches that of the anemometer unit. Any other co-axial cable will cause large output signal fluctuations and may damage the anemometer.
5) Probe supports (model no. 1150, 1152); and
6) Hot film probe (TSI 1210-20W serial no. 93311) liquid probe.

<u>3.2.2 Calibration of the hot film anemometer:</u>

Before the anemometer could be used for measuring the velocity profile of the jet, it had to be calibrated. The injection mechanism could generate a theoretical mean jet velocity of between 6 in/s (.1524 m/s) to 40 in/s (1.016 m/s). Since the lower limit of this velocity was relatively small, it was not feasible to use a constant head tank to create a jet with a steady velocity. There was no other equipment readily available that could generate such a wide range of velocities for calibration purposes. Instead of using a jet with constant velocity, the same effect could be achieved by towing the anemometer at a given velocity in a body of stationary water. This method was used to calibrate the hot film probe.

A D.C. motor having a .152 m diameter pulley was used to tow a trolley located above a water channel, at the required velocities. Figure 3.1 shows a schematic of the towing mechanism on the water channel and Figure 3.2 presents two photographs of the actual system. A D.C. power supply was used to vary the speed of the motor and therefore the velocity of the trolley.

In order to measure the actual velocity of the trolley, a simple electrical circuit was used. A battery was connected to an oscilloscope such that the scope always measured the voltage of the battery. A part of the metal wire connecting this circuit was exposed and two metal

Figure 3.1 Schematic of the flying anemometer calibration system

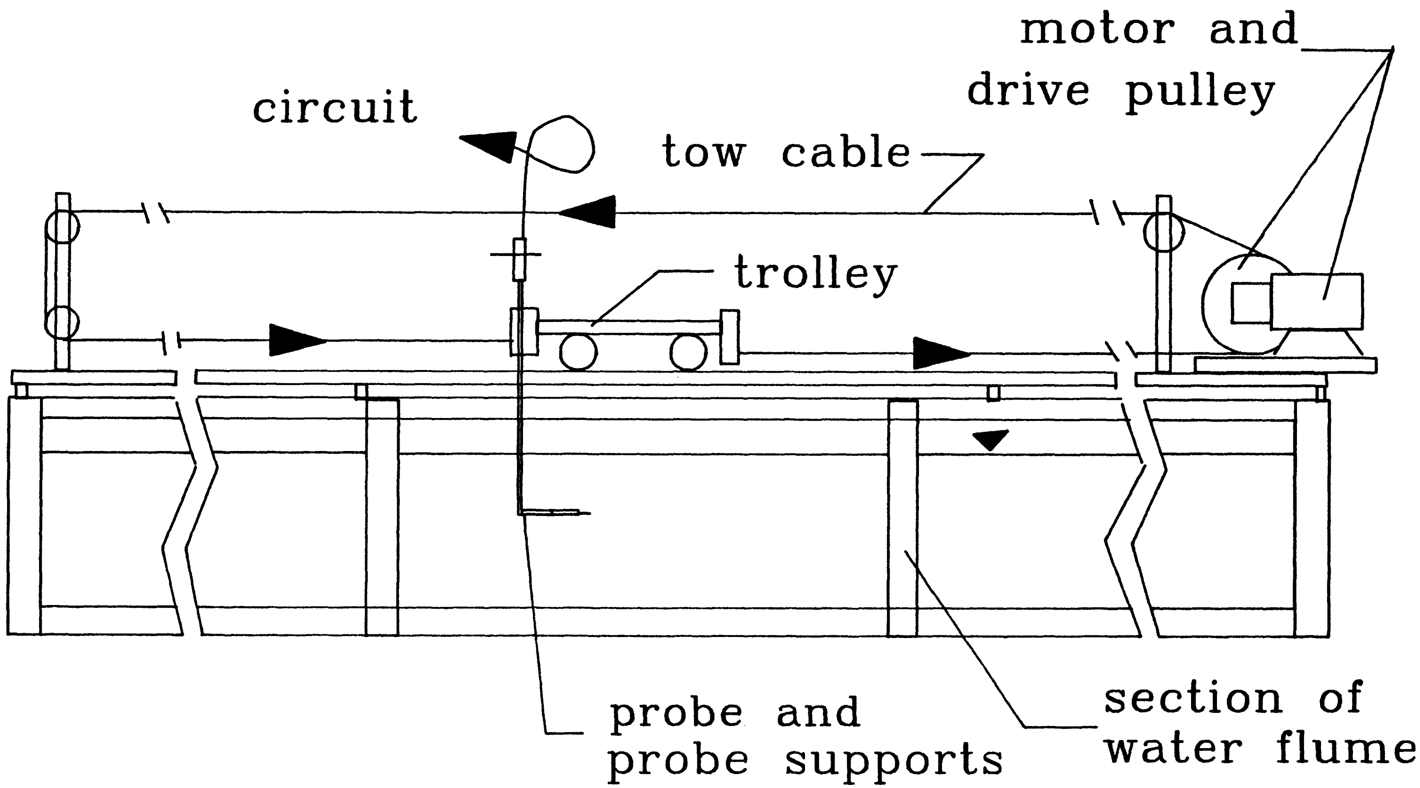

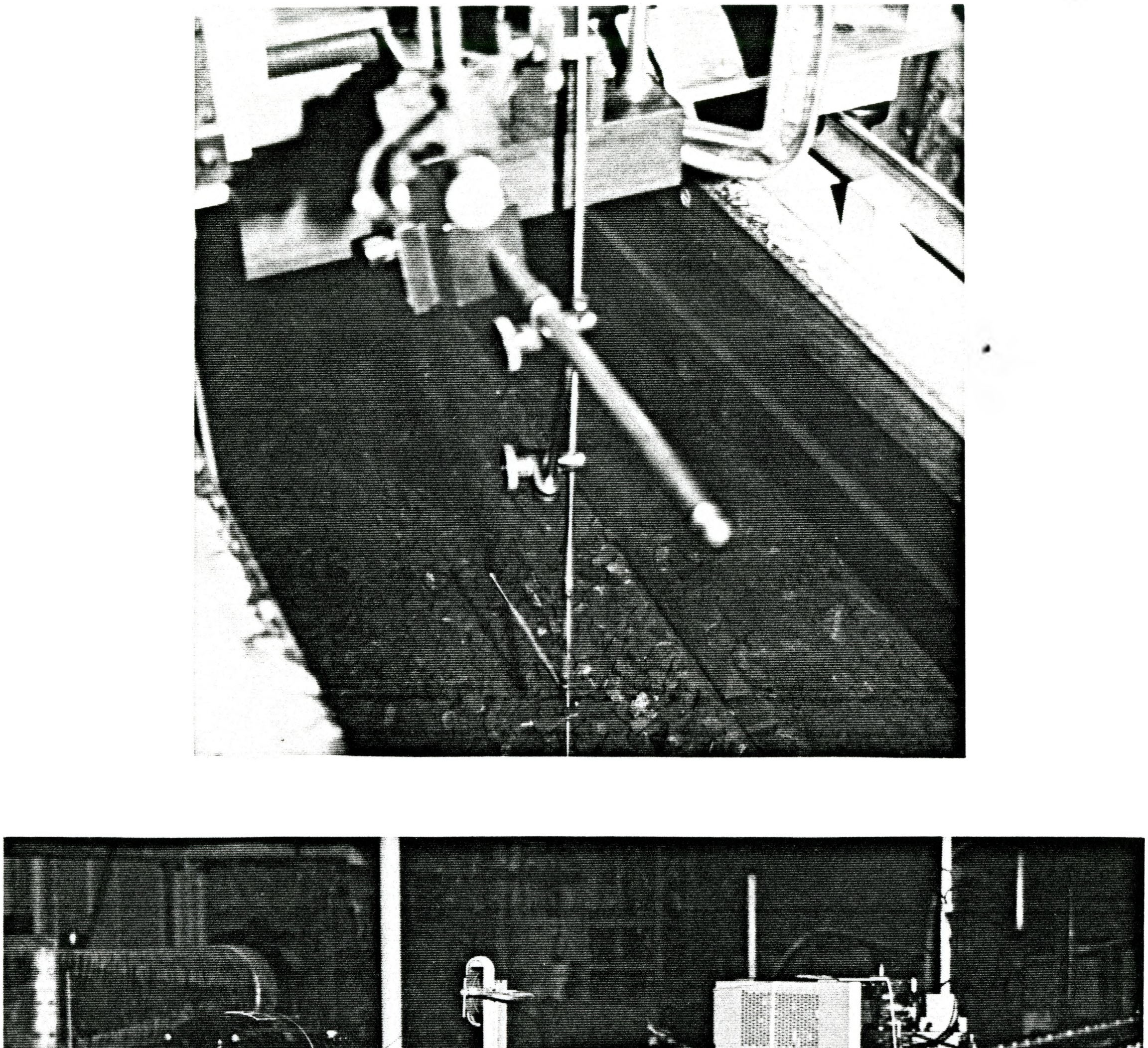

Figure 3.2 Photographs of the anemometer calibration system

bars were clamped onto the frame of the tank and they were 6 feet apart. The exposed wires were positioned in such a way that every time they went pass the metal bars, the circuit to the scope would be shorted. This created a spike on the scope and the time between the two spikes could be measured from the oscilloscope trace and hence the velocity of the trolley could be determined.

As the hot film probe was towed along the tank, the voltage output from the anemometer was very constant between the contact points. This meant the velocity of the trolley remained constant within the 6 feet calibration distance. The anemometer was then subjected to a range of velocities between .152 to .914 m/s. The results are plotted on the calibration curve shown in Figure 3.3. Using ENPLOT2 (a graphics computer software package), a calibration curve was fitted to the experimental results to obtain a relationship between the measured voltage and the velocity. The relationship was:

$$Voltage = 6.13449 + 6.6536 * (Velocity * 0.3048)^{.325112}$$

Using the calibration curve, the hot film anemometer was then used to measure the velocities of the jet exiting the ejection tube during the formation stage of a vortex ring.

Fig. 3.3 Calib. curve for hot film probe
Model # TSI 1210-20W, Ser. no. 93311

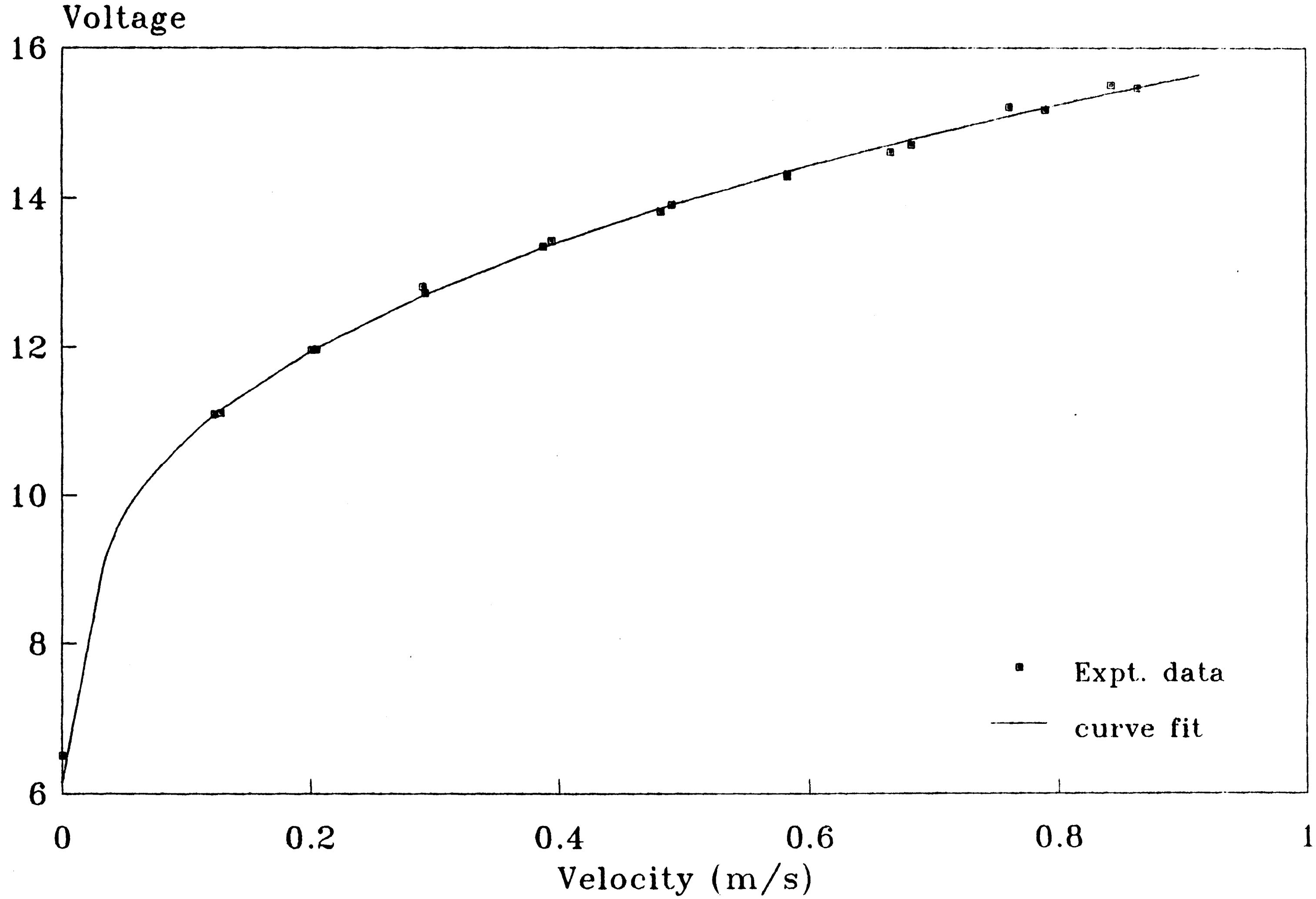

3.3.1 Description of the mounting mechanism for the hot wire anemometer:

After the hot film probe was calibrated, the probe was mounted onto the tank for measuring the velocity profile of the jet. The probe was mounted at two locations close to the exit of the injection tube. The first location was approximately 0.8 cm above the opening of the injection tube and the second location was approximately 1 cm inside the opening of the injection tube. The probe support was mounted onto a traversing mechanism that permitted the probe to travel across the diameter of the injection tube. Figures 3.4 and 3.5 present a schematic of the mounting mechanism for the probe and a picture of the traverse mechanism.

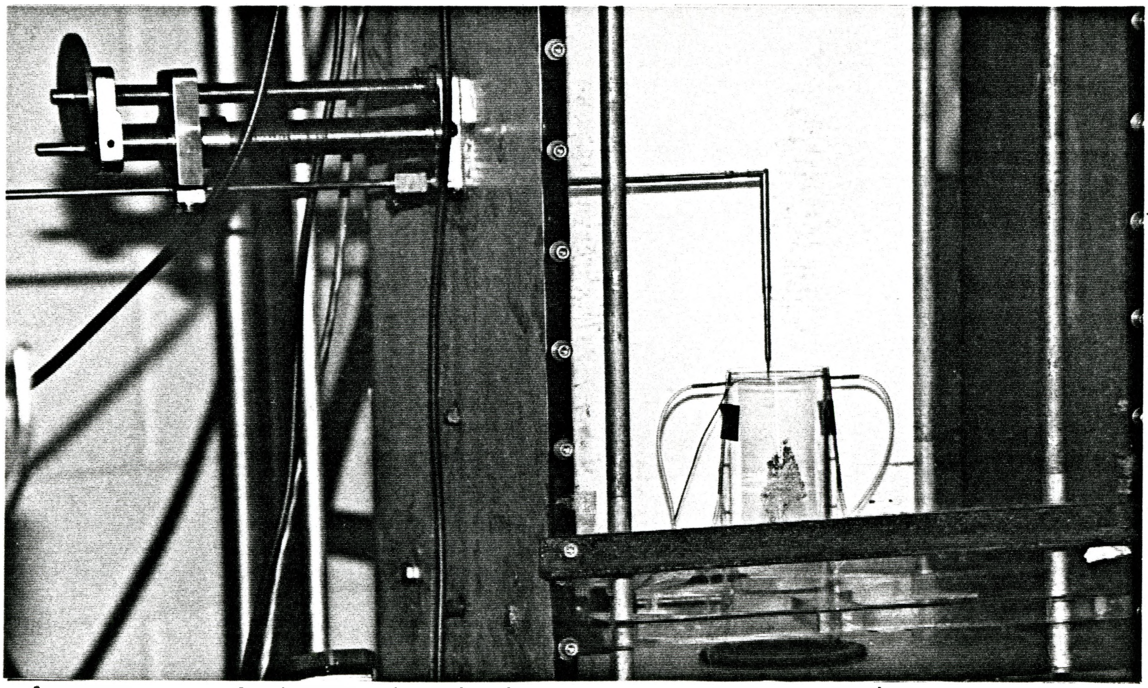

Figure 3.4 Photograph of the anemometer mounting mechanism.

Figure 3.5 Schematic of the traverse mechanism and the locations of the probe

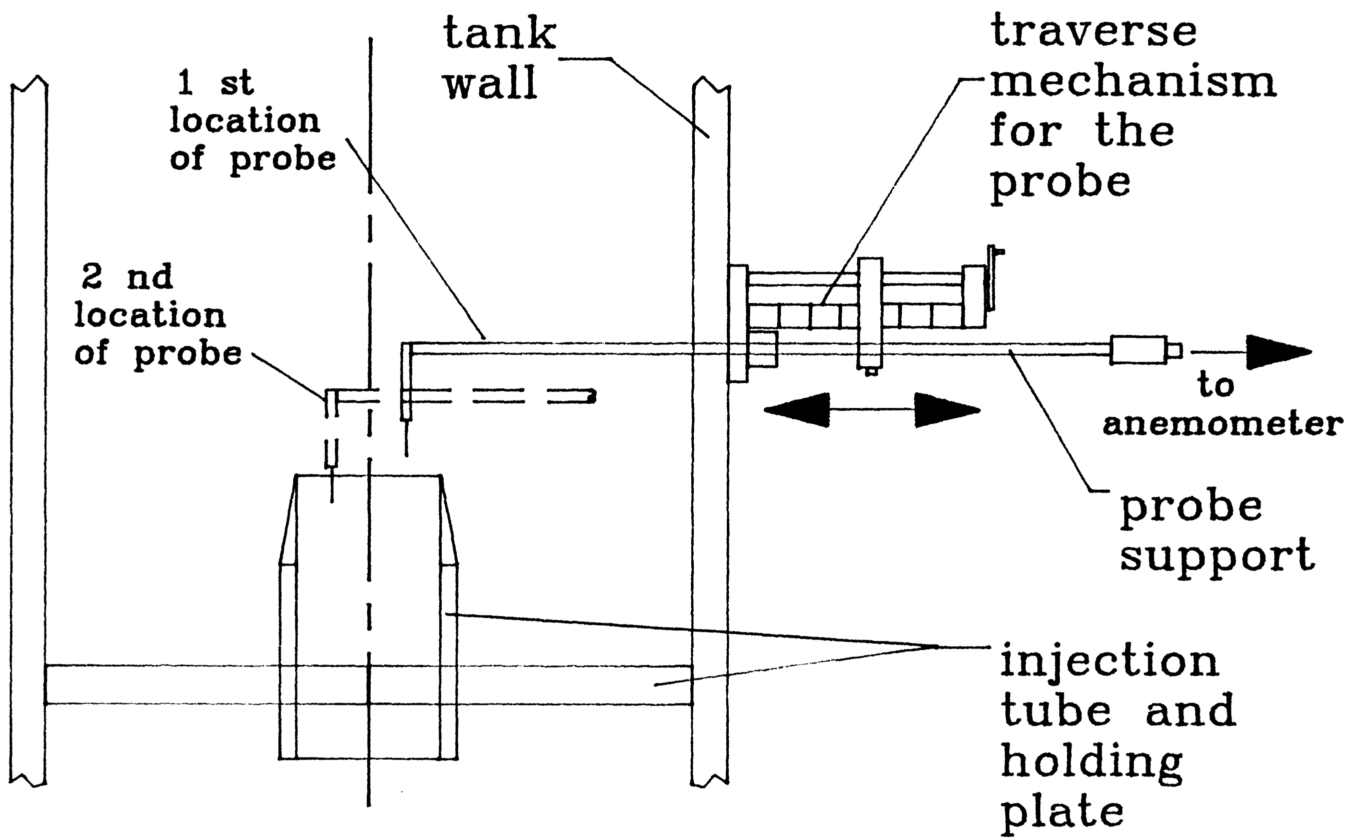

3.3.2 Measurements of the velocity profile of the jet:

Four different theoretical jet velocities were used in the measurements, .203, .330, .483 and .635 m/s. The first set of measurements were taken where the hot film probe was mounted at a distance of .8 cm above the exit plane of the injection tube. The locations which most of the first set of measurements were taken were: -25.4, -20.3, -15.2, -10.1, -5.1, 0.0, 5.1, 10.2, 15.2, 20.3, 22.9, 24.1, 25.4, 26.7, 27.9 and 30.5 mm along a diameter of the tube. These results were shown in Figure 3.6 to 3.9.

The second set of measurements that were taken with the probe mounted at a location of .010 m below the exit plane of the injection tube. The locations which the second set of measurements were taken are: -23.8, -22.9, -21.6, -20.3, -17.8, -15.2, -10.2, -5.1, 0.0, 5.1, 10.2, 15.2, 17.8, 20.3, 21.6, 22.9 and 23.8 mm along a diameter of the tube. These results are shown in Figure 3.10 to 3.13. A table of the relationship between the percentage power supplied to the motor and the theoretical jet velocity is given below in Table 3.1:

| % Power | Theo. Vel. (m/s) |
|---|---|
| 15 | .203 |
| 30 | .330 |
| 50 | .483 |
| 70 | .635 |

Table 3.1. Relationship between power supplied and theoretical jet velocity

Fig 3.6. Displacement of plate vs. time
15%power, L/D=2.8, .8cm form tube

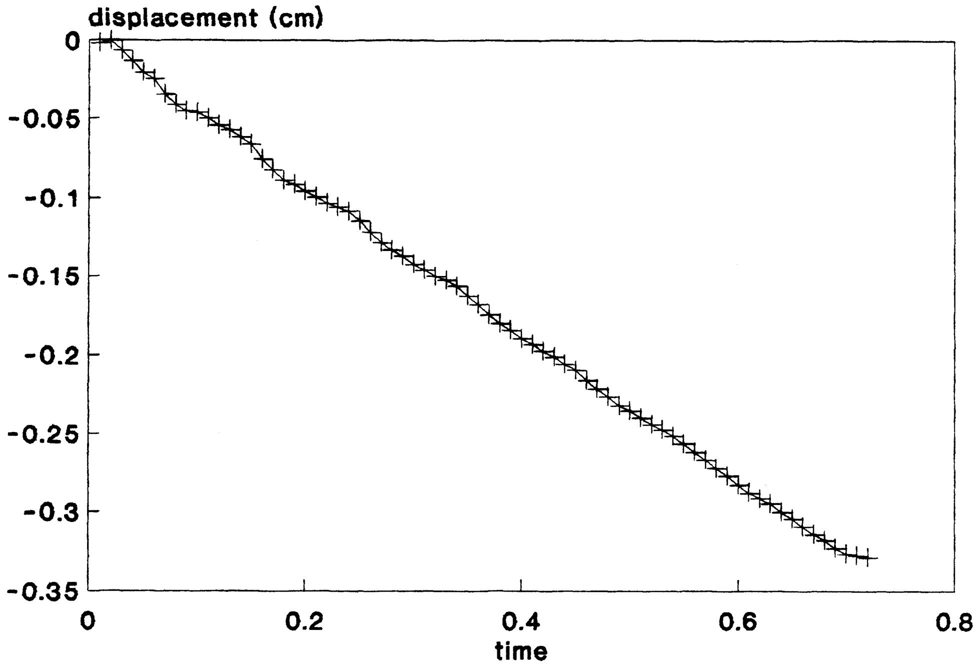


Velocity profile of jet vs. time
15%power, L/D =2.8

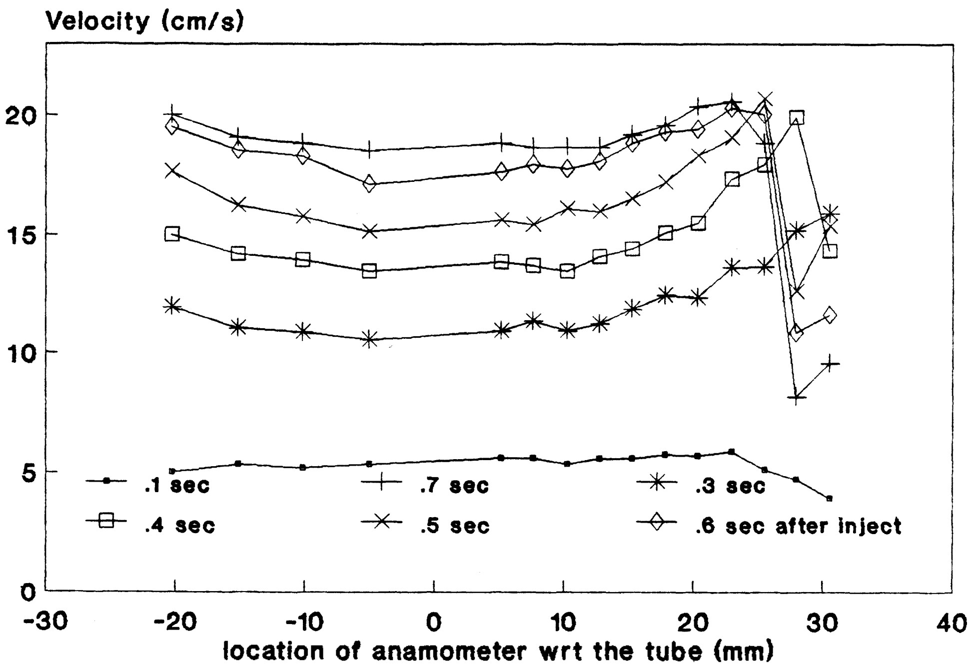

Fig 3.7 Displacement of plate vs. time
30%power, L/D=2.8, .8cm from tube

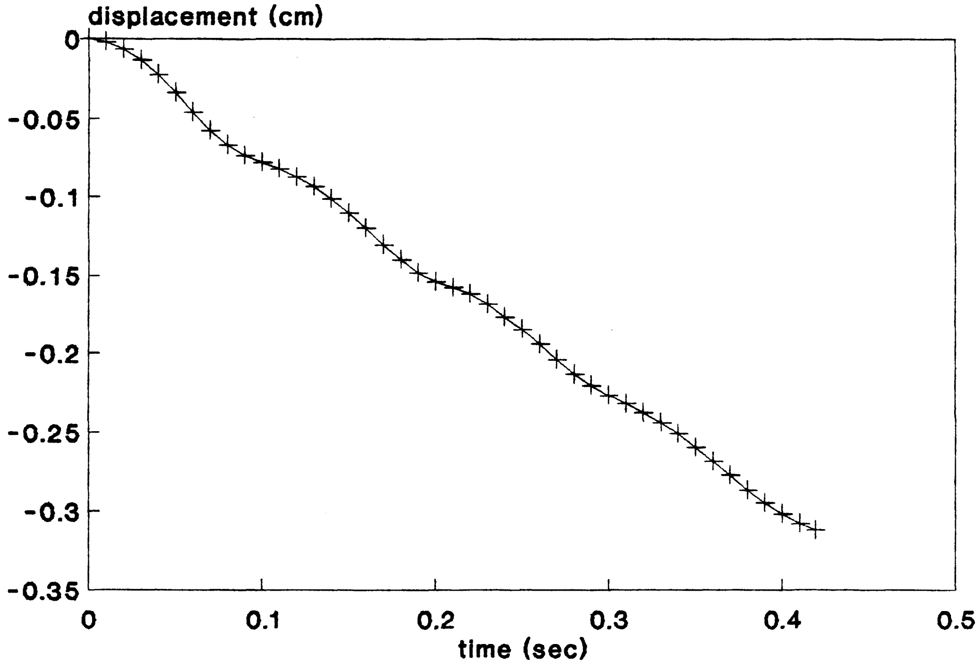


Velocity profile of jet vs. time
30%power, L/D=2.8, .8cm from tube

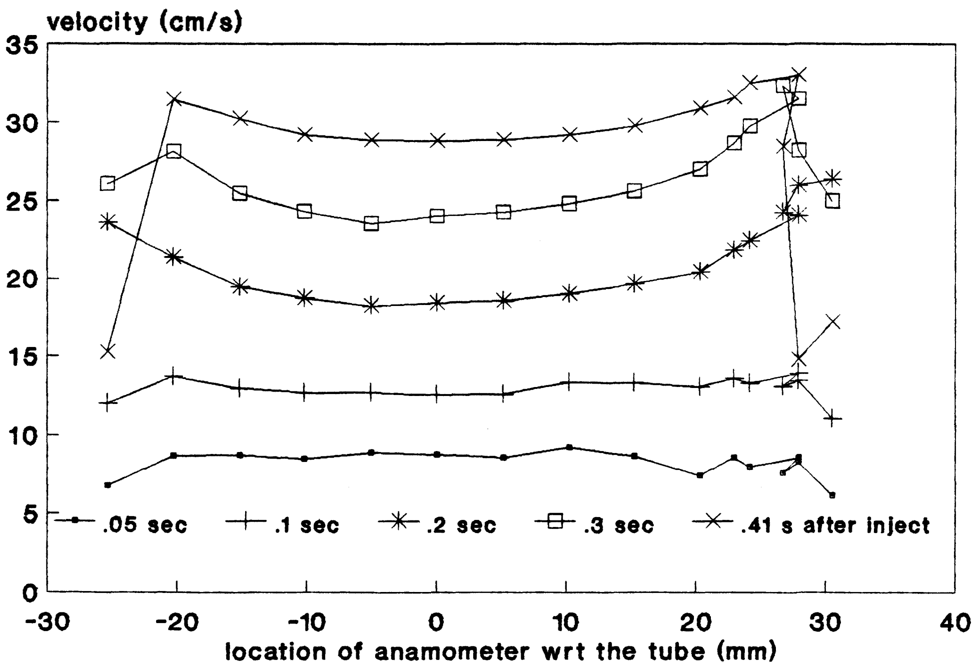

Fig 3.8 Disp. of injection plate vs. t
50% power, L/D=2.8, .8 cm above tube

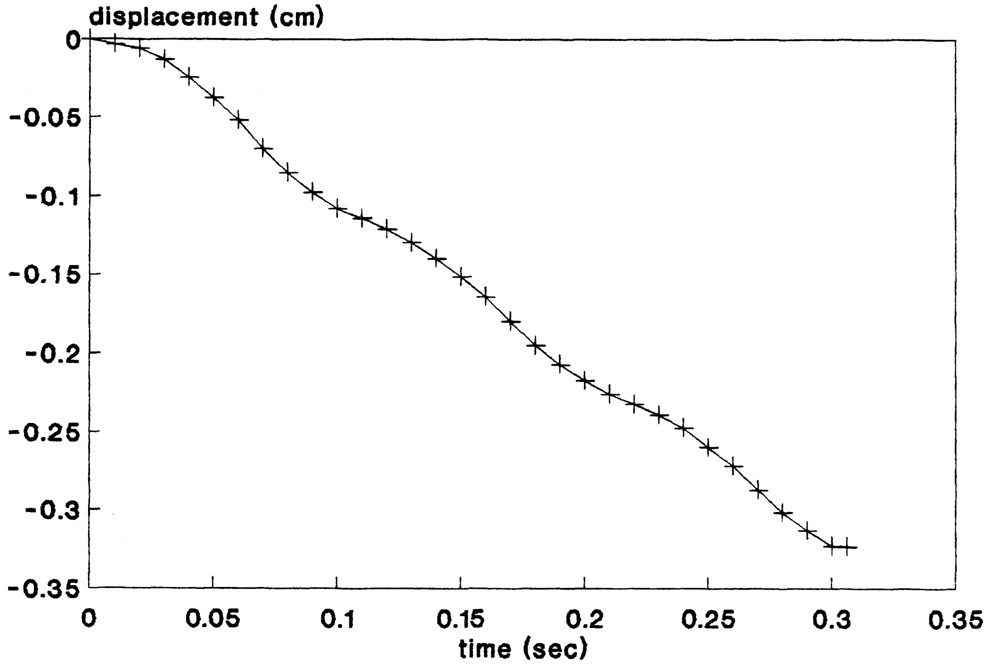


Velocity profile of jet vs. time
50%power, L/D=2.8, .8 cm form tube

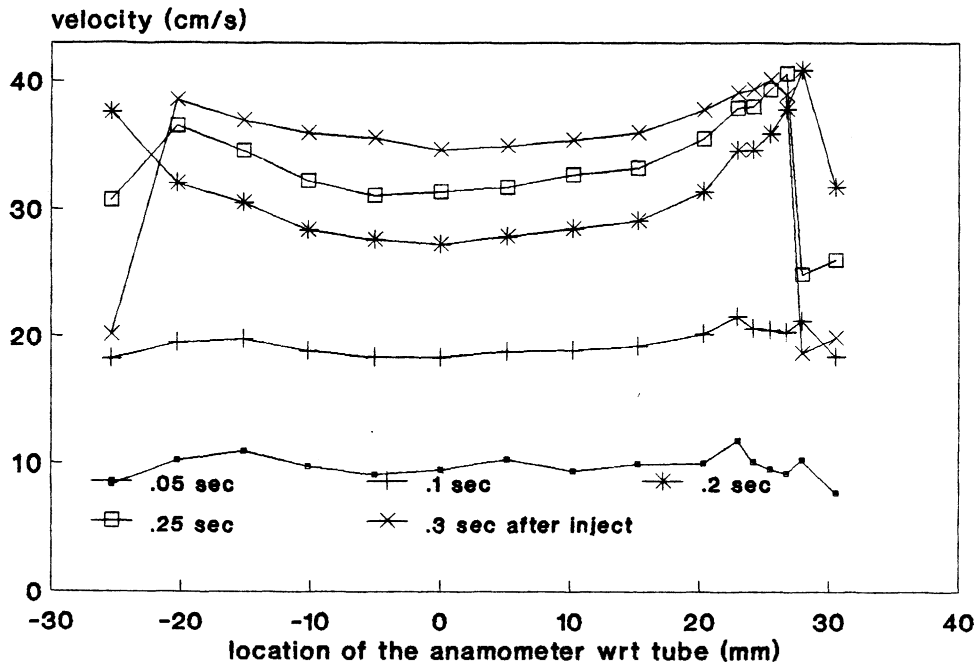

Fig 3.9 Displacement of plate vs. time
70%power, L/D=2.8, .8cm form tube

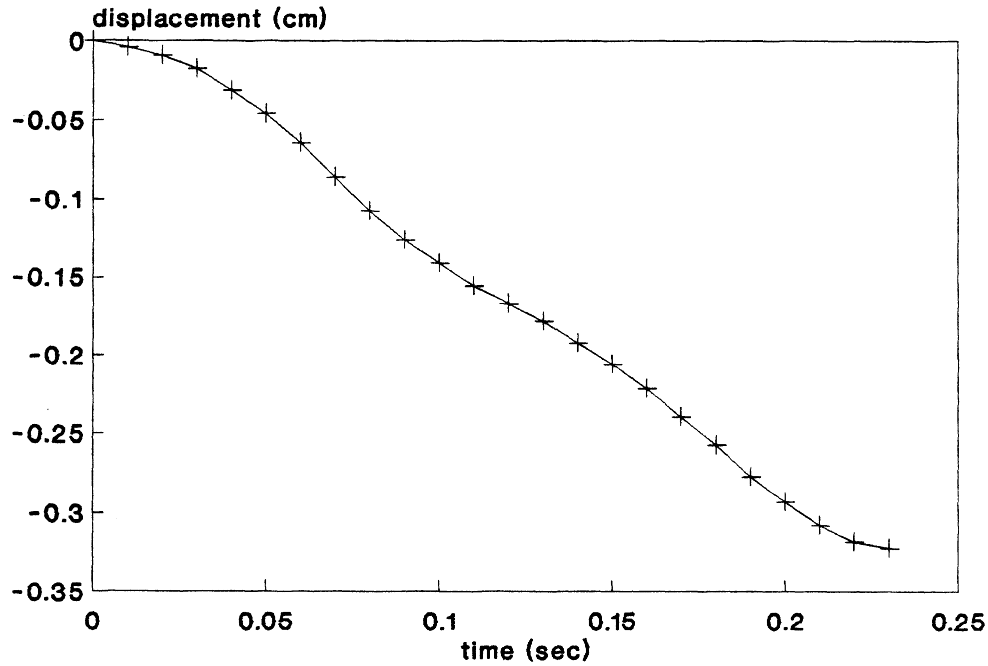


Velocity profile of jet vs. time
70%power, L/D=2.8, .8cm from tube

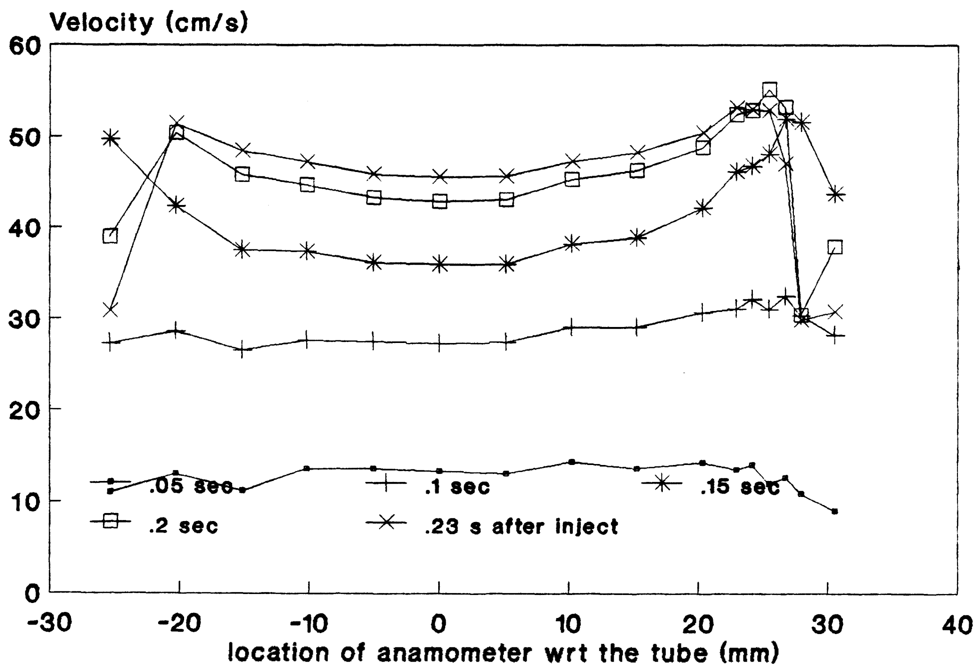

Fig 3.10 Vel. trace of jet and disp. of injection plate vs. time
15%power, Vjideal= 20.3 cm/s

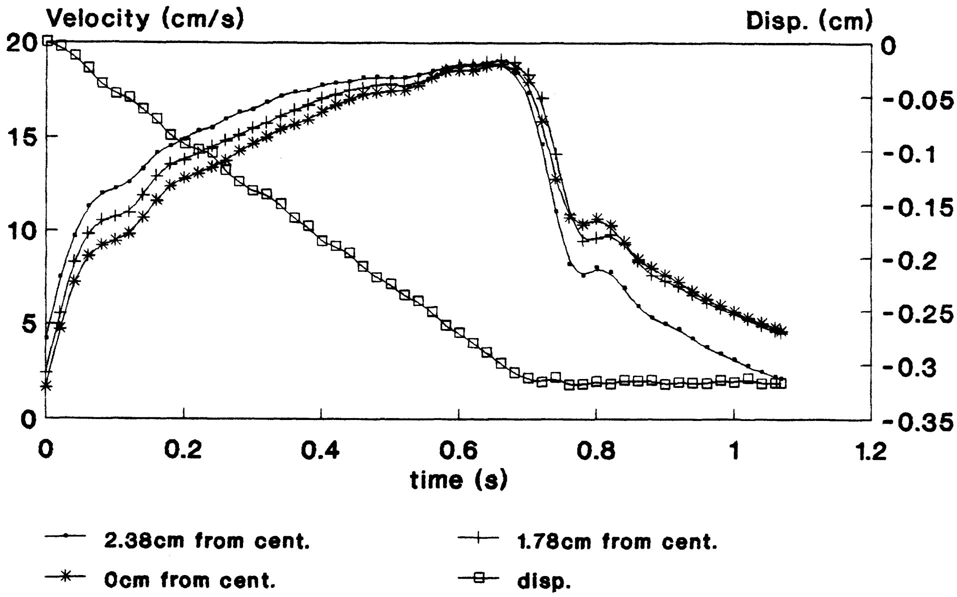


From:15%p-int

Velocity profile of jet vs. time
15%power, L/D=2.8, 1 cm inside tube

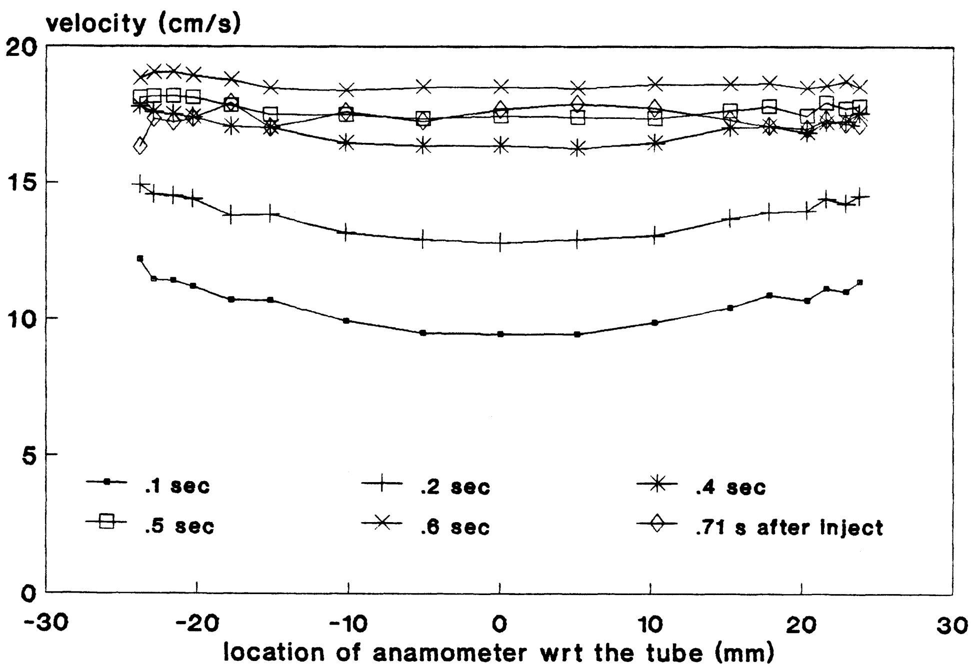

Fig 3.11 Vel. trace of jet and disp. of injection plate vs. time
30%power, Vjideal= 33.5 cm/s

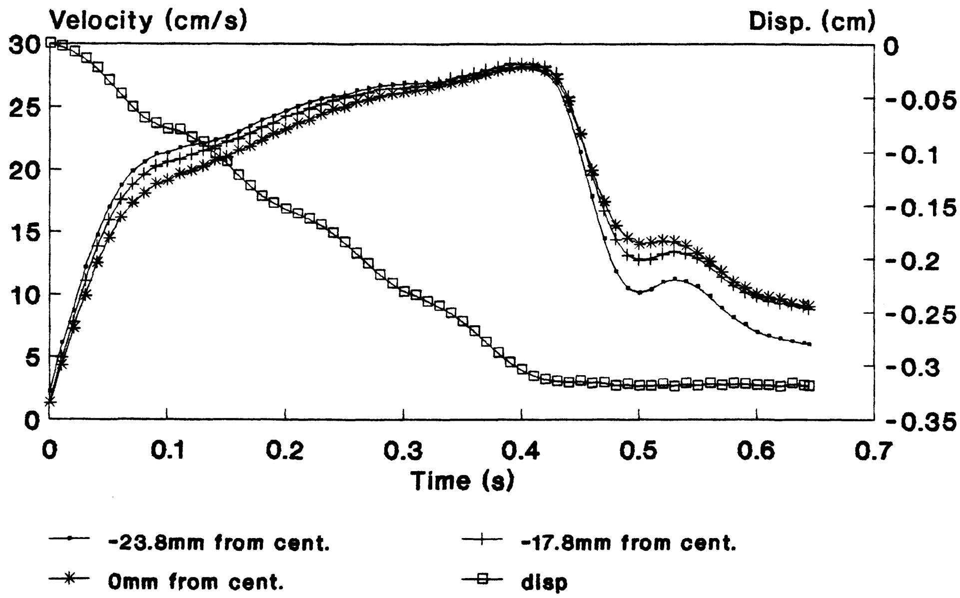


From: 30%p-int

Velocity profile of jet vs. time
30%power, L/D=2.8, 1 cm inside tube

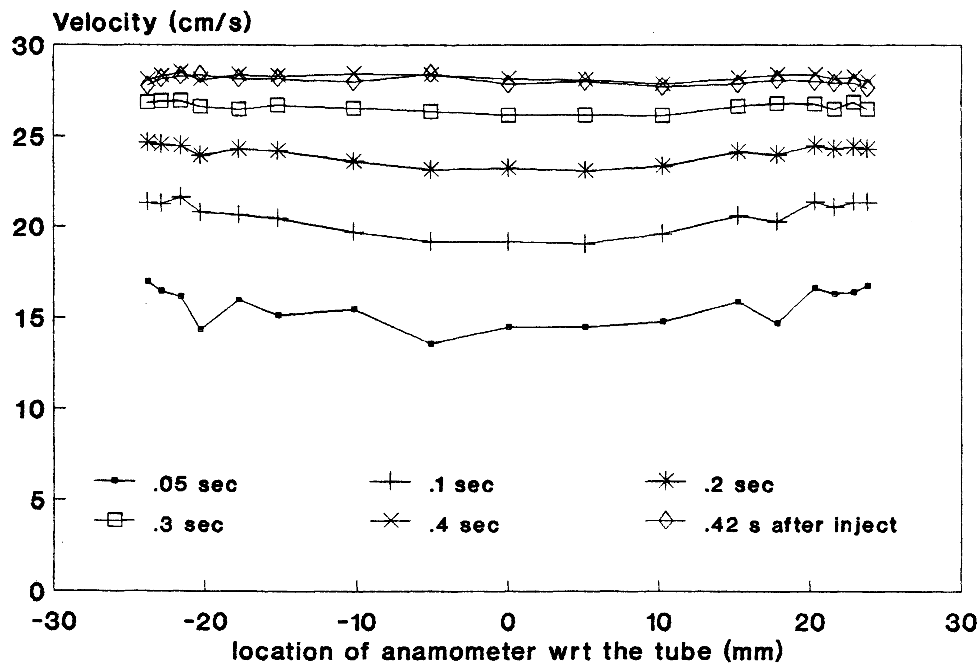

Fig 3.12 Vel. trace of jet and disp. of injection plate vs. time
50%power, Vjideal= 50.5 cm/s

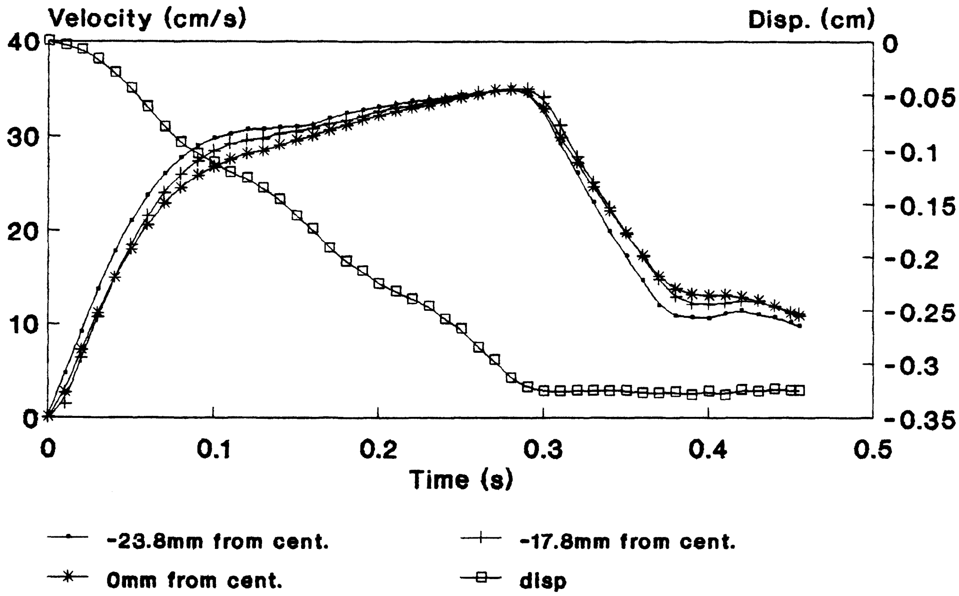


From: 50%p-int

Velocity profile of jet vs. time
50%power, L/D=2.8, 1cm inside tube

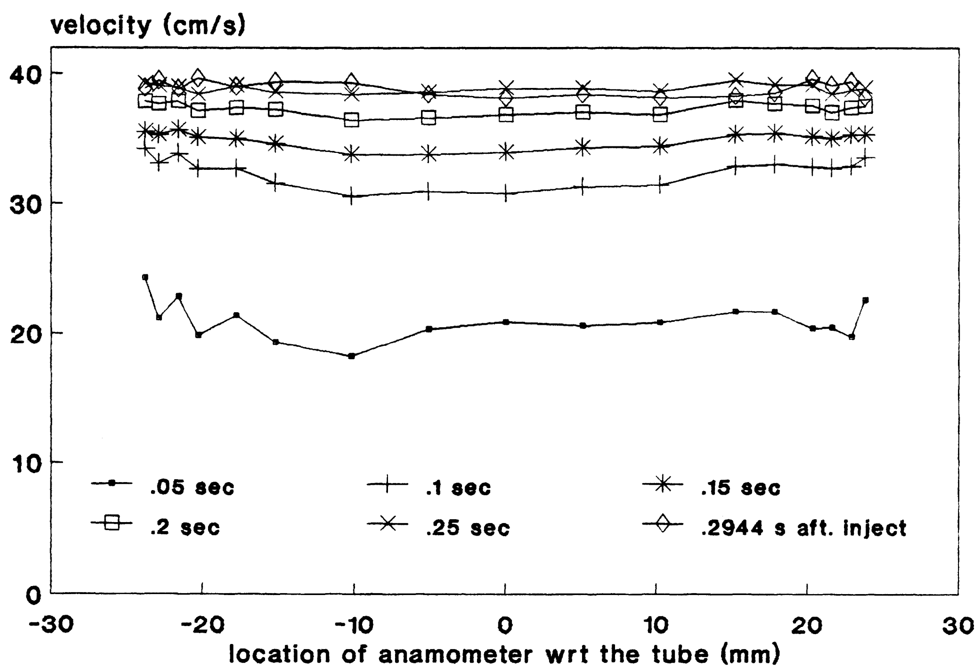

Fig 3.13 Vel. trace of jet and disp. of injection plate vs. time
70%power, Vjideal= 64.3 cm/s

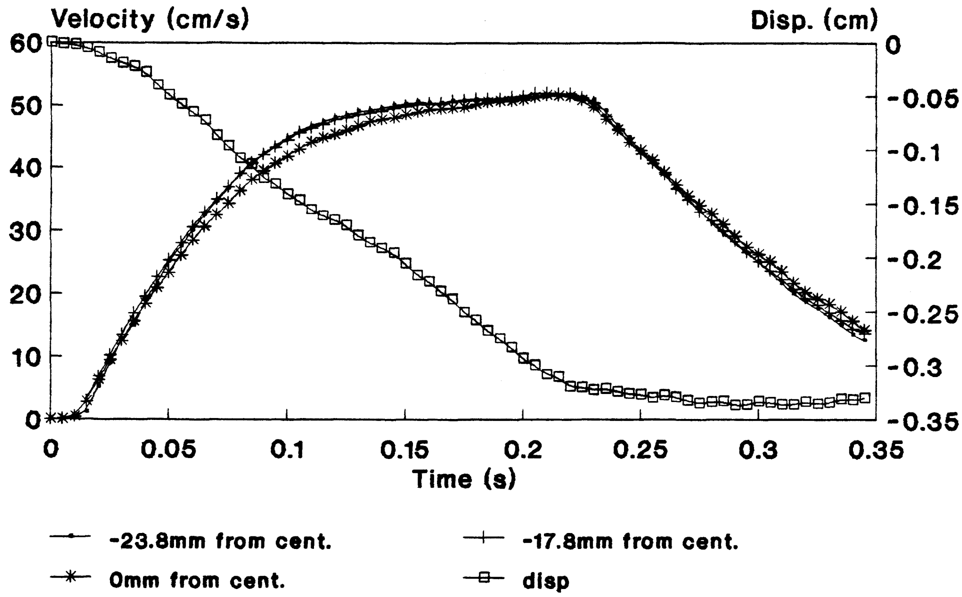


From: 70%p-int

Velocity profile of jet vs. time
70%power, L/D=2.8, 1cm inside tube

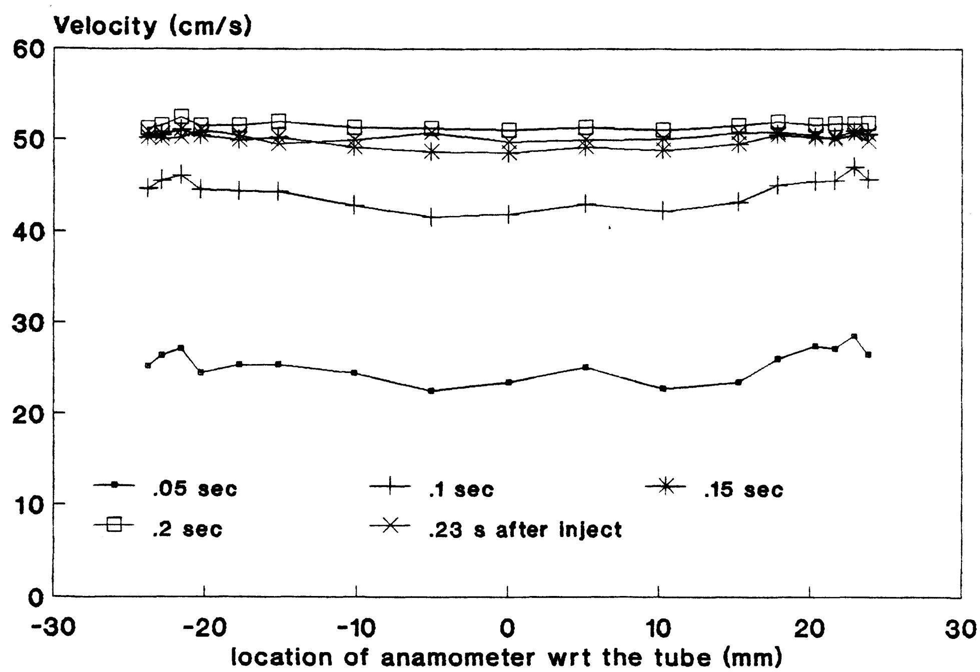

## 3.4 Discussion:

### 3.4.1 Measurements in a place 0.8 cm above the exit plane of the tube

With the hot film probe located at a distance of 0.8 cm above the exit plane of the injection tube, the first set of velocity measurements were obtained. The velocity measurements of the jet showed that the velocity at the centre of the tube was less than the velocity close to the edge of the injection tube, as shown in Figures 3.6 to 3.9. This could have been caused by the roll up of the fluid as it left the injection tube. As the fluid was ejected from the tube, vorticity was generated in the boundary layer of the jet. This vorticity caused the fluid close to the boundary to roll up after it separated at the exit of the tube. As this volume of fluid finished one rotation, it met with the portion of the jet that was still being injected to form a vortex ring. This may have caused the higher velocity obtained at locations close to the wall of the tube especially at the later stage of the injection period. This hypothesis should be further examined using flow visualization techniques.

### 3.4.2 Measurements at 10.2 mm below the exit of the tube:

Since the velocity profile of the jet at this location was affected by the roll up of part of the jet, the velocity profile of the jet had to be obtained at locations where the hot film probe was placed at the exit plane of the tube or inside the tube a short distance below the exit plane. Due to the limitations of the injection mechanism, the hot film probe could not be mounted right at the exit plane of the tube. Instead, it was mounted inside the tube at a distance of 10 mm below the tube opening. Figures 3.10 to 3.13 present the results obtained with the probe mounted at this location.

These results confirmed the assumption that the velocity profile of the jet would not attain its maximum velocity at the beginning of the injection. The average measured velocities of the jet leaving the tube were smaller than the theoretical jet velocities assuming no leakage at the wall. This was presumably due to leakage through the annular gaps between the injection plate and the wall of the tank during the injection period. Due to this over estimation of the velocity profile, the volume and energy of the jet had to be recalculated based on the measured velocity profile.

### 3.4.3 Calculation of the actual volume and energy of the jet:

The velocity profile of the jet was measured at nine locations along the radius of the injection tube. The total volume and energy of the jet were estimated using these measurements. Judging from the results obtained, the measurements from the left hand side of the tube were very similar to the measurements from the right. Consequently, only the right hand side of the velocity profile shown in the Figures 3.10 to 3.13 was used for the calculation of the volume and energy of the jet.

The volume and energy calculations for the jet were defined by the quantity and velocity of fluid that crossed the plane where the probe was located during the injection period. The area of the tube was divided into sections, each section was defined by the distance from the mid point between the last and the present data point to the mid point between the present and the next data point. The measured velocity was taken as the mean velocity over the entire section. There were two exceptions to this which were:

1) the larger radius of the second to last data point was defined at the location of the last data point;

2) for the last data point to satisfy the no slip condition at the wall boundary, the velocity profile was assumed to decrease linearly from the last data point to the wall boundary where the velocity of the jet reached zero.

| Location of probe(mm) | Radius of segment(mm) |
|---|---|
| 0.0 | 0.0 - 2.5 |
| 5.1 | 2.5 - 7.6 |
| 10.2 | 7.6 - 12.7 |
| 15.2 | 12.7 - 16.5 |
| 17.8 | 16.5 - 19.1 |
| 20.3 | 19.1 - 21.0 |
| 21.6 | 21.0 - 22.2 |
| 22.9 | 22.2 - 23.8 |
| 23.8 | 23.8 - 25.4 |

Table 3.2. Location of each segment wrt location of the probe

With these assumptions, the total volume of the jet was given by,

$$Volume\ of\ jet = \sum_{tbegin}^{tend} U_{measured}\, \pi\ (\ r_2^2 - r_1^2\ )\ \Delta t$$

except for the very last segment where the velocity was assumed to have a linear velocity profile to satisfy the no slip condition at the wall boundary. The volume of fluid past through this segment was obtained by integrating the assumed velocity profile over the area of the segment, that is,

$$dvolume = \int_{r_1}^{r_2} U(r)\ dA$$

$$= \frac{U_{measured}\ 2\ \pi\ 1.9015*10^{-3}}{0.063}$$

For the calculation of the energy of the jet, two more assumptions were made;

1) the radial component of the velocity profile did not change appreciatively and was not significant compared with the axial component within the period each measurement was taken, i.e. the radial velocity inside the jet was zero, $U_{radial} \approx 0$.

2) the axial component of the velocity was assumed to be the same between the period each data point was taken, i.e. Va=constant. The time between each measurement was either .0005 sec or .0002 sec which is the sampling rate of the oscilloscope.

With the two assumptions above, the calculation for the energy of the jet was simplified to;

$$Energy = \sum_{tbegin}^{tend} 0.5\ U_{measured}^{3}\ \rho\ \pi\ (\ r_2^2 - r_1^2\ )\ \Delta t$$

For the last segment, the energy was obtained by integrating the velocity profile over the cross sectional area that is,

$$dEnergy = \int_{r_1}^{r_2} 0.5\ U_{measured}^{3}\ \rho\ dA$$

$$= 3.73978*10^{-6}\ \pi\rho \left(\frac{U_{measured}}{0.63}\right)^{3}$$

These calculations were done using a BASIC computer program, and the results are shown in Figures 3.14 and 3.15. The theoretical jet velocities presented on these Figures were based on the velocity of the injection plate. Assuming there was no leak through the gap between the plate and the wall, $U_j$ is given by:

$$U_j = \frac{144\ U_{plate}}{\pi} = \frac{Volumetricflowrate}{\pi}$$

The theoretical volume of the jet was calculated by assuming that there was plug flow with a uniform velocity profile and the length of this plug was .142 m, i.e. Lm/Dm = 2.8 . The volume is given by:

$$Volume_{theoretical} = \left(\frac{Lm}{Dm}\right) \frac{\pi}{4}\ Dm^3 = 17.6\ in^3$$

The theoretical energy of the jet is calculated using:

$$E_{theoretical} = \frac{1}{2}\ \rho\ Volume_{theoretical}\ U_j^2$$

Figure 3.14 shows that the volume of the jet leaving the orifice was less than that of the theoretical prediction and it decreased as the theoretical jet velocity increased. In Figure 3.15, it is seen that the ratio of the energy of the jet based on empirical data to the theoretical energy of the jet, decreased as the theoretical jet velocity increased.

Fig 3.14 Comparison between meas. volume & ideal volume of the jet

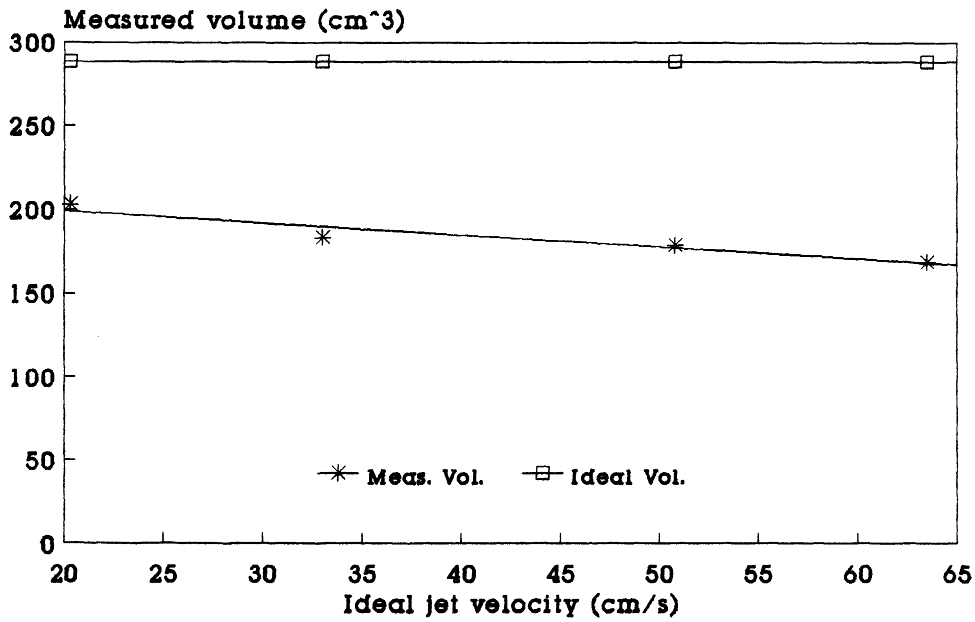


Measurements done at 1cm inside injection tube
Ideal vol. = 288 cm^3

Fig 3.15 Comparison between act. and measured jet energy

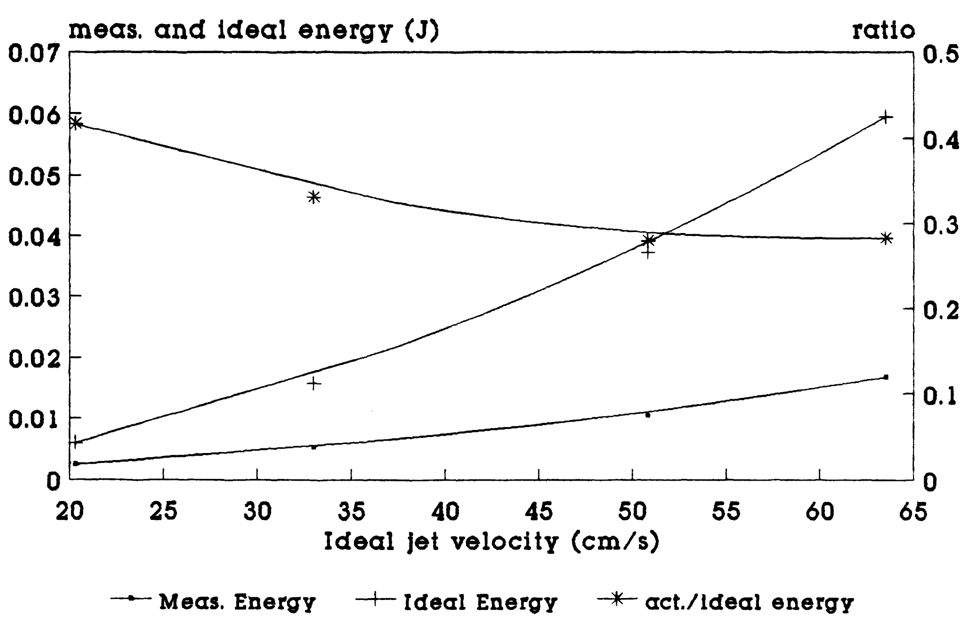


Measurements done at 1cm inside injection tube

This ratio ranged from 40% to 28% of the theoretical energy of the jet and was so low due to fluid leakage through the annular gaps around the injection plate. As shown in Table 3.5, the energy of the jet calculated from the average measured jet velocity was much closer to the value calculated based on the actual velocity profile of the jet. The tabulated results based on the data in Figure 3.15 and 3.16 are shown in Table 3.3.

| % Power | Duration of injection (sec) | Stroke Length (cm) | Theoretical Jet Velocity (cm/s) |
|---|---|---|---|
| 15 | .7100 | 0.3162 | 20.32 |
| 30 | .4285 | 0.3142 | 33.53 |
| 50 | .2944 | 0.3239 | 50.55 |
| 70 | .2300 | 0.3228 | 64.26 |

Table 3.3. Generation parameters during the formation of a vortex ring.

| % Power | Calc. Volume of jet (cm^3) | Plug Length Lm (cm) | Average Calc. jet vel. (cm/s) |
|---|---|---|---|
| 15 | 203.2 | 9.91 | 14.2 |
| 30 | 183.5 | 9.14 | 21.1 |
| 50 | 178.6 | 8.89 | 30.0 |
| 70 | 168.8 | 8.38 | 36.3 |

Table 3.4. Calculated velocity and volume of the jet from the hot film probe measurement where,
Plug length = Calc. Volume of jet / Area of orifice:
Averaged calculated jet velocity ($U_{javg}$) = Calc. Vol. of jet / ( Area of orifice * Duration of injection)

| % Power | Calc. Energy of jet (J) | $E_{jet}$ (J) | $E_{theo.\,jet}$ (J) |
|---|---|---|---|
| 15 | 0.0025 | 0.0021 | 0.0060 |
| 30 | 0.0052 | 0.0041 | 0.0157 |
| 50 | 0.0104 | 0.0080 | 0.0372 |
| 70 | 0.0168 | 0.0111 | 0.0595 |

Table 3.5. The energy content of the jet obtained using various method of calculation where, $E_{jet} = 0.5 * \rho * Volume_{measured} * U_{javg}^2$

The average velocity and the equivalent plug length of the jet that form a vortex ring are useful when investigating the behaviour of vortex rings penetrating stratified layers of fluids. This is because previous experimental results showed that the depth of penetration of a vortex ring into a stratified layer was a function of these two parameters. Latto (1987) suggested that optimum vortex rings should be generated with an Lm/Dm ratio of 2.8, that is a plug length of .142 m for a .0508m diameter orifice, however, the measured Lm/Dm ratios for these experiments only ranged from 2 to 1.7. Since the measured Lm/Dm ratio was less than the optimum value, in order to increase the Lm/Dm ratio to the optimum value, plastic flaps were installed onto the injection plate, as described in Chapter 2, to minimize the fluid leakage through the annular gap between the plate and the wall during the injection period. The following section describes the velocity measurements of the jet after the injection plate was modified and compares these results with the results obtained before the modification.

### 3.4.4 Velocity measurements of the jet after the modification to the injection plate:

In section 3.4.3, the data in Figure 3.14 indicated the volume of fluid that leaked through the gap during the injection period was fairly significant. The volume of fluid that went through the orifice was only 60% - 70% that of the theoretical volume of the jet. In order to minimize this leakage, plastic flaps were installed onto the upper surface and around the edge of the injection plate, see Figure 2.4. After this modification, hot film anemometry was used to obtain a new set of data on the jet velocity profile. These measurements were performed with the same theoretical Lm/Dm ratio as before and similar power level or theoretical jet velocity, with the probe at .010 m below the exit plane of the orifice. The results were compared with those obtained before the modification. The graphs for the velocity trace and the velocity profile of the jet obtained after the modification were shown in Figures 3.16 to 3.19. Finally, the volume and energy of the jet were calculated for this new setup.

Fig. 3.16 Vel. trace of jet and disp. of injection plate vs. time (modified)
15%power, Vjideal= 19.8 cm/s

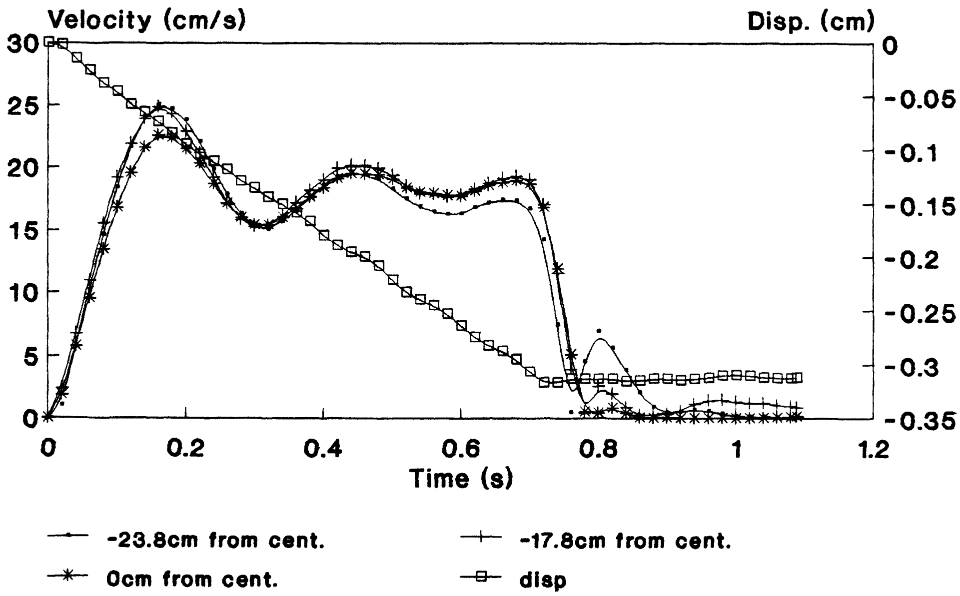


From: 15%p-i-s

Velocity prifile of jet vs. time
15% power (modified), L/D=2.8

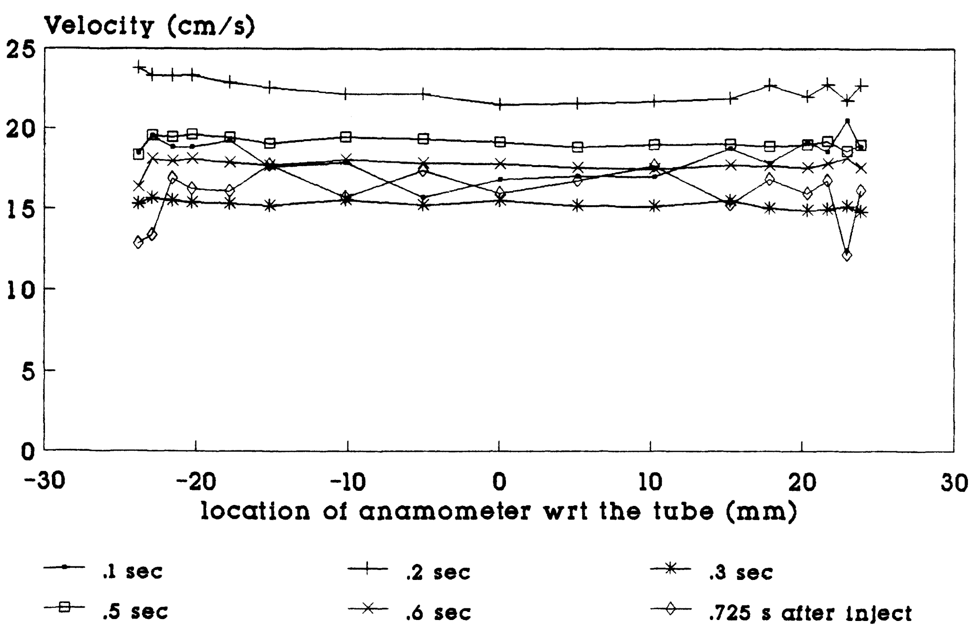

Fig 3.17 Vel. trace of jet and disp. of injection plate vs. time (modified)
30%power, Vjideal= 32.5 cm/s

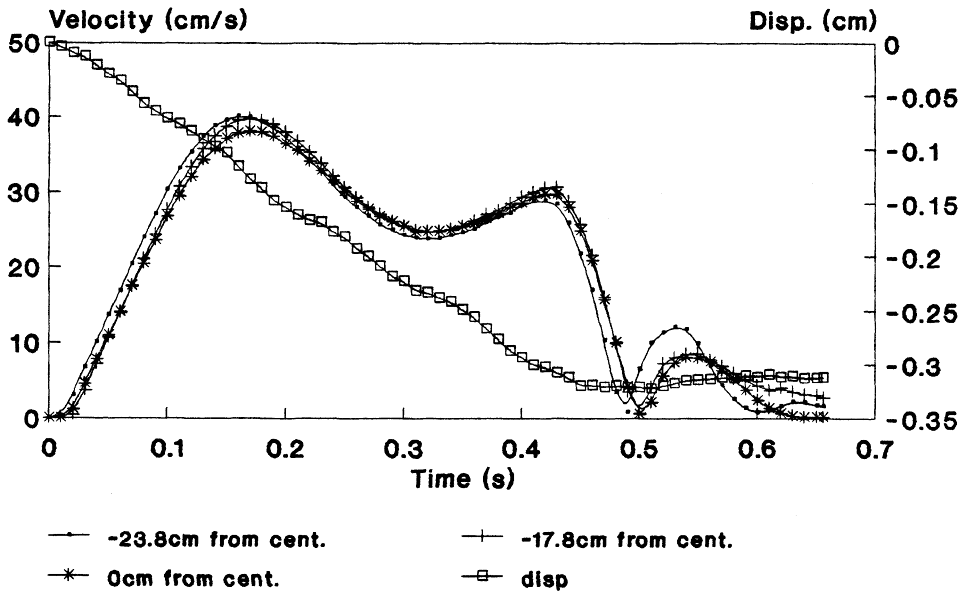


From: 30%p-i-s

Velocity profile of jet vs. time
30% power (modified), L/D=2.8

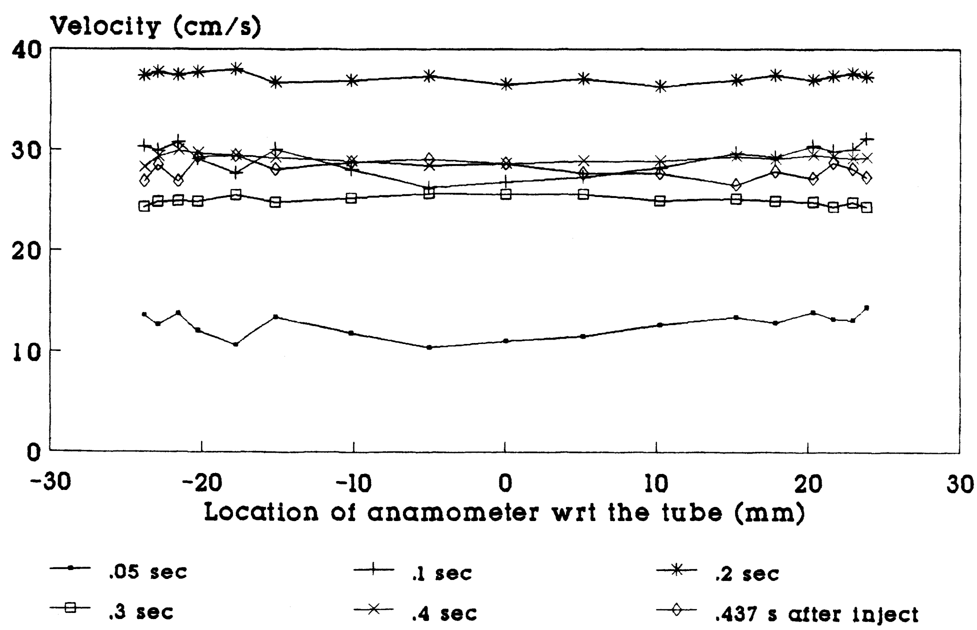

Fig. 3.18 Vel. profile of jet and disp. injection plate vs. time (modified)
50%power, Vjideal= 49.8 cm/s

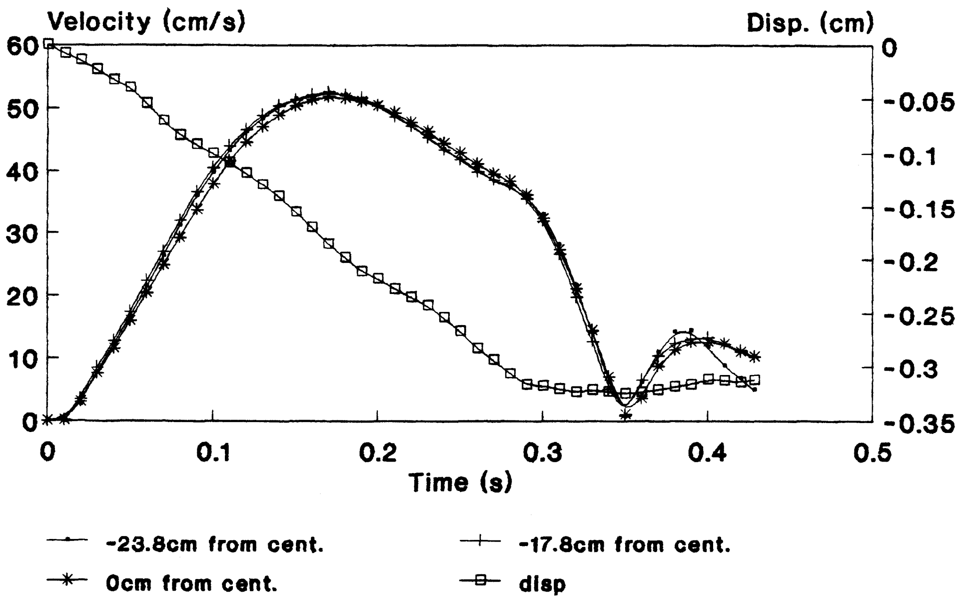


From: 50%p-i-s

Velocity profile of jet vs. time
50% power (modified), L/D=2.8

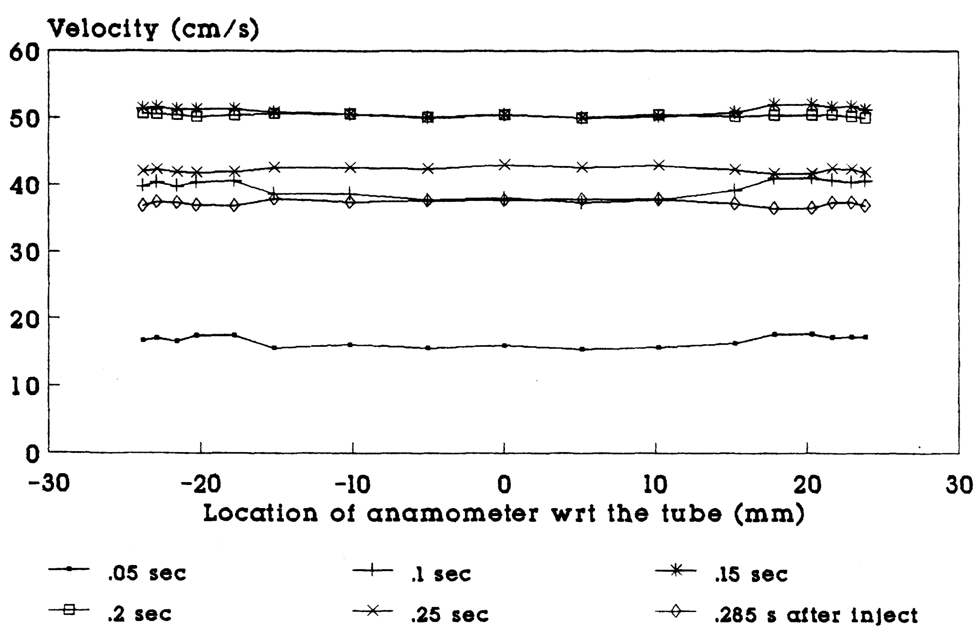

Fig 19 Vel. trace of jet and disp. of injection plate vs. time (modified)
70%power, Vjideal= 66.8 cm/s

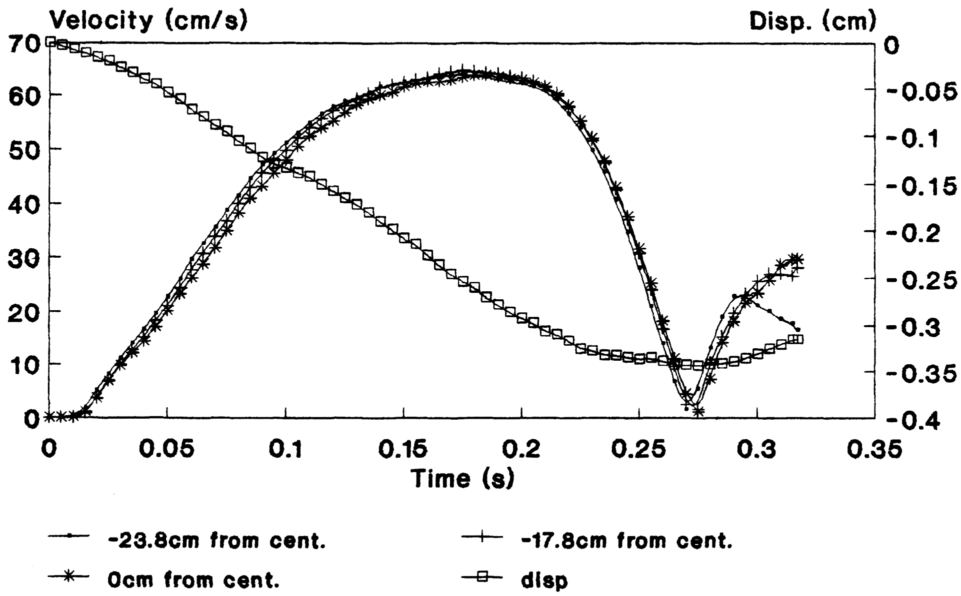


From: 70%p-i-s

Velocity profile of jet vs. time
70% power (modified), L/D=2.8

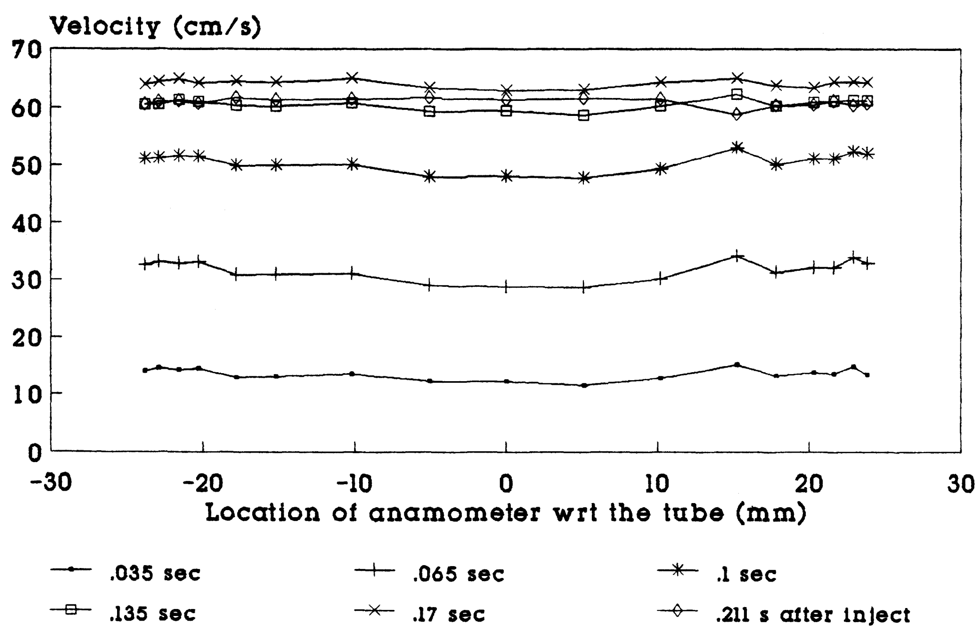

There was a large difference between the new velocity profiles of the jets during the injection period and those obtained before the modification, see Figures 3.10 to 3.13. At the very beginning of the injection period, the jet generated by the modified injection mechanism had a higher acceleration than the jet obtained with the original mechanism. This showed that the addition of the plastic flaps prevented most of the fluid from leaking out through the gap and resulted in a higher acceleration of the jet at the beginning of the injection period.

The other noticeable different was the maximum velocity attained by the jet during the injection period. After the modification to the plate, the jets with theoretical average jet velocities of .198, .325 and .498 m/s, attained a maximum jet velocity that was higher than the theoretical jet velocity except for the case where the average theoretical jet velocity was the highest, i.e. .668 m/s. This maximum velocity was obtained immediately after the acceleration period of the jet. This peak in the measured jet velocity may be caused by the time it took for the jet to decelerate and adjust itself to the average theoretical jet velocity. However before the modification, the maximum velocities of the jet in every case had a much lower value than the average theoretical jet velocities and the velocities did not reach a maximum value until the very end of the injection period.

After the equipment modification, at the end of the injection period the velocity of the jet decreased to zero and then it increased again to a much lower value than before. Flow visualization experiments at the exit of the orifice showed the formation of a second vortex ring with opposite vorticity to that of the primary ring. As this secondary ring rolled across the hot film probe, the probe accordingly responded. Since this hot film anemometer was not designed to measure velocity directions, any flow across the film surface will result in a response irrespective of its direction.

The formation of the secondary vortex ring could be caused by two factors. First, before the primary ring travelled away from the tube, the flow induced by the rotation motion of the primary ring separated at the inside edge of the orifice and a secondary ring with opposite vorticity was formed. This phenomena was also observed by Maxworthy (1977). A second factor could be the over shoot of the injection plate at the end of the injection period. The injection plate may have slightly bounced back to its original stop position, and a small volume of fluid would be sucked back into the orifice. As this ingested fluid separated at the edge of the orifice, a secondary vortex ring would also be formed.

Before the modification, flow visualization experiments showed the jet velocity did not decrease to zero at the end of the injection period. This could be caused by the inertia of the fluid above the plate moving through the annular gap and thereafter through the ejection tube, after the plate had stopped. Therefore, the velocity of the jet did not drop to zero after injection, which was not the case for the modified plate.

The same type of calculations as those used in section 5.3 were used to calculate the volume and energy in the jet. The results are given in Tables 3.6 to 3.8.

| % Power | Duration of injection (sec) | Stroke Length (cm) | Theoretical Jet Velocity (cm/s) |
|---|---|---|---|
| 15 | .7250 | .3147 | 19.8 |
| 30 | .4370 | .3109 | 32.5 |
| 50 | .2850 | .3091 | 49.8 |
| 70 | .2110 | .3078 | 66.8 |

Table 3.6. Generation parameters during the formation of a vortex ring.

| % Power | Calc. Volume of jet (cm^3) | Plug Length Lm (cm) | Average Calc. jet vel. (cm/s) |
|---|---|---|---|
| 15 | 280.2 | 13.72 | 19.1 |
| 30 | 255.6 | 12.70 | 29.0 |
| 50 | 224.5 | 11.18 | 41.4 |
| 70 | 196.6 | 9.65 | 48.5 |

Table 3.7. Calculated velocity and volume of the jet from the hot film probe measurement.

Flow visualization experiments showed that for the ring formed with the longest plug length i.e. 0.137 m, Lm/Dm = 2.7, a secondary ring with the same sign of vorticity was formed immediately after the primary ring during the injection period. This ring was eventually sucked into the primary ring and destroyed. This phenomenon was not observed for rings generated with a shorter plug length. Since the effect of this phenomenon on the traverse of a vortex ring is unknown, the optimum Lm/Dm ratio for a tube type vortex ring generator should be reevaluated for the design of tube type vortex ring mixers.

| % Power | Calc. Energy of jet (J) | $E_{jet}$ (J) | $E_{theo.\ jet}$ (J) |
|---|---|---|---|
| 15 | 0.0065 | 0.0051 | 0.0057 |
| 30 | 0.0153 | 0.0107 | 0.0152 |
| 50 | 0.0271 | 0.0192 | 0.0355 |
| 70 | 0.0370 | 0.0231 | 0.0640 |

Table 3.8. The energy content of the jet obtained using various method of calculation.

From Table 3.7 and 3.8, it can be seen that the average measured velocity, volume and energy of the jet after the injection plate modification was much closer to the theoretical value than those values obtained with the original injection mechanism. This meant the modification had successfully minimized the leakage through the gap during the injection. However, Figures 3.20 and 3.21 showed that although the addition of plastic flaps minimized the leakage through the gap, the measured volume and the ratio between the measured energy and the theoretical energy of the jet still decreased as the theoretical jet velocity increased. Therefore, the addition of the plastic flaps was not able to stop the leakage completely.

Fig 3.20 Comparison between meas. and theoretical volume of the jet(modified)

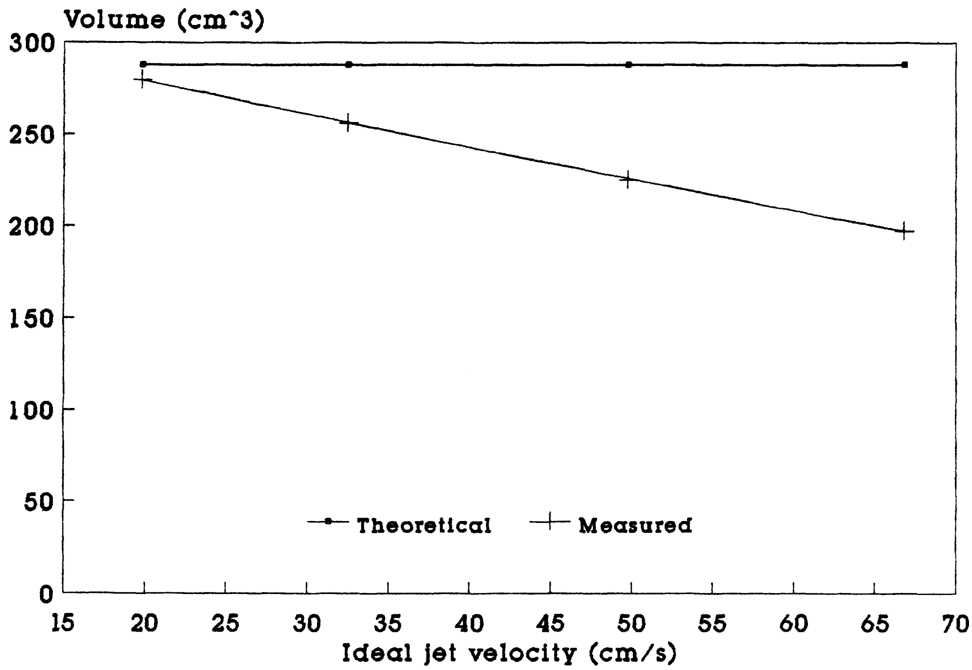


Theoretical jet vol. = 288 cm^3

Fig. 3.21 Comparison between meas. and theoretical energy of the jet(modified)

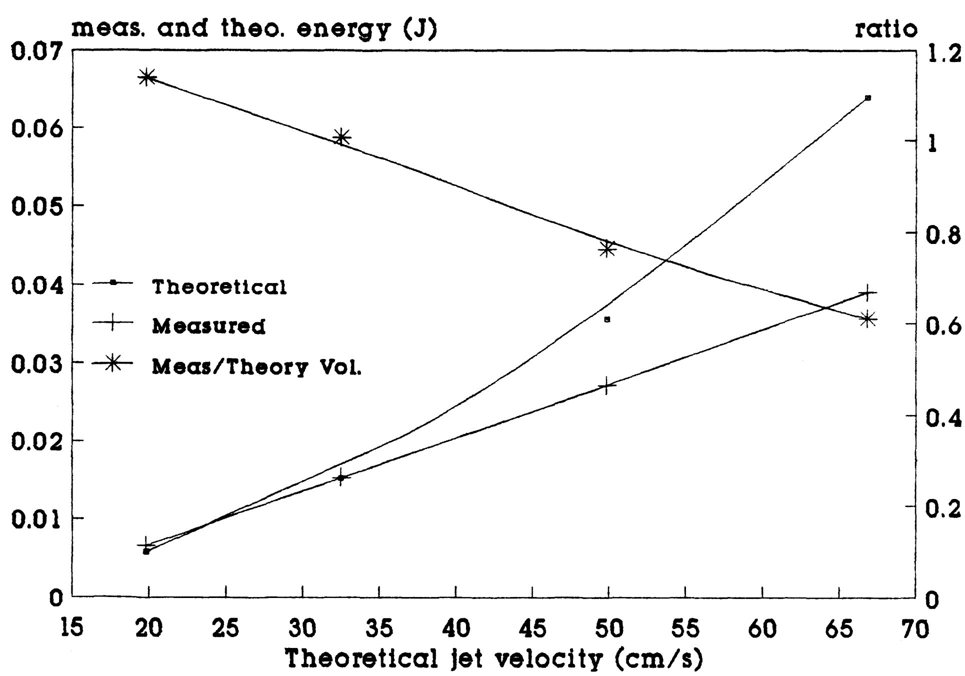

3.4.5 Correlations relating the measured volume of the jet and averaged jet velocity to the theoretical jet velocity:

For the injection mechanism without modification, the measured volume of the jet or the ratio between the plug length of the jet to the diameter of the injection tube is related to the theoretical jet velocity by:

$$\frac{Lm}{Rm} = 4.10744 - 0.0320744\, U_j \tag{3.1}$$

and the relation between the theoretical jet velocity and the averaged measured jet velocity is:

$$U_{javg.} = 1.61126 + 0.505345\, U_j \tag{3.2}$$

For the injection mechanism with the modification to minimize the leakage through the gaps during the injection, the measured Lm/Rm ratio is related to the theoretical jet velocity by:

$$\frac{Lm}{Rm} = 6.09321 - 0.0868094\, U_j \tag{3.3}$$

and the relation between the theoretical jet velocity and the averaged measured jet velocity is:

$$U_{javg.} = -0.686383 + 1.1572\, U_j - 0.0153077\, U_j^2 \tag{3.4}$$

These correlations are also given in Figures 3.22 and 3.23.

N.B. These relationships only apply to the injection mechanism tested in this report. $U_j$ and $U_{javg}$ are in inches per second.

Figure 3.22 L and Vjmeas. vs Vjtheo.
L = 4.10744 - 0.0320744 * Vjtheo.
Vjavg. = 1.61126 + 0.505345 * Vjtheo.

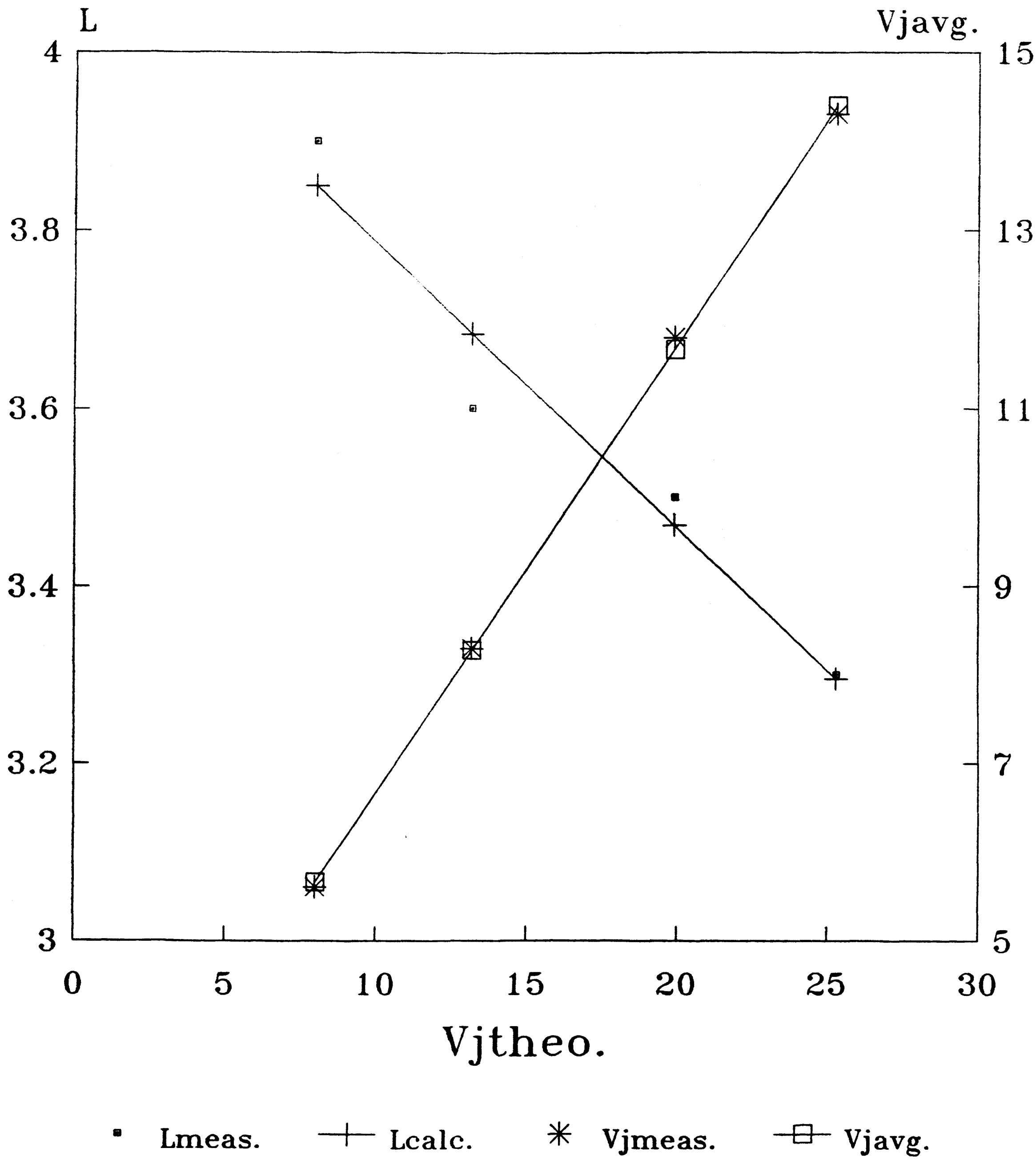

Figure 3.23 L and Vjmeas. vs Vjtheo.
L = 6.09321 - 0.0868094 * Vjtheo.
Vjavg.= -.686+1.16*Vjtheo.-.015*Vjtheo^2

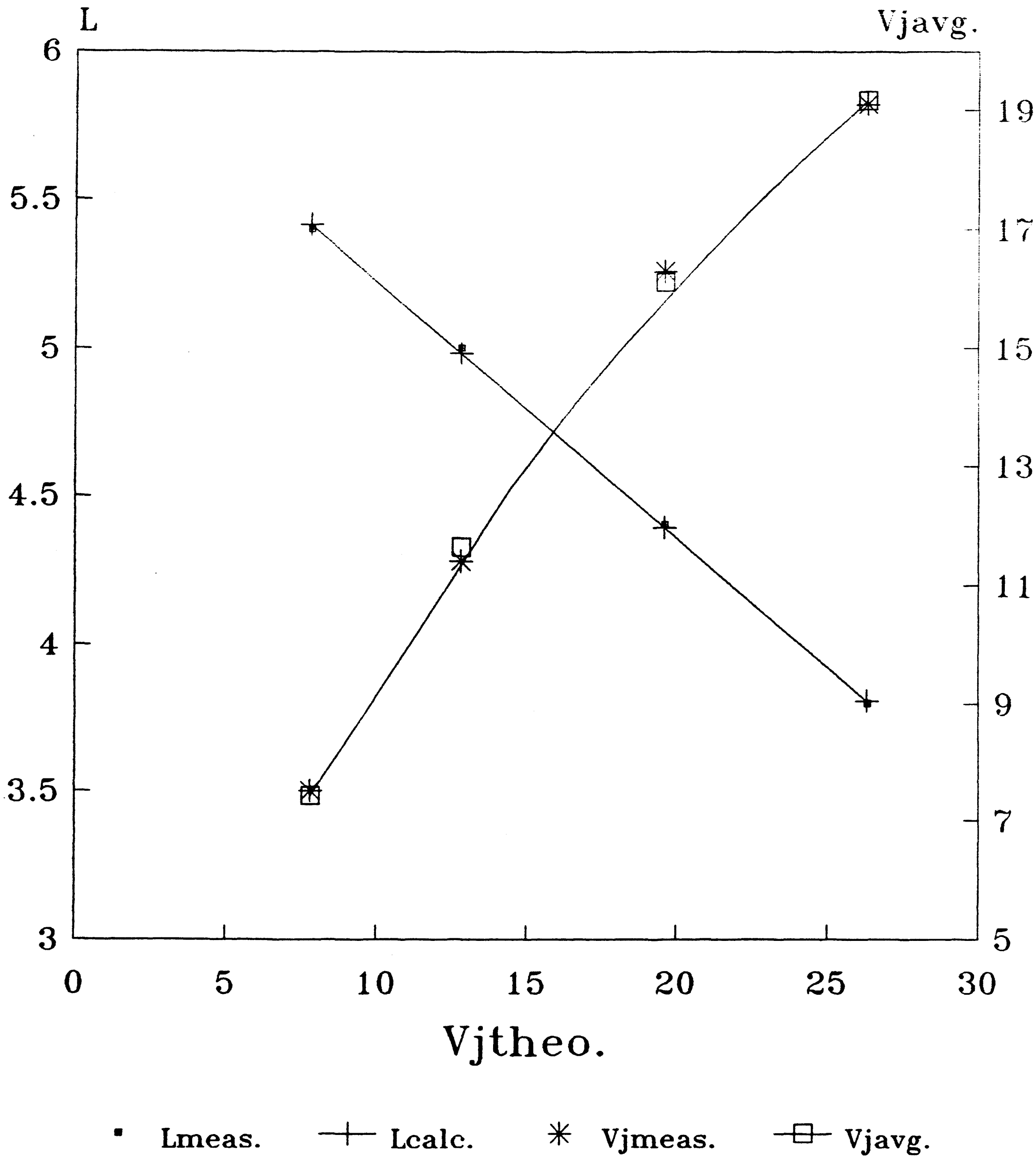

3.5 Conclusion:

The above discussion on the measurements of the volume of the jet and average jet velocity showed that as the theoretical jet velocity increased, the leakage of fluid through the gap increased. This decreased the average measured velocity and volume of the jet leaving the orifice. Hence the plug length of the jet was still shorter than the actual generation value of 0.142 m, Lm/Dm =2.8, even after the plate modification. The leakage through the gap could be further minimized by installing more plastic flaps on the under side of the injection plate. However this modification was not suitable for this experimental setup because it would create large amount of friction between the plastic flaps and the wall of the tank. As the injection began, the water that would ordinarily have leaked through the gap would be held back and the pressure exerted by this water would push the plastic flaps harder against the wall of the tank, and would have restricted the movement of the plate. Also, with no water leaking through the gap, there was nothing to prevent the plate from rubbing against the wall of the tank. This may have caused vibration while the plate is moving down and may have affected the generation of a vortex ring.

Therefore, with no further modification to prevent the leakage of water from the bottom of the injection plate during the injection period, the following empirical correlations between Lm and $U_j$ were used

$$\frac{Lm}{Rm} = 6.09321 - 0.0868094\, U_j$$

and the relation between the $U_{jtheo}$ and the $U_{javg}$ is:

$$U_{javg.} = -0.686383 + 1.1572\, U_j - 0.0153077\, U_j^2$$

# Chapter 4

# A Study of the Effects on a Vortex Ring after it has Penetrated into a Stratified Layer

## 4.1 Introduction:

In this chapter, the study on vortex ring travelling in two layers of stratified fluid having different densities is discussed. The research included a flow visualization study on the mixing caused by a vortex ring as it travels vertically in a tank of stratified fluid. An empirical correlation between the maximum penetration depth of a vortex ring into a stratified layer, the density gradient between the two layers of fluid and the initial energy in the ring, was obtained. As a result of this study, it was clearly shown why vortex ring mixers are so effective for the destratification of fluids and what kind of vortex ring should be generated for different mixing and destratification applications.

## 4.2 Literature Review:

Only studies on vortex rings that travel perpendicular to the stratified layer are reviewed as being pertinent to the present study. These studies can be divided into two types: 1) vortex rings penetrating a stratified layer having a sharp change in density gradient, and 2) vortex rings penetrating a stratified layer having a linear change in density gradient. In most of these studies, the stratified layers were water and an aqueous brine solution.

Linden (1973) was one of the first to address the problem of vortex rings penetrating into a stratified layer having a sharp change in density gradient. He studied vortex rings that could barely penetrate the stratified layer. As the ring reached the interface between the two layers of fluid, it began to recoil and collapse. Eventually the ring fell back into the layer of fluid where the ring was generated. As the ring fell back, fluid from the other fluid layer was sucked into the ring due to the inertia of the ring and mixed with the fluid in the ring.

Hecht et al (1980), Honji et al (1976) and Maxworthy (1977) studied the effects of vortex rings that penetrated through the interface of a stratified layer. Both Honji et al (1976) and Maxworthy (1977) used a stratified layer with a linear change in density gradient. Honji et al (1976) observed that after a ring penetrated into the stratified layer, it began to elongate and slow down. Eventually it fell back into the layer of fluid where it was generated. Maxworthy (1977) had similar observations on the slowing down of the ring after it penetrated through a stratified layer. Moreover, he observed that the shape of the ring remained relatively constant at the initial stage of penetration. The shape of the ring and the core began to distort only after the vortex ring had travelled far into the stratified layer. Maxworthy (1977) explained that the slow down of the ring was related to the production of baroclinic vorticity, due to the density gradient between the fluid in the core and the surrounding fluid, which cancelled the vorticity inside the core of the ring. He also observed a strong jet of fluid, caused by the rejection of the negative vorticity produced in the ring, in the opposite direction to the ring motion. Hecht et al (1980) developed an axisymetric wake computer code to simulate the penetration of a ring into the stratified layer. With their program, they were able to predict the slow down and decrease in size of the ring. Their prediction agreed very well with their experimental data for a ring that was travelling in a stratified layer with a linear change in density gradient. However, their prediction for the case with sharp change in density gradient was not as accurate as that for a linear density change.

So far, all the studies mentioned dealt with a single vortex ring penetrating through a stratified layer and the vortex ring experienced decrease in size and velocity after it penetrated into the stratified layer. Then, Baird et al (1979) attempted to use vortex rings, fired at a 20 seconds time interval, as a means for mixing a tank of fluid containing a stratified layer of brine and water with a sharp change in density gradient. Through these experiments, he determined the mixing efficiency $\epsilon$ of the rings was 9% - 30% depending on the density gradient and the initial properties of the ring. The equation for the mixing efficiency was given as:

$$\epsilon = \frac{\textit{theoretical minimum energy required}}{\textit{energy actually required}}$$

where the minimum theoretical energy was equal to the increase in potential energy during the mixing process. The mixing efficiency was plotted against the Froude number Fr and is illustrated in Figure 4.1. The Fr was defined as,

$$Fr = \frac{\textit{Initial energy in a ring}}{\textit{Work required to move the ring in the stratified layer}}$$
$$= \frac{E_v}{2\ \Delta V\ g\ \phi H\ (\rho_d - \rho_l)}$$

where,

$E_v$ - kinetic energy of the ring which is equal to kinetic energy in the jet,

$\Delta V$ - Volume of the jet,

$\Phi H$ - Distance travelled, and

$\rho_d$, $\rho_l$ - density of denser and lighter fluid.

This showed vortex ring mixing was much more energy efficient

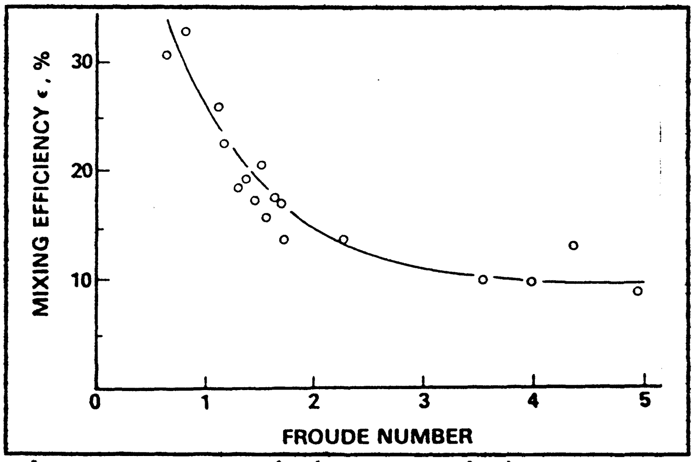


Figure 4.1 Mixing efficiency vs. Froude number (Fr). Baird(1979)

than the impeller mixers which have an energy efficiency in the range of 0.6% - 1.1%. Therefore, the use of vortex rings have a lot of potential for improvements in various mixing processes. It can be seen from Figure 4.1, as the Fr increased the mixing efficiency decreased, Baird et al (1979) attributed the decrease in efficiency to vortex rings hitting the bottom of the vessel. As the ring hit the bottom of the vessel, the energy in the ring was dissipated and wasted. Shortly afterwards, Latto (1987) independently developed the idea of using vortex rings for mixing and developed a series of novel vortex ring mixers. His initial primary interest was in the destratification and mixing of slaked lime slurries. These experiments were later extended to the mixing of stratified layers consists of hot and cold water using his vortex ring mixers. Once again, it showed the great efficiency of vortex rings mixing. Another advantage of the vortex ring mixers observed by Latto (1989) was, they are able to create extensive mixing throughout a vessel immediately after a mixer is started and a homogeneous mixture can be obtained in a short period of time. This is particularly useful when chemical reactions are taking place and a uniform mixture is required.

## 4.3 Experimental Procedure:

In these experiments, all the runs were performed in the tank described in Chapter 2. A vortex ring was generated near the bottom of the tank and it travelled towards the top through an interface of a stratified layer. Two types of stratified layers were used. They were: 1) hot/cold water and 2) brine (of various densities)/water stratified layers. In order to visualize the location and the size of the ring, red dye was injected into the generating jet, and therefore into the vortex ring, as a tracer to the path of the fluid ejected during the formation of the ring. Another method to visualize vortex rings travelling in a stratified layer was to mix red dye into one layer of the stratified fluid while leaving the other layer colourless. This method allowed the observation of the interaction between the two layers of stratified fluid, as the vortex ring was travelling through the liquids. All the tests were recorded using a video camera and then analyzed using a digital video frame grabber.

### 4.3.1 Dimensional analysis of important variables:

A dimensionless analysis using the Buckingham Pi theorem was performed to assess nondimensional parameters that are of importance. This permitted a reduction of the number of parameters that have to be varied during the experiments. These variables are:

$\rho_1$ - density of solution where the ring was generated;

Lm - theoretical plug length of the fluid injected;

Rm - radius of the injection orifice;

$U_{javg}$ - average jet velocity;

$\mu$ - viscosity of the fluid;

$g\Delta\rho$ - buoyancy force on the ring due to the density gradient between the two fluids of the stratified layer;

Xm - maximum penetration depth;

Li - distance of the orifice from the opening of the orifice; and

$X_{wall}$ - distance of walls of the tank from the centre of the orifice.

Since there were 9 variables and 3 basic units, there would be 6 different Pi groups. The three basic parameters chosen were:

$$\mu\ ,\ V_j\ ,\ Rm$$

After performing the analysis, the resulting Pi groups obtained were:

$$\frac{Xm}{Rm} = f\left(\frac{\rho_1 Vj\, Rm}{\mu}\ ,\ \frac{Rm^2 g\Delta\rho}{\mu\, Vj}\ ,\ \frac{Lm}{Rm}\ ,\ \frac{Li}{Rm}\ ,\ \frac{X_{wall}}{Rm}\right)$$

by dividing the second term by the first term in the equation above, two of the pi groups were combined together to form the Richardson number (Ri) i.e.:

$$Ri = \frac{g\Delta\rho\, Rm}{\rho_1 Vj^2}$$

This is the ratio between the potential energy accumulated in the fluid in the ring and the initial kinetic energy originally present in the ring and is in fact the inverse of the Froude number Fr. By introducing this dimensionless group, the viscosity of the fluid was eliminated. This meant the relationship obtained through these experiments should be applicable to any fluid and is independent of the viscosity of these fluids. By the use of non dimensional groups, the number of parameters that had to be varied in the experiments was reduced. The effects on the maximum penetration depth of a vortex ring into a stratified layer, due to the variation of the parameters on the right hand side of the above equation were studied in the experiments described in this chapter.

Before describing the experimental results, flow visualization experiments on vortex rings penetrating a stratified layer were used to help explain why vortex rings were so efficient as a mixing process, especially for the destratification of stratified fluid.

## 4.4 Flow visualization studies on vortex rings travelling in a stratified fluid:

In order to understand what happens along the path of a vortex ring when it is travelling in a stratified fluid, flow visualization experiments were performed. The history of a ring travelling in a stratified layer can be divided into three phases: 1) the generation phase; 2) the traverse phase where a ring travels in a body of fluid that has the same density as the fluid in the ring; and 3) the penetration and decay phase when a ring has penetrated through the interface and travels in a fluid that has a density different with the fluid in the ring. In Figures 4.6, 4.8, 4.12, 4.13, 4.14 the location where the picture was taken correspond to the window showed in Figure 4.2a. Similarily, in Figures 4.9, 4.10, 4.11 the location where the picture was taken correspond to the window showed in Figure 4.2b.

### 4.4.1 Generation phase of a vortex ring:

As Maxworthy (1977) observed, a vortex ring is generated by the separation and the roll up of a pulsating jet at the exit of an orifice. Figure 4.3 a-h shows the trace of streaks of red dye used to indicate the roll up of the jet and rotation of the fluid during the generation of a vortex ring. If the plug length (Lm), or the duration, of the jet is too long, a secondary ring with vorticity of the same sign will form as shown in Figures 4.3b and c. Due to the proximity of this secondary ring to the

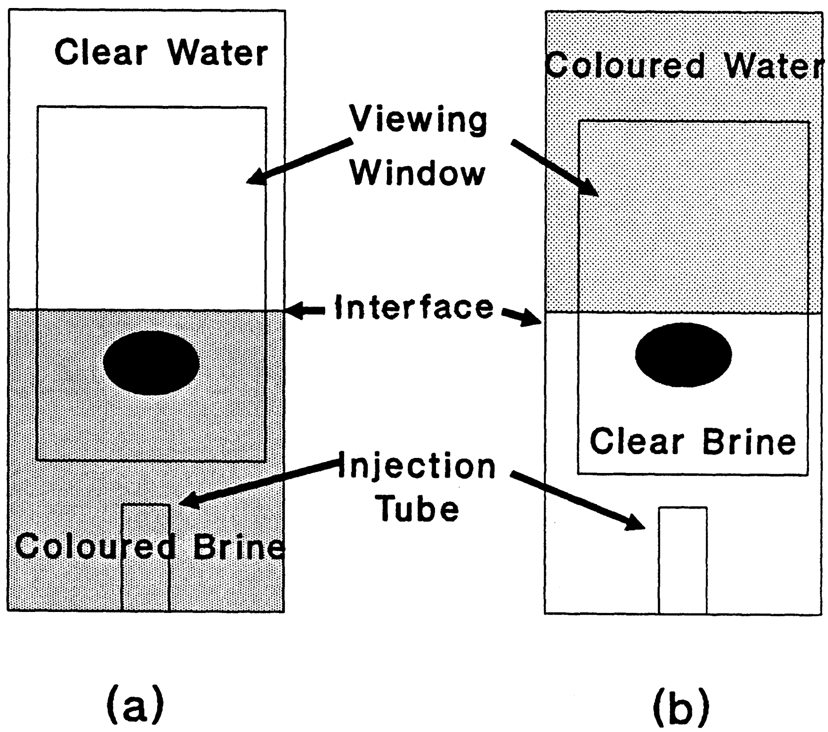


Figure 4.2 The locations of the windows correspond to the location on the tank where the pictures are taken. a) correspond to Figures 4.6, 4.8, 4.12, 4.13, 4.14; b) cprresponds to Figures 4.9, 4.10, 4.11.

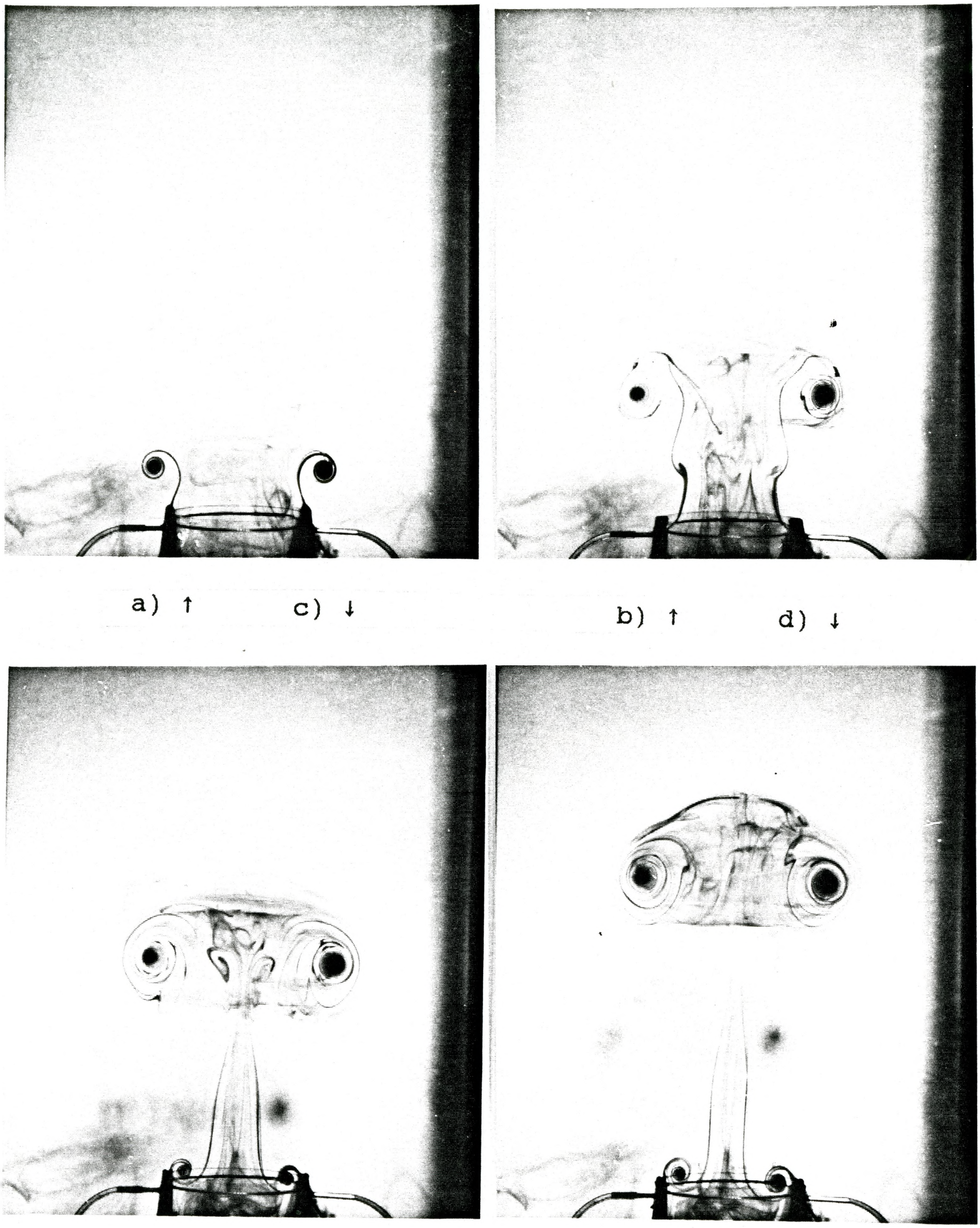


Figure 4.3 Continue on page 90.

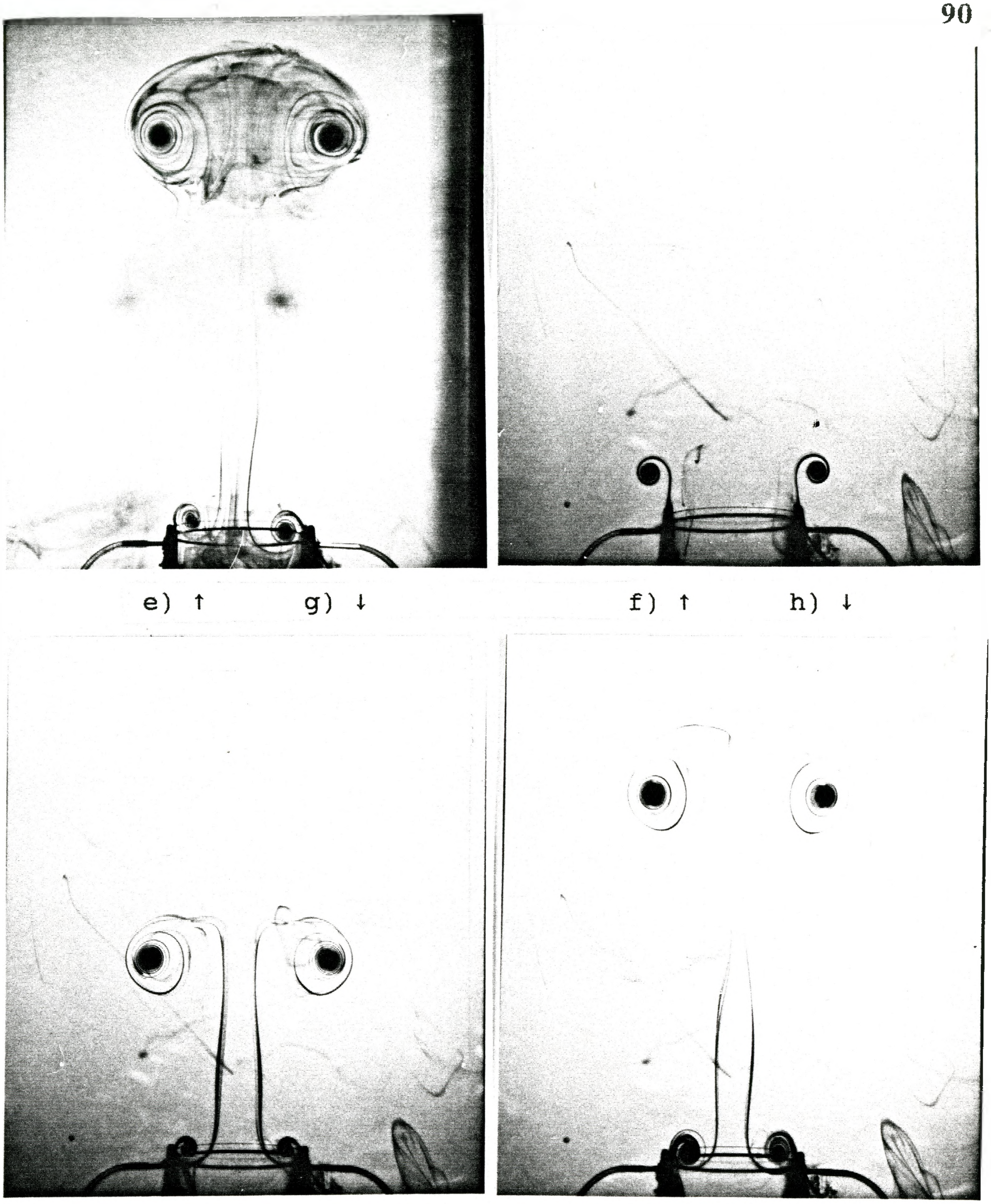


Figure 4.3 The generation of a vortex ring due to the separation of a jet at the exit of the orifice. (a-e) As the plug length of the jet becomes too long, ($Lm \geq 0.145$) a secondary ring was formed and sucked into the primary ring. (f-g) As Lm decreases ($Lm \approx 0.112$) the secondary ring disappear. (c-e, g-h) The flow induced by the ring separated at the edge of the tube which formed another ring at the opening of the tube.

primary ring, it is sucked into the primary ring and combined into one vortex ring. At the same time, before the ring leaves the orifice, the fluid flow induced by the rotational motion of the ring separates at the inside edge of the orifice. This results in the formation of a secondary vortex ring with vorticity of opposite sign to that of the primary ring as shown in Figures 4.3 c-e, g-h. This ring separates from the orifice and travels towards the bottom of the tank if it accumulates enough vorticity. This phenomena was also observed by Maxworthy (1977) as shown in Figure 4.4; two vortex rings were formed by one pulsating jet, which is especially true for orifice plate type generators where the motion of the secondary vortex ring is not obstructed by the wall as in the case of a tube type generator. However, orifice type generators were not tested in Maxworthy's (1977) study.

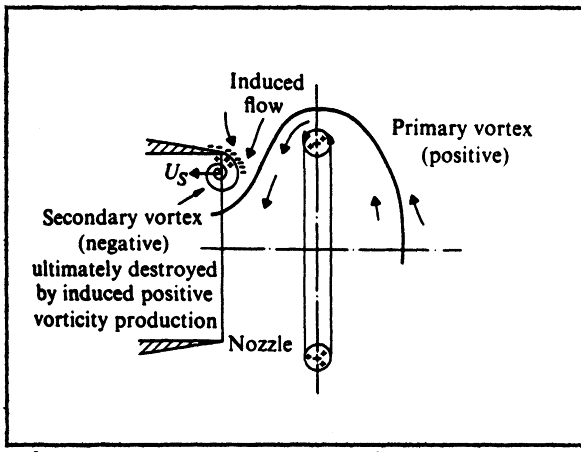


**Figure 4.4** Formation of the secondary vortex ring at the orifice. Maxworthy(1977)

4.4.2 Traverse phase of a vortex ring:

After a vortex ring is fully formed, it begins to travel away from the generating orifice. The interface of the stratified layer is still a few ring diameters away from the ring and it is travelling in a fluid having the same density as the fluid in the ring. Under this condition, the ring is travelling at virtually constant velocity and the wake behind it is very small, as shown in Figure 4.5. Very little mixing occurs between the surrounding and the fluid in the ring for this case.

<u>4.4.3 Penetration and decay phase of a vortex ring:</u>

As seen in Figure 4.6, when a ring containing brine approaches the interface, it pushes the layer of lighter fluid (water) that is close to the interface, around the surface of the ring and into the brine layer. Then, depending on the Richardson number (Ri) for the ring, the ring may or may not be able to penetrate through the interface and travel into the layer of water. For high Ri, the buoyancy force acting on the ring becomes so large that it prevents the ring from penetrating the

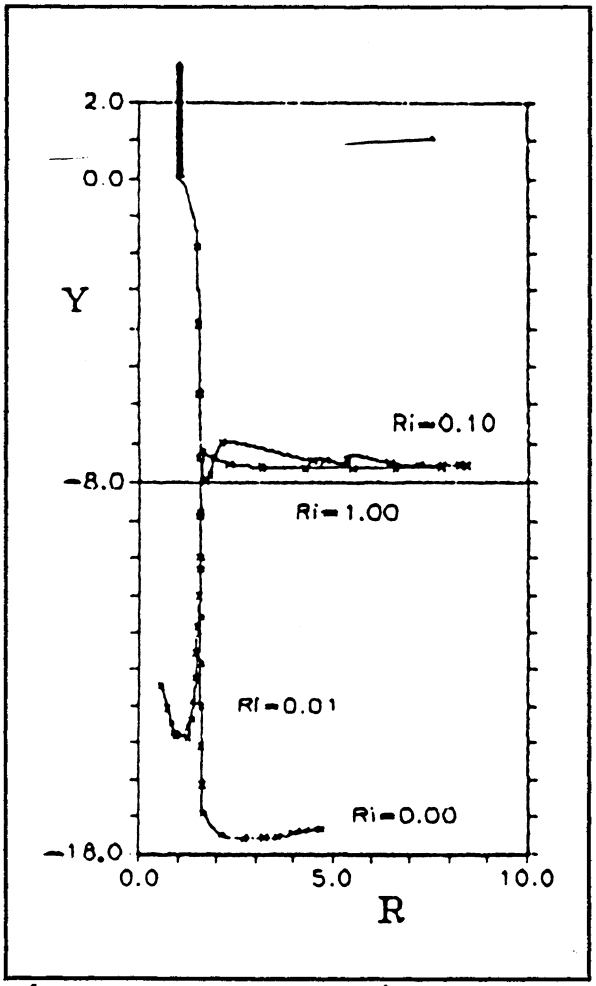


Figure 4.7 Penetration depth Y vs. Ri. R is the radius of the core of the ring. Latto (1988)

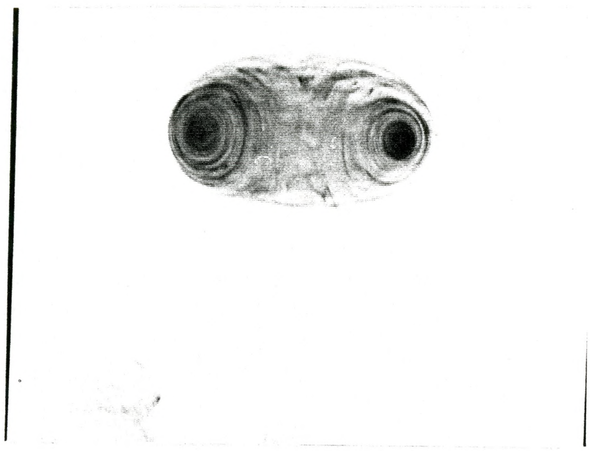

a) ↑

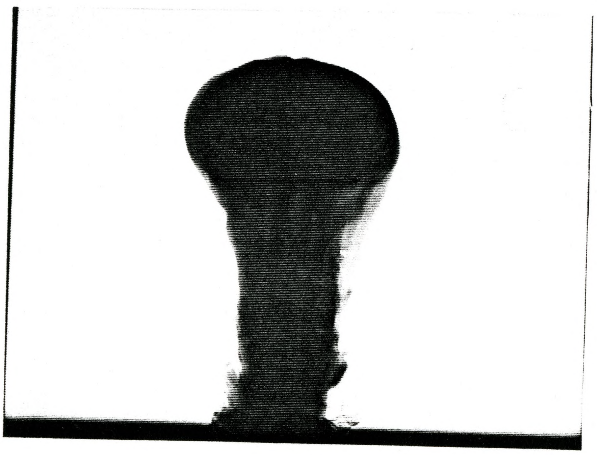

b) ↑

Figure 4.5 The wake of the ring (a) travelling in a fluid with a uniform density is smaller than the ring (b) that is travelling in a stratified fluid.

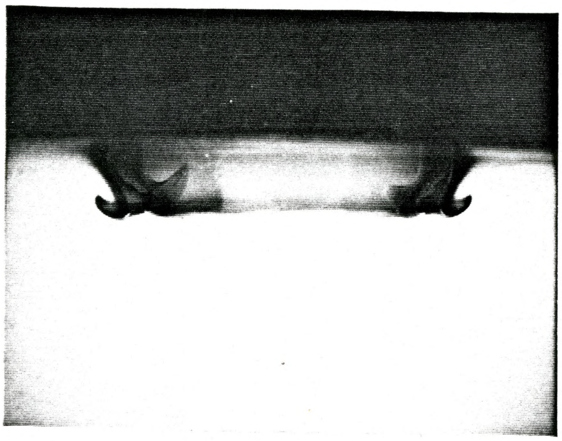

a) ↑

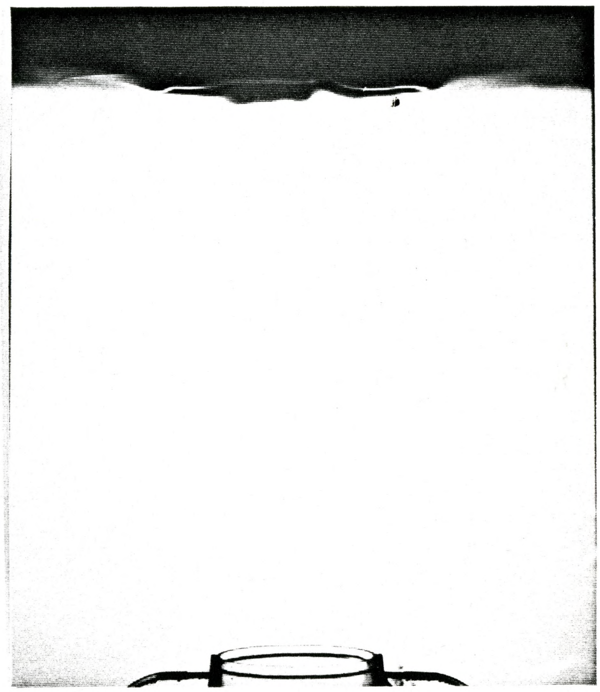

b) ↑

Figure 4.6 Water being pushed into the brine layer as the ring reaches the interface a) Ri = 0.27; b) Ri = 0.10.

interface. As Ri was decreased, the depth of penetration increased, as showed by Latto (1988), see Figure 4.7. Theoretically when Ri = 0, that is when there is no density gradient in the fluid, a ring is capable of travelling an infinite distance. However, due to the transition of a ring from a laminar to a turbulent condition and considering the viscosity of a fluid plays a role, the distance travelled by a ring in a viscous fluid will be finite; and approximately 200 times the orifice diameter, as observed by Baird et al (1979).

4.4.3.1 Rings with large Ri:

For Ri > 0.1, a ring is only capable of penetrating a very short distance into the upper stratified water layer, after which it falls back into the brine layer. Figure 4.8 shows that under these conditions, a vortex ring does not produce very much mixing in the water layer, except for some large amplitude surface waves at the interface after a ring fell back into the brine layer, which aids in the mass transfer between the two layers. Most of the mixing occurs in the brine layer where a small volume of water is sucked into the brine layer as a ring falls back into the brine layer. Similar observations were also reported by Linden (1973). After a ring fell back into the brine layer, it began to roll across the lower surface of the interface and disintegrate into small eddies, see Figure 4.9. This process mixed the entrained water

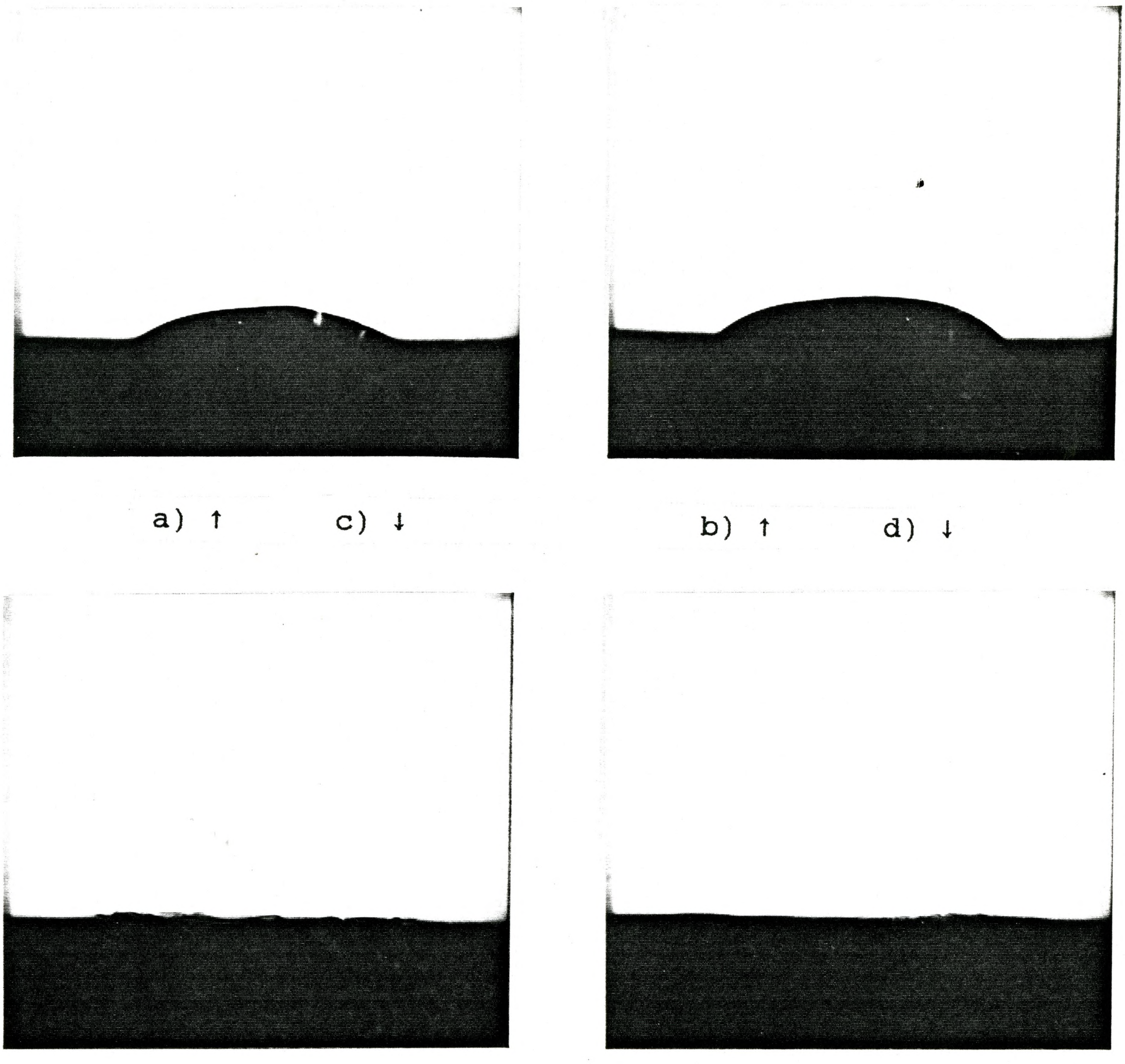


Figure 4.8 A sequence of picture showing a dyed brine ring travelling into the water layer. The ring was not able to penetrate the interface of the stratified layer. Ri = 0.27.

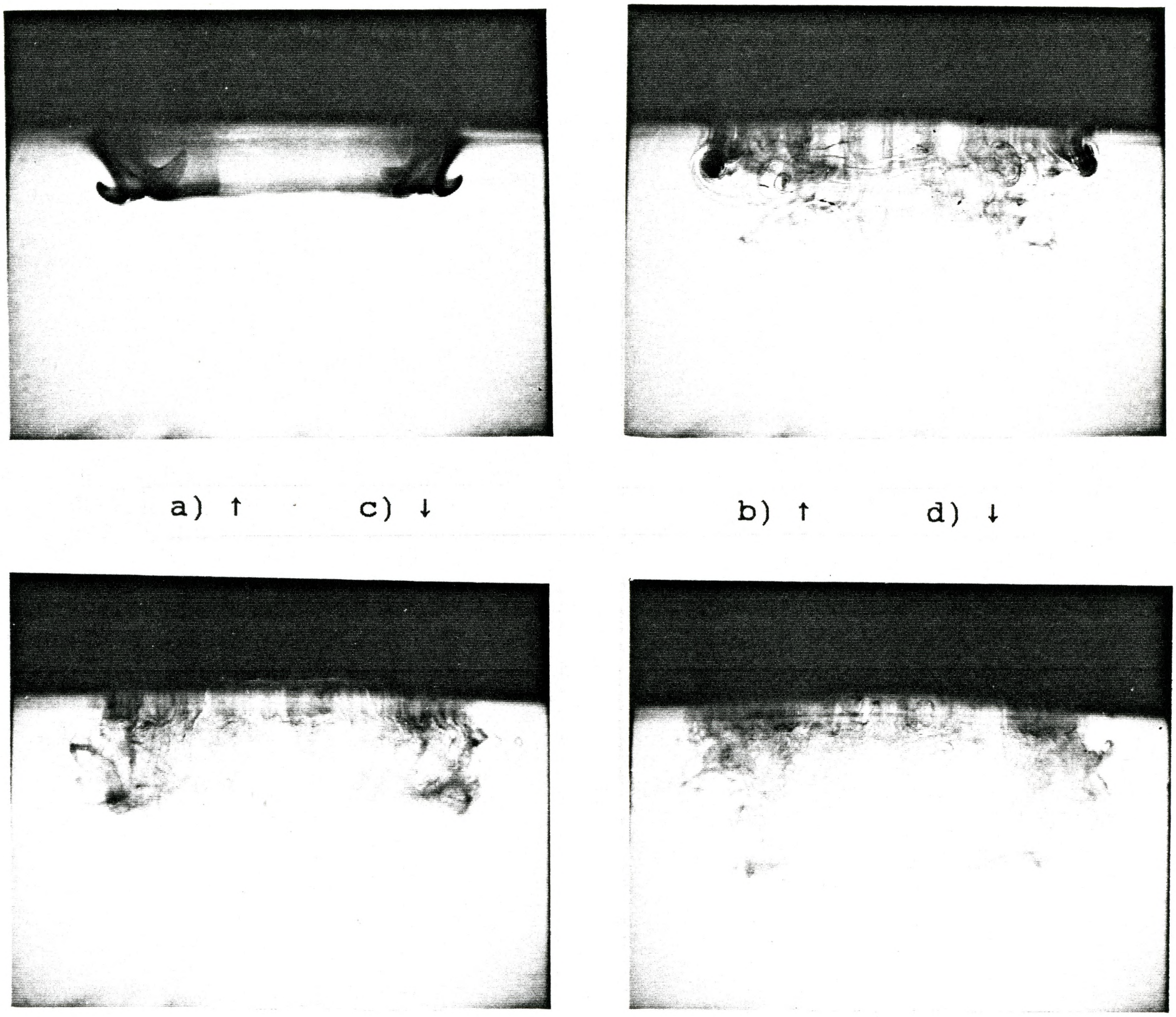


Figure 4.9 As the ring approaches the interface, it pushes some of the water into the brine layer and disperses it across the bottom of the interface. Ri = 0.27.

with the brine around the interface and hence reduced the density gradient between the fluid around the interface. Even under this adverse condition, a vortex ring is still capable of agitating the interface of a stratified layer, even though slowly. Vortex rings generated with a Ri $\approx$ 0.1, will appear to be good for processes like liquid-liquid extraction, since the rolling motion of the ring across the interface will improve the rate of mass transfer between the two fluids and will not mix the two fluids together quickly.

#### 4.4.3.2 Rings with small Ri:

For Richardson number between, $0 \leq Ri \leq 0.1$, a ring is capable of penetrating through the interface and travels into the water layer. While a ring is travelling in the water layer, it entrains water from its surrounding. This is visualized by the coloured wake that fell back into the brine layer, as shown in Figures 4.10 and 4.11. At the same time a portion of the fluid inside the ring is detrained into the wake of the ring, see Figures 4.12, 4.13 and 4.14, due to the production of baroclinic vorticity inside the ring, as described by Maxworthy (1977). This reduces the vorticity inside the core of a ring. As the vorticity inside a ring decreases, it is no longer capable of keeping the same volume of fluid, therefore part of the fluid inside the ring has to be discharged into the wake.

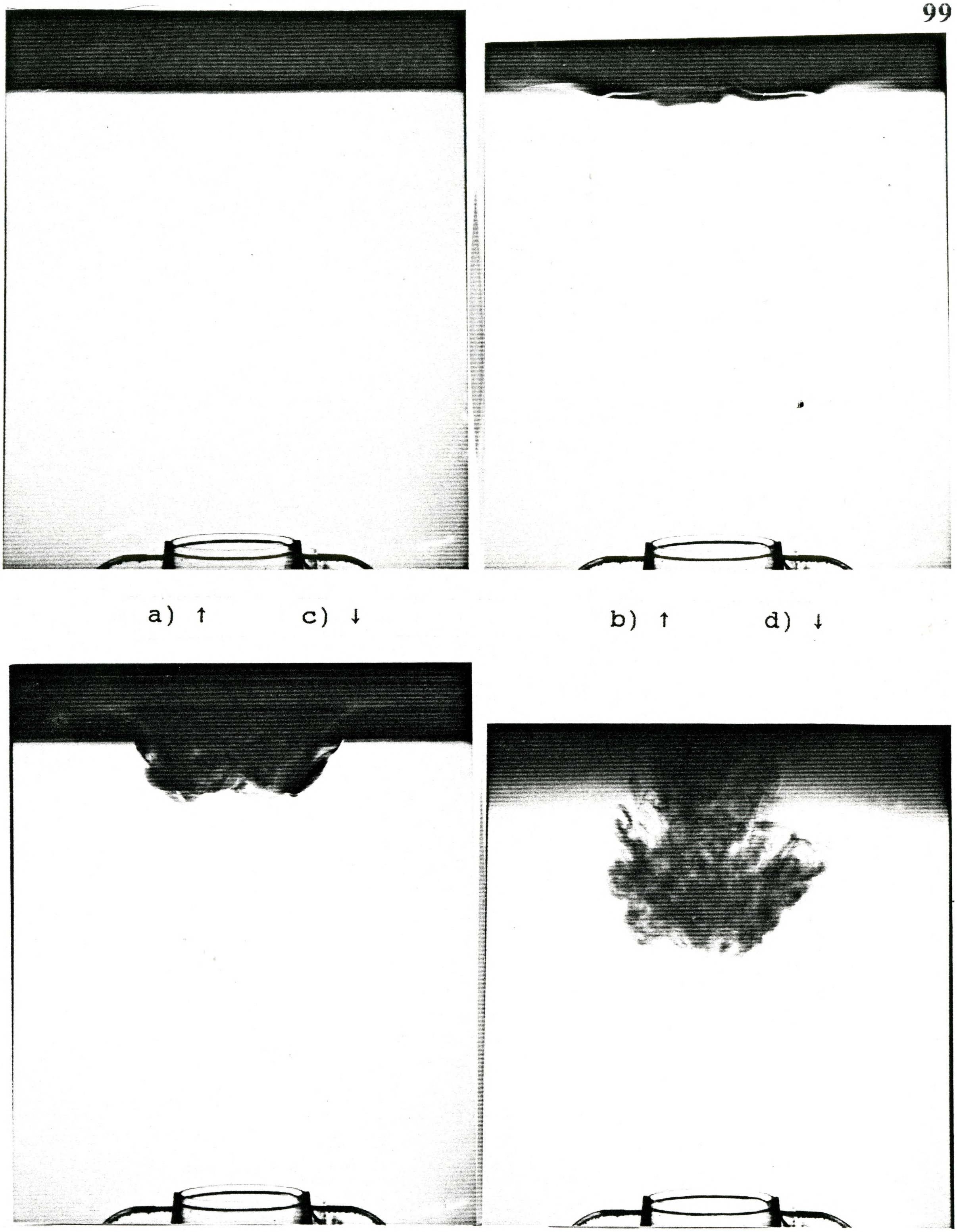


Figure 4.10 As Ri decreases, the ring is able to carry more brine into the water layer. Hence, the wake of the ring disperse more brine and water mixture back into the brine layer. Ri = 0.01.

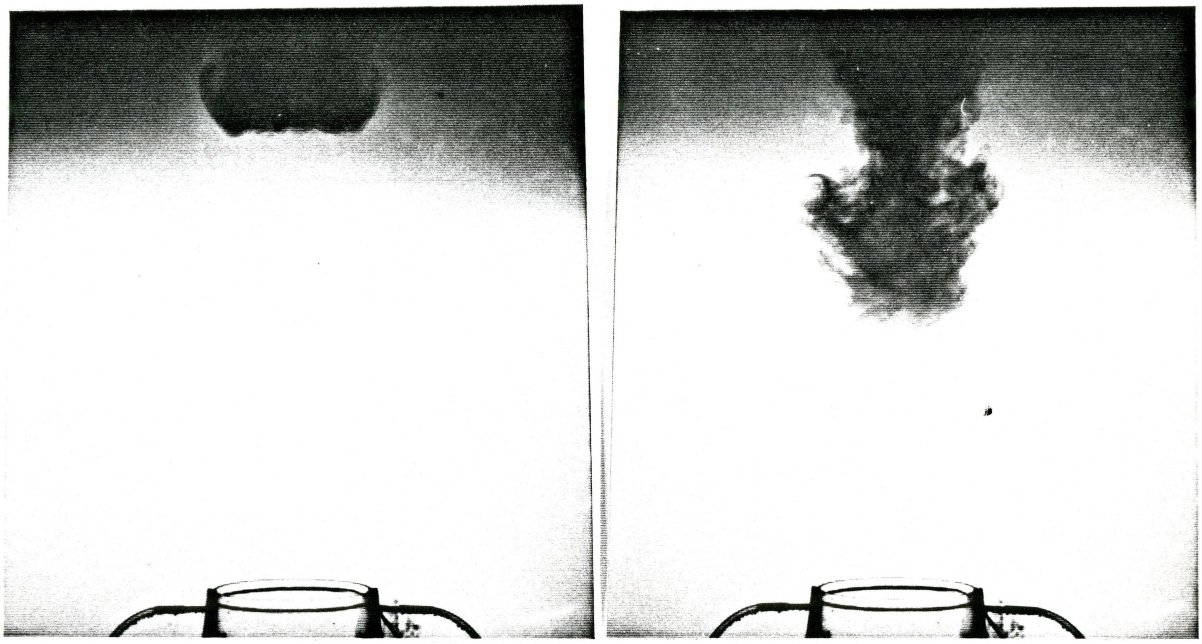

a) ↑ c) ↓ b) ↑ d) ↓

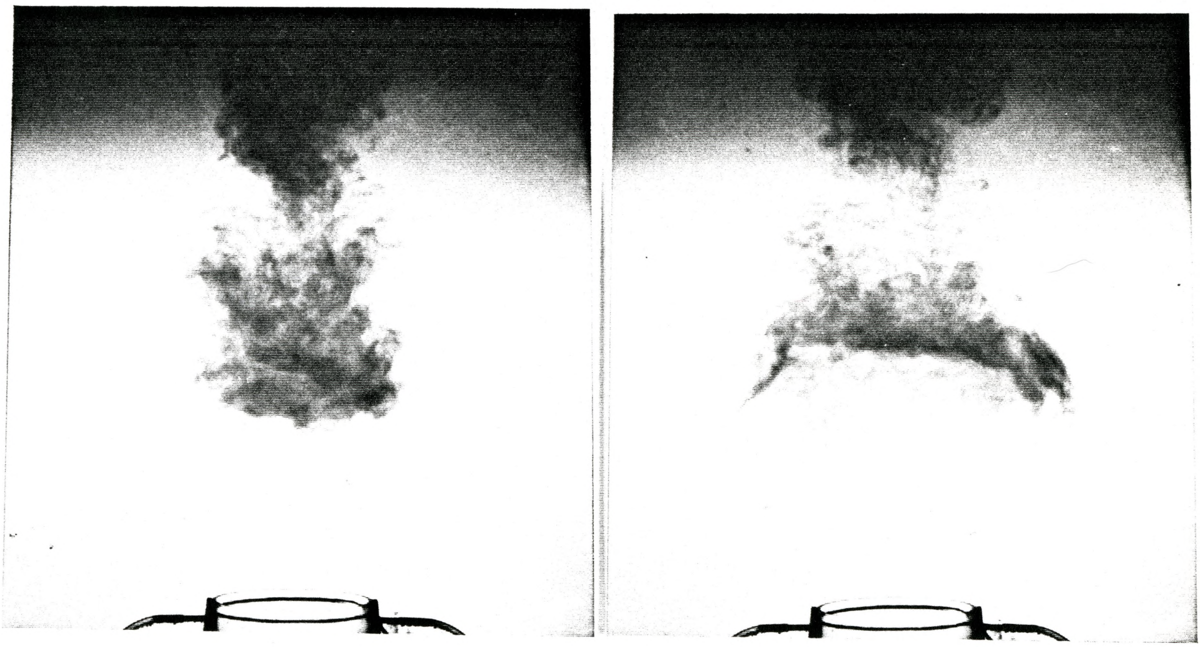

Figure 4.11 As Ri further decreases, the wake of the ring was able to cause even more mixing in the brine layer by carrying more brine and water mixture deeper into the brine layer. Similar results were obtained for Ri = 0.04 and 0.02.

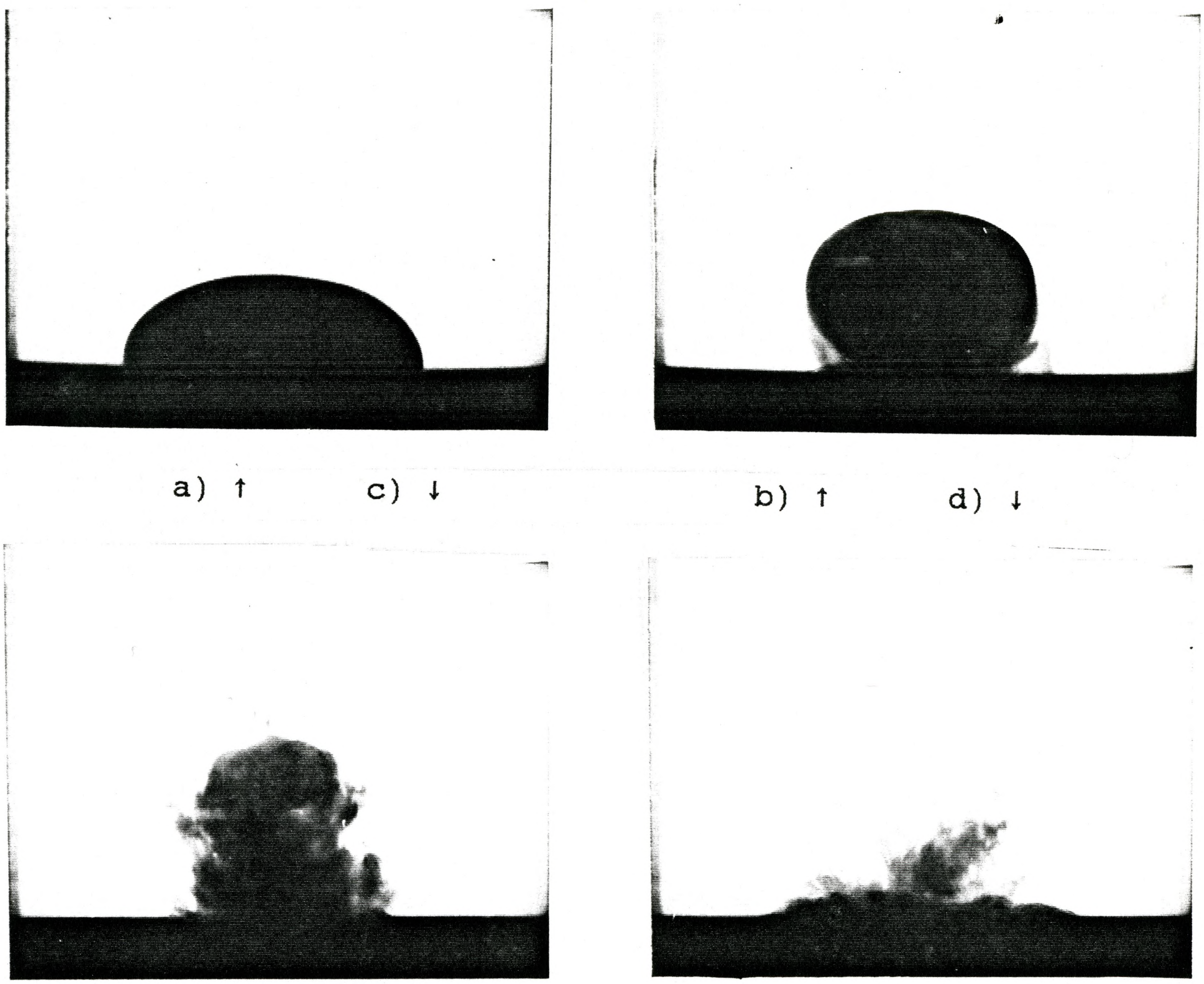


Figure 4.12 This sequence showed the ring was able to penetrate the interface but did not travel far into the interface. Ri = 0.1

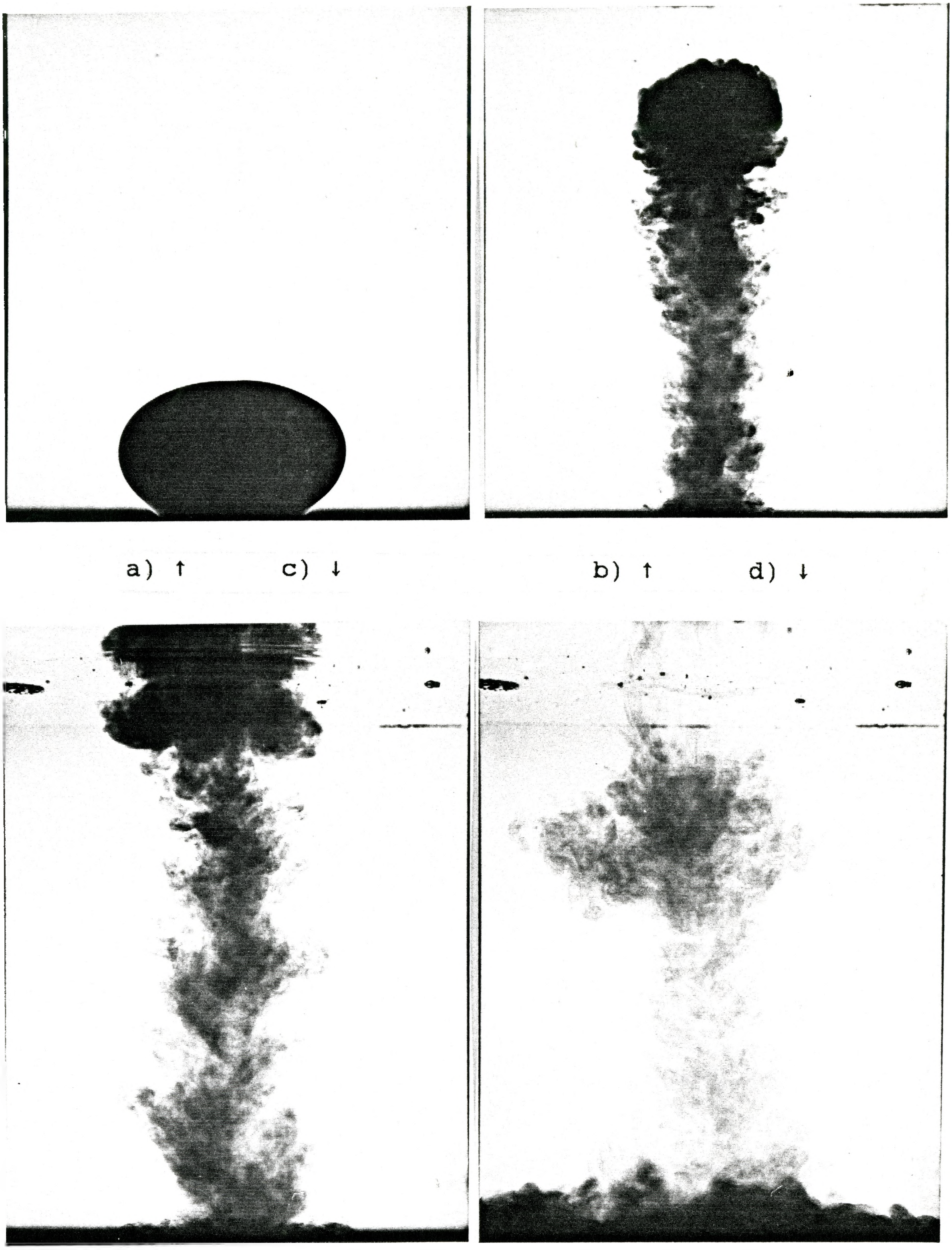


Figure 4.13 The ring was strong enough to penetrate the interface and reach the water surface at Ri = 0.04.

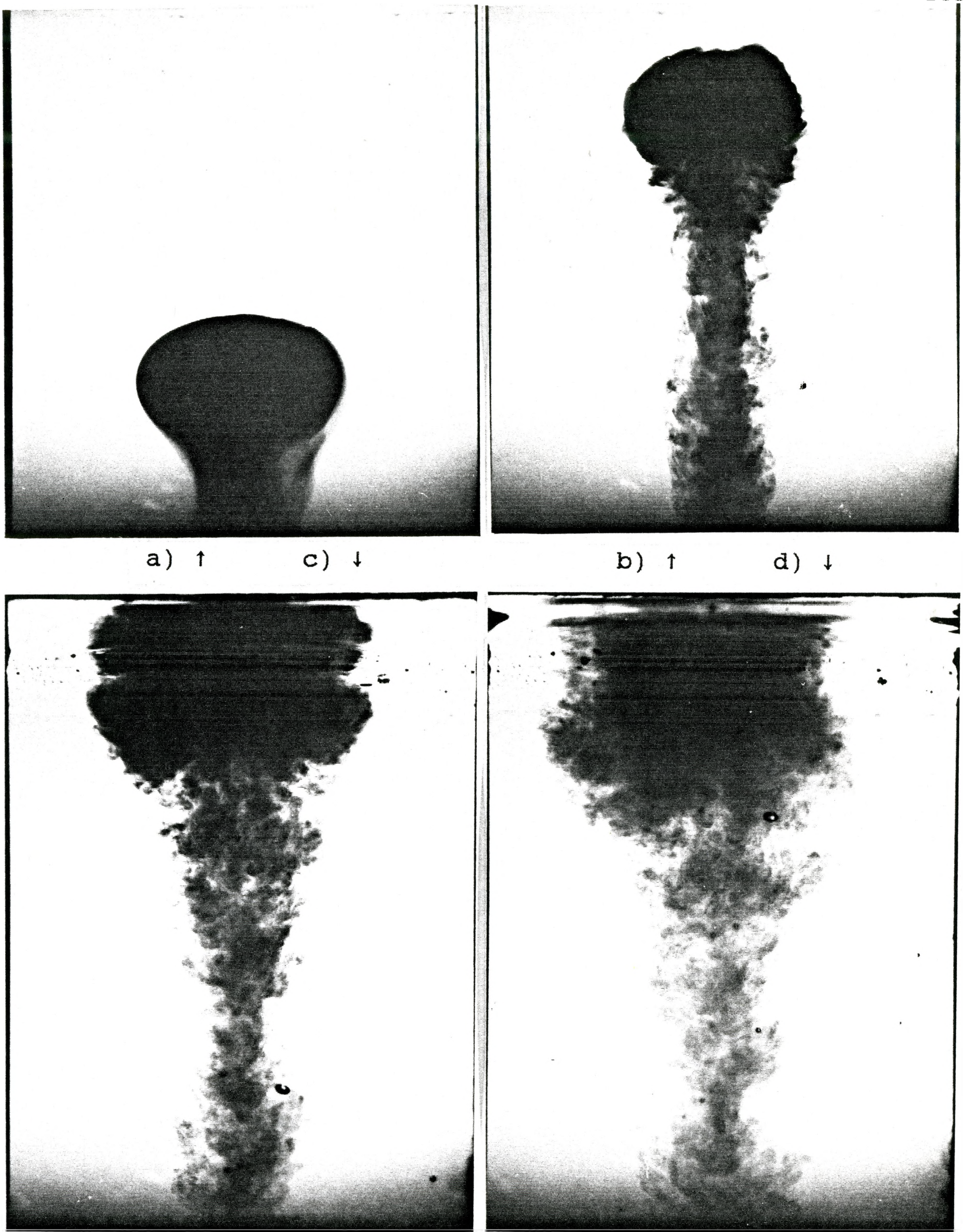


Figure 4.14 As the strength of the vortex ring increases, it is able to carry more brine deep into the water layer and disperse it in the water layer. Ri = 0.02

It is observed that the detrainment rate of a ring increases with Ri. The detrained fluid brings with it a small amount of vorticity in the form of small eddies, see Figures 4.12, 4.13 and 4.14, which enhances the mixing of this detrained fluid with the surrounding water. As more and more fluid is detrained from the ring, a situation is reached where the vorticity inside the ring was no longer capable of maintaining the integrity of the ring and it decays catastrophically to form a lot of small eddies. The depth of penetration of a vortex ring before the final decay depends on the value of Ri. Vortex rings with Ri = 0.1 are able to penetrate the interface but are not able to travel very far into the stratified layer, as showed in Figure 4.9. Vortex rings that had enough momentum or vorticity, $0.1 < Ri < 0$, are able to travel noticeably further into the stratified layer than when $Ri > 0.1$. Those rings that reach the top of the water layer will roll along the surface, similar to rings that roll along the underside of the interface, as they decay, see Figures 4.13 and 4.14. The vortex ring then breaks up into small eddies and disperses the brine in the ring across a localized area to which a decayed vortex ring reaches. For those type of rings with $0.1 < Ri < 0$, the majority of the mixing occurs due to the entrainment of surrounding water and subsequent mixing it within the ring, and then discharges into the wake of a ring. If a ring can travel far into a stratified layer, it can cause more mixing between the fluid inside the ring and the surrounding ambient fluid.

4.4.3.3 What happens to the fluid in the wake:

As a ring carries its fluid into the water layer, it acquires potential energy due to the density gradient between the brine and water. Due to this density gradient, negative vorticity is produced inside the ring, as observed by Maxworthy (1977). When this brine solution inside a ring is detrained, it falls back towards the stratification interface at a relatively high velocity. As this stream of brine impinges on the interface, it causes large amplitude oscillations at the interface, and because of its high velocity, this stream of brine and water mixture is able to reach deep into the brine layer. This results in additional mixing as the lower density mixture comes into contact with the brine. Since this mixture has a lower density than the brine, after this stream of fluid has dissipated its energy, it rises back up to the interface. These results can be observed in Figures 4.9, 4.10 and 4.11. Similarly, the brine that is dispersed by the ring as it decays in the water layer, falls back towards the top of the interface, because it has a higher density than water. This results in the formation of a third layer of fluid between the brine and the water layer, the density of this layer of fluid is between that of the brine and the water.

The observation described above were for the mixing of two layers of stratified fluid, caused by a single vortex ring. If vortex rings are continuously fired through a density interface, it will result in a decrease in density gradient between the two layers of fluid. This means a reduction in the Richardson number and the detrainment rate of fluid from a ring after it penetrates into the stratified layer. Hence these vortex rings are able to carry more brine into the water layer and cause even more mixing between the two layers of fluid. Eventually, the density gradient between the two layers will disappear and result in diluted brine solution with a uniform density.

## 4.5 Experimental results:

A summary of the results of the experiments performed is given in this section. Other information on the initial parameters including, the densities of the two fluids, the theoretical jet velocity and the averaged measured jet velocity, are given in appendix B.

The first sets of experiments were performed with hot and cold water stratified layers. The specifications of these experiments were:

| Filename | Li(m) | Rem | Ri | Lm/Dm |
|---|---|---|---|---|
| EXPT2 | .432 | 8640 | 0.03 | 1.7 |
| EXPT4 | .330 | 3670 | 0.17 | 1.9 |
| EXPT6 | .373 | 5740 | 0.06 | 1.8 |
| EXPT7 | .368 | 3670 | 0.14 | 1.9 |

Lm/Dm - the plug length of the fluid injected measured using the hot film anemometer. This value is obtained by substituting the theoretical jet velocity into the equation (3.1) given in chapter 3.

The second set of experiments were performed using brine and water as the stratified layers with the unmodified injection mechanism (injection mechanism with a peripheral gap around the plate). Specifications for these experiments were:

| Filename | Li(m) | Rem | Ri | Lm/Dm |
| --- | --- | --- | --- | --- |
| SEPT11-2 | .292 | 7550 | 0.14 | 1.7 |
| SEPT12-1 | .224 | 4240 | 0.10 | 1.9 |
| SEPT14-2 | .193 | 7250 | 0.13 | 1.7 |

The final set of experiments were performed using brine and water stratified layers and a modified injection system, where the leakage of fluid through the gaps around the injection plate during the injection was minimized. The specifications for these experiments were:

| Filename | Li(m) | Rem | Ri | Lm/Dm |
| --- | --- | --- | --- | --- |
| 2PDEC14 | .203 | 7520 | 0.15 | 2.5 |
| 2PDEC142 | .203 | 7520 | 0.15 | 2.5 |
| 4PDEC17 | .203 | 7290 | 0.06 | 1.7 |
| EXPT20 | .203 | 10780 | 0.08 | 2.2 |
| EXPT21 | .203 | 12780 | 0.06 | 1.9 |
| EXPT22 | .203 | 7800 | 0.14 | 2.5 |
| EXPT24 | .203 | 7310 | 0.06 | 2.5 |
| EXPT25 | .203 | 10220 | 0.03 | 2.2 |
| EXPT26 | .203 | 4450 | 0.18 | 2.7 |
| EXPT27 | .203 | 10600 | 0.03 | 2.2 |
| EXPT28 | .203 | 7570 | 0.06 | 2.5 |
| EXPT29 | .203 | 10540 | 0.08 | 2.2 |
| EXPT30 | .203 | 6010 | 0.11 | 2.6 |

All the experiments described above were recorded using a video camera and then analyzed using a digital video frame grabber.

In the analysis, the core diameter and the location of the core of the vortex ring with respect to the location of the injection tube were measured.

After the ring penetrated into the water layer, the fluid inside the ring began to mix with the water surrounding it. As the mixing spread to the core of the ring, the centre of the core was no longer clearly visible. Hence the errors in the measurement of the core diameter and the location of the core increased, especially after the ring had penetrated far into the stratified layer.

It was possible to obtain the traverse velocity of a ring from a distance and time trace of the core of the ring. These results are presented in Figures 4.15 - 4.34 where the dimensionless diameter and traverse velocity of the ring are plotted against the dimensionless distance travelled.

After analyzing the data from the experiments, the maximum penetration depth, the core diameter and the traverse velocity of the ring while it was travelling in the brine layer, and the detrainment rate of the ring while it was travelling in the water layer, were determined. These data are presented in the following table in the form of dimensionless variables:

| Filename | $X_p/R$ | D/Dm | $U_v/U_j$ | dR/dX |
|---|---|---|---|---|
| EXPT2 | 9.2 | 1.31 | 0.334 | - |
| EXPT4 | .85 | 1.3 | 0.235 | - |
| EXPT6 | 3.6 | 1.36 | 0.285 | - |
| EXPT7 | 0.2 | 1.36 | 0.243 | - |
| SEPT11-2 | 1.6 | 1.36 | 0.421 | - |
| SEPT12-1 | 1.2 | 1.4 | 0.321 | - |
| SEPT14-2 | 2.5 | 1.37 | 0.429 | - |
| 2PDEC14 | 0.88 | 1.51 | 0.454 | - |
| 2PDEC142 | 1.6 | 1.51 | 0.42 | -0.81 |
| 4PDEC17 | 5.1 | 1.54 | 0.45 | -0.17 |
| EXPT20 | 10.2 | 1.38 | 0.53 | -0.11 |
| EXPT21 | 14.2 | 1.35 | 0.53 | -0.10 |
| EXPT22 | 3.5 | 1.41 | 0.50 | -0.44 |
| EXPT24 | 13.7 | 1.44 | 0.48 | -0.11 |
| EXPT25 | 21.9 | 1.39 | 0.51 | -0.06 |
| EXPT26 | 0.8 | 1.46 | 0.36 | - |
| EXPT27 | 23.6 | 1.36 | 0.41 | -0.05 |
| EXPT28 | 12.6 | 1.42 | 0.51 | -0.10 |
| EXPT29 | 8.8 | 1.43 | 0.49 | -0.13 |
| EXPT30 | 6.9 | 1.41 | 0.47 | -0.24 |

where;

dR/dX - detrainment rate, as defined by Maxworthy (1977), which is the change of the core diameter of the ring with respect to the distance travel by the ring.

These results will be discussed in more detail in the discussion section.

Figure 4.15 Dv/D and Vv/Vj vs. X/R
Re=8640, Ri=0.03

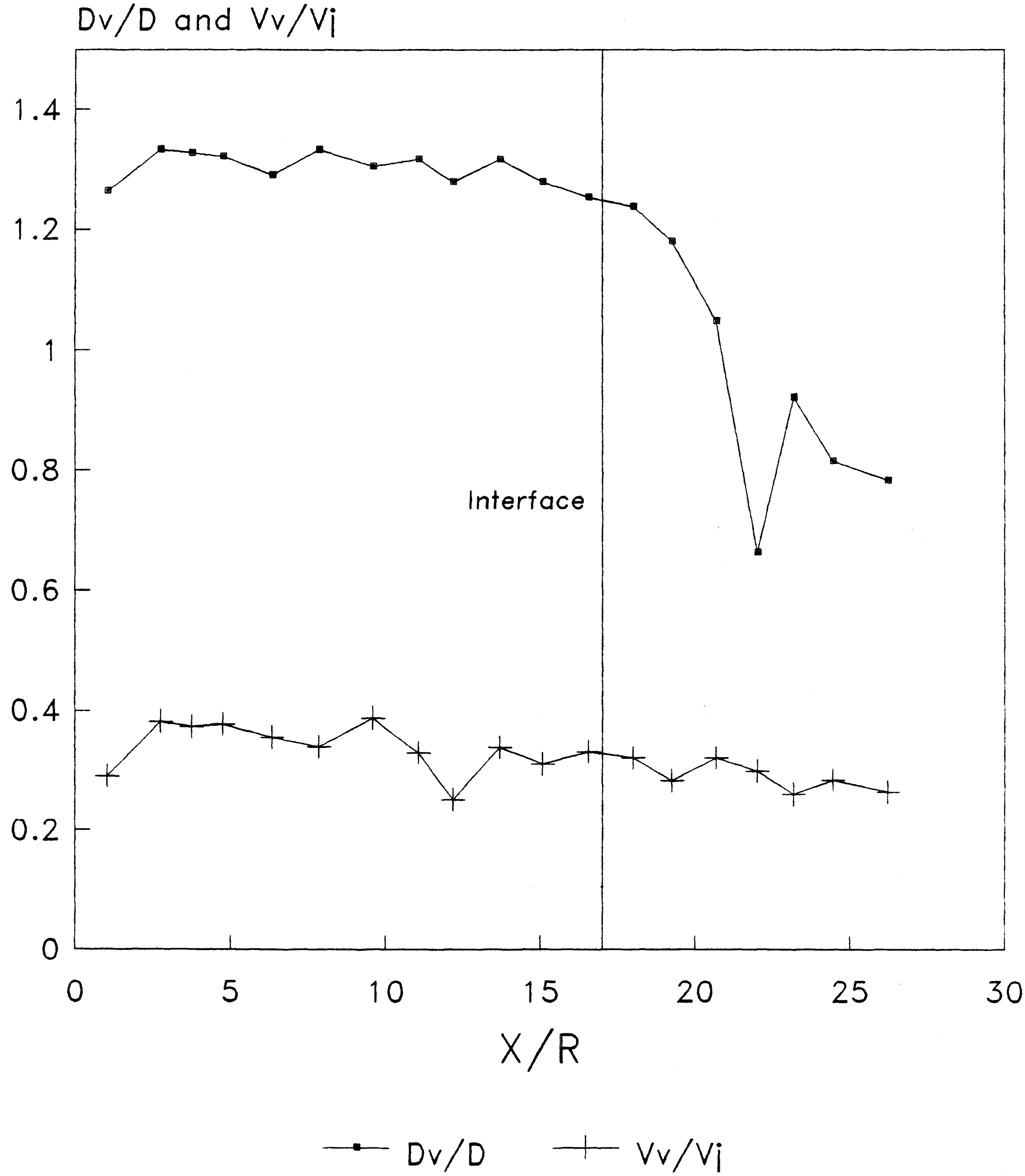


from: expt2

Figure 4.16 dv/d and Vv/Vj vs x/r
Re=3670, Ri= 0.17

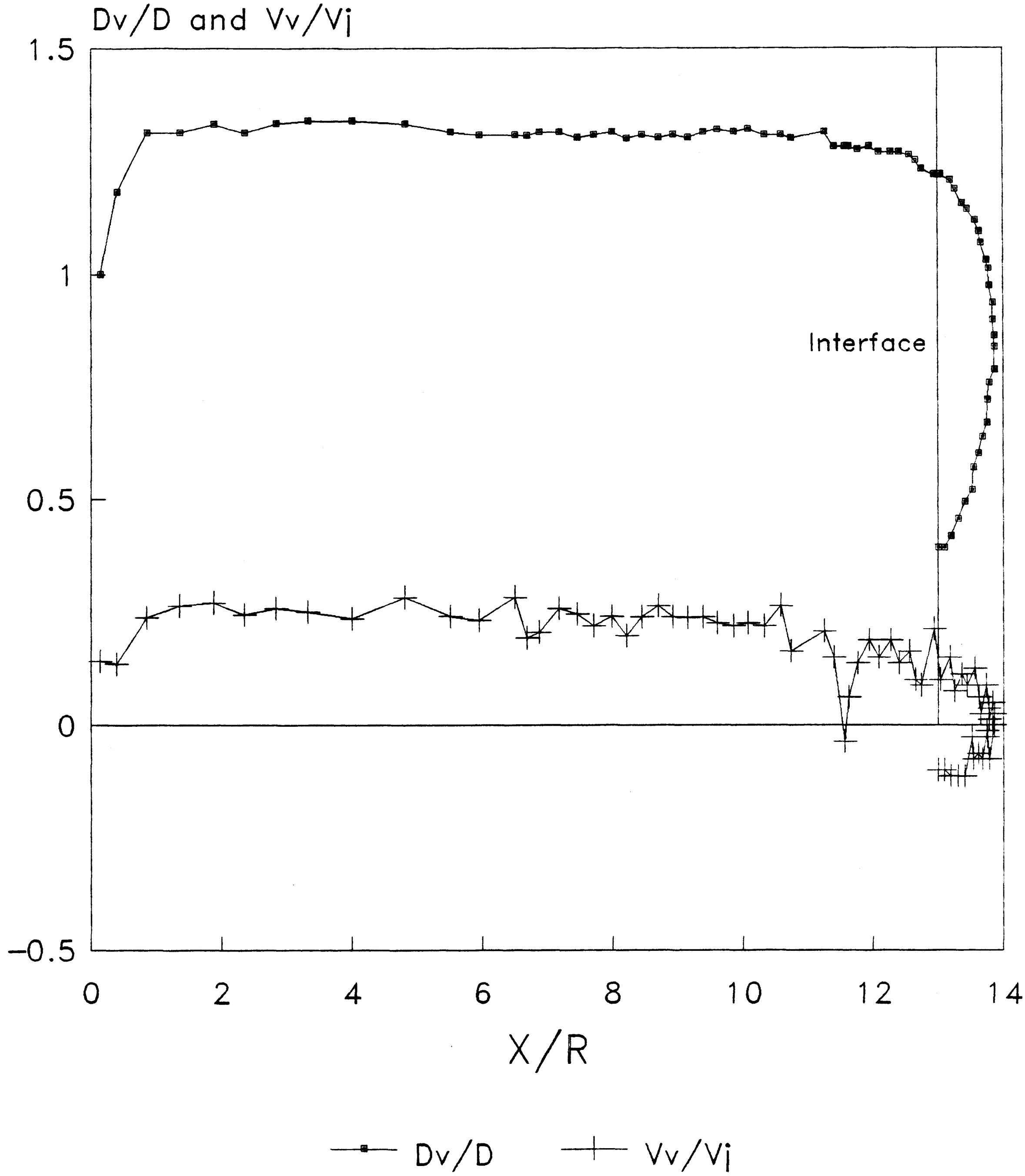


from: expt4

Figure 4.17 Dv/D and Vv/Vj vs. X/R
Re=5740, Ri =.06

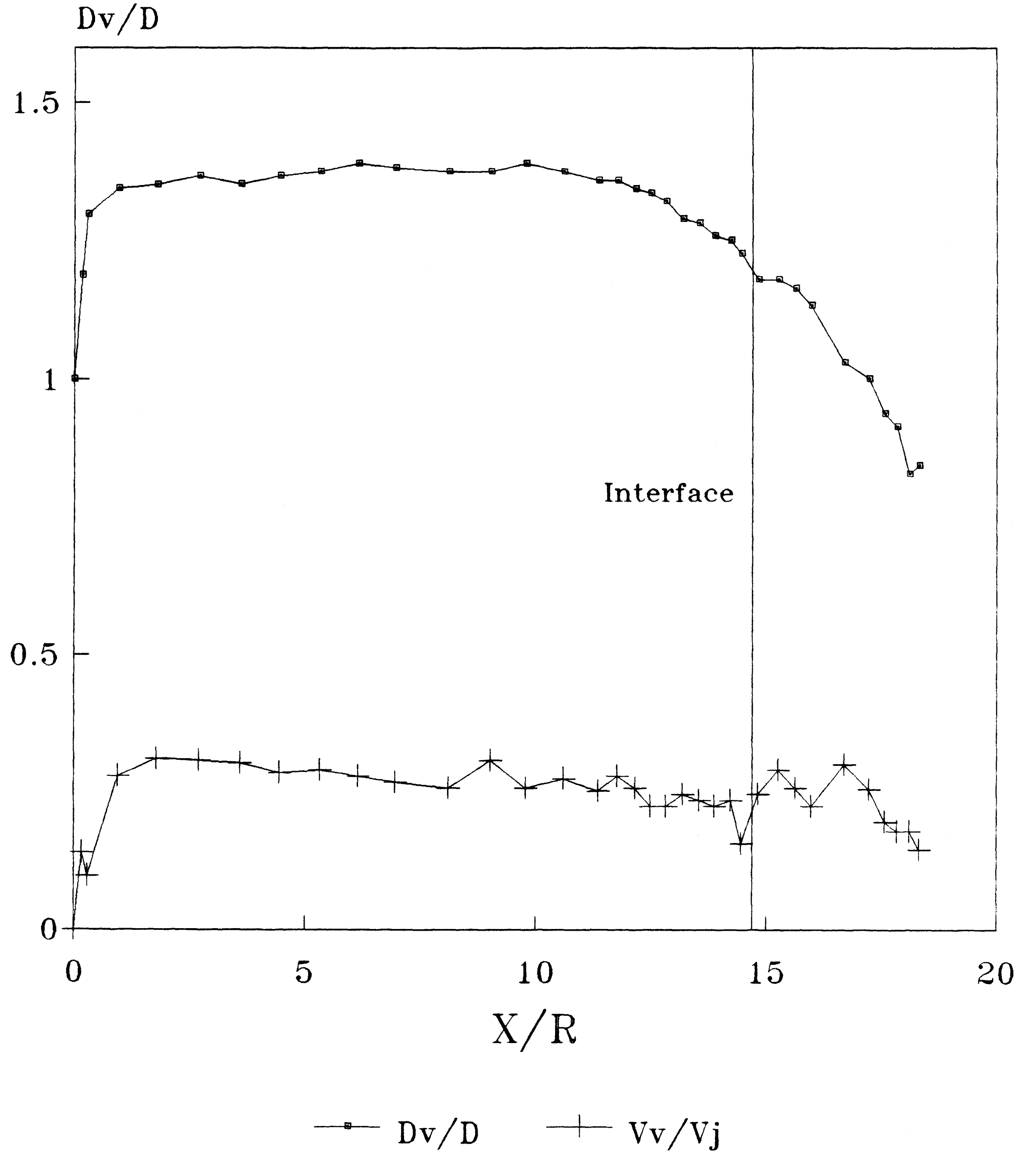


expt6-2

Figure 4.18 Dv/D and Dv/Dj vs X/R
Re=3670, Ri=.14

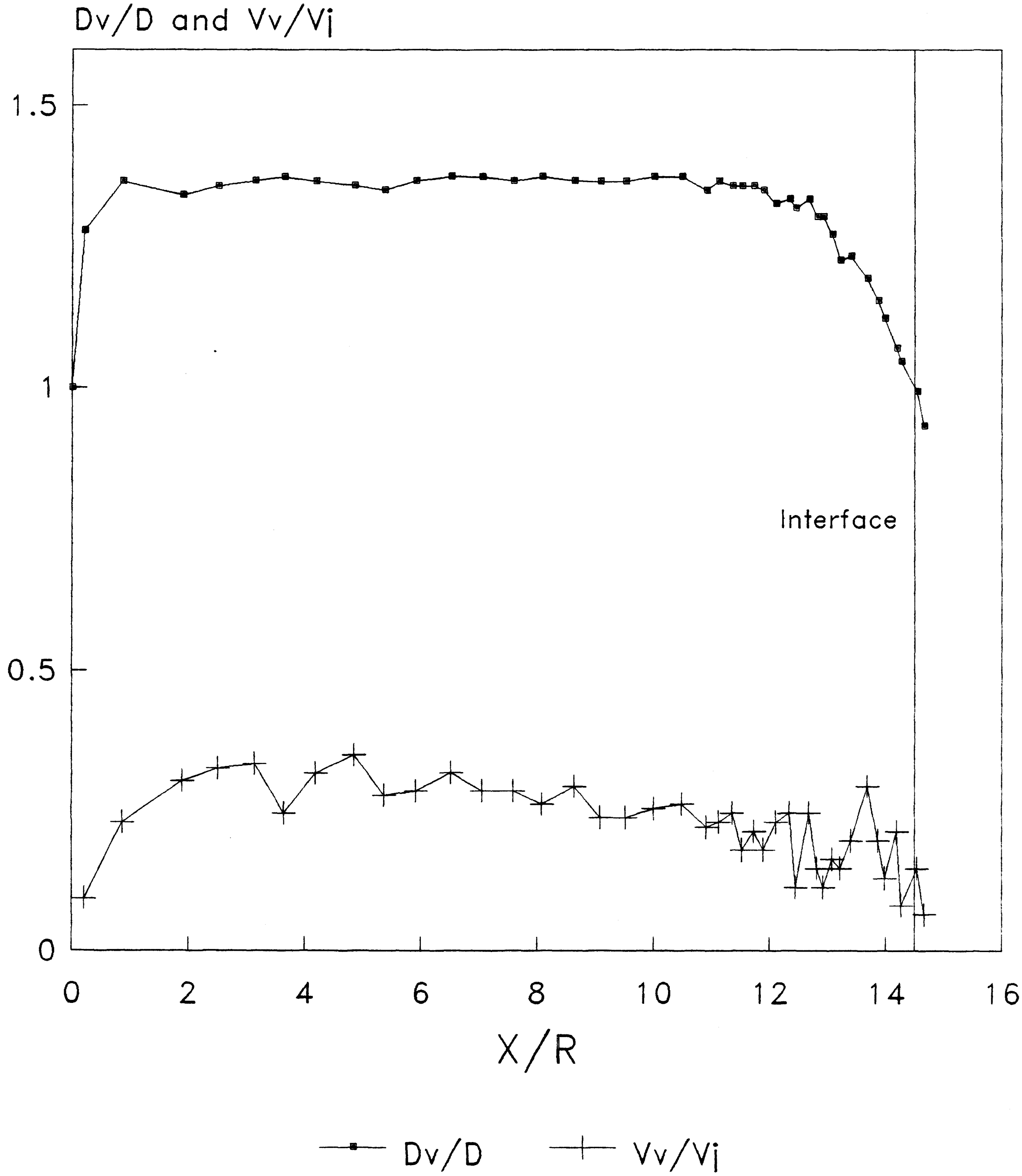


from: expt7

Figure 4.19 Dv/D and Vv/Vj vs. X/R
Re=7550 ,Ri=.14

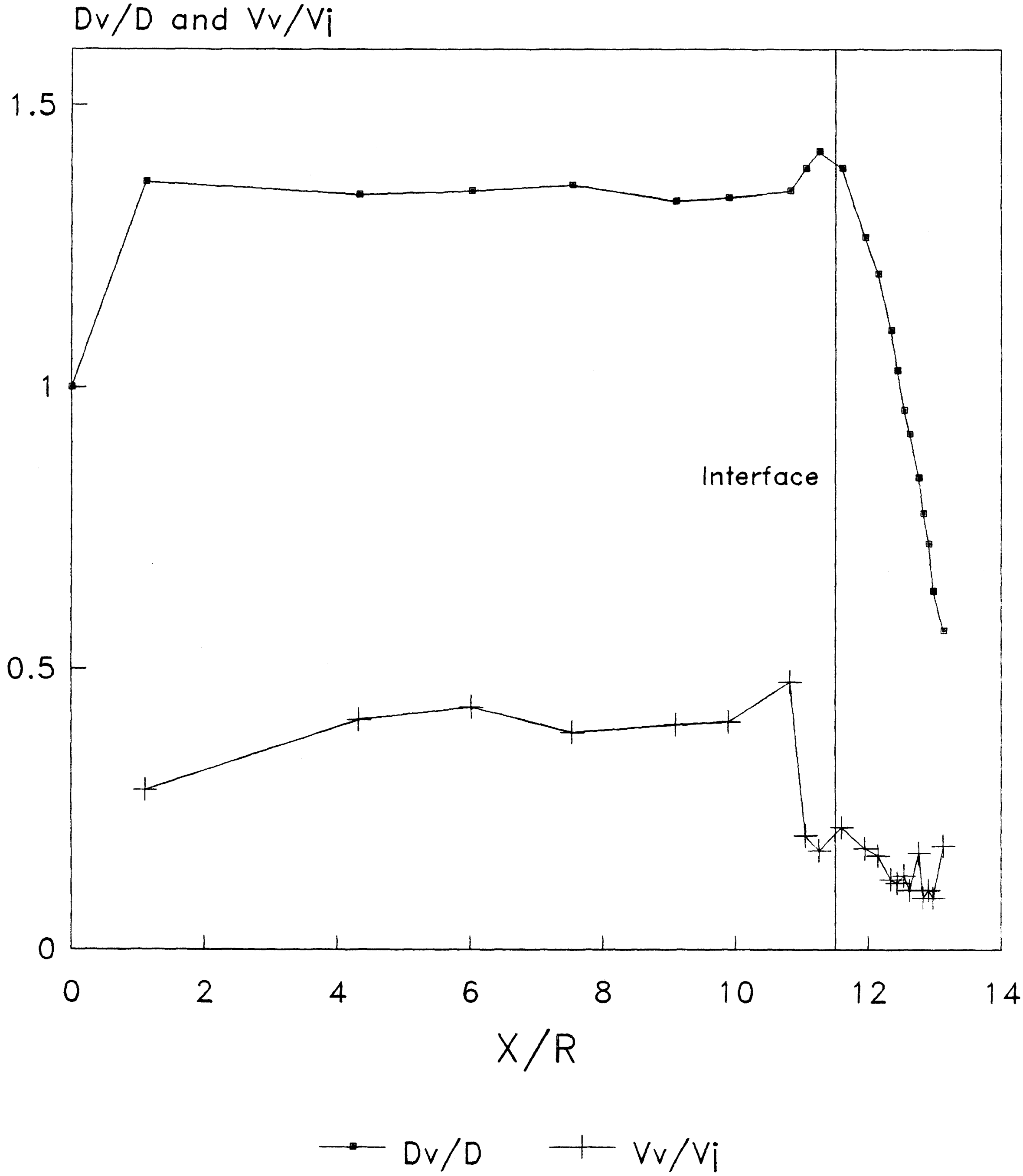


from : sept11

Figure 4.20 Dv/D and Vv/Vj vs X/R
Re=4240, Ri=.10

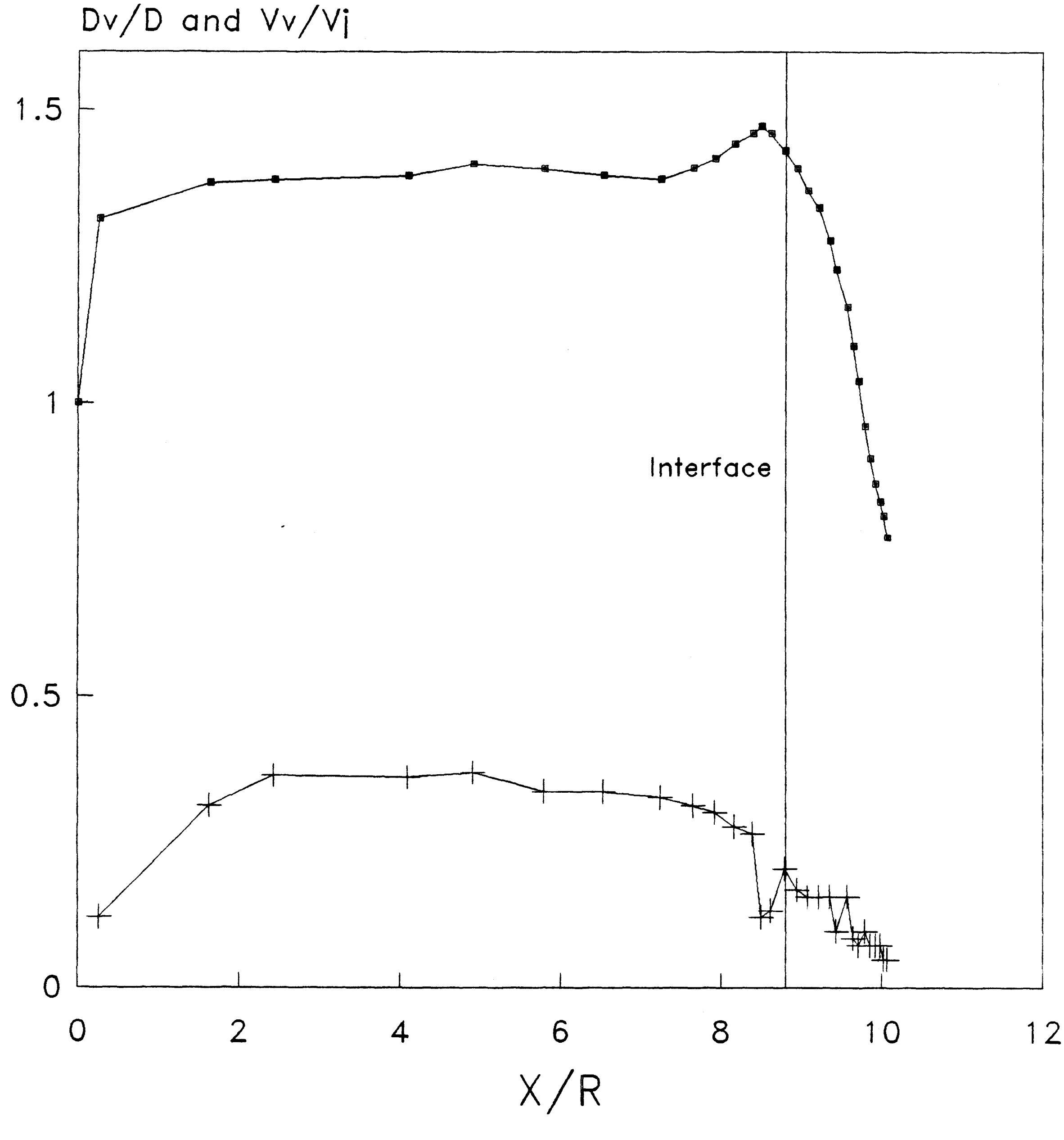


from: sept12-1

Figure 4.21 Dv/D and Vv/Vj vs X/R
Re=7250, Ri=.13

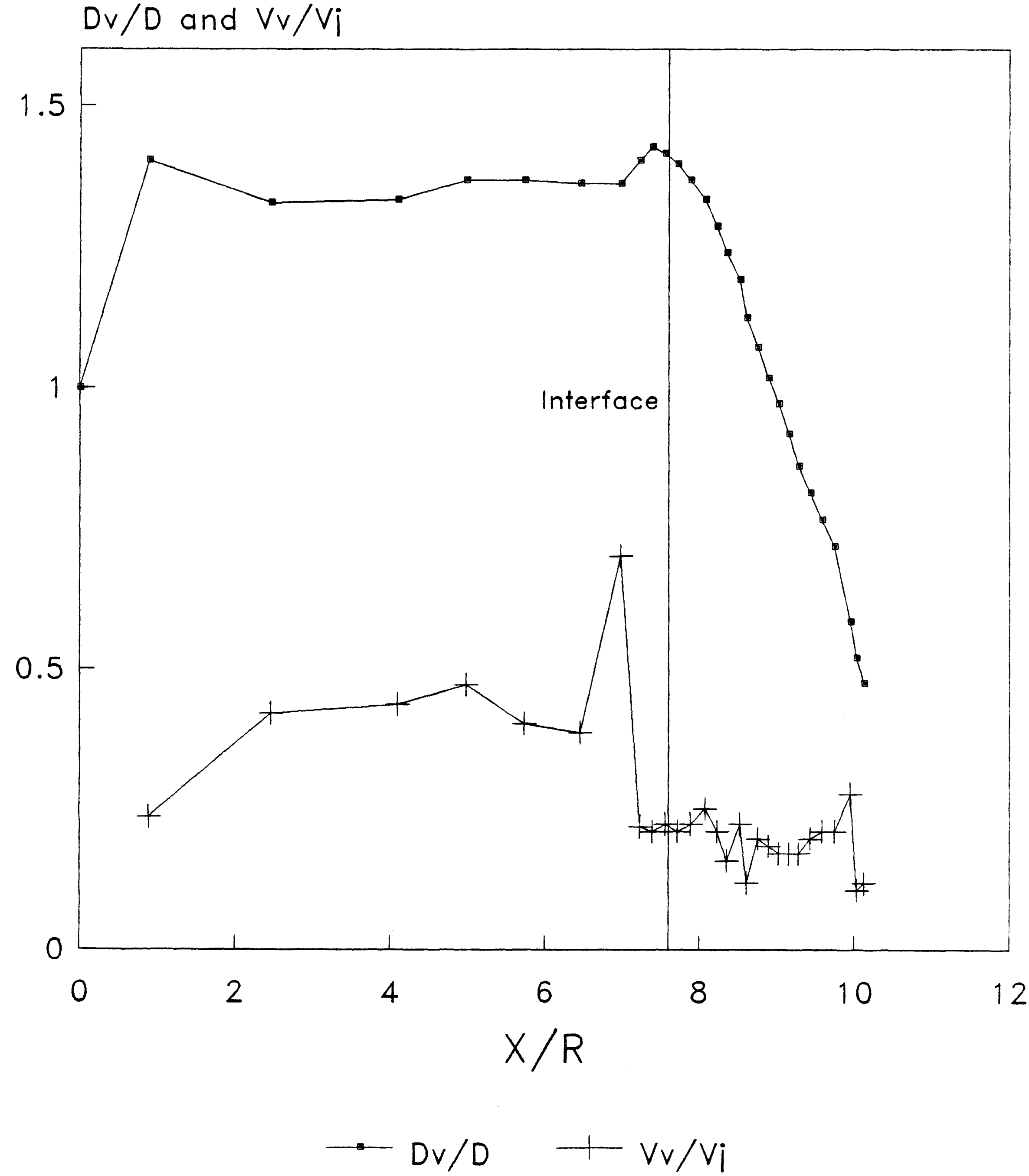


from sept14-2

Figure 4.22 Dv/D and Vv/Vj vs. X/R
Re=7520, Ri=.15

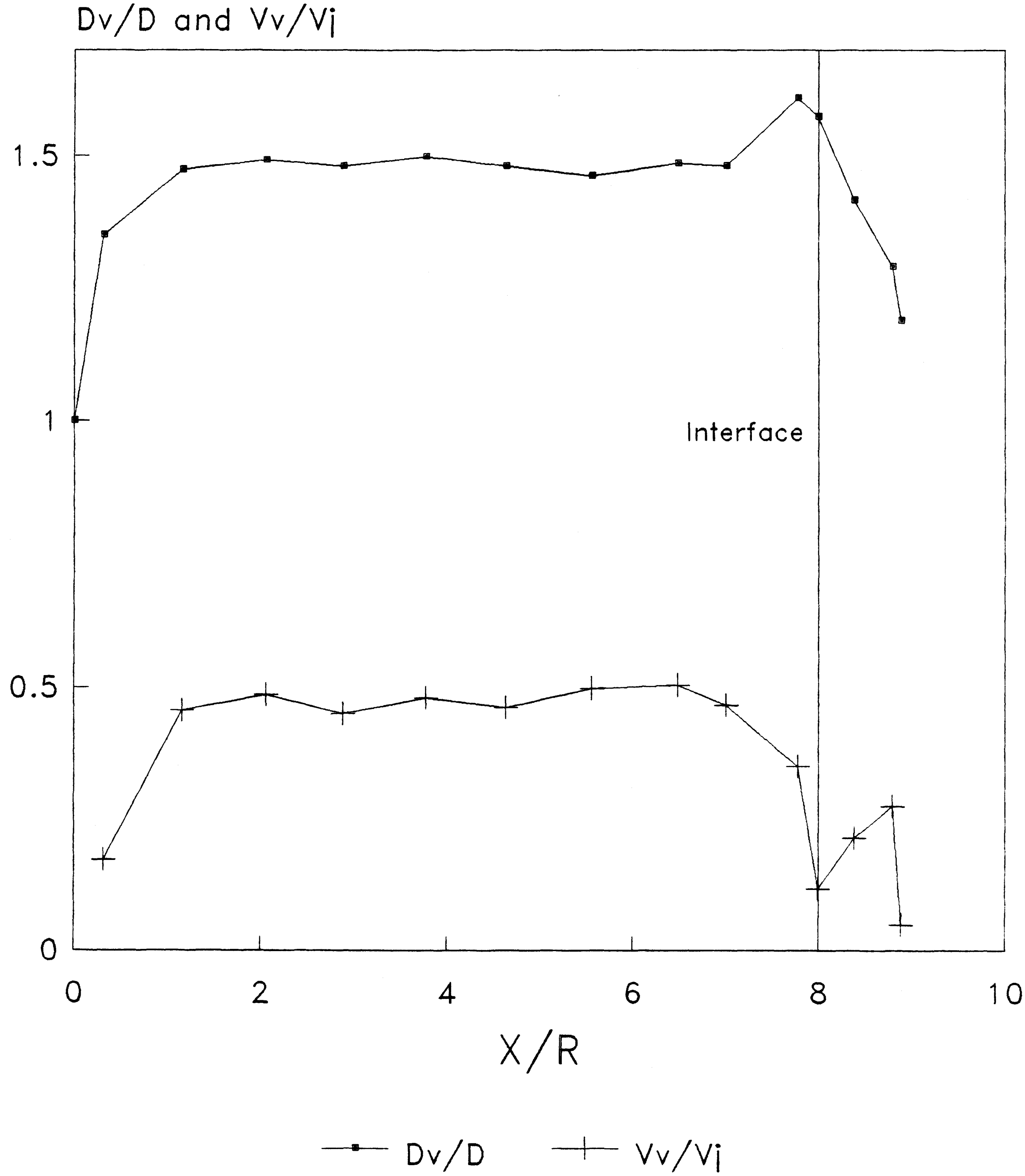


from: 2pdec14

Fig 4.23 Dv/D & Vv/Vj vs. X/R (2nd trial
Re=7520, Ri=.15

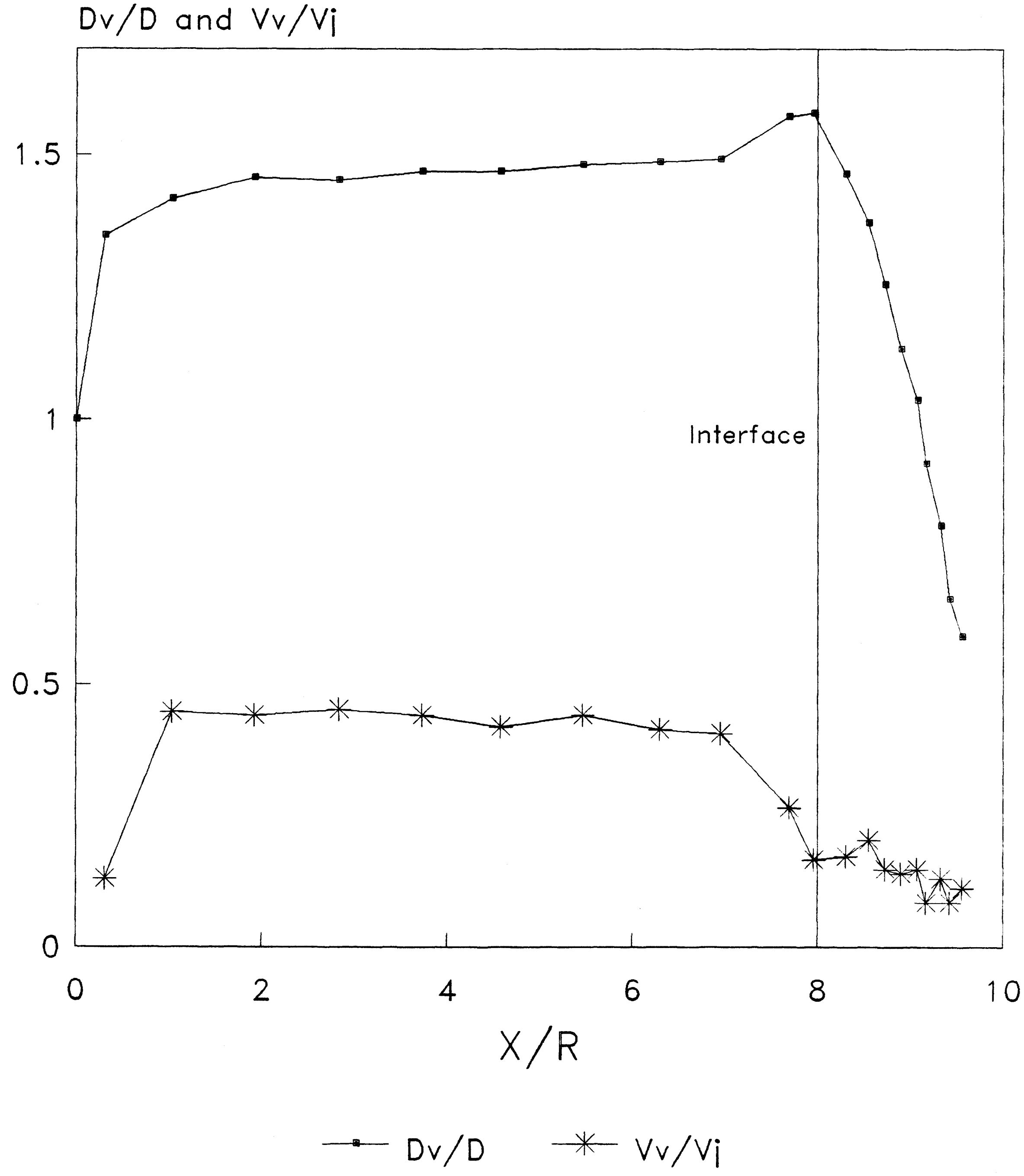


from 2pdec142

Figure 4.24 Dv/D & Vv/Vj vs. X/R
Re=7290, Ri=.06

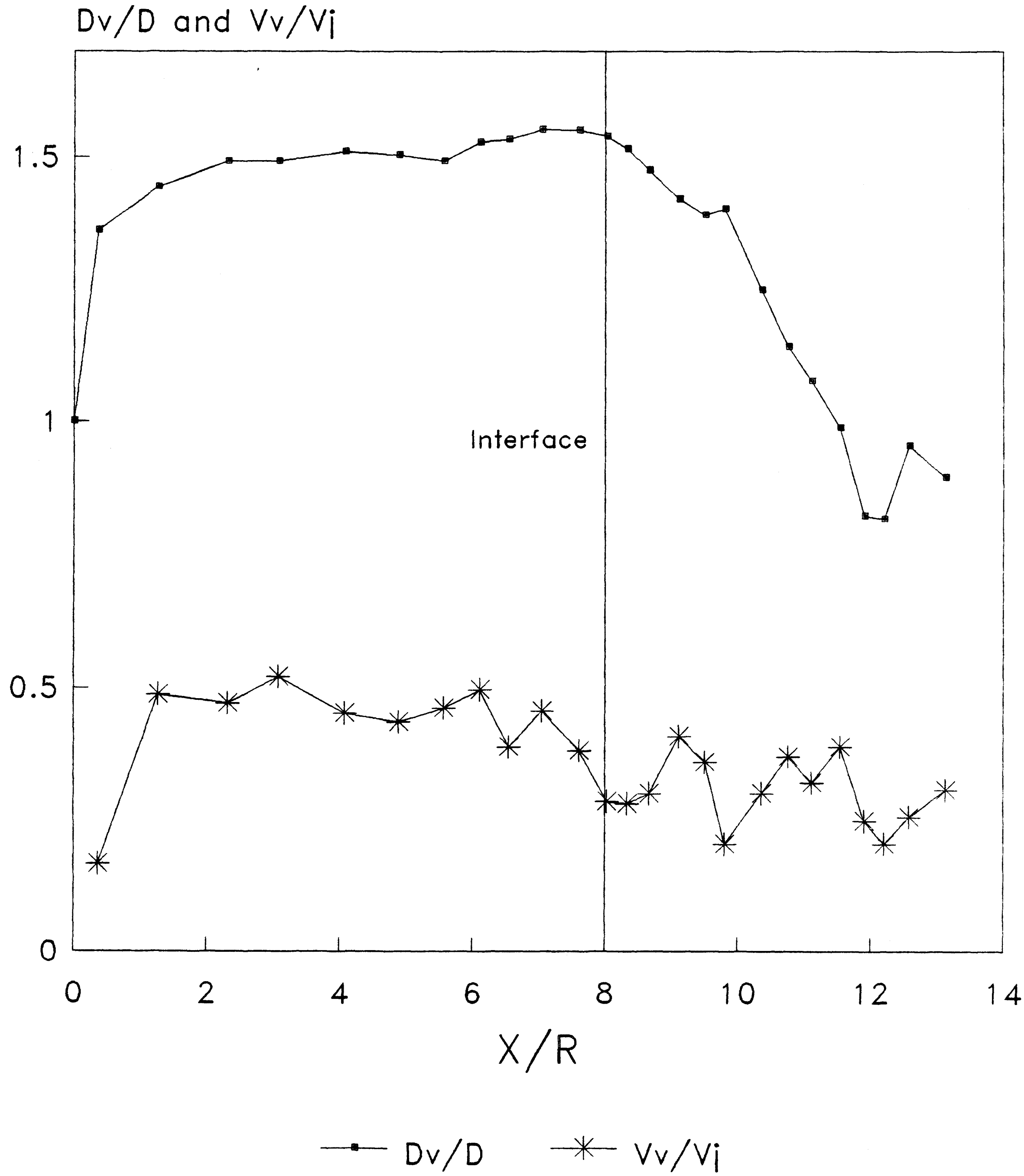


from: 4pdec17

Figure 4.25 Dv/D & Vv/Vj vs. X/R
Re=10780, Ri=.08

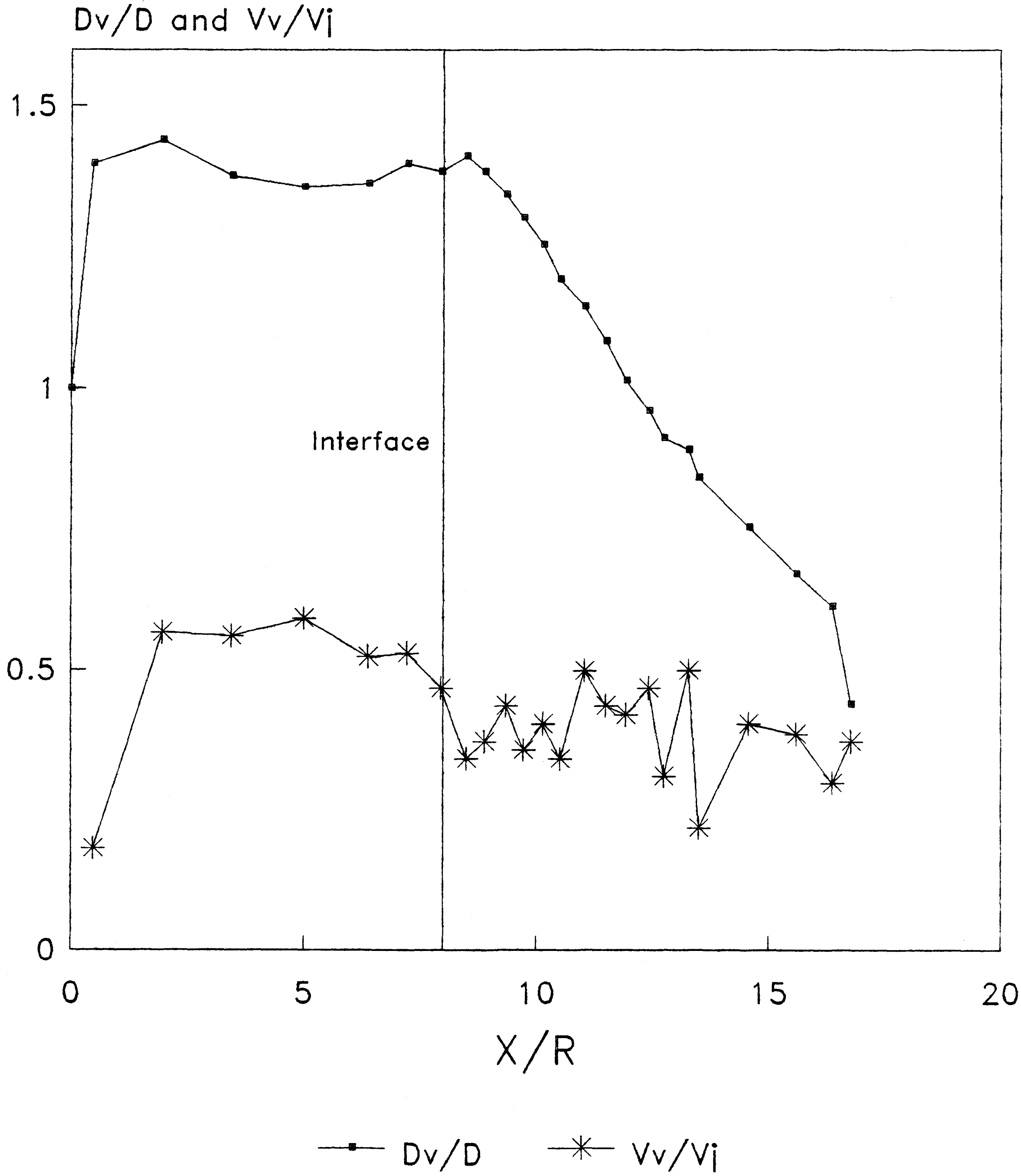


from: expt20

Figure 4.26 Dv/D & Vv/Vj vs. X/R
Re=12780, Ri=.06

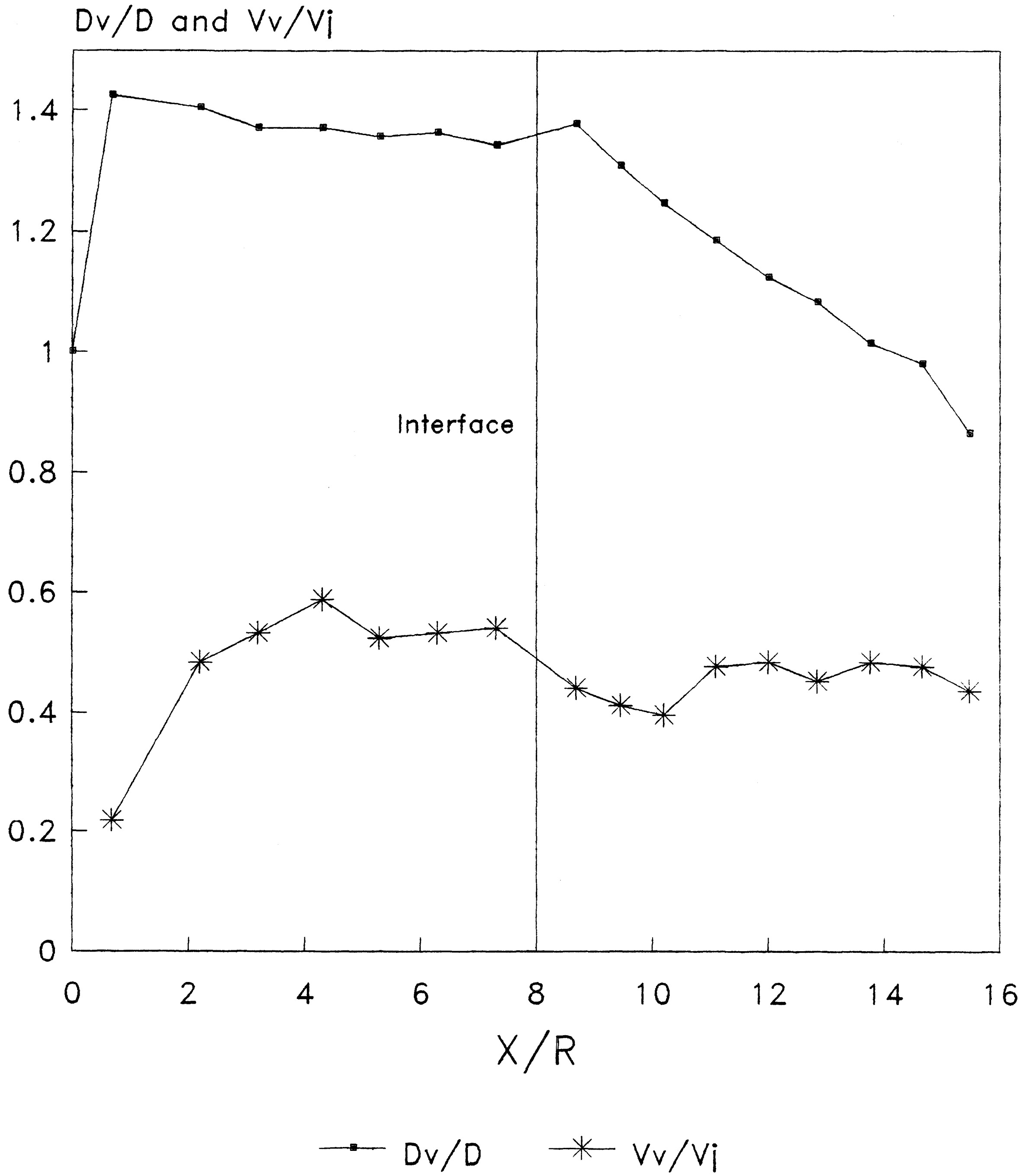


from: expt21

Figure 4.27 Dv/D and Vv/Vj vs. X/R
Re=7800, Ri=.14

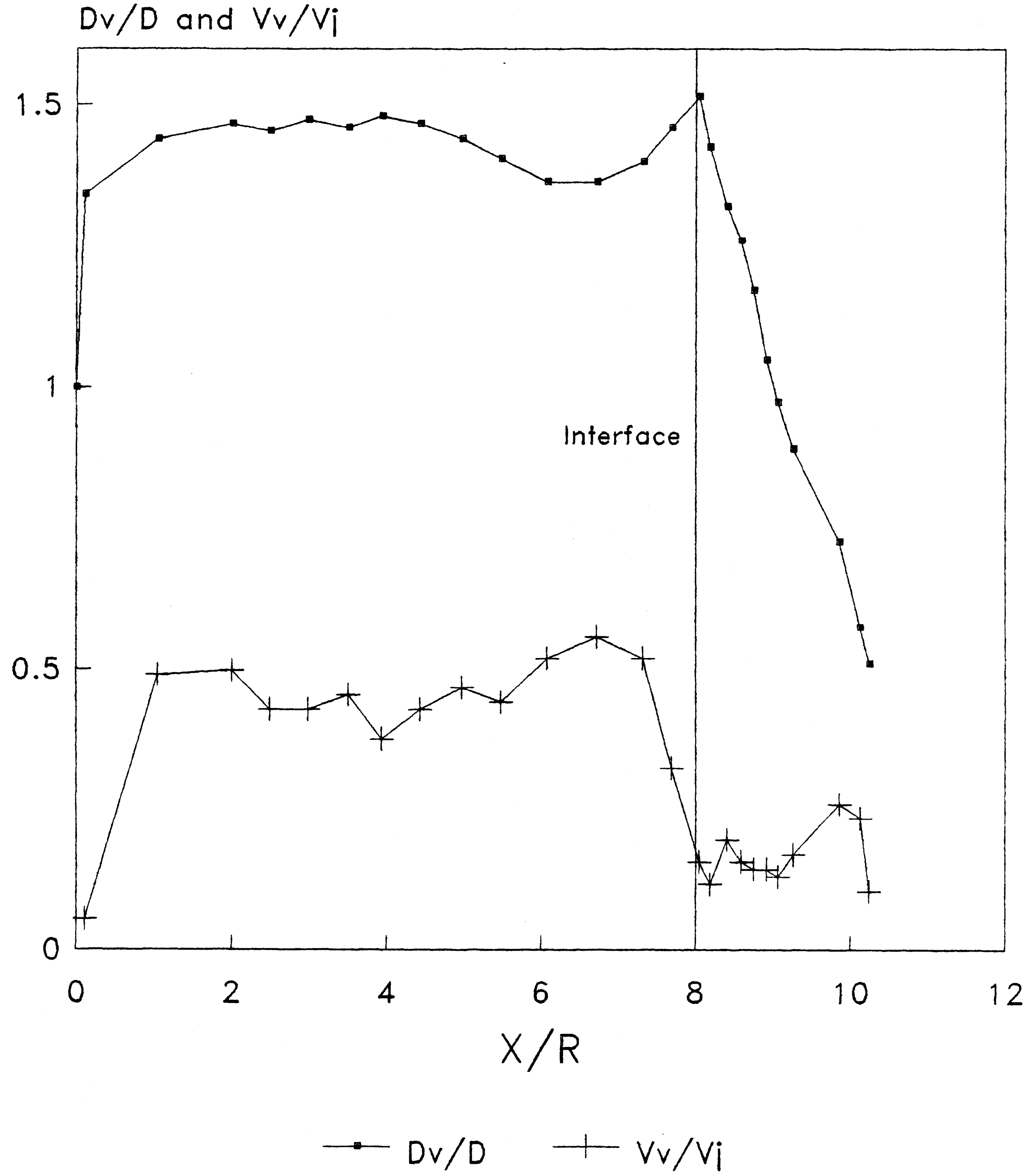


from: expt22

Figure 4.28 Dv/D & Vv/Vj vs. X/R
Re=7310, Ri=.06

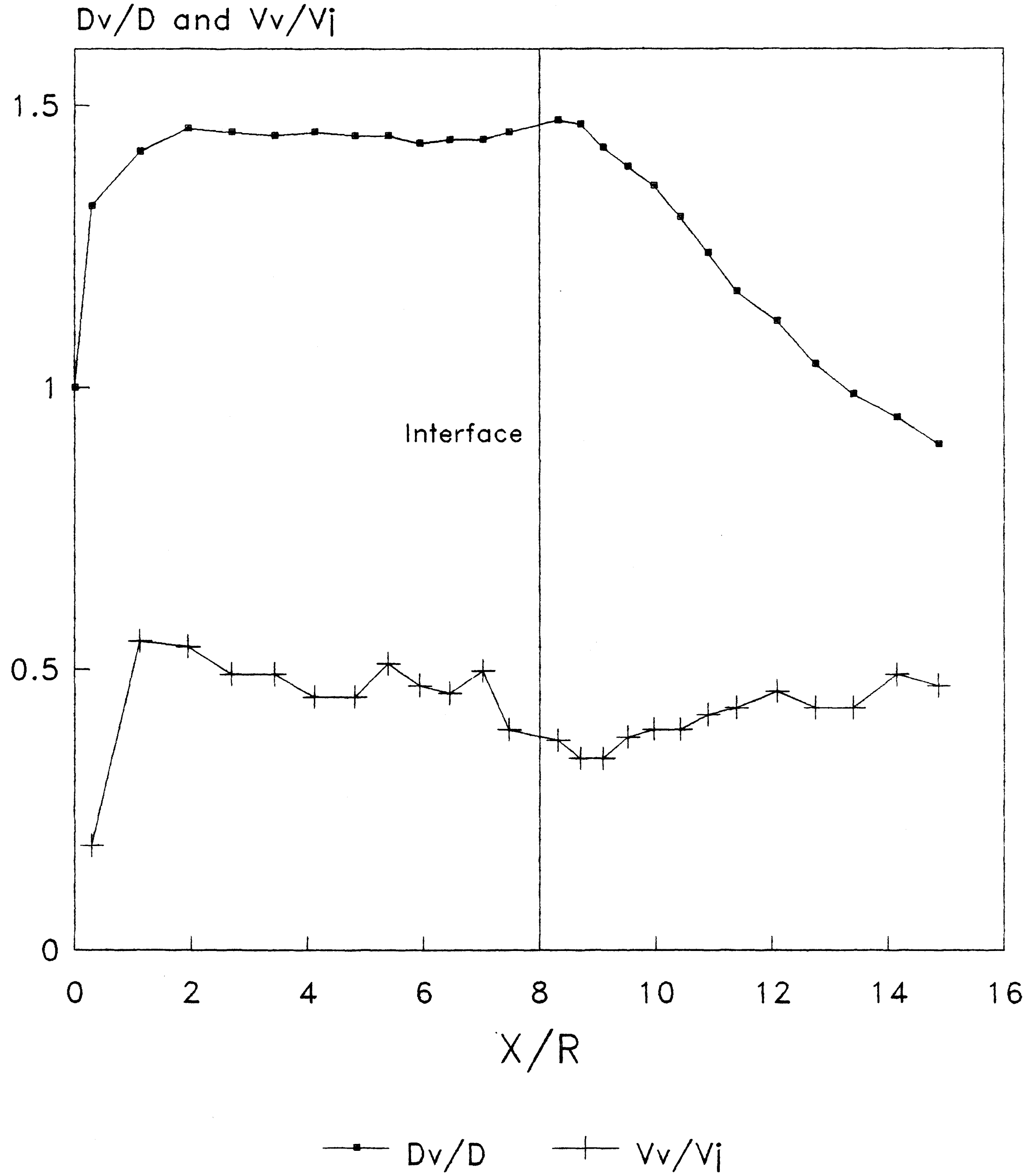


from: expt24

Figure 4.29 Dv/D & Vv/Vj vs. X/R
Re=10220, Ri=.03

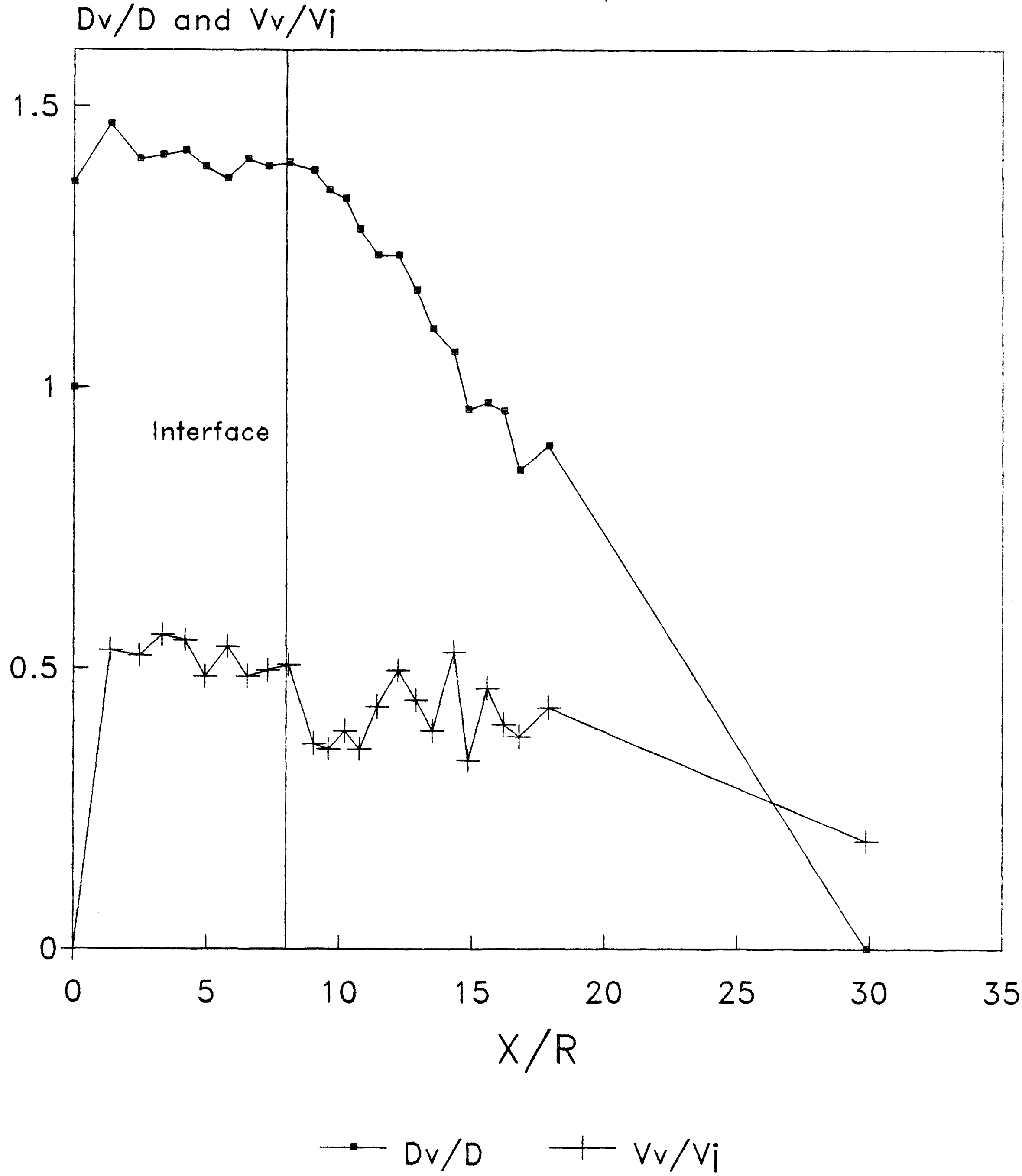


from: expt25

Figure 4.30 Dv/D & Vv/Vj vs. X/R
Re=4550, Ri=.18

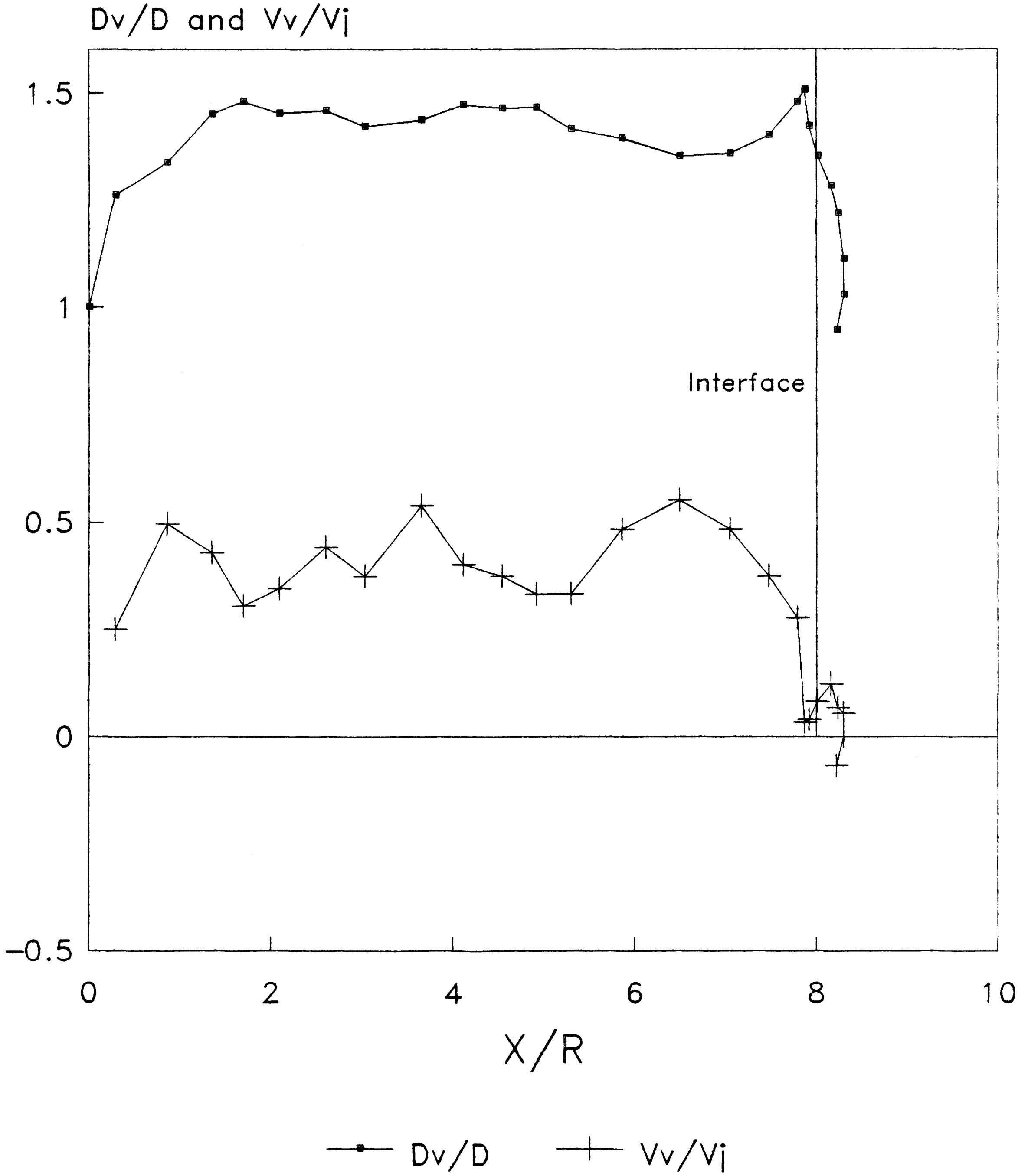


from: expt26

Figure 4.31 Dv/D & Vv/Vj vs. X/R
Re=10600, Ri=.03

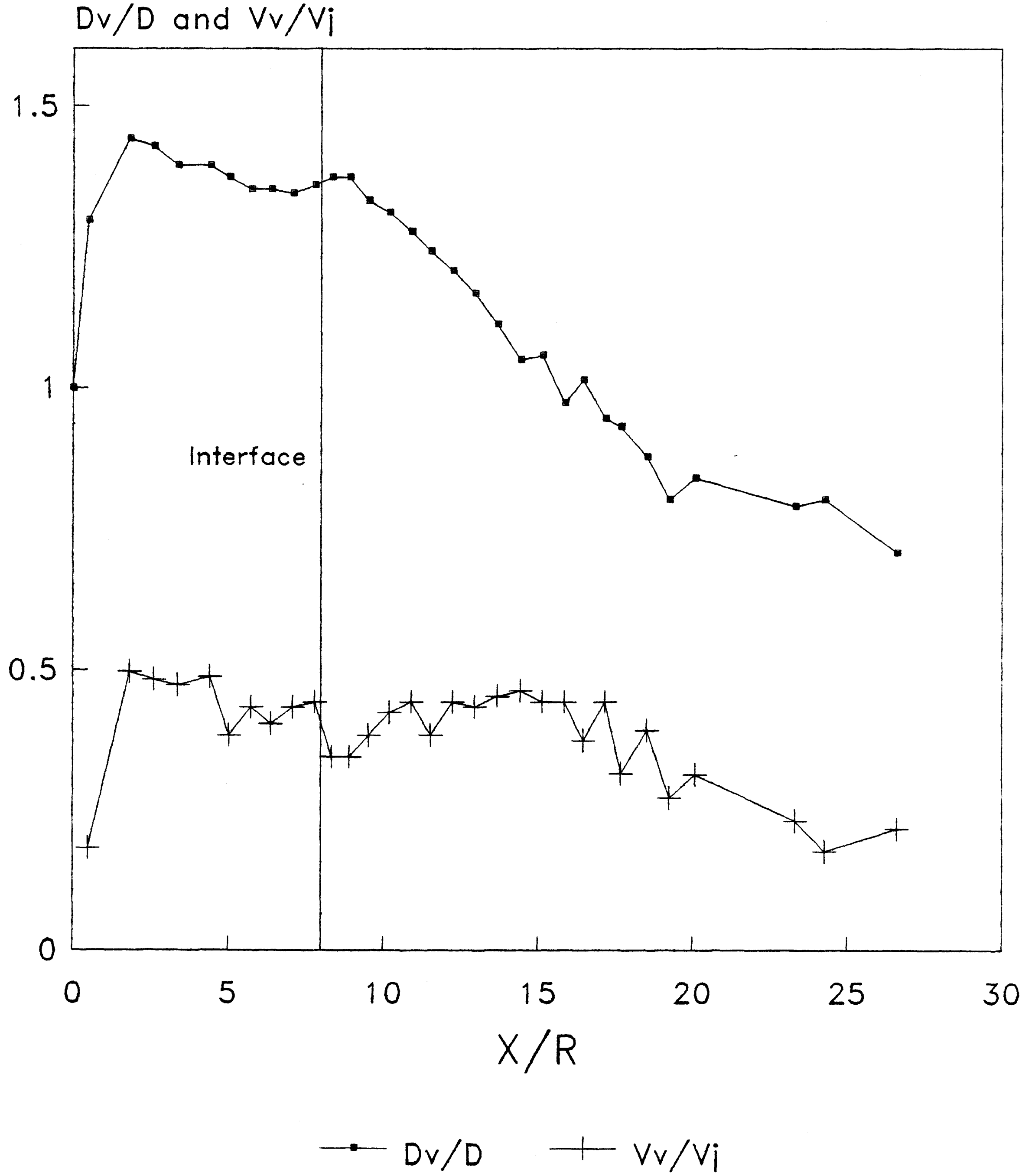


from: expt27

Figure 4.32 Dv/D & Vv/Vj vs. X/R
Re=7570, Ri=.06

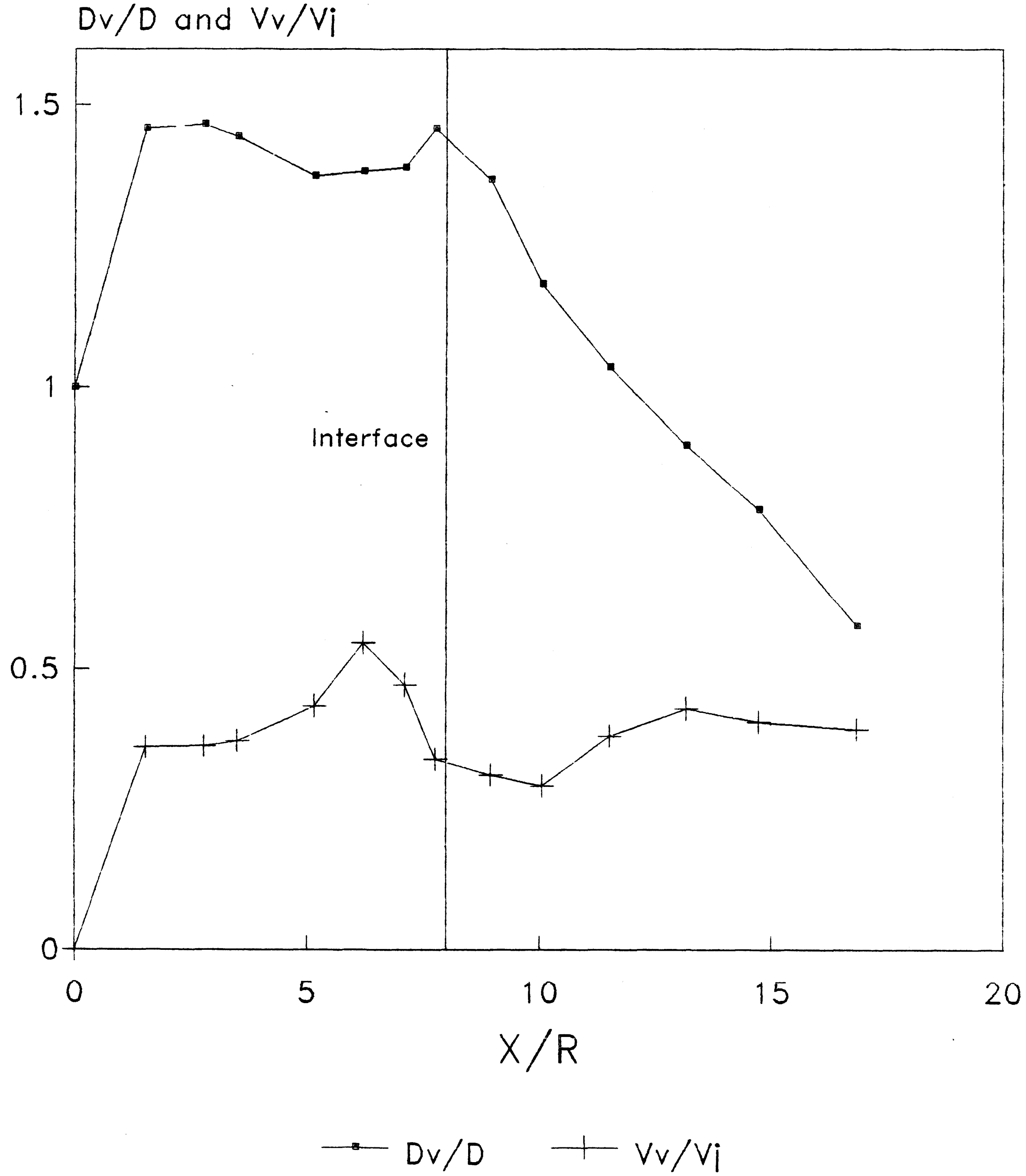


from: expt28

Figure 4.33 Dv/D and Vv/Vj vs. X/R
Re=10540, Ri=.08

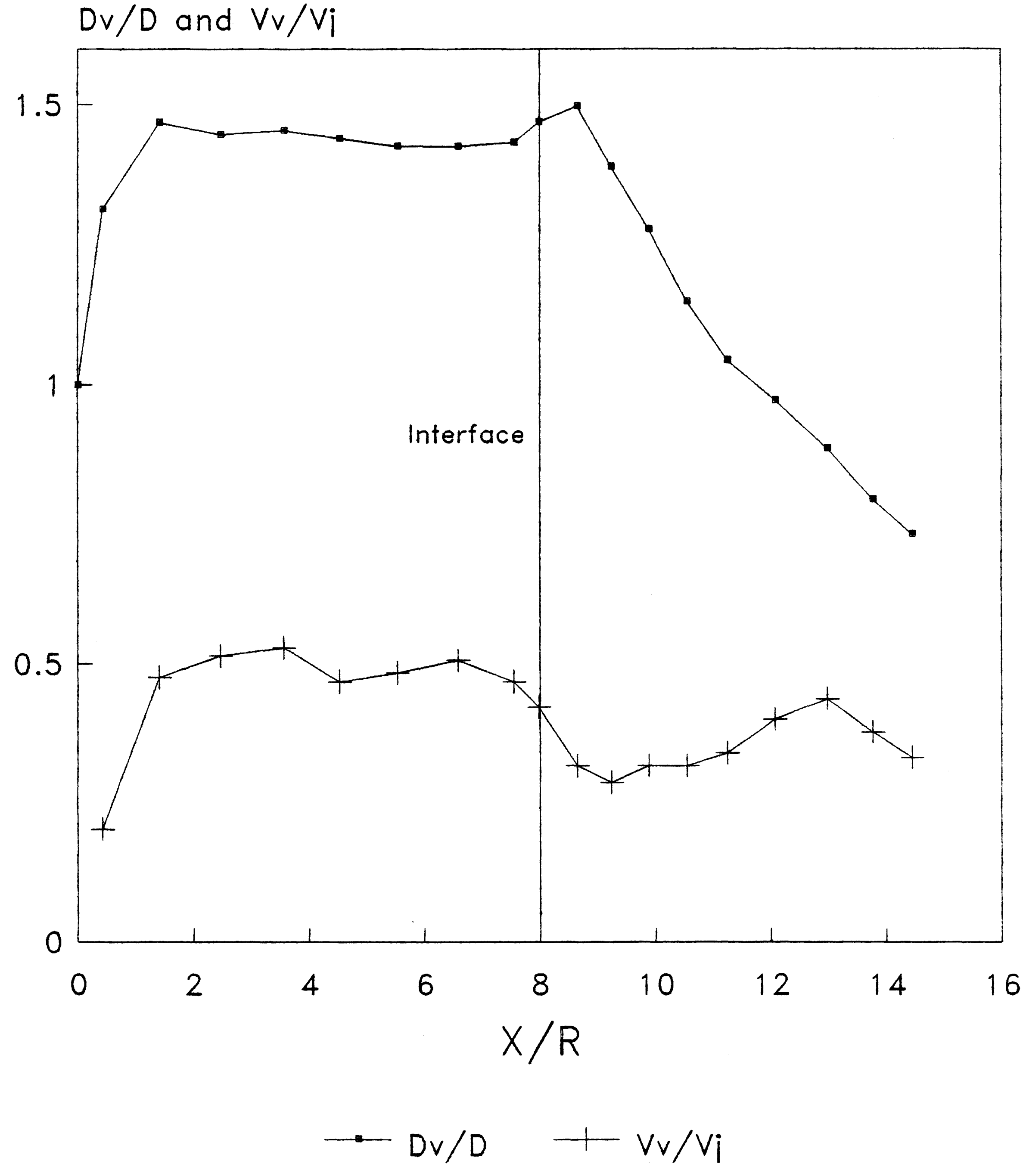


from: expt29

Figure 4.34 Dv/D & Vv/Vj vs. X/R
Re=6010, Ri=.11

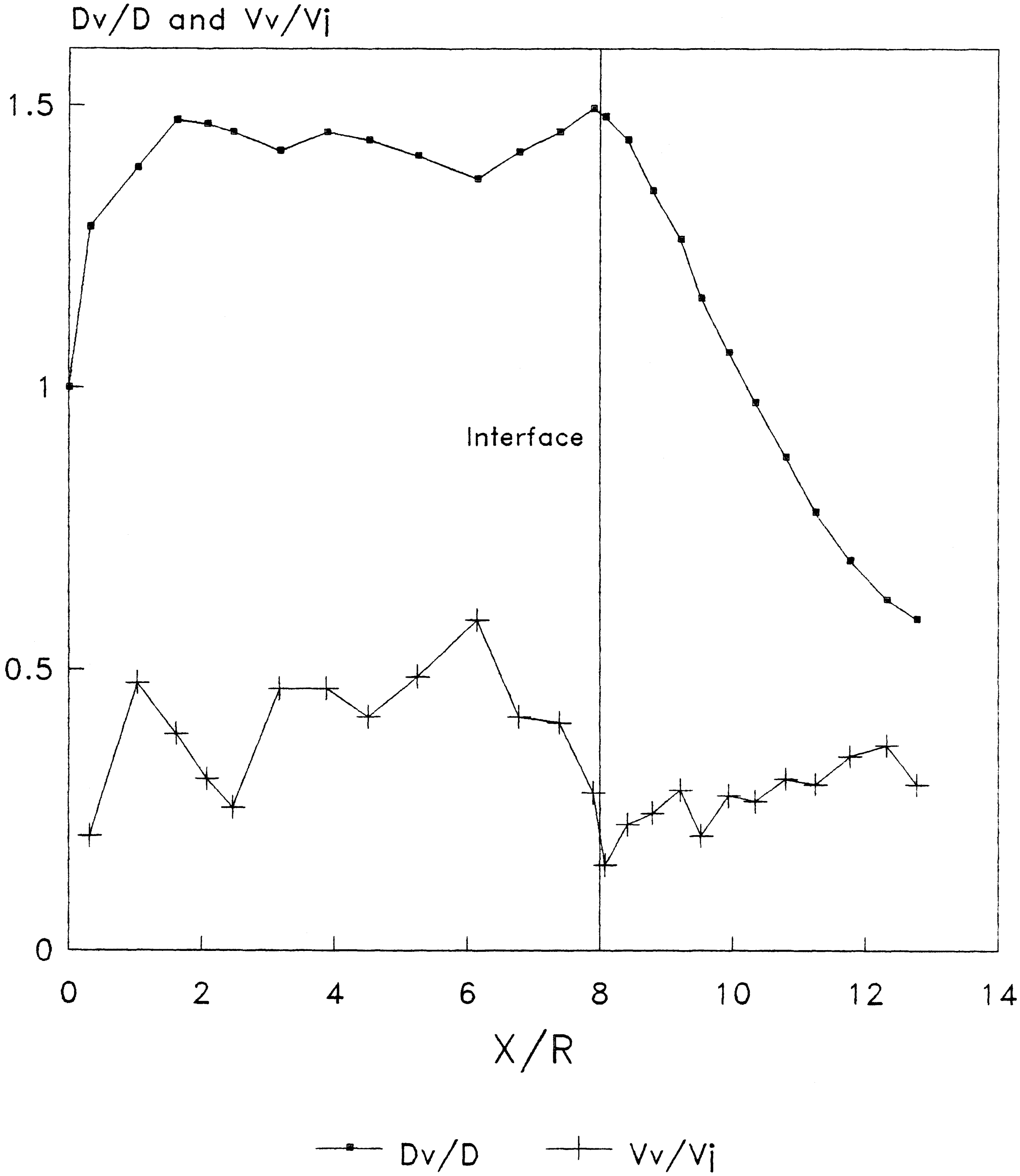


from: expt30

### 4.6.1 Modelling the maximum penetration depth of a vortex ring travelling into a stratified layer using the momentum equation:

The first model described below, developed by Chow(1987), used the continuity equation and the momentum equation to predict the maximum depth of penetration of a vortex ring after it passed through the interface of a stratified layer. In order to simplify the calculations, the following assumptions were made by Chow(1987) about the rings that penetrated into the stratified layer.

1) The detail structure of the ring is ignored, i.e. it ignored the existence of the concentrated core of vorticity inside the volume of the vortex ring. The vortex ring was assumed to be an oblate spheroid travelling with an initial linear velocity Vv (traverse velocity of the ring) before it penetrated into the stratified layer.
2) The effect of the stratified layer on the distribution of vorticity inside the ring is neglected.
3) The velocity of the detrained fluid is assumed to be equal and opposite to the traverse velocity of the vortex ring. This means that the vortex ring will not gain extra forward momentum from the detrainment of fluid into its wake.
4) The entrainment and/or detrainment rate of the vortex ring is assumed to be constant throughout the entire period the ring

was travelling in the stratified layer.

5) The shape of the ring remained similar while it is travelling in the stratified layer.

The first two assumptions were justified on the basis of flow visualization experiments. In these experiments, vortex rings carrying coloured brine solution travelled towards a layer of colourless water. At the initial stage, after the ring penetrated the stratified layer, there was a very distinct boundary between the ring and the surrounding fluid. Also very little mixing occurred at the front of the ring. Hence the decrease in the volume of the vortex ring was mainly due to the detrainment at the rear of the ring. From these observations, it was assumed that the vortex ring was a moving oblate spheriod of fluid that detrained fluid into a wake in its path. The third assumption was made because there was insufficient information about the velocity of the wake behind the ring and it was felt that this was a reasonable assumption. Experimental results showed that the decrease in size of the ring was virtually linearly related to the distance travelled by the ring in the stratified layer, which justified the fourth assumption. Although Maxworthy (1979) observed that the shape of the ring remain similar only during the initial period after the ring penetrated into the stratified layer, the fifth assumption was made to simplify the equations so that a closed form solution could be obtained. After these initial assumptions, the continuity and momentum equations were considered.

Continuity equation:

The continuity equation can be written as:

$$V * \sigma - V_o * \sigma_o = \rho * V_e = \rho * (V - V_o) \quad (4.1)$$

where the mass of the fluid entrained into the ring is equated to the mass of the ring at time (t) minus the initial mass of the ring. Differentiating both sides wrt (R) we get,

$$\frac{d(V * \sigma)}{dR} = \rho \frac{dV}{dR} \quad (4.2)$$

or

$$\frac{d\sigma}{(\rho - \sigma)} = \frac{dV}{V} \quad (4.3)$$

Equation (4.3) can be rewritten into alternative form,

$$\frac{d((\sigma-\rho) * V)}{dR} + \frac{d(\rho * V)}{dR} = \rho \frac{dV}{dR} \quad (4.4)$$

Simplifying Equation (4.4) gives,

$$\frac{d}{dR}[gBV] = \frac{gV}{\alpha\rho_o}\frac{d\rho}{dx} \quad (4.5)$$

where,

$$B = \frac{(\rho - \sigma)}{\rho_o} \tag{4.6}$$

Momentum equation:

The momentum equation can be written as;

$$\frac{d}{dt}\,[\sigma U V] = -\frac{1}{2} C_D' \rho U^2 A + (\rho - \sigma) g V \tag{4.7}$$

In this equation the rate of change of momentum of the ring is equated to the drag force and buoyancy force that is acting on the ring. Substituting Equation (4.5) into (4.7) and rearranging we can obtain;

$$\frac{d(U^2)}{dR} + \left(6 + \frac{3}{4} C_D'\right) \left(\frac{\rho}{\sigma}\right) \frac{U^2}{R} = \left(\frac{\rho}{\sigma} - 1\right) \frac{2g}{\alpha} \tag{4.8}$$

In Equation (4.8), $C_D$' and $\alpha$ are assumed to be constant, but $\rho/\sigma$ is generally not a constant due to the change in the density of the fluid in a ring $\sigma$ created by entrainment of the surrounding fluid. In this case, $\sigma$ is related to the core radius of the ring R or the distance travelled by the ring X. For a vortex ring travelling in a stratified layer with a step change in density gradient, by integrating Equation (4.2) we get;

$$\frac{(\rho - \sigma)}{(\rho - \sigma_o)} = \frac{V_o}{V} = \left(\frac{R}{R_o}\right)^3 \tag{4.9}$$

Rearranging Equation (4.9) we get;

$$\frac{\rho}{\sigma} = \frac{R^3}{(R^3 - E)} \quad where \quad E = B_o R_o^3 \tag{4.10}$$

where,

$$B_o = \frac{(\rho - \sigma_o)}{\rho} \tag{4.11}$$

Substituted Equation (4.10) into Equation (4.8), the final form of the differential equation is;

$$\frac{d(U^2)}{dR} + \frac{NR^2}{(R^3-E)}(U^2) = \frac{2gE}{\alpha}\left(\frac{1}{R^3-E}\right) \tag{4.12}$$

where, $N = 6 + \frac{3}{4} C_D$.

This is a first order linear differential equation which can be solved by the integrating factor method. The general solution for Equation (4.12) is of the form;

$$\left(\frac{U}{U_o}\right)^2 = \left[\frac{1-B_o}{1-\frac{B}{\eta^3}}\right]^{\frac{N}{3}} \eta^{-N}\left[1 + \frac{B_o}{\alpha\,(1-B_o)^{\frac{N}{3}}}\left(\frac{1}{Fr_o}\right)G(\eta)\right] \tag{4.13}$$

where,

$$G(\eta) = \frac{1}{(N-2)}\left[\eta\,(\eta^3-B_o)^{\frac{N-6}{3}}\left(\eta^3 - \frac{2\,(N-4)}{(N-5)}B_o\right) + \frac{(N-3)\,(N-6)}{(N-5)}B_o^2\,(\eta-1) - (1-B_o)^{\frac{N-6}{3}}\left(1-\frac{2\,(N-4)}{(N-5)}B_o\right)\right] \tag{4.14}$$

for $6 < N < 10$.

When a ring reaches its maximum penetration depth, it will stop travelling forward, and therefore the ratio of U/Uo = 0. Since all the parameters on the right hand side of Equation (4.13) are known except for the value of $\eta$ which is the ratio of $R/R_o$, by substituting U/Uo = 0 into equation (4.13), the final value of R/Ro can be determined. Since dR/dx is a constant, by integrating and rearranging dR/dx, it can be shown that the ratio of R/Ro is related to the penetration depth by;

$$X_m = \frac{\eta R_o - 1}{\alpha} \tag{4.15}$$

and therefore the maximum distance travelled by the ring can be calculated from Equation (4.15).

In order to obtain a solution to Equation (4.13), the following parameters are required. They are;

1) $\sigma$ - density of the vortex ring,

2) $\rho$ - density of the ambient fluid,

3) $R_o$ - initial core radius of the vortex ring,

4) $U_o$ - initial velocity of the vortex ring,

5) $C_D'$ - drag coefficient on the vortex ring ($C_D'$ = .096) Maxworthy (1974), and

6) $\alpha$ - entrainment rate of the vortex ring from Maxworthy (1974), $\alpha$ = 0.011.

After all these values were substitute into the right hand side of Equation (4.13), $\eta$ was varied until the left hand side of Equation (4.13) reached or approached zero. The results are presented in Figure 4.35 which shows that the right hand side of Equation (4.13) goes to zero when $\eta$ is approximately 1.08 - 1.09. However, flow visualization experiments showed that the size of the vortex ring decreased after the vortex ring penetrated the stratified layer. Therefore, this theoretical solution is incorrect and unacceptable as it predicts a growth of the ring after it has penetrated into the stratified layer.

The primary cause of the failure of this model appears to be the assumption that the vortex ring continues to entrain fluid after it penetrates into the stratified layer. Although this might be true, as Maxworthy (1977) suggested, that the vortex ring is entraining fluid from its surroundings, the behaviour of this ring is dominated by the detrainment from the vortex ring into its wake. Following the failure of Chow's model, this momentum model was modified. This time the detrainment rate of the vortex ring was taken into account.

Figure 4.35 Results from Chow's model: RHS of eqn. 9 vs. $\eta$.

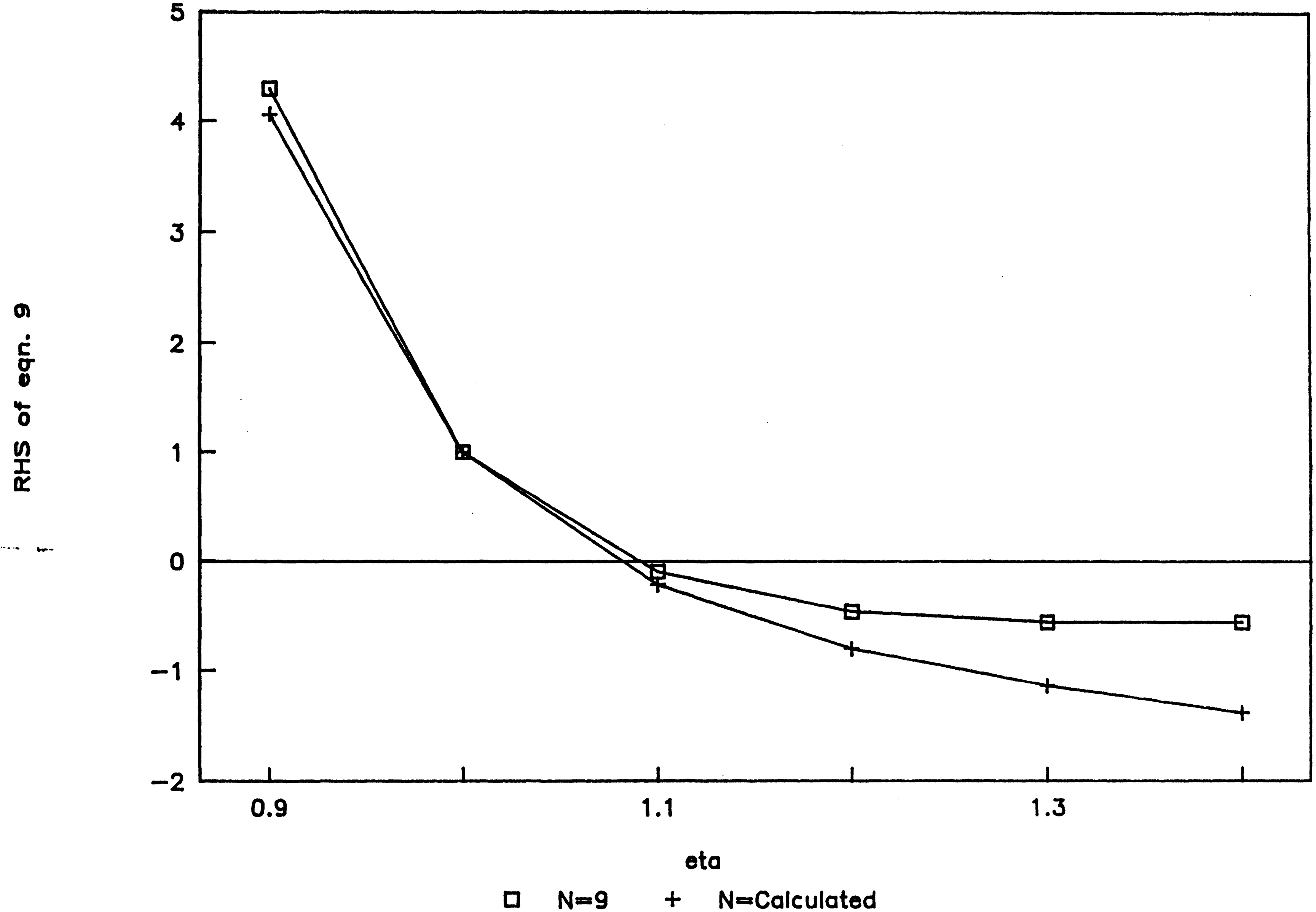

### 4.6.2 Modified momentum balance model:

After reviewing the reason for the failure of the initial momentum balance model, a second model was developed with modifications which covered the short comings of the initial model. The revised model assumes that the size of the vortex ring, after it penetrates into the stratified layer, is governed by the detrainment rate of the vortex ring (dR/dx). The detrainment rate was assumed to be a constant, as observed from the experimental result. Experiments showed that the detrainment rate of fluid from the ring was much faster than the entrainment rate of surrounding fluid. Hence, the entrainment of surrounding fluid into the ring was neglected in this model. Furthermore, the change in density of the fluid in the ring due to the entrainment of fluid was also neglected

#### Continuity equation:

With these assumptions, the continuity equation can be written as,

$$\frac{d}{dt}\,(V-V_o)\,\sigma = \dot{m} \tag{4.16}$$

Since V, R and x are only a function time and density only, Equation (4.1) can be transformed into,

$$\sigma\,\frac{dV}{dR}\,\frac{dR}{dx}\,\frac{dx}{dt} = \dot{m} \tag{4.17}$$

where,

$$\frac{dR}{dx} = \alpha_d \qquad \text{and} \qquad \frac{dx}{dt} = U$$

Moreover the volume of the vortex ring can be given as,

$$V = K\pi R^3 \tag{4.18}$$

By differentiating Equation (4.18) wrt dR we can get,

$$\frac{dV}{dR} = 3K\pi R^3 \tag{4.19}$$

Substituting Equation (4.19) into Equation (4.17) we get,

$$\dot{m} = 3K\pi R^2 \sigma \alpha_d U \tag{4.20}$$

In order to use the continuity equation in the form of Equation (4.20), the momentum Equation (4.7), needs to be modified.

**Momentum equation:**

Since the mass flow rate of fluid out of the ring was equal to,

$$\dot{m} = \sigma U \tag{4.21}$$

The momentum equation can be written as,

$$\dot{m}U + m\frac{dU}{dt} = -\frac{1}{2}C_D \rho U^2 K_2 \pi R^2 - (\sigma - \rho)\, gV \tag{4.22}$$

Substituting Equation (4.20) into Equation (4.22) and realising that,

$$\frac{du}{dt} = \frac{dU}{dR}\cdot\frac{dR}{dx}\cdot\frac{dx}{dt} = \frac{dU}{dR}\alpha_d U \qquad (4.23)$$

The final form of the momentum equation becomes,

$$\begin{aligned}&\sigma V\alpha_d U\frac{dU}{dR} + 3K\pi R^2\sigma\alpha_d U^2 = \\ &-\frac{1}{2}C_D\rho U^2 K_2\pi R^2 - (\sigma-\rho)\,gV\end{aligned} \qquad (4.24)$$

Rearranging Equation (4.24) gets,

$$U\frac{dU}{dR} + \left(3 + \frac{\frac{1}{2}C_D\rho K_2}{\sigma\alpha_d K}\right)\frac{U^2}{R} = -\frac{(\sigma-\rho)\,g}{\sigma\alpha_d} \qquad (4.25)$$

Reducing Equation (4.25) into a non-dimensionalizing form by replacing U with $U^*$ and R with $R^*$. Then,

$$U^* = \frac{U}{U_j} \qquad and \qquad R^* = \frac{R}{Rm}$$

After substituting these dimensionless variables into Equation (4.25)

and rearranging we obtain,

$$U^*\frac{dU^*}{dR^*} + \left(3 + \frac{1}{2}\frac{C_D\rho_2 K_2}{\rho_1\alpha_d K}\right)\frac{U^{*2}}{R^*} = -\frac{Ri}{\alpha_d} \qquad (4.26)$$

Let z = $U^{*2}$, then dz = 2 $U^*$ d $U^*$ and realizing the following terms are

constants in the calculation.

Equation (4.26) can be written as,

$$C_1 = 2\,(3 + 0.048\frac{\rho}{\sigma\alpha_d})$$

$$C_2 = -\frac{2Ri}{\alpha_d}$$

$$\frac{dz}{dR^*} + C_1 \frac{z}{R^*} = C_2 \tag{4.27}$$

This equation is a first order linear differential equation which can be solved by the variation of parameters method, with the initial conditions of,

$$@\ x = 0,\ R_o^* = \frac{R_o}{Rm},\ U_o^* = \frac{U_o}{U_j}$$

The closed form solution is given in terms of the constants $C_1$ and $C_2$ as follows,

$$U^{*2} = -\frac{C_2}{C_1 - 1} R^* + \left( \frac{U_o^{*2}}{R_o^{*C_1}} + \frac{C_2}{(C_1-1)\ (R_o^{*C_1-1})} \right) R^{*C_1} \tag{4.28}$$

Empirical data were substituted into Equation (4.28) to determine the variation of the velocity with respect to the change in radius of the vortex ring. By setting $U^* = 0$, the maximum penetration depth into a stratified layer of a vortex ring could be determined. When $U^* = 0$, the ring still had a certain diameter or $R^*$. With this value of $R^*$, the maximum penetration can be obtained from,

$$\frac{R_o^* - R^*}{\alpha_d} = \frac{X_p}{Rm} \tag{4.29}$$

The results from four different experiments were used to test this model to determine whether it would be able to predict the maximum penetration depth of a vortex ring that was travelling into a stratified layer. These four experiments were identified as: 2PDEC142, EXPT22, EXPT28 and EXPT30. The experimental data required by the model were: $\rho_H$, $\rho_L$, detrainment rate, Ri, $U_o^*$ and $R_o^*$. After substituting these initial conditions into Equation (4.28), the value of $R^*$ was varied until the value of $U^*$ approached zero. As $U^* = 0$, this meant the vortex ring had reached its maximum penetration depth into the upper stratified layer. This distance can be determined by substituting the value of $R^*$, where $U^* = 0$, into Equation (4.29). The calculated values of $R^*$ and $U^*$ were plotted against X/R and are shown in Figures 4.36 - 4.39. A comparison between the experimental results and the results obtained from the model are given below:

| Filename | Calculated Xp/R | Experimental Xp/R |
|---|---|---|
| 2PDEC142 | 0.31 | 1.6 |
| EXPT22 | 0.51 | 3.5 |
| EXPT28 | 1.57 | 12.6 |
| EXPT30 | 0.68 | 6.9 |

Table 4.1 A comparison of the maximum penetration depth attained by a vortex ring travelling in a stratified fluid between the calculated and measured value.

These results show that the maximum penetration depths of the ring predicted by the model, for the four test cases, were appreciably smaller than the actual empirical values obtained in the experiments. The reasons for the discrepancies between this model and the experimental data are discussed in the next section.

Figure 4.36 U* and R* vs. X/R
Numerical Results

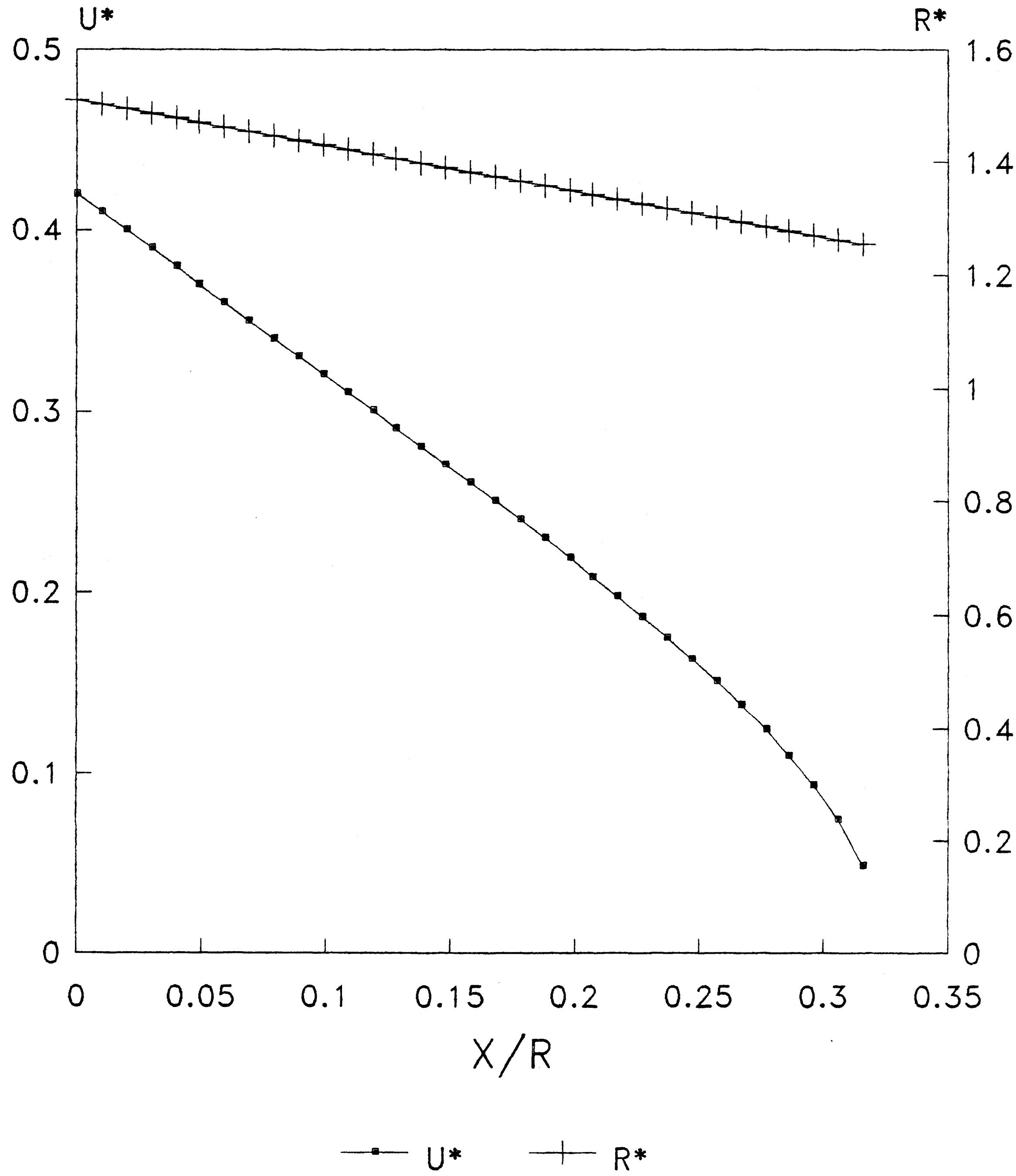


newstra1

Figure 4.37 U* and R* vs. X/R
Numerical Results

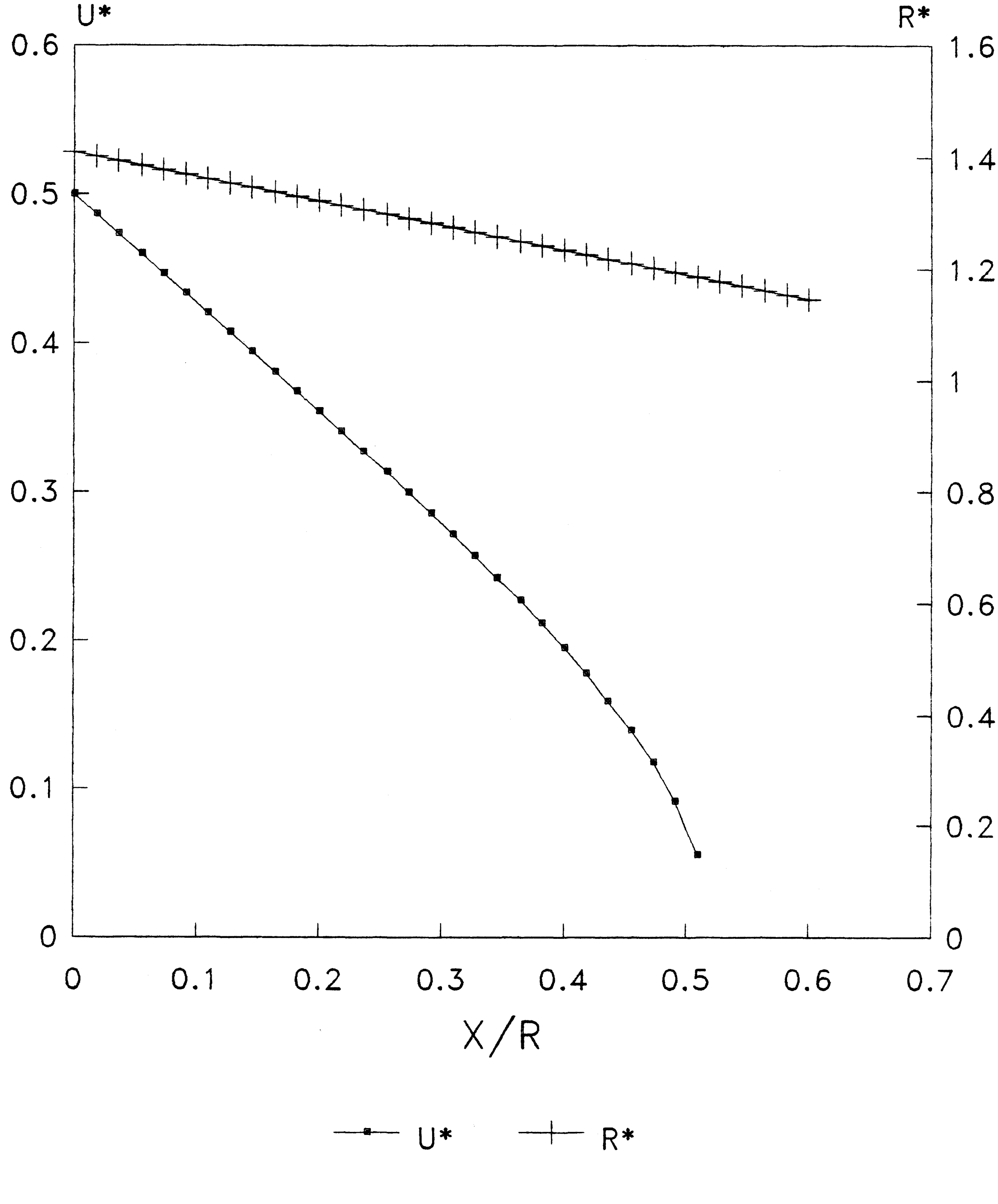


newstra2

Figure 4.38 U* and R* vs. X/R
Numerical Results

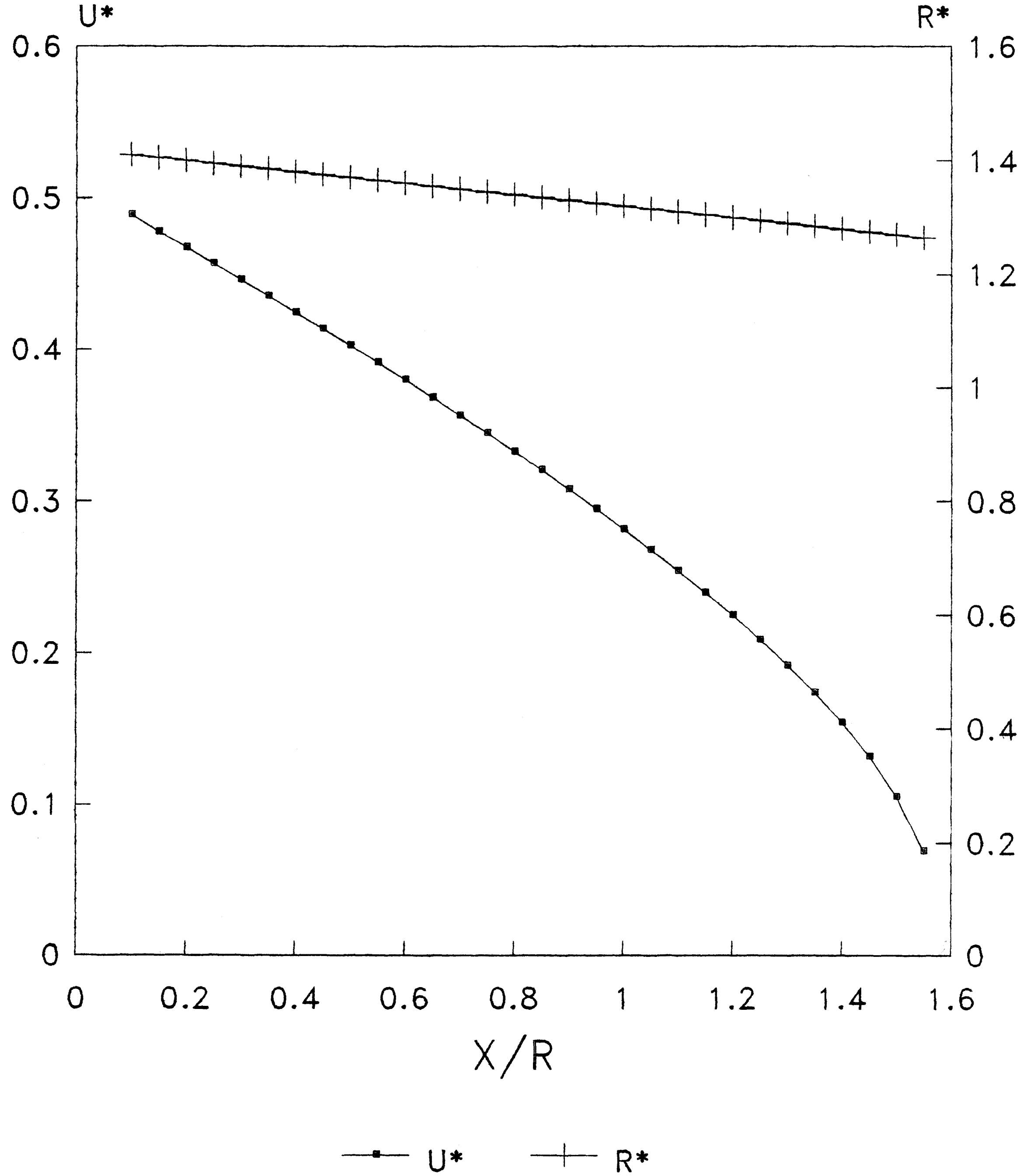


newstra3

Figure 4.39 U* and R* vs. X/R
Numerical Results

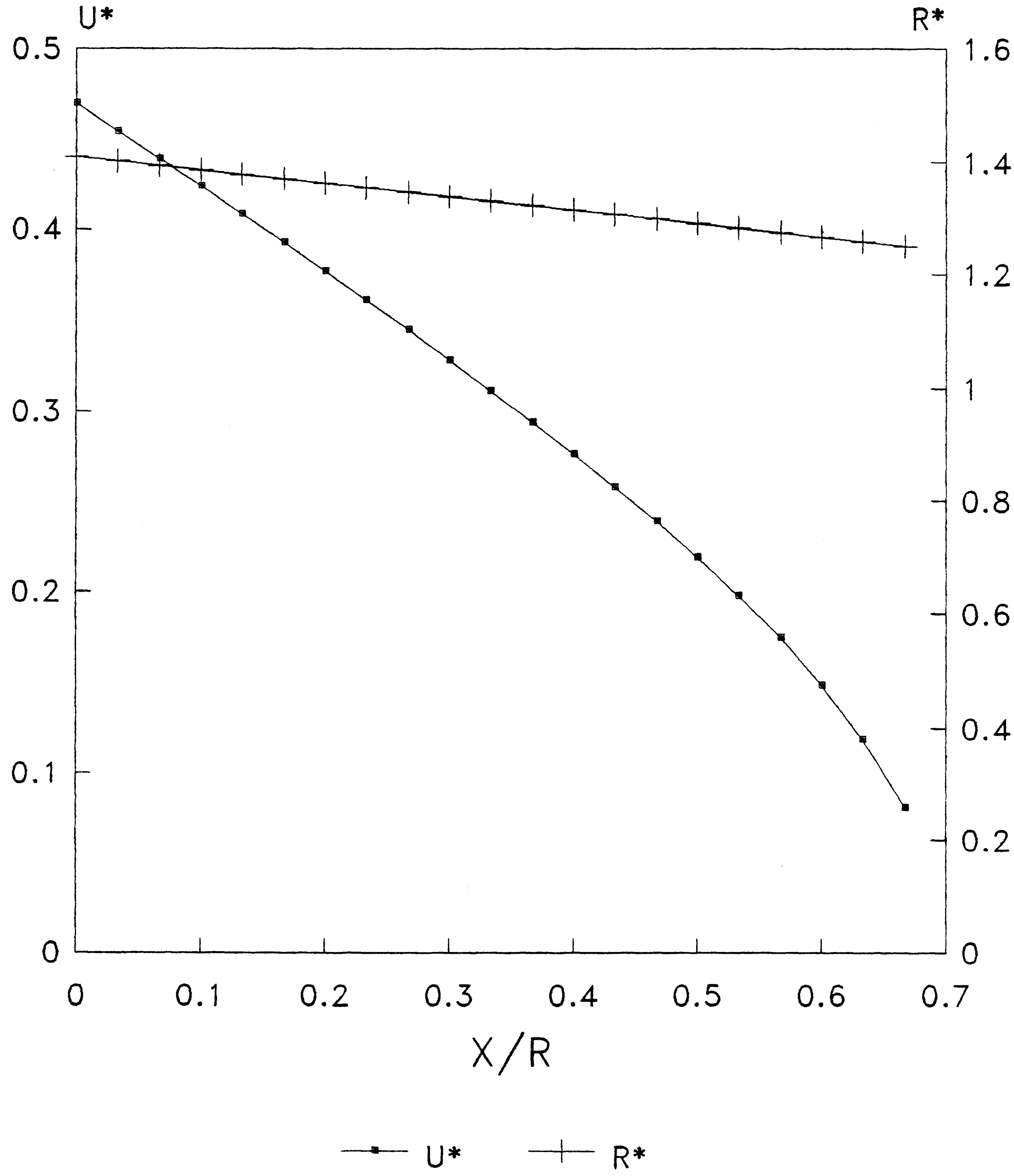


newstra4

Discussion:

The first item to be discussed is the derived dimensionless variables. A total of five dimensionless parameters were derived, Xm/R, Lm/Rm or Lm/Dm, Li/Rm, Xwall/Rm and Ri. Only three of these five parameters were varied in this study. The two variables that were held constant being Li/Rm =8 and Xwall/Rm =6 or Xwall/Rcore =4. Referring back to the literature review in Chapter 2, it was recommended by Brasseur (1986) that the ratio of Xwall/Rcore should be greater than or equal to 5 in order to prevent the proximity of the walls of the tank from reducing the velocity of the ring. In the present case, Xwall/Rcore was only 4 which meant the ring would possibly be slowed down due to the close proximity of the walls of the tank. This led to the decision to limit the value of Li/Rm to 8. With Li/Rm=8, the fully formed ring would be approximately 3Rm from the interface of the stratified layer. This meant the ring only had to travel a short distance before arriving at the interface, and therefore minimized the effect of the walls on the velocity of the ring. Once a ring penetrated into the stratified layer, the dominant effect acting on the ring was the buoyancy force due to the density gradient between the fluid inside the ring and its surrounding. Since the size of a ring continued to decrease after it penetrated the interface, the wall effect became less significant. Another reason for choosing Li/Rm =8 was that Latto (1986) determined that optimum vortex rings could be generated when $Lm/Dm = 2.8$ or $Lm/Rm = 5.6$. Therefore by choosing $Li/Rm = 8$, it allowed enough space for the ring to form properly during its generation stage before travelling towards the interface of the stratified layer.

Two types of stratified layers were used in these experiments. The first type of stratified layer consisted of hot/cold water. The disadvantage of this type of stratified layer was the lack of control of the density distribution at the interface due to heat transfer and mixing between the hot and cold water layer while the tank was being filled. Figure 4.40 presents a typical temperature distribution, obtained using five thermocouples in a region close to the interface. The temperature distribution was almost linear in this region. Since the density of water is proportion to the temperature, this meant there was a relatively large variation of density in the vicinity of the interface. However a sharp density gradient was required, and therefore this type of stratified layer was not used any more in later experiments. It was decided that a more convenient fluid combination would be brine and water.

Figure 4.40 Temperature around the interface of the stratified layer (proportional to the density of the fluid) vs. the location of the thermal couple.

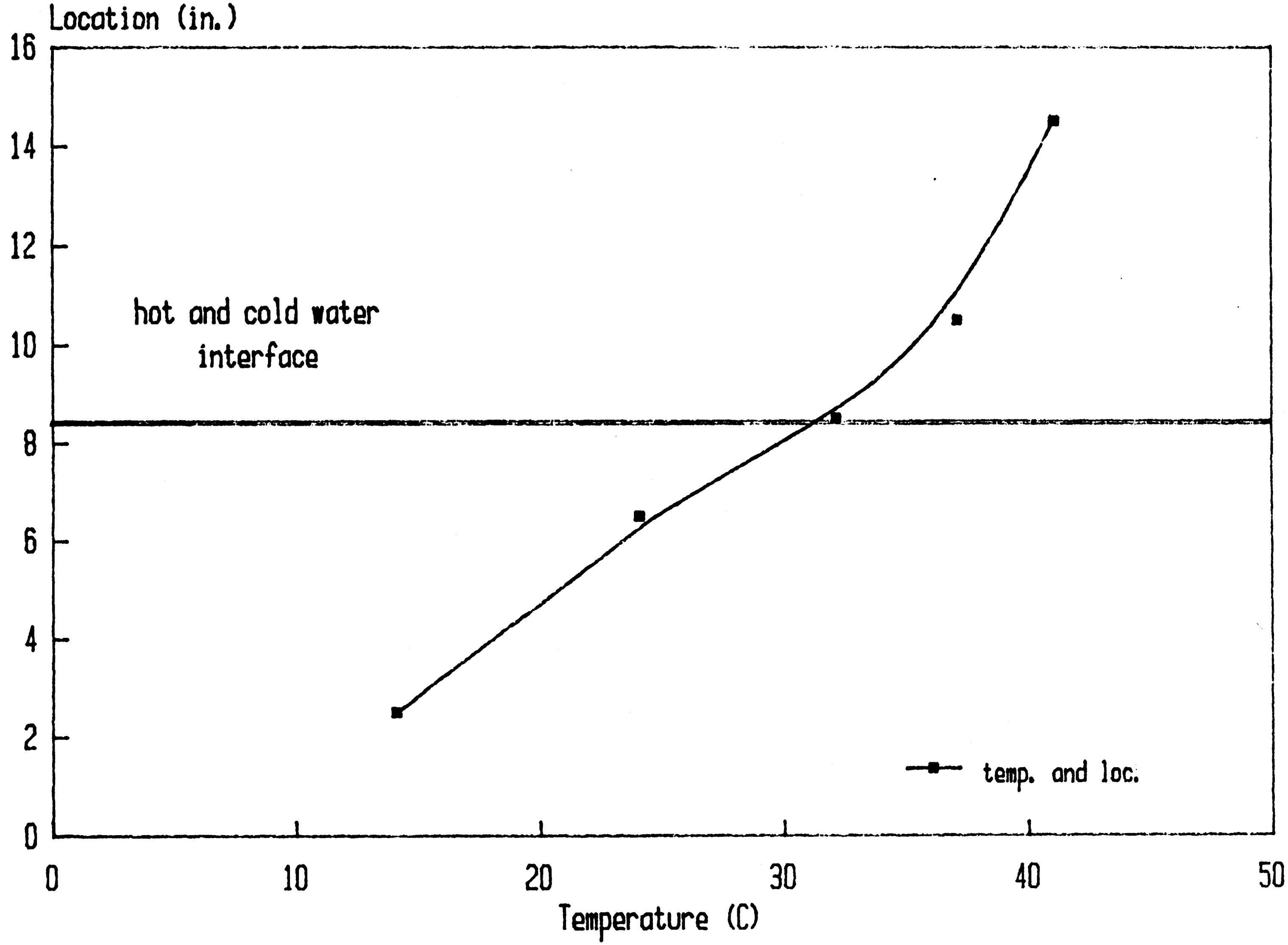

The advantages of this type of stratified layer were:

1) A stratified layer with a step change in density gradient can be obtained. This was observed by the sudden change in refractive index at the interface in all the video recordings of the experiments.

2) The density of the brine could be varied by diluting with water, and therefore the dependence of the penetration depth on the Reynolds number could also be investigated.

Baird et al (1979) indicated the need to be able to predict the maximum penetration depth that a vortex ring could travel into a stratified fluid. This information, as described by Baird (1979), would greatly affect the mixing efficiency of vortex ring mixers. In this Chapter, a momentum balance model was developed in an attempt to predict the penetration depth of a vortex ring travelling in a stratified fluid. Results showed the model always under predicted the actual penetration depth of the vortex rings. This meant the momentum balance model over predicted the momentum loss from the ring, while it was travelling in the stratified fluid. In other words, linear momentum loss through detrainment apparently is not the mechanism which causes a vortex ring to slow down after it travels through a stratified layer. Hence this model was not suitable for predicting the maximum penetration depth of a vortex ring when it travels in a stratified fluid. Either a more accurate theoretical model or an empirical relationship between the penetration depth of a ring and the corresponding Richardson number Ri had to be obtained.

Irdumsa et al (1983) showed due to the difference in boundary conditions, vortex rings generated from a tube are larger in size and have slower translational velocity than those rings generated from an orifice plate. In the present experiments, only a tube type generator was used. The measurements of the core diameter and the traverse velocity obtained between the period after the ring was completely formed to where it came close to the interface of the stratified layer are shown in Figure 4.41. The following linear relationship was fitted to these data:

$$\frac{Dv}{Dm} = 0.14349 \frac{Lm}{Dm} + 1.090691$$

These results were compared with those obtained by Latto (1986), who observed that for rings generated from an orifice plate, Dv/Dm = 1.28 when Lm/Dm = 2.8. Substituting the value of Lm/Dm = 2.8 into the above equation gives Dv/Dm = 1.49 for rings generated from a tube. This meant rings generated at a tube were considerably larger than rings generated at an orifice plate.

Figure 4.41 Dv/D vs. L/D

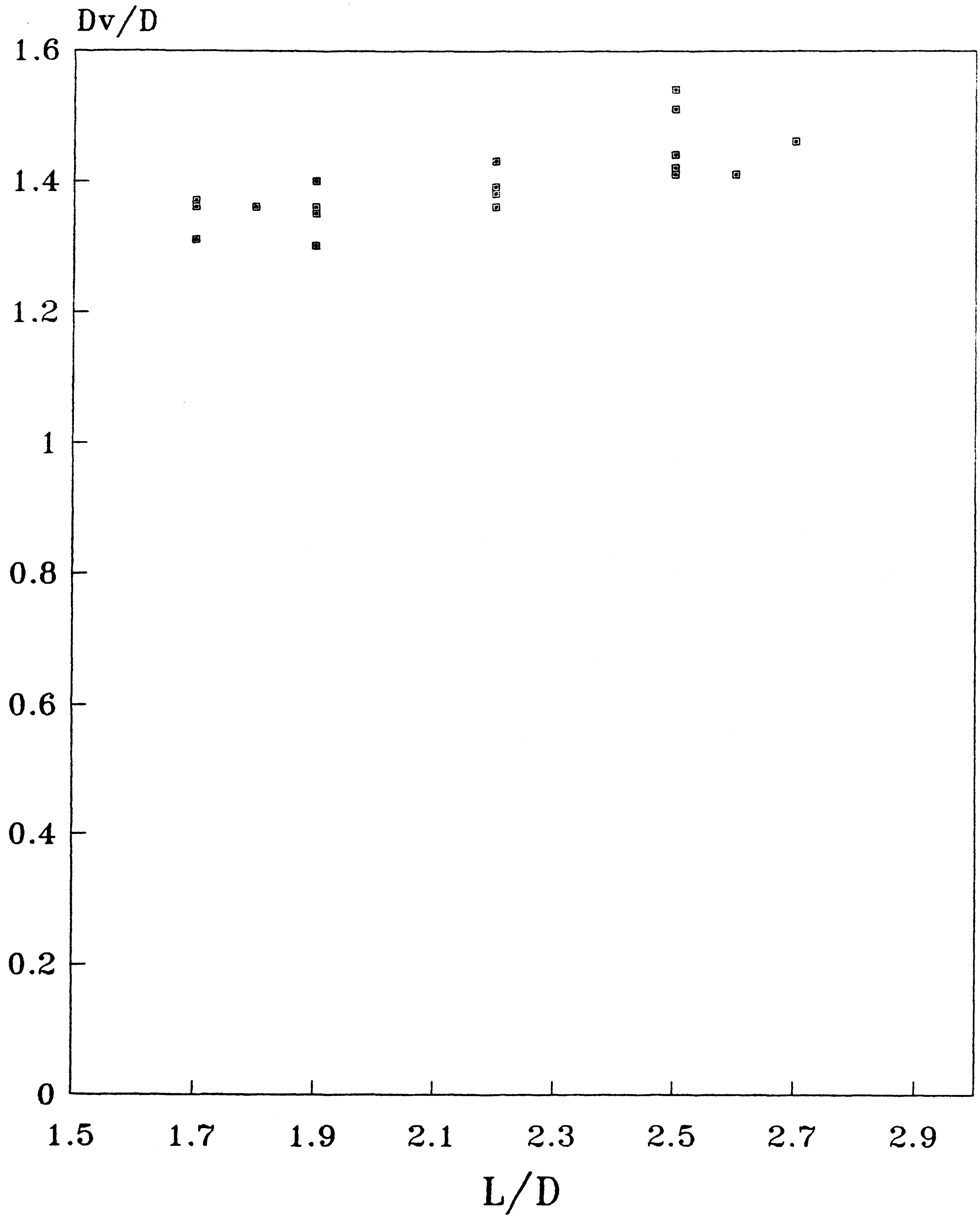

Irdumsa et al (1983) derived a theoretical curve that would distinguish the difference between rings generated from a tube and an orifice. Experimental data obtained in this thesis were fitted to this curve and the results are shown in Figure 4.42. In all the experiments performed, the value of $U^*$ was always less than unity. According to Irdumsa (1983), when $U^* < 1$, vortex rings were generated at a tube. This corresponds to the equipment that was used to generate vortex ring in the present experiments. However, there seems to be a discrepancy between the experimental data and the theoretical values, as $U^*$ continued to decrease, and the value of $D^*$ did not increase any further. It seemed there is a limit to the maximum size the ring could attain, no matter how much further the value of $U^*$ was decreased. This was not observed by Irdumsa et al(1983).

# Figure 4.42 D* vs U*

Theory: U* = 2.4711 * D*^-2

Irdumsa et al (1983)

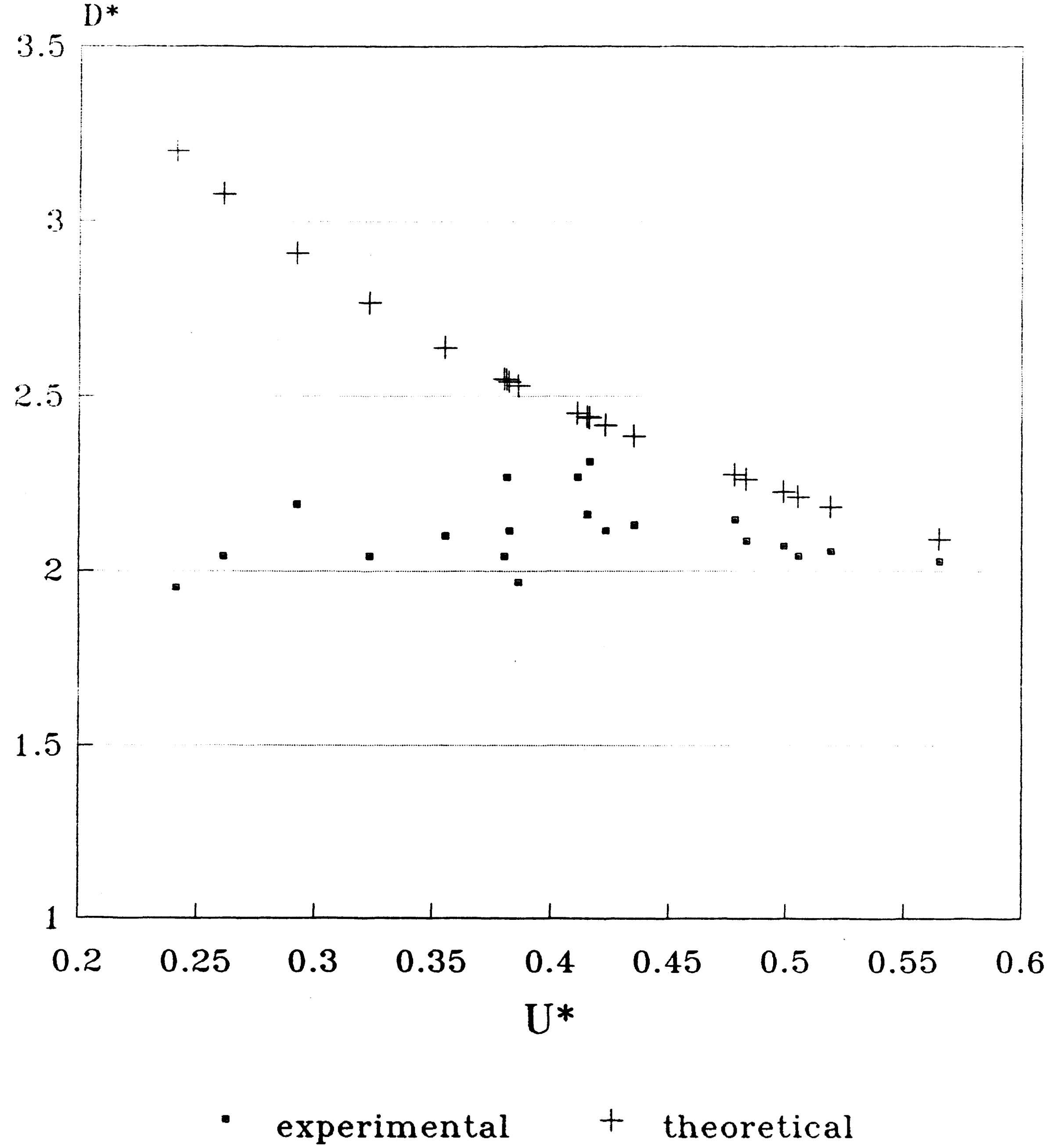

Since an accurate theoretical penetration depth model was not achieved, a series of experiments were performed in order to obtain an empirical relationship relating the maximum penetration depth and Ri. The results of these experiments were shown in Figure 4.43. Only the data from the brine and water stratified layer experiments were used in the graph. The Figure shows that all the data points, except two, appear to follow the same trend or fell along a single curve. The range of jet Reynolds number, $Re_{jet}$, used was between 4000 - 11000. The experiments were limited to this range of Re because the experimental apparatus was not able to generate a jet with a higher velocity. However, within this range of Re, it showed that the relationship between the penetration depth (Xm/Rm) and Ri was independent of Re. This was demonstrated at Ri of 0.06, 0.03 and 0.12 where Xm/Rm was almost the same for various $Re_{m}$. This supported the original proposal of combining the two non-dimensional 'Pi' groups together to form a Ri which would eliminate the affect of the viscosity of the fluid.

Figure 4.43 Xp/R vs. Ri at various Reynolds number

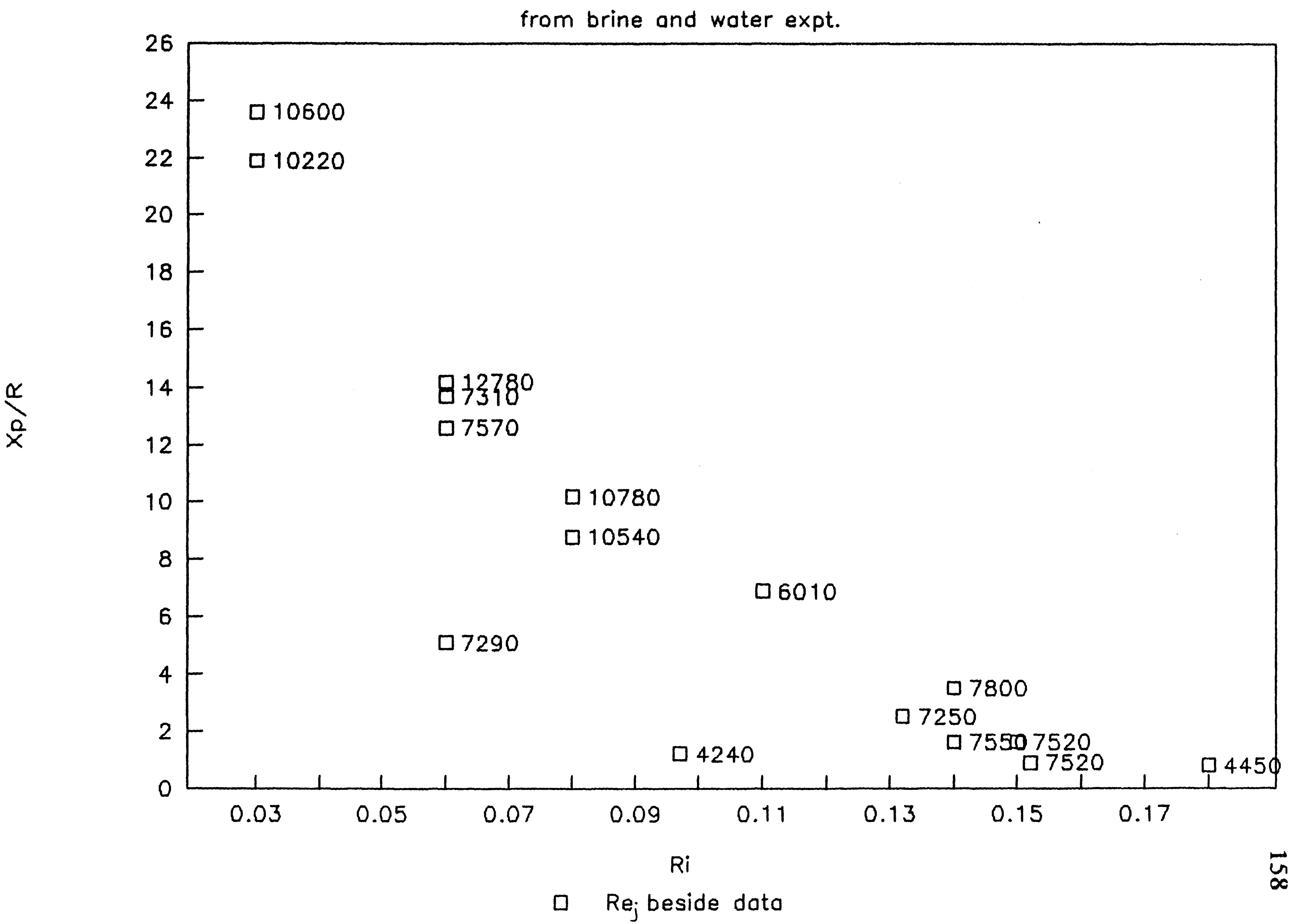

Since Figure 4.43 showed some form of power relation between Xm/Rm and Ri, a log plot was tried. In this case it would be Xm/Rm vs. $\log_{10}$Ri and the results are given in Figure 4.44. The resulting data could be correlated with a straight line. A linear regression performed with these data points resulted in the following equation:

$$\frac{Xm}{Rm} = -29.7\log_{10}Ri - 22.7 \qquad (4.30)$$

where $0.17 < Ri < 0.027$.

This relationship could be used to predict the maximum penetration depth of a vortex ring travelling in a stratified layer with a sharp density gradient. It shows that when Ri = 0.17, a vortex ring will not be able to penetrate an interface, or Xm/R = 0. On the other hand, it also shows that when $Ri \rightarrow 0$, $Xm \rightarrow \infty$, which correspond to the results of a vortex ring travelling in an ideal fluid with uniform density and no viscosity. This type of vortex ring could travel a very long distance, (up to 200 times the diameter of the orifice), as noted by Baird et al (1977). Although Equation (4.30) does not take into account the proximity of the wall boundaries of the tank, it is anticipated that it will still hold true for a larger tank than the one used in this study, with a larger Xwall/Rm ratio and an interface that is further away from the orifice than was investigated. More experimental data obtained under similar initial conditions obtained from an undergraduate thesis project, Strange (1991), were also added to the empirical relationship between Xm/R and Ri to determine how well this relationship would fit with other experimental data. The result is shown in Figure 4.45. Although these data were a little scattered at low Ri, they happen to follow the empirical curve fairly well.

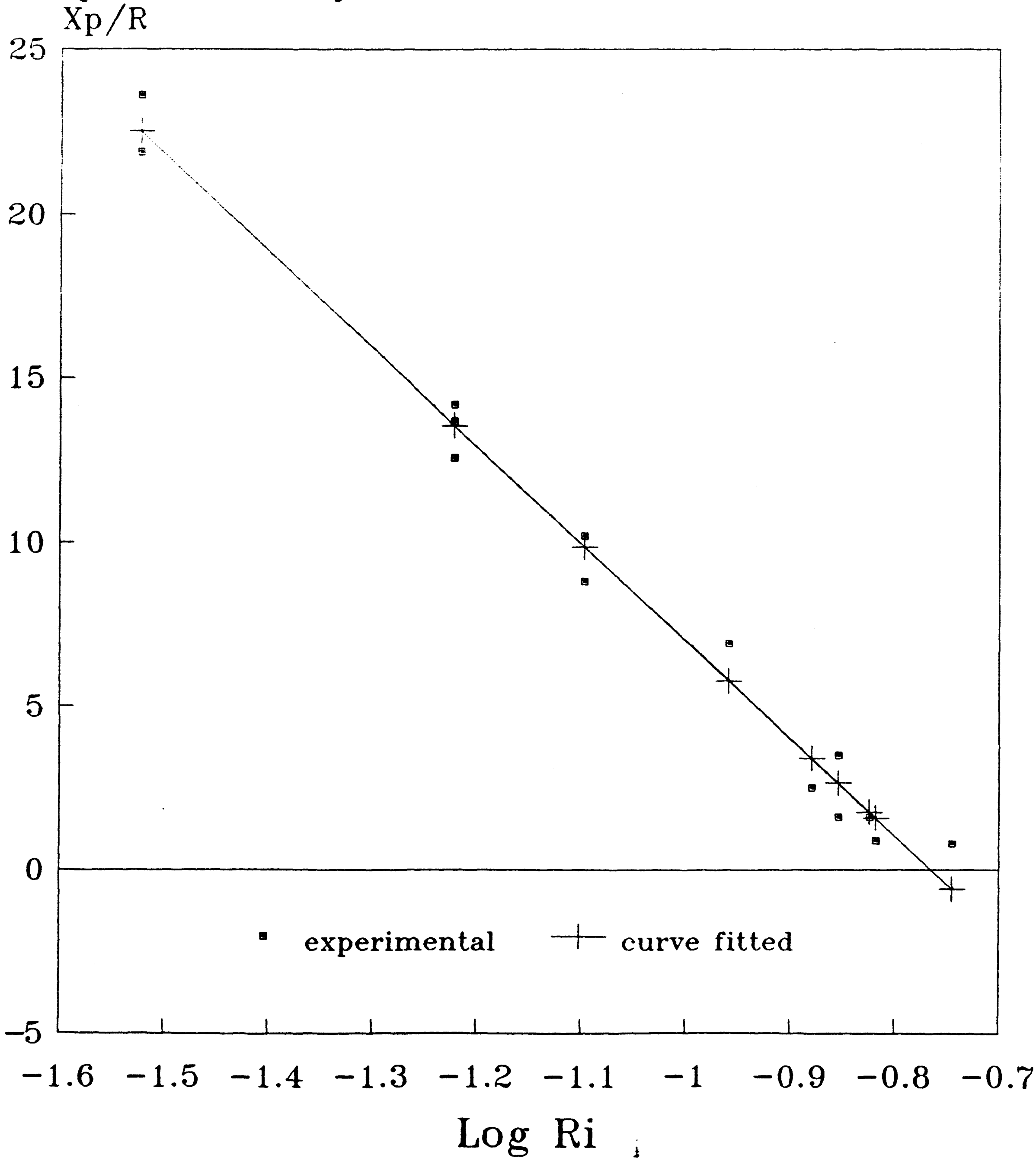


Figure 4.44 Xp/R vs. $\log_{10}$Ri

# Figure 4.45 Xp/R vs. log Ri

From brine and water expt.

$Xp = -29.7(\log Ri) - 22.7$

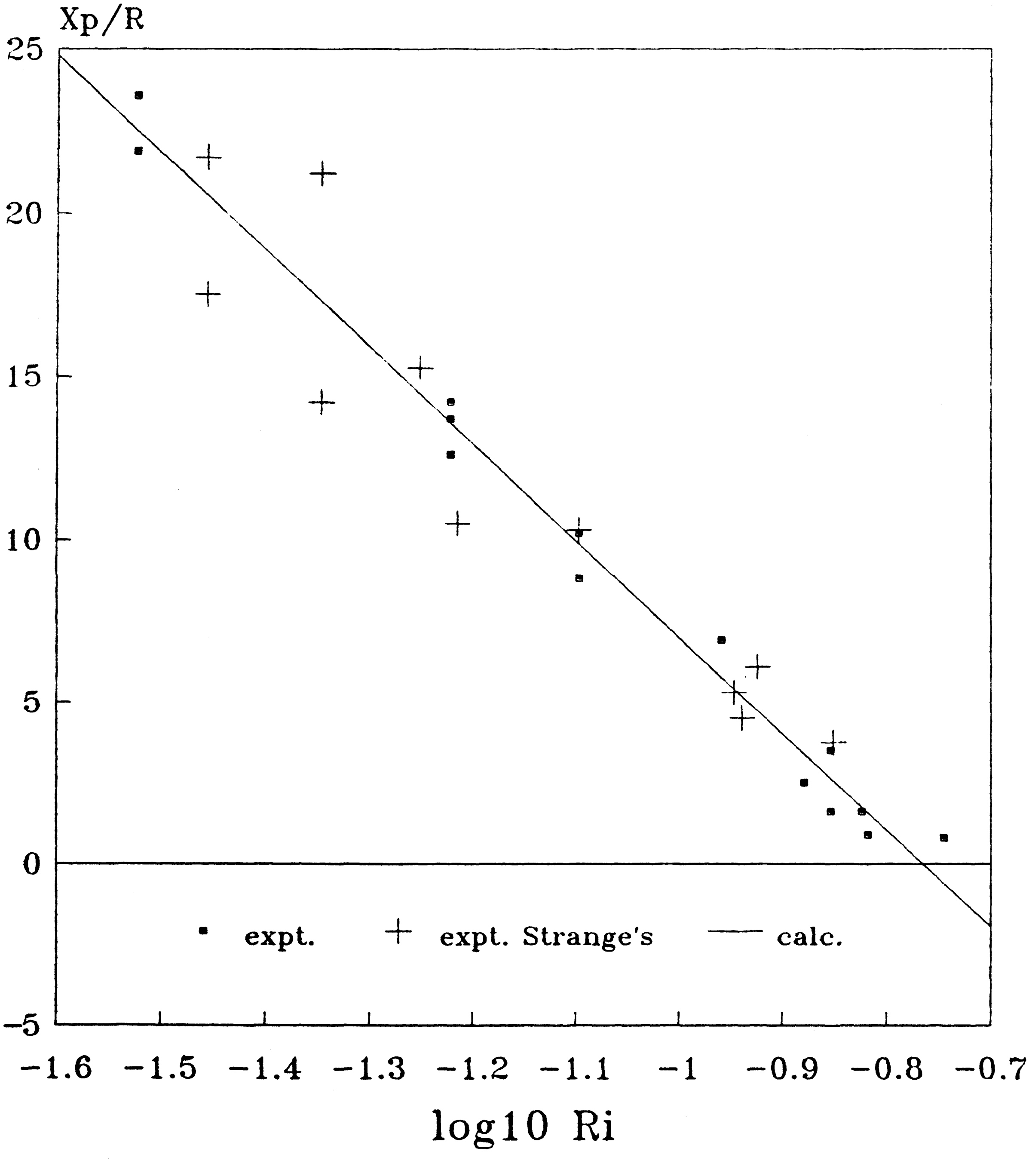


d:\stratify\hgdata\23b

4.8 Conclusion:

In this chapter, the importance of a knowledge about the velocity and volume of the jet injected during the formation of a vortex ring was demonstrated. Without the correlation between the volume of the jet and the theoretical jet velocity, obtained in Chapter 3, Figure 4.43 of Dv/Dm vs. Lm/Dm and Figure 4.44 of maximum penetration depth vs. Ri, could not be obtained .

Through the use of various flow visualization techniques, the amount of mixing that was caused by a single vortex ring when it travelled in a stratified fluid was demonstrated. When a vortex ring travels in a fluid with different density than that of the fluid in the ring, it mixes this surrounding fluid with the fluid in the ring by continuously entraining and then detraining it. Mixing also occurs in the wake that is deposited behind the ring as this wake falls back into the denser layer of fluid. Even after the decay of a ring, it breaks up into smaller eddies and subsequently produces more mixing with the surrounding fluid. Since one vortex ring can generate considerable mixing, it explains why vortex ring mixers are so efficient for destratification processes.

The experimental results showed that a tube type generator generates vortex rings that are both bigger in size and have a slower traverse velocity than those generated by an orifice or a plate type generator. With these data, an empirical correlation relating the penetration depth of a vortex ring into a stratified layer to the density gradient between the two layers of fluid and the initial energy in the ring, i.e. Xm/Rm vs. Ri, was obtained. This relationship was:

$$\frac{Xm}{Rm} = -29.7 \log_{10} Ri - 22.7$$

where 0.17 < Ri < 0.027.

This relationship will assist in the design and operation of tube type vortex ring mixers for the mixing of stratified layers with a sharp change in density gradient. This will optimize the mixing efficiency of these mixers by preventing a vortex ring from energetically impacting the bottom of a vessel or energetically breaking the surface of a liquid and dispersing most of its energy during impact.

# Chapter5

# Numerical Simulation of the Effect on a Vortex Ring due to the Proximity of One Wall

## 5.1 Introduction:

When using vortex ring mixers to mix a liquid in a tank, the number mixers and their locations in a tank have considerable effect on the efficieny of the mixing process. If two vortex ring mixers are operated too close together or the mixers are located too close to the wall of a vessel, the strength of the vortex rings produced by the mixers will be reduced because of interference with the rings beside it or its own images. This will reduce the efficiency of these type of mixers, as a vortex ring will not able to carry a volume of fluid an appreciable distance from its generation point.

Previous studies by Baird et al (1977) and Brasseur et al (1986) showed that vortex rings generated in a volume of unbounded fluid would travel away from the orifice in a straight line at a fairly constant velocity for a long distance. Brasseur et al (1986) also showed the proximity of walls around the ring reduced the traverse velocity of the ring considerably. Then Oshima et al (1975), (1984) and (1986) demonstrated both numerically and experimentally that two vortex rings, when travelling side by side, are attracted towards each other and eventually collide. This phenomena is similar to that of a vortex ring travelling parallel and close to a wall. In such a case, a ring will turn away from its path, hit a wall and disintegrate. This premature disintegration of vortex rings may reduce the efficiency of vortex ring mixers and can be avoided by positioning the mixer or the trajectory of a vortex ring away from the vessel walls.

In the research reported in this thesis, the effect of the proximity of one wall on the path of a vortex ring was studied analytically using numerical simulation. Inviscid flow theory, or the Biot Savart law was used. The result showed that when a vortex ring travels very close to a wall, the side nearest to the wall will slow down and cause the vortex ring to turn towards the wall and eventually hit the wall. A recommendation on how far the orifice of the mixers should be located from the wall of the vessel is given so that the wall effect on the vortex ring is minimized.

## 5.2 Theory:

Inviscid flow theory was used in this simulation to determine the effect on the path of a vortex ring travelling close to a wall. In order to simplify the calculation, the following assumptions were made:

1) The vortex ring has reached steady state.
2) The vortex ring has a thin core of vorticity of strength K.
3) The circular core of the vortex ring is divided into small segments of line vortex. As the division is increased, the segments of line vortex approached the shape of a circular vortex ring.

According to inviscid flow theory, the effect of a wall could be produced by putting an imaginary vortex ring at equal distance on the other side of the wall as shown in Figure 5.1.

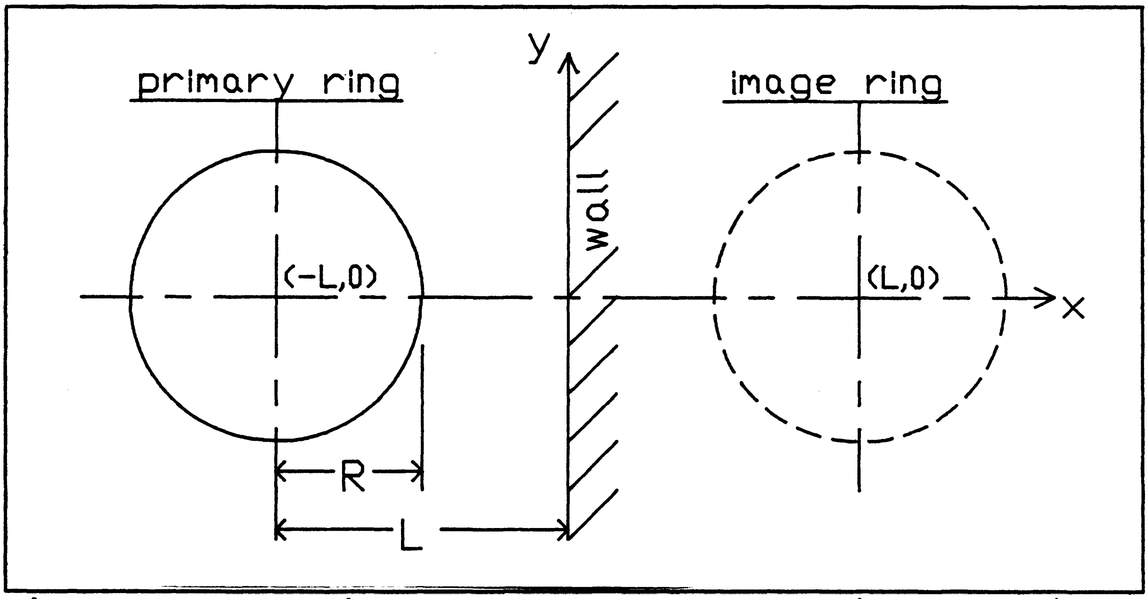


Figure 5.1. Locations of the core of the primary and image ring at the beginning of the simulation. i.e. @ t=0.

The Biot Savart law was used to determine the velocity induced by the image on the primary ring. The equation used to calculate the induced velocity at any point was given in differential form that is,

$$\delta\bar{q} = \frac{K ds}{4\pi} \frac{\bar{t} \times \bar{r}}{|\bar{r}|^3} \quad (5.1)$$

where,

$\delta\bar{q}$ - velocity induced at a point due to a segment of the core of the vortex ring,

K - the amount of circulation in the segment of the core of the vortex ring,

t - unit tangent vector of the segment ds,

$\bar{r}$ - the vector from the segment of the vortex core to the point where the induced velocity was calculated, and

$|\bar{r}|^3$ - magnitude of the vector r. See Figure 5.2.

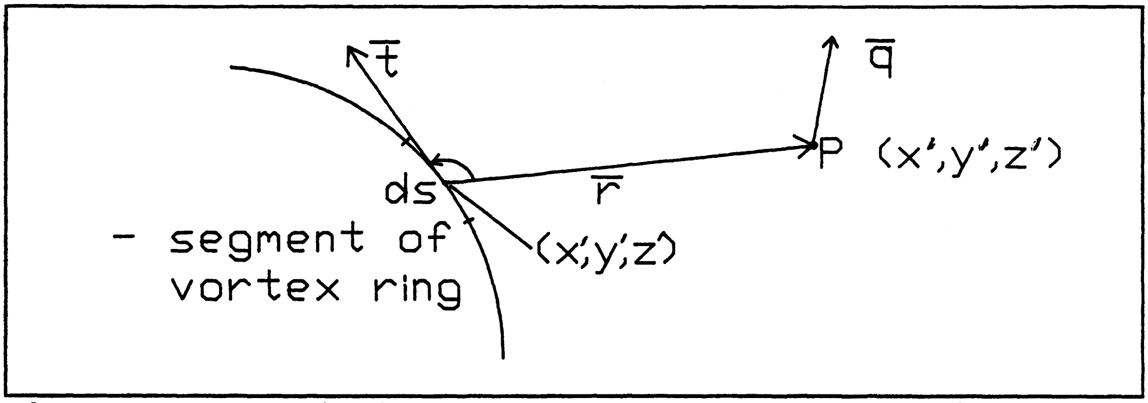


Figure 5.2 Description of the parameters of the Biot Savart law

A computer program in BASIC was developed to calculate the three components of the induced velocities, a copy of this program is given in Appendix C. In this program, both the primary and image rings were discretized into small segments of 2 to 10 degrees depending on the type of calculations. After discretizing the core of the ring into small segments and realizing that the unit tangential vector could be written as,

$$\bar{t} = \frac{dx'}{ds}\hat{i} + \frac{dy'}{ds}\hat{j} + \frac{dz'}{ds}\hat{k} \quad (5.2)$$

the three components of the velocity q could be expressed as,

$$
\begin{aligned}
du &= \frac{K}{4\pi|\overline{r}|^3}\,[(z-z')\,dy' - (y-y')\,dz'] \\
dv &= \frac{K}{4\pi|\overline{r}|^3}\,[(x-x')\,dz' - (z-z)\,dx'] \\
dw &= \frac{k}{4\pi|\overline{r}|^3}\,[(x-x')\,dy' - (y-y')\,dx']
\end{aligned}
\qquad (5.3)
$$

where,

x, y and z were the cooridnates where the value of the induced velocities were calculated and x', y' and z' were the coordinates of the segment of the line vortex, see Figure 5.2.

These three equations were used in the computer program to calculate the induced velocities caused by the vortex ring and its image. All the variables used in this simulation were dimensionless so the results could be generalized for future comparison with experimental data. The transformations are given in Table 5.1,

| Original Parameters | Dimensionless Parameters |
|---|---|
| u | $\hat{u} = u/(K/R)$ |
| (x-x') | (x-x') / R |
| dx' | dx'/R |
| dt | $dt/(R^2/K)$ |

Table 5.1. Transformation of variables in equation 5.3 into dimensionless variables.

## 5.3 Calculations:

Two sets of calculations were performed to determine the effect of the induced velocity on the path of the vortex ring. The first set calculated the tendency of a vortex ring to turn towards a wall in a vessel. The second set of calculations simulated a vortex ring turning towards a wall and how the core of the ring changed its shape as it approached a wall. The results of the calculations are described below.

### 5.3.1 Calculation of the induced velocity at two locations in the ring due to the proximity of the wall:

The first set of calculations used the inviscid flow theory to calculate the induced velocity due to both the primary and image rings at two locations along the core diameter of the ring. The two locations are at 1/2 core radius from the centre of the ring along the x - axis, i.e. at $(-L-\frac{1}{2}R, 0)$ and $(-L+\frac{1}{2}R, 0)$, refer to Figure 5.1. The calculation were performed for the initial stage when the primary and image ring met. At this time, the core of the two rings were still in a plane and their axis were parallel to each other.

The first step was to test the convergence of the program. The convergence was determined by calculating the velocity induced at the centre of the ring due to the primary ring only. It was found that the solution converged to a dimensionless induced velocity of 0.5 when the core of the primary ring was divided into segments of 2 degrees. Once the size of each segment was determined, the velocity induced by only the primary ring, and the primary ring and its image, at the two locations specified above could be determined. The results of this calculation are given in Section 5.4.1.

5.3.2 Numerical simulation of vortex ring turning towards a wall:

The results of the calculations given in Section 5.4.1 showed that the presence of a wall close to the path of a vortex ring resulted in the slowing down of the traverse velocity of the ring and caused the ring to turn towards the wall. The Biot Savart law was then used to simulate a vortex ring turning towards a wall when it was travelling too close to it. However, for the calculation of the self induced velocity, the Biot Savart law was not very appropriate. This was because for vortex rings with an infinitely thin core, the self induced velocity of the vortex ring approaches infinity as the value of 'r' approaches zero, as showed in Equation (1). This observation was also made by Batchelor (1967). Obviously, in reality a vortex ring would never travel at infinite velocity in a real fluid because of the viscous effects. Therefore, a self induced or transverse velocity was assumed for the vortex ring.

Two methods were used to approximate the self induced velocity of a vortex ring. The first method was to use the Biot Savart law to calculate the self induced velocity of a ring. As mentioned above, the self induced velocity goes to infinity as r approaches zero. However, in this case the size of each segment was kept finite at 10°, which prevented the self induced velocity from going to infinity.

The second method was to assume that the traverse velocity of the ring was constant. From previous experimental results by Baird et al (1979), it was shown that the traverse velocity of a vortex ring was relatively constant after the ring was generated. The direction of this velocity vector was assumed to be the unit vector defined by the cross product of the tangents of the two nearest segments, as shown in Figure 5.3.

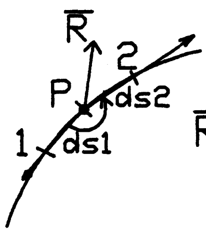


$$\overline{R} = \overrightarrow{P1} \times \overrightarrow{P2}$$

**Figure** 5.3. Method for calculating the direction of the self induced velocity.

Since the exact value of the self induced velocity was not known, an arbitrary value of 0.4 was chosen for this simulation. This self induced velocity was chosen because the distance travelled by the ring using this method was approximately the same as that of the ring where the self induced velocity was calculated. The results of this simulation are given in Section 5.4.2.

## 5.4 Results and Discussion:

### 5.4.1 Results from the calculation of the induced velocity along the core diameter of the vortex ring:

The results of the calculations showed that the velocity induced by the primary ring at the two locations along the core diameter of the vortex ring is 0.6228. The velocities induced by both the primary and image rings at these two locations are listed in Table 5.2:

| $X_{wall}/R$ | Ur | Ul |
|---|---|---|
| 1.25 | 0.57967 | 0.61221 |
| 1.75 | 0.61221 | 0.61858 |
| 2.00 | 0.61636 | 0.61987 |
| 3.00 | 0.62122 | 0.62184 |
| 5.00 | 0.62248 | 0.62256 |
| 7.50 | 0.62270 | 0.62271 |
| 10.00 | 0.62274 | 0.62275 |

Table 5.2. Listing of the velocities induced by both the primary ring and its image at the two specified locations. $X_{wall}/R$ is a dimensionless distance of the centre distance of the vortex ring from the wall.

Table 5.2 shows that the velocity of the point closer to the wall is slower than the point further away from the wall. This indicates that a vortex ring begins to turn towards the wall because the part of the ring that is close to the wall is travelling at a slower speed than the part that is further away from the wall. Figure 5.4 shows the variation of ratio between the velocity of the left and the right portions of a ring, Fig 5.4 Effect of the proximity of wall on the velocity of the vortex ring

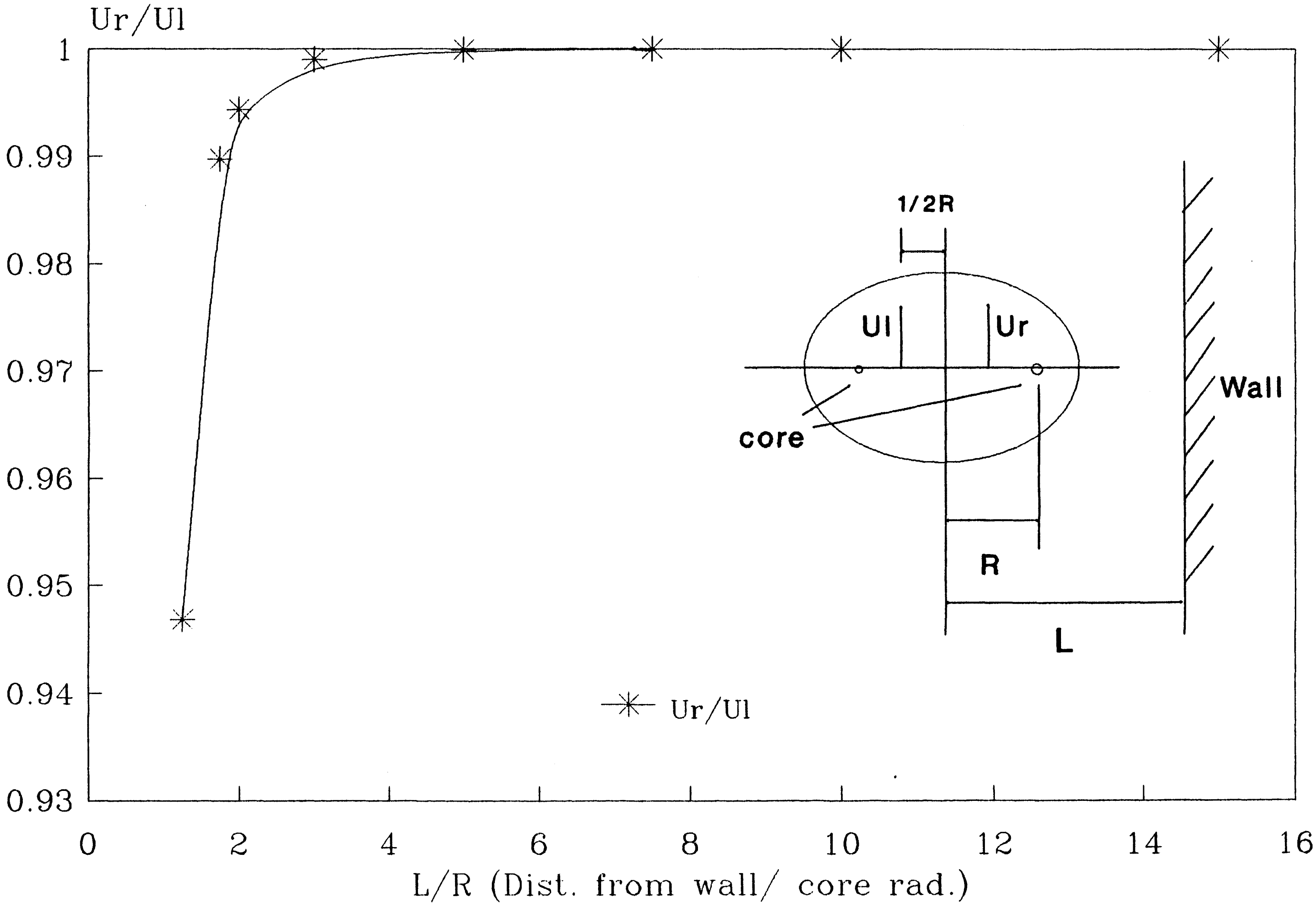

Ur/Ul, as the mean distance of the ring from the wall changes. Ur/Ul approach 1 as $X_{wall}/R \geq 5.0$. This means that in order to prevent the vortex ring from turning towards a wall, the centre of the ring must be at least 5 core radii from the wall.

The proximity of the wall along the path of the ring has another effect on the trajectory of the ring. As the ring travels relatively close to a wall, the forward velocity of the ring decreases while it turns towards the wall. It can be seen from Figure 5.5 that the ratio between the velocity on the right Ur with the wall effect and the velocity at the same point of the ring without the proximity of the wall $Ur\infty$ approaches 1 as $X_{wall}/R \geq 5.0$. For $X_{wall}/R < 5.0$, $Ur/Ur\infty < 1.0$, the rings are travelling too close to the wall of the vessel and they will slow down and turn towards the wall.

Fig 5.5 Effect of the proximity of wall
on the velocity of the vortex ring
Ur/U@ (N.B. Ur=Ul=0.62278 @ )

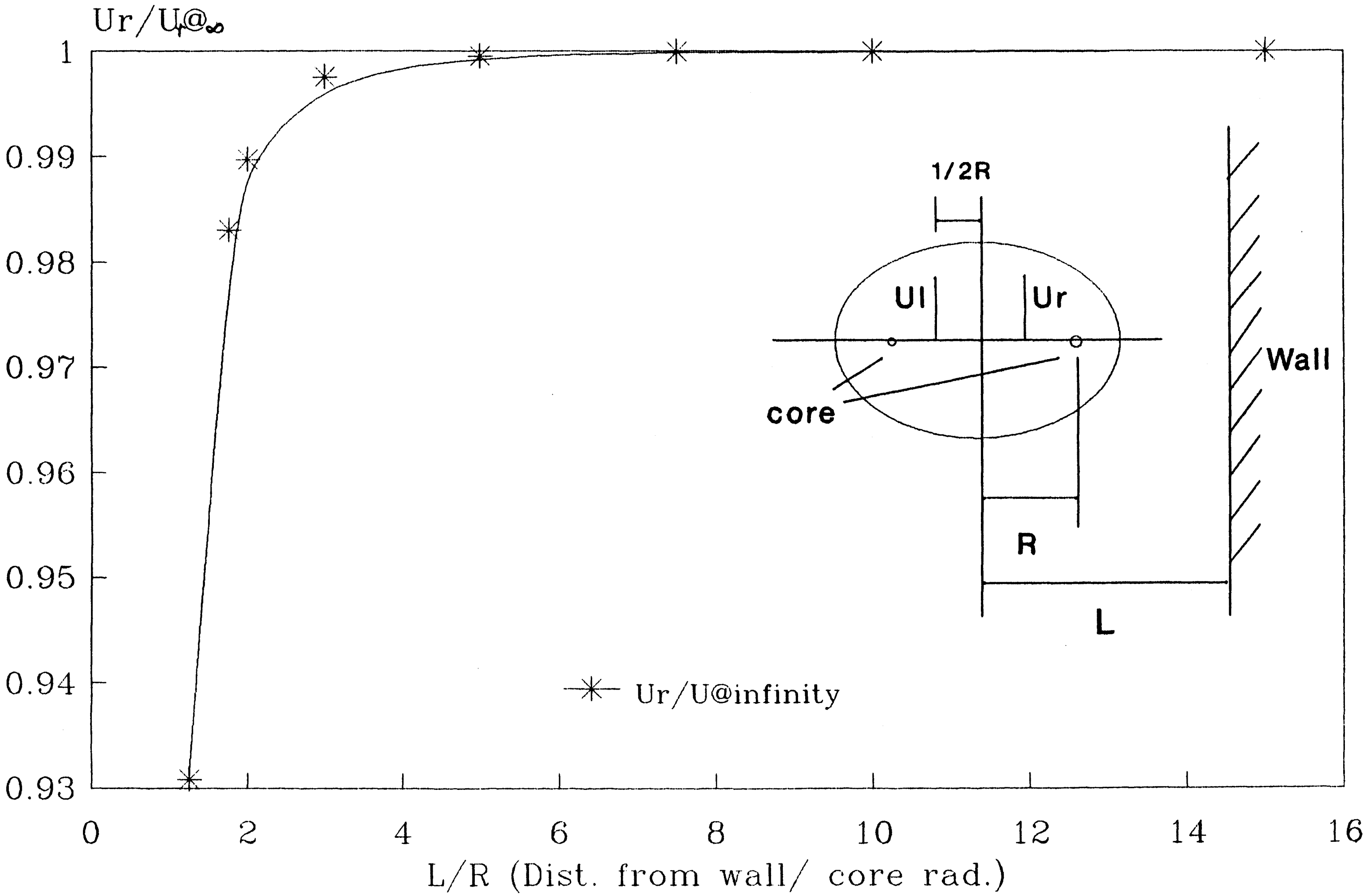

5.4.2 Simulation of a vortex ring travelling towards the wall:

Two computer programs were written in BASIC for this particular simulation. In the first program, the self induced velocity was assumed to be constant; the simulation using this program is called "ring 1". In the second program, the self induced velocity was calculated using the Biot Savart law; the simulation using this program is called "ring 2". A comparison of the results from these two programs together with some experimental data indicates which model is more reliable in predicting the path of the vortex ring when it is travelling adjacent to a wall.

Two sets of results were computed for comparison purposes, the initial conditions for which are specified in Table 5.3, the results of which are presented in Figure 5.6 - 5.15.

| | Constant self induced velocity (ring 1) | Self induced velocity calc. from Biot Savart law (ring 2) |
|---|---|---|
| $\Delta\theta$(deg) | 10 | 10 |
| dt | 0.2 | 0.2 |
| $X_{wall}/R$ | 1.25 \| 1.5 | 1.25 \| 1.5 |

Table 5.3. Input parameters for the computer program that simulate the path of a vortex ring close to a wall.

At time equal to zero, all vortex rings started at the same initial locations for both programs, see Figure 5.6. As time proceeded, both rings 1 and 2 moved away from their original positions and began to turn towards the wall. For the case where $X_{wall}/R = 1.5$ the comparison was reasonably close at time of 1.0, see Figure 5.7. However, at a time of 2.0, ring 1 had moved closer to the wall than ring 2, see Figure 5.8. Also, the side of ring 1 that was nearest to the wall was slowed down considerable more than that of ring 2. At a time of 2.4, see Figure 5.9, ring 1 is pulled even closer to the wall than at a time of 2.0. Eventually, at a time of 2.6, the ring 1 became unstable, as seen in Figure 5.9. On the other hand, ring 2 kept on moving forward without disintegrating up to a time of 4.0, see Figure 5.10. Furthermore, ring 2 also moved towards the wall at a slower rate than that of ring 1.

The other set of data was for $X_{wall}/R = 1.25$ keeping all the initial parameters constant. The original position of both vortex rings is shown in Figure 5.11. As the vortex rings got closer to the wall, ring 1 was attracted towards the wall much faster than ring 2 as shown in Figure 5.12 for a time of 1.0. The right hand side of the rings were slowed down more than that for $X_{wall}/R = 1.5$. This showed that the proximity of a wall slows down a vortex ring and causes it to turn towards the wall.

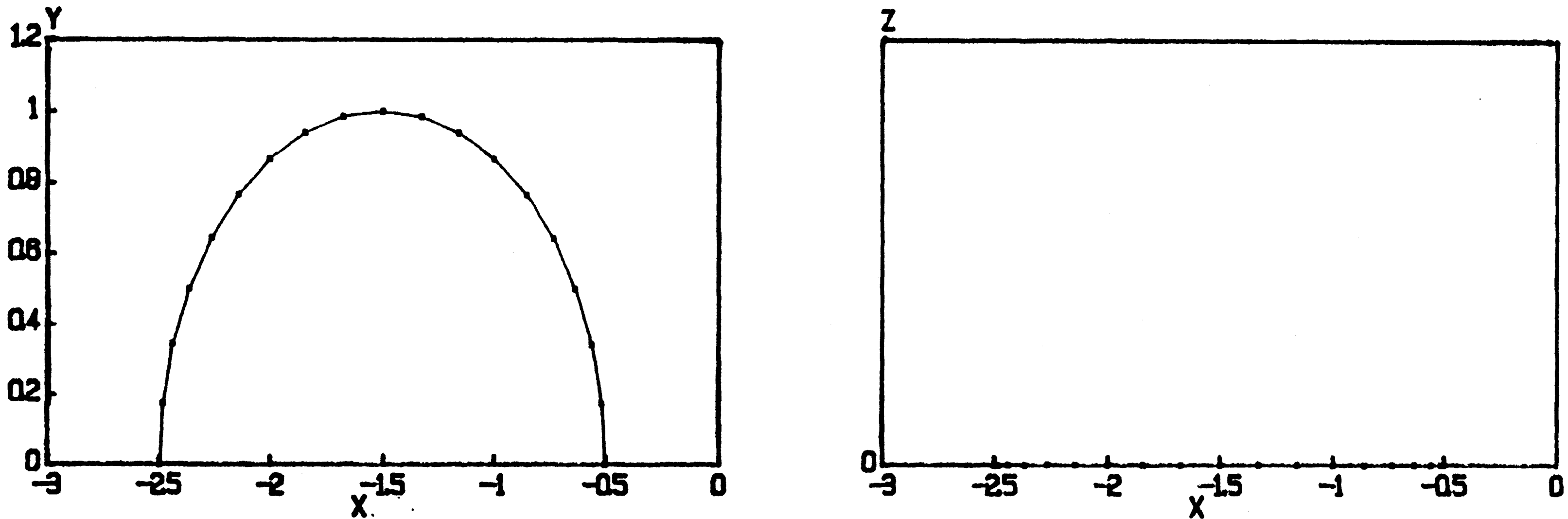


a)

b)

Figure 5.6 a) The shape of ½ of the core of the rings in the X-Y plane and b) The shape of the core of the rings in the X-Z plane; at time = 0.0.

a) Constant Vel. Method @ T = 1.0 b)

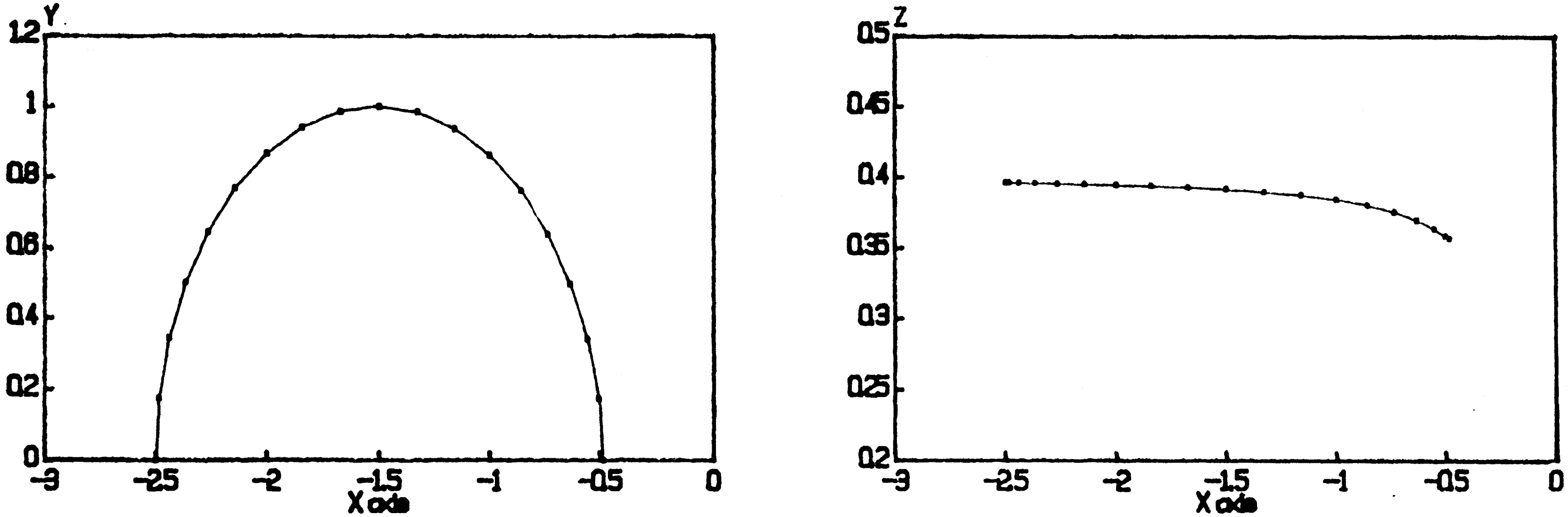


a) B.S. Law @ T = 1.0 b)

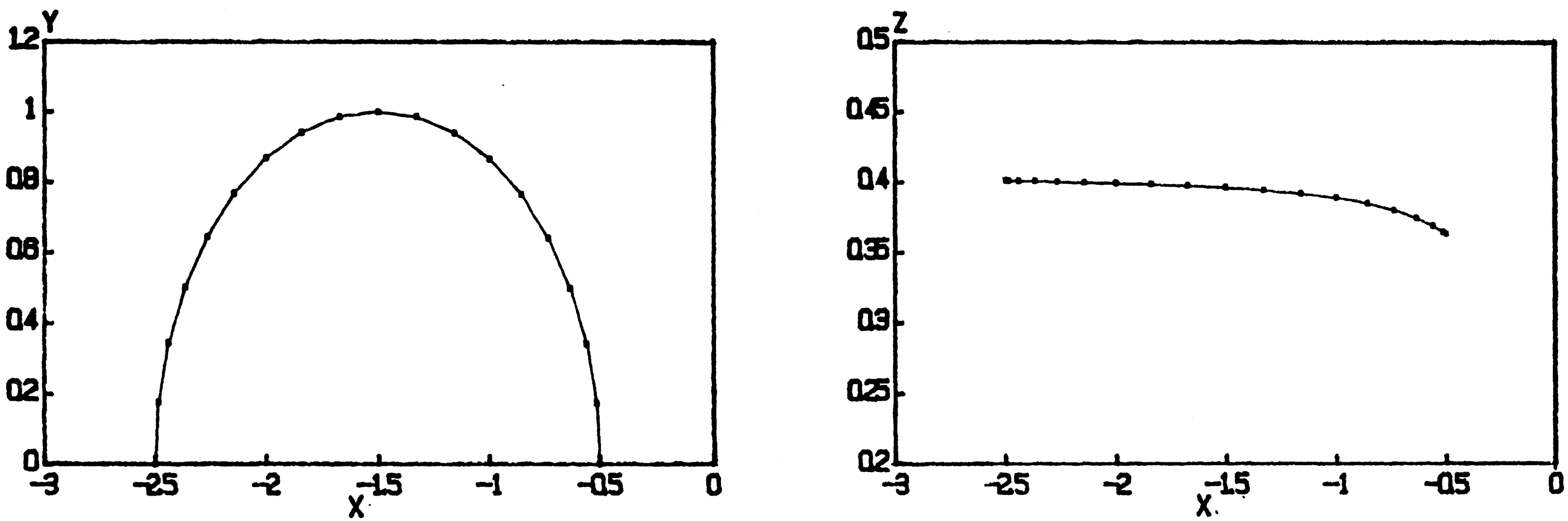


Figure 5.7 a) The shape of ½ of the core of the rings in the X-Y plane and b) The shape of the core of the rings in the X-Z plane; at various time steps calculated by: i) B.S. Law and ii) constant velocity method

a) Constant Vel. Method @ T = 2.0 b)

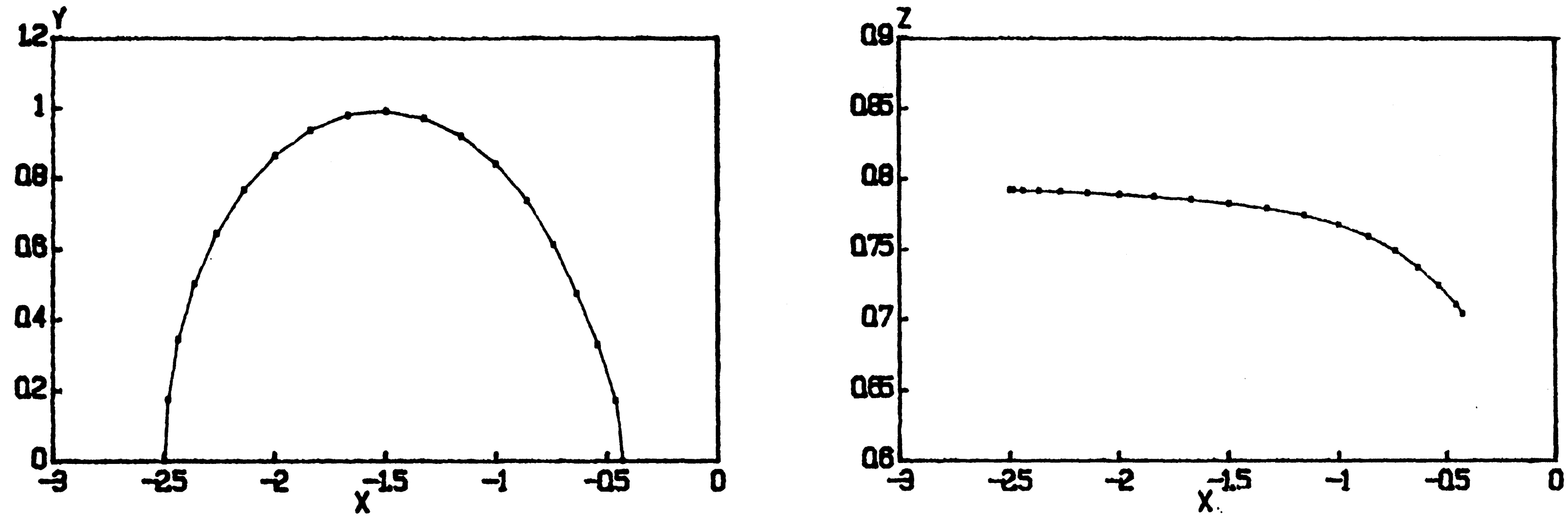


a) B.S. Law @ T = 2.0 b)

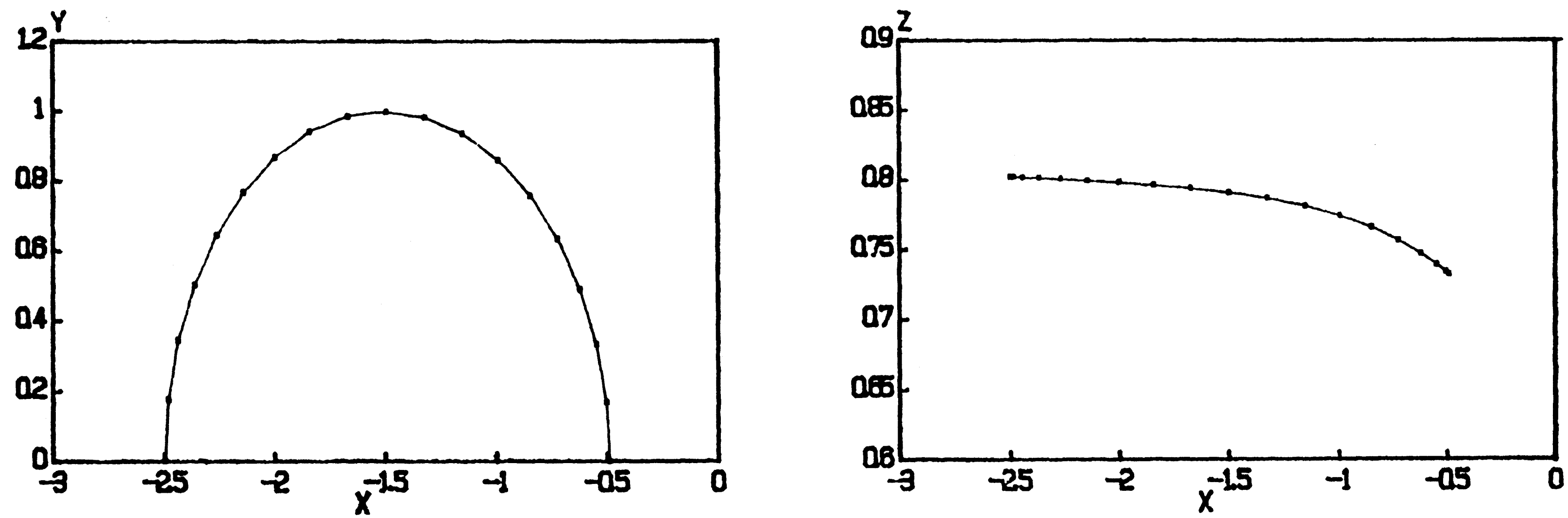


Figure 5.8 a) The shape of ½ of the core of the rings in the X-Y plane and b) The shape of the core of the rings in the X-Z plane; at various time steps calculated by: i) B.S. Law and ii) constant velocity method

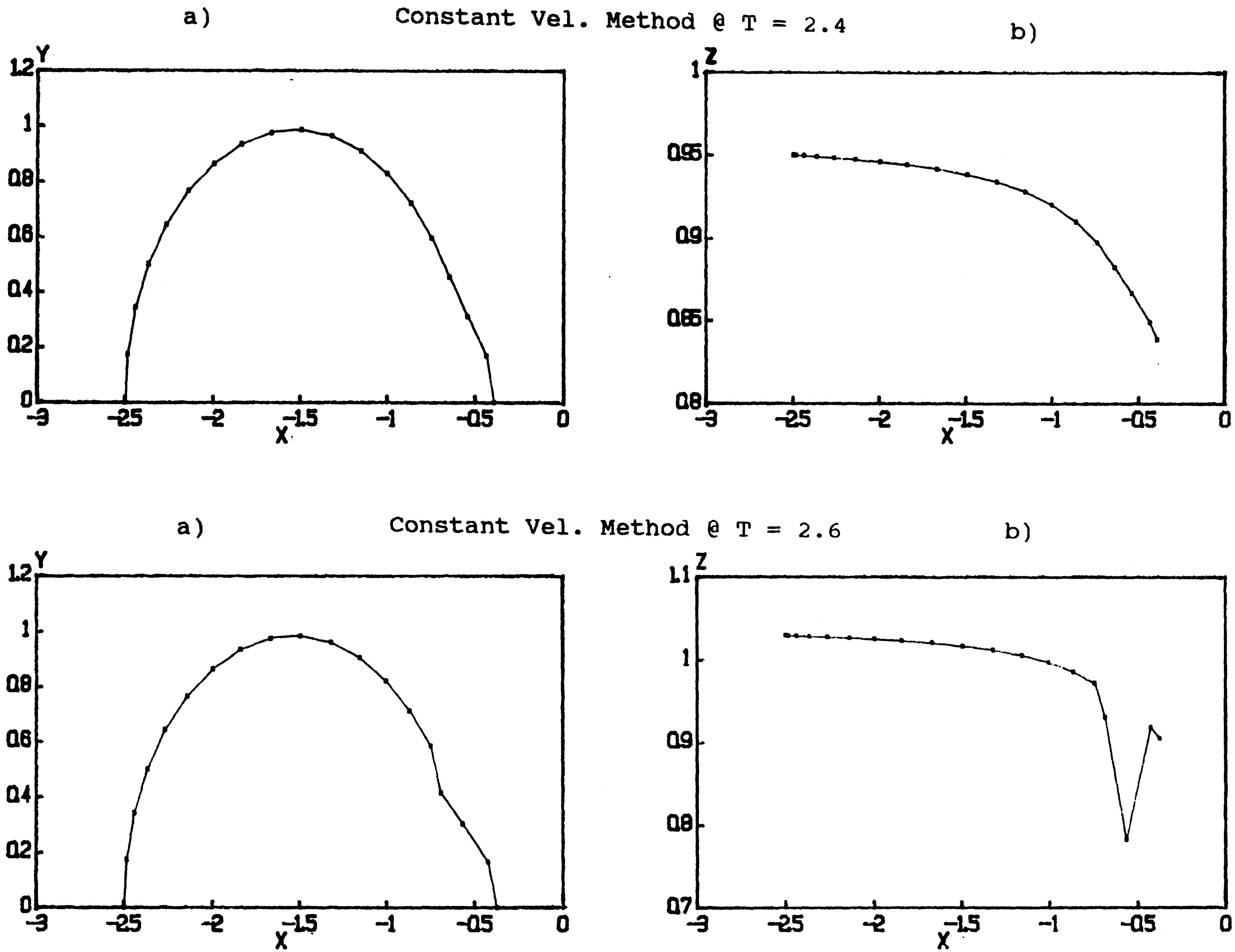


Figure 5.9 a) The shape of ½ of the core of the rings in the X-Y plane and b) The shape of the core of the rings in the X-Z plane; at various time steps calculated by constant velocity method.

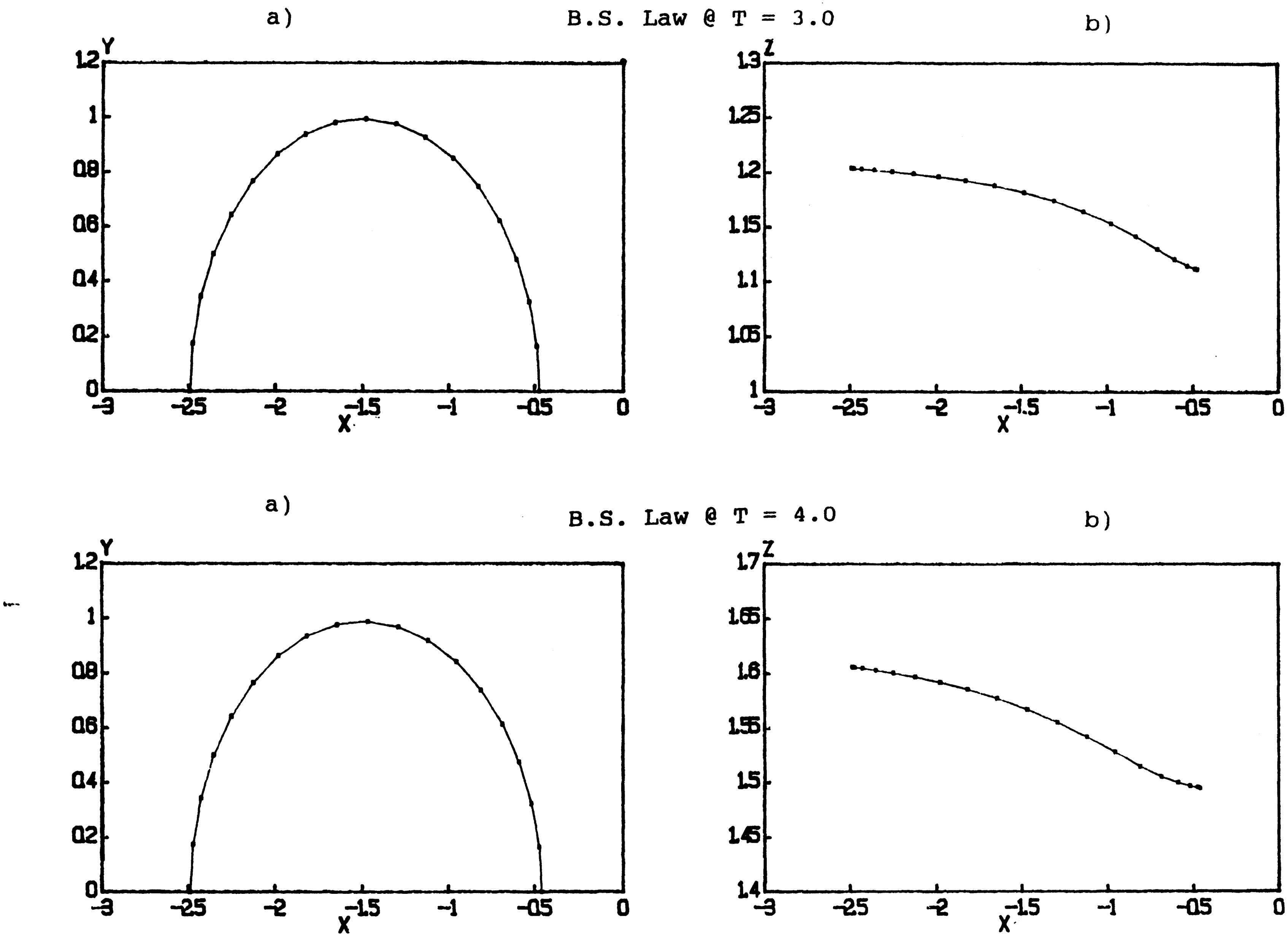


Figure 5.10 a) The shape of ½ of the core of the rings in the X-Y plane and b) The shape of the core of the rings in the X-Z plane; at various time steps calculated by B.S. Law.

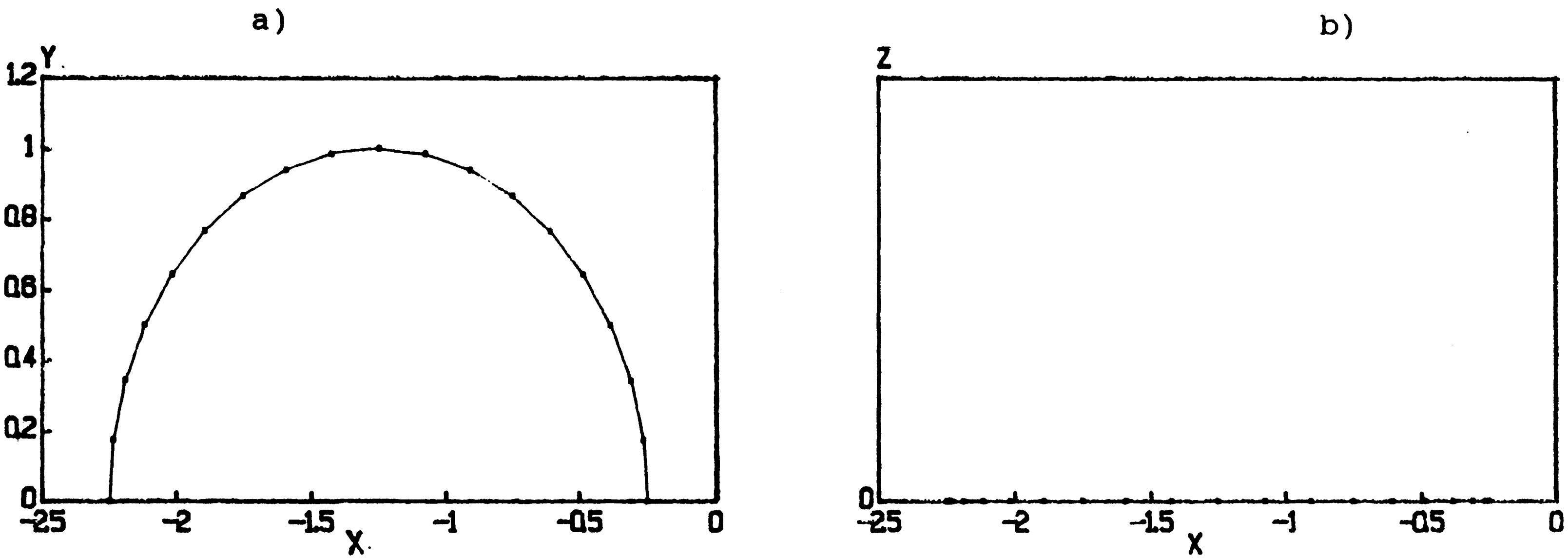


Figure 5.11 a) The shape of ½ of the core of the rings in the X-Y plane and b) The shape of the core of the rings in the X-Z plane; at time = 0.0.

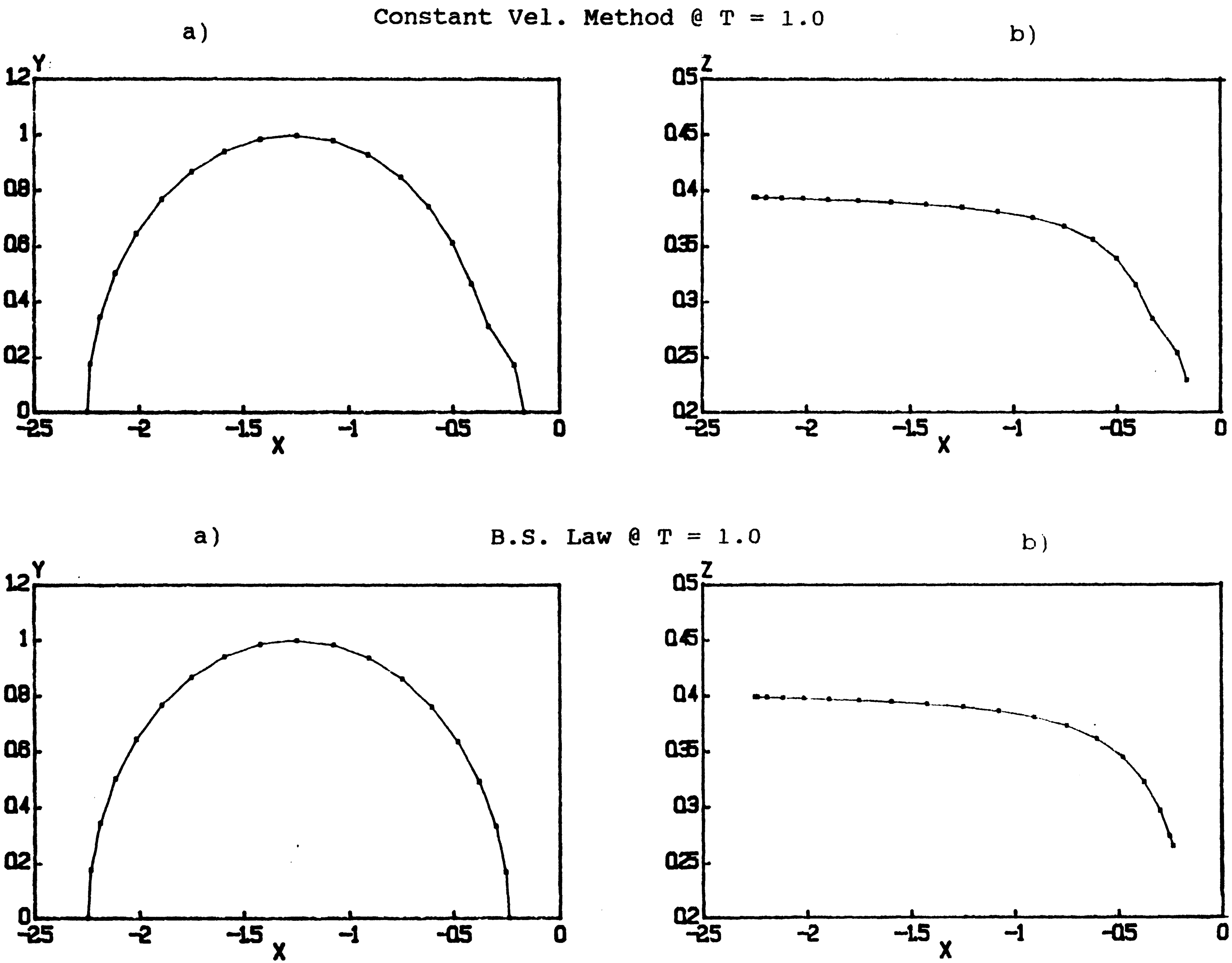


Figure 5.12 a) The shape of ½ of the core of the rings in the X-Y plane and b) The shape of the core of the rings in the X-Z plane; at various time steps calculated by: i) B.S. Law and ii) constant velocity method

a) Constant Vel. Method @ T = 1.2 b)

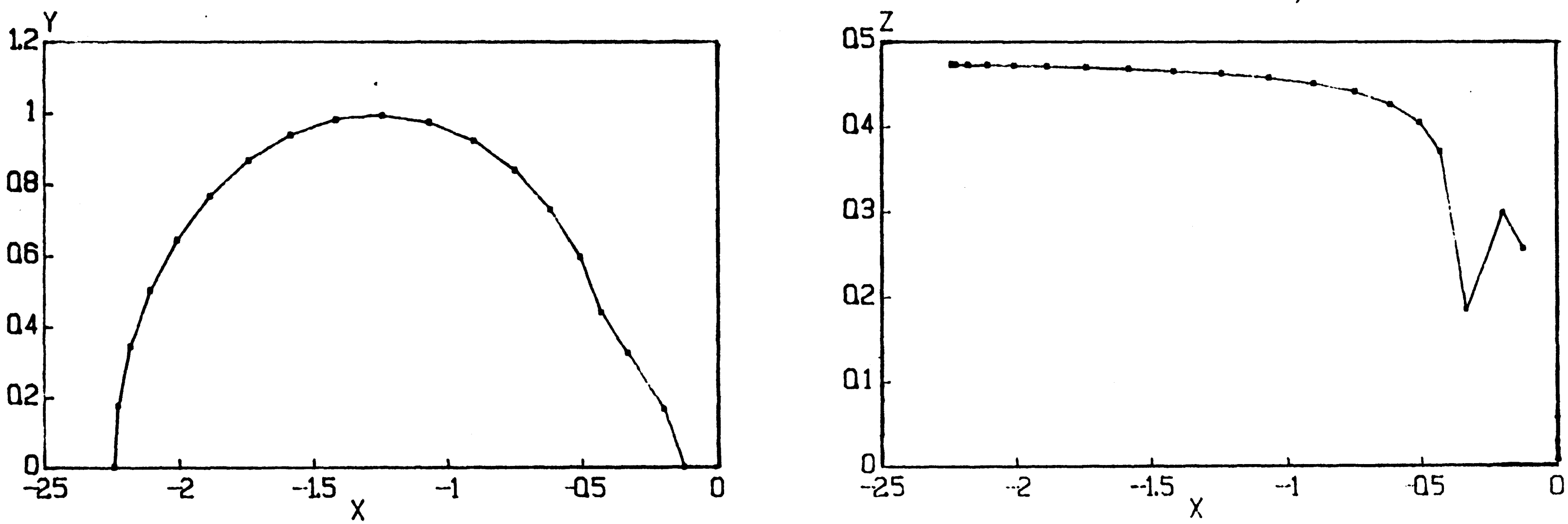


Figure 5.13 a) The shape of ½ of the core of the rings in the X-Y plane and b) The shape of the core of the rings in the X-Z plane; at various time steps calculated by constant velocity method.

a) B.S. Law @ T = 2.0 b)

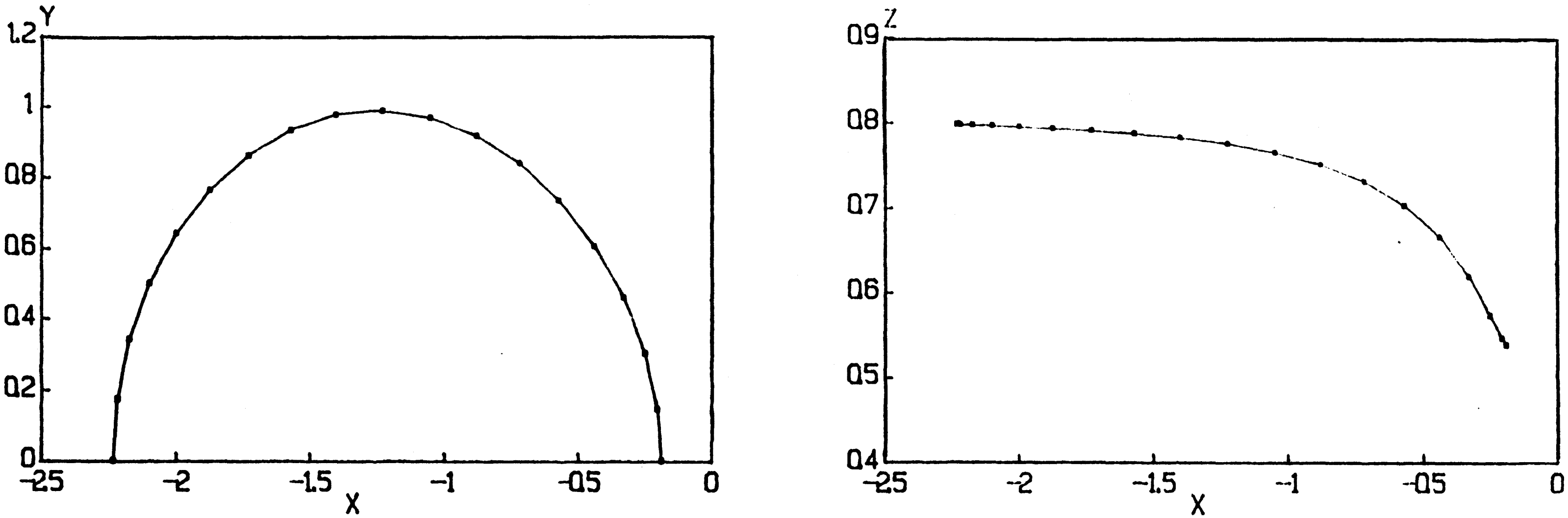


a) B.S. Law @ T = 3.0 b)

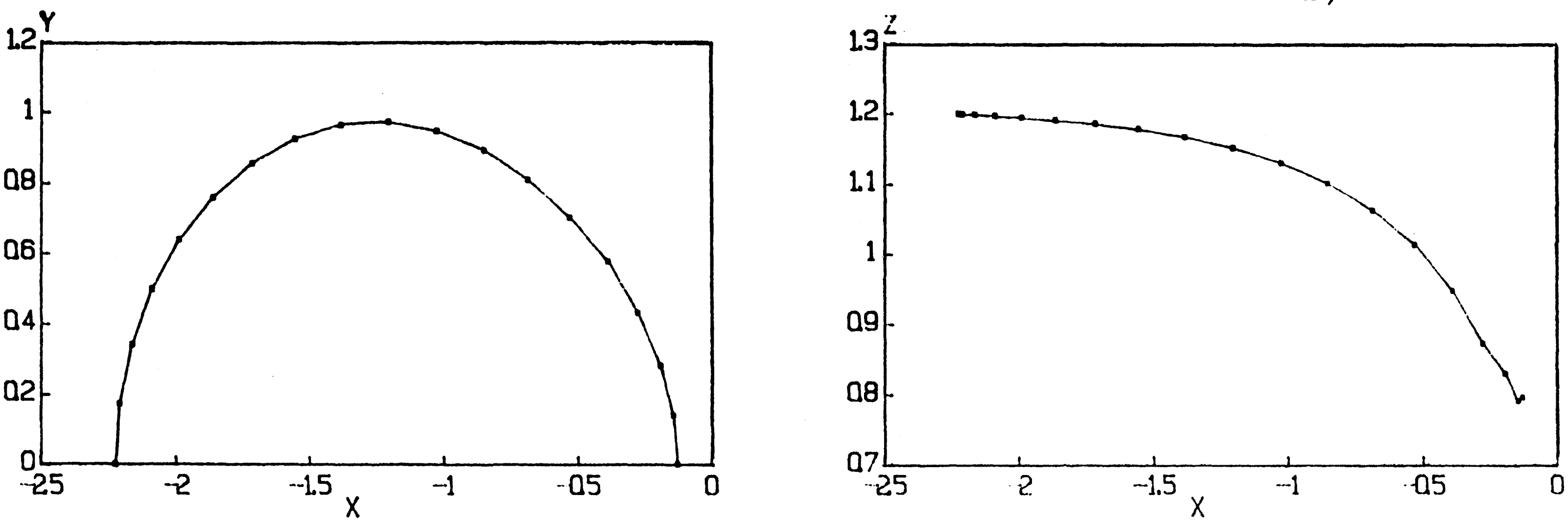


Figure 5.14 a) The shape of ½ of the core of the rings in the X-Y plane and b) The shape of the core of the rings in the X-Z plane; at various time steps calculated by B.S. Law.

a) B.S. Law @ T = 3.2 b)

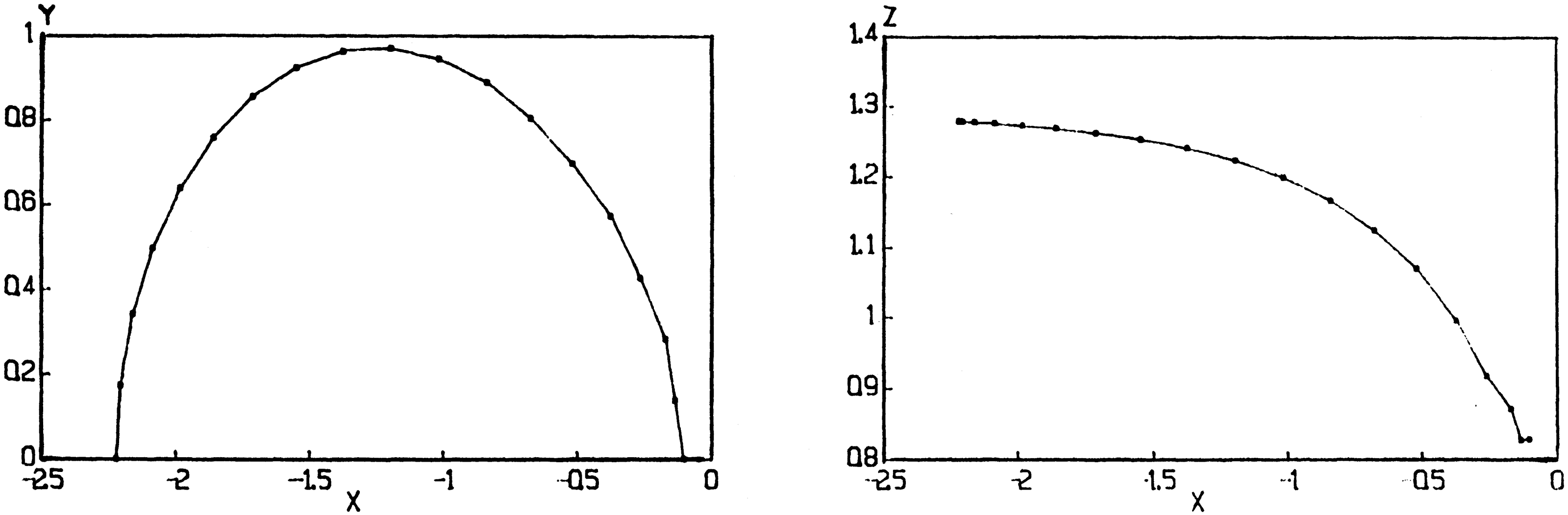


a) B.S. Law @ T = 4.0 b)

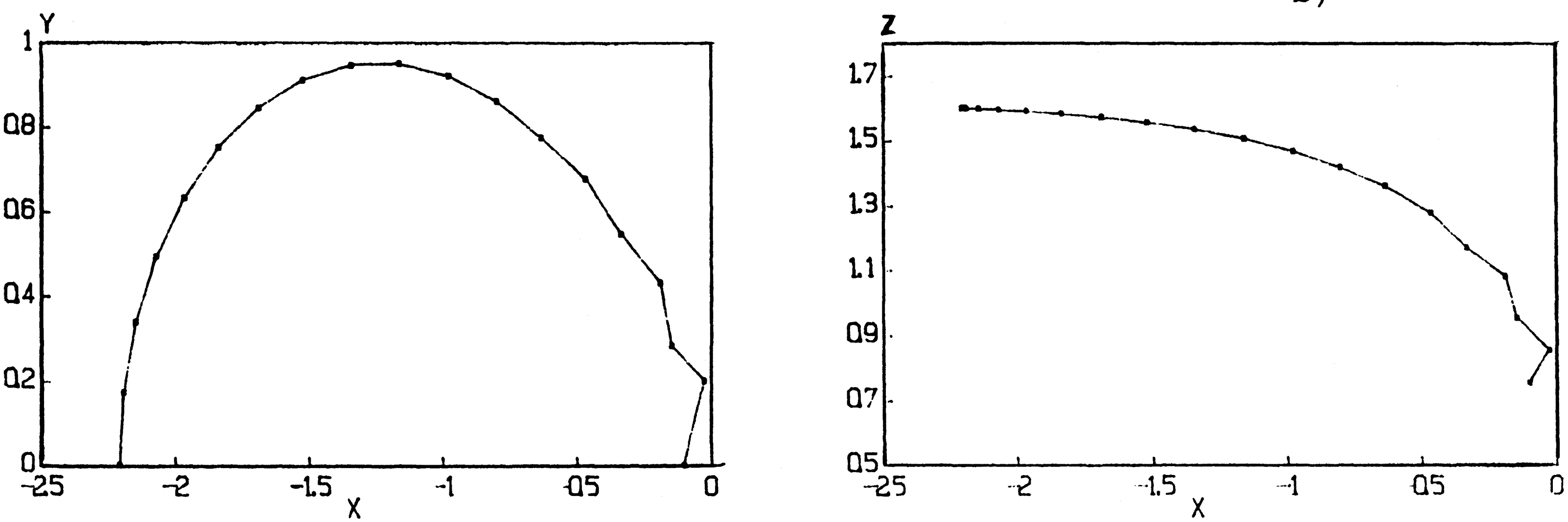


Figure 5.15 a) The shape of ½ of the core of the rings in the X-Y plane and b) The shape of the core of the rings in the X-Z plane; at various time steps calculated by B.S. Law.

At a time of 1.2, ring 1 became unstable, see Figure 5.13, while ring 2 was still propagating forward without hitting the wall or becoming unstable. Ring 2 was still travelling forward at times of 2.0 and 3.0, see Figure 5.14. At a time of 3.2, see Figure 5.15, while ring 2 was still propagating forward, its core came very close to the wall. Finally, at a time of 4.0 the core of ring 2 collided and bounced off the wall.

From the above results, it is clear that the assumption of constant self induced velocity over predicted the movement of the vortex ring and resulted in an early disintegration of the vortex ring. On the other hand, although the Biot Savart law might not be the most appropriate relationship for calculating the self induced velocity on the primary ring, the numerical results obtained using the Biot Savart law seemed to give a better agreement with the experimental results of Oshima et al (1984) than the numerical results of this study, obtained using the constant self induced velocity assumption. As shown in Figure 5.16, when two vortex rings travel close together, they will not collide with each other together until they have travelled a distance from the opening of the orifice. However, further experiments have to be performed to verify this observation.

Figure 5.16 Experiments from Oshima et la(1984) showing the effect of two vortex rings travelling too close to each other.

## 5.Conclusion:

The results of the computer simulation, using the Biot Savart law, on the effect on the path of a vortex ring due to the proximity of one wall are presented. The induced velocities at two points along the core diameter of a vortex ring due to the present of the ring and its image were calculated. The results showed that as a ring gets closer to a wall, the tendency of the ring to turn towards the wall dramatically increases and the proximity of a solid boundary also decreases the traverse velocity of the ring. In order to minimize the effect of a wall on the path of the vortex ring, the centre of the ring should be at a distance of at least 5 times ($X_{wall}/R$) from the wall. Since R is the core radius of the ring and the core radius of the ring is approximately 1.5 times the radius of the orifice for tube type generators, then the centre of the orifice or the mixer orifice should be 7.5 $X_{wall}/Rm$ from the wall of a vessel.

The path of a vortex ring with an infinitely thin core travelling close to a wall was simulated using two methods for calculating the self induced velocity. These were; 1) the constant velocity assumption and 2) the Biot Savart law assumption. Both set of results showed that a vortex ring will turn towards a wall under certain conditions. From Section 5.3.1, it was shown that when a vortex ring is travelling closer to the wall, with $X_{wall}/R = 1.25$, it turns towards the wall much sooner than for a ring for which $X_{wall}/R = 1.50$. Also, the Biot Savart law assumption seemed to give a closer approximation to the experimental results, even though the self induced velocity calculated by this method never converges due to the limitation of the invisid flow theory. However, this observation has to be verified with further experimental data.

Overall Conclusion:

Through the use of flow visualization techniques and hot film anamometry, it showed the difference between a ring generated at a tube and an orifice. In this study, all the vortex rings were generated at a tube and they were all larger in size and slower in velocity than rings generated at an orifice under similar conditions. This is deemed to be a significant factor when considering the destratification of fluid in a vessel as the maximum penetration depth of the ring depends on the initial traverse velocity and size of the ring before it penetrated into the stratified layer.

By using the proper kind of flow visualization techniques, the amount of mixing caused by one vortex ring penetrating through the stratified layer was demonstrated. Experiments showed that mixing occurred throughout the period the ring was travelling in the stratified layer. As the ring penetrated into the stratified layer, it continued to entrain the surrounding fluid into the ring and then detrain it into a wake behind the ring. This wake of denser fluid fell through the interface back into the layer of denser fluid and then dispersed by means of eddies and mixed with the surrounding denser fluid. After the ring decayed in the lighter fluid layer, the vorticity inside the ring broke up into small eddies. All these observations showed that the ring continued to mix the surrounding fluid with the fluid in the ring once it penetrated into the stratified layer, which explained why vortex ring mixers are so effective for the destratification of stratified fluid.

In order to improve the design of vortex ring type mixers for the destratification of fluid, a theoretical model and an empirical relationship was obtained to predict the maximum penetration depth of a vortex ring into a stratified layer. The theoretical model used was developed on the basis of the momentum balance equation. Comparison between experimental results and calculated results from the model showed the model constantly under predicted the maximum penetration depth the ring could achieve. The failure of this model meant an empirical relationship had to be used to estimate the maximum penetration depth of a vortex ring travelling in a stratified fluid. The following empirical relationship for a tube type vortex ring mixer was obtained:

$$\frac{Xm}{Rm} = -29.7 \log_{10} Ri - 22.7$$

where $0.17 < Ri < 0.027$.

This equation was obtained for the following conditions: $Xwall/Rm = 6$; $Li/Rm = 8$ and $L/Dm \approx 2 - 2.8$. It is expected that this equation will still hold true for a longer distance between the generation orifice and the interface of the two layers of stratified fluid than Li/Rm = 8, e.g. if the value of Xwall/Rm is increased to 7 or 8, then Li/Rm can be increased to approximately 10. By reducing the effects of the proximity of the boundaries of the vessel, a vortex ring can maintain a constant translational velocity for a longer distance while travelling towards the interface, hence the initial conditions of the vortex ring will be the same as in the case where Xwall/Rm = 6. Further experiments had to be performed to verify the assumptions given above. In order to apply the equation to the actual mixer, a relationship between the pressure supplied to the drive piston and the average jet velocity during the injection has to be obtained. Ri can be calculated using the averaged measured jet velocity and substituted into the above equation to obtain Xm/R or the maximum penetration depth of a vortex ring travelling in a stratified layer.

Another factor that can affect the normal path of a vortex ring is the proximity of another ring or a wall boundary. If a vortex ring collides with a wall and disintegrates, much of the energy in the ring is wasted in the collision, by preventing this collision from occurring the energy in the ring can be conserved and used for the mixing of the fluid in the vessel. Using invisid flow theory, the effect of a solid boundary or a wall was simulated by placing another vortex ring at equal distance on the other side of the boundary. This ring was usually called the image ring or the image of the primary ring. Through the use of the Biot Savart law, the tendency of two vortex rings being attracted towards each other or a single vortex ring turning towards a wall boundary of the tank was calculated. Results showed that in order to prevent this phenomena from occurring, the centre of a vortex ring had to be 5 times the core radius from the wall boundary of the ring or the centre to centre distance between two vortex rings had to be 10 times the core radius of the rings. Assuming the ratio between the core radius of the ring R and the radius of the injection orifice Rm is 1.5, the turning effect of a ring could be minimized if the centre of the generating orifice is 7.5 Rm from the wall of the tank or the distance between two generating orifice is 15 Rm. This information is valuable when designing the locations of vortex ring mixers for specific tank geometries, by preventing the vortex rings from colliding with the wall of the tank most of the energy in the ring can be used for the mixing of the fluid.

# Reference:

Baird M.H.I., Rohatgi A. and Wairegi T.,"Mixing effects and hydrodynamics of vortex ring",Can. J. Chem. Eng., (1979), vol.57.

Baird M.H.I., Wairegi T. and Loo H.J.,"Velocity and momentum of vortex rings in relation to formation parameters", Can. J. chem., (1977), vol. 55.

Brasseur J.G.,"Evolution characteristics of vortex ring over a wide range of Reynolds numbers",AIAA/ASME 4th Fluid Mechanics, Plasma Dynamics and Lasers Conference, May 1986.

Chow - Private communication. (1987)

Glezer A. and Coles D., "An experimental study of a turbulent vortex ring",J. Fluid Mech., (1990), vol. 211, pp243-283.

Honji H., Tatsuno M.,"Vortex rings in a stratified fluid", Journal of Physical Society of Japan, V41 n6 Dec 1976.

Hecht A.M., Bilanin A.J., Hirsh J.E., and Snedeker R.S.,"Turbulent vortices in stratified fluids", AIAA Journal, (July, 1980), Vol. 18, No. 7.

Irdumsa J. and Garris C.A., "Energetics of vortex ring formation", 83-WA/Aero-4, ASME, 1983.

Latto B.,"New mixer for slurries and stratified fluid",12th international conference on slurry technology, March-April 1987.

Latto B.,"Novel vortex ring mixers for slurries and stratified liquids", Proceeding of the Fourteenth International Conference on Cool and Slurry Technology, Coal and Slurry Technology Association, April 1989.

Latto B., Papple M.L.C., Shoukri M., Barid M.H.I., "Mixing of thermally stratified fluids by injecting a series of vortex rings - a numerical simulation", Transaction of Institution of Chemical Engineers, Vol. 68, Part A, September 1990.

Linden P.F.,"The interaction of a vortex ring with a sharp density interface: a model for turbulent entrainment", J. Fluid Mech., (1973), Vol. 60, Part 3.

Maxworthy T.,"The structure and stability of vortex ring",J. Fluid Mech., (1972), vol. 51, part 1, pp15-32.

Maxworthy T.,"Turbulent vortex ring",J. Fluid Mech., (1974), vol.64, part 2, pp227-239.

Maxworthy T.,"Some experimental studies of vortex rings",J. Fluid Mech., (1977), vol. 81, part 3, pp465-495.

Oshima Y. and Kuwahara K.,"Experimental and Numerical Study of Vortex Interaction", AIAA 17th Fluid Dynamics, Plasma Dynamics and Laser Conference, June, 1984.

Oshima Y., Noguchi T. and Oshima K.,"Numerical study of interaction of two vortex rings", Fluid Dynamics Research, 1, (1986). p215-227

Oshima Y. and Asaka S.,"Interaction of two vortex rings moving side by side", Natural Science Report, Ochanomizu University, Vol. 26, No. 1, 1975.

Papple M.C.I., Shoukri M., Latto B., Baird M.H.I., "Numerical simulation of the transport of vortex rings in an initially stratified fluid", Chemical Engineering Communication, Vol. 103, 1991.

Perrakis K.K. and Papailiou D.D.,"Turbulent vortex ring and entrainment mechanism",A.I.A.A., 1988.

Sallet D.W. and Widmayer R.S., "An experimental investigation of laminar and turbulent vortex rings in air",Z. Flugwiss, 22 (1974), Heft 6.

Strange B., Undergraduate Thesis Project, Department of Mechanical Engineering, McMaster University, 1991.

Wooller J. and Hinwood J.B.,"The time dependent properties of non-bouyant vortex rings",Fifth Australian Conference on Hydraulics and Fluid Mechanics, December 1974.

## Biblography

G.K. Batchelor, An Introduction to Fluid Dynamics, Cambridge University Press, G. Britain, 1967.

# Appendix A

## A.1. Hardware set up for the frame grabber:

The High Res Technologies HRT-512-8 digital video frame grabber is used to analysis the experimental results collected using the video camera. The video frame grabber comes with its own software which was modified to suite the requirements for the measurements of the location and core diameter of the vortex ring after it is generated. This frame grabber will run with an IBM XT or AT compatible computer with a mouse. The mouse must be Microsoft Mouse compatible (the one that is currently in use is a Logitech serial mouse). A mouse is essential for moving the cursor within a freezed image to measure the location and size of the vortex ring.

The frame grabber board can be installed onto any empty expansion slot in an IBM XT or AT compatible computer whether it is an 8 bit or a 16 bit slot. If the frame grabber is installed into a computer for the first time, the program INSTALL.BAS must be run. This program prompts for a base address where the video image is stored and passes this address to a file HRTML.BAS which contains the machine code routines to communicate with the frame grabber. This INSTALL.BAS program will also prompt the operator to adjust the dip switches on the frame grabber board to the correct base address. This initial set up is only required when the frame grabber is installed into a computer for the first time. After the frame grabber board is installed into the computer, the NTSC video output from either a VCR or a video camera is connected to the video input of the frame grabber, top RCA jack. The digitized video output at the bottom RCA jack can be connected to any monitor. One reminder from the manufacturer is, **NEVER** turn the video camera or the monitor off or on while the computer is running. These equipment must be turned on before the computer is started.

## A.2. Software set up for the frame grabber:

After installing the hardware, the software can be loaded for analyzing the video images recorded during the experiments. The software written for this particular application is written in BASICA which has to run with DOS version 3.3. In order to execute the program, the following command must be typed at DOS prompt.

>basica grabber4 <CR>

Then the software will prompt for the name of the data file where the measurements will be saved.

### A.2.1. Vertical calibration routine:

The calibration routine measures the number of pixel a within one inch vertical distance, shown on the video image.

To begin, freeze a frame on the video recorder, then press "0" on the keyboard. The image is then digitized or frozen. A cursor will show up on the monitor. For the convenience of measuring the location of the ring, a scale is always shown on the left hand side of the recording. In order to calibrate the frame grabber for a set of measurement, move the cursor to any spot on the scale and enter "0 <CR>", then move the cursor to another location that is one inch vertically away from the original location and enter "0 <CR>" again. Now the frame grabber is calibrated for this set of measurement and a second screen will show up on the computer monitor.

### A.2.2. Measurements of the location and core diameter of the vortex ring:

The second screen presents the different operations that the frame grabber can perform. However, the measurements of the properties of the vortex ring only require function 0 and E. **Function 0** initiate the procedure for acquiring the measurements and **function E** will save all the measured values on to a diskette.

After "0" is pressed, the lower window on the screen will prompt for the **first input**, which is the frame number, which will be used for the calculation of the time elapsed later on. For **second input**, the users are asked to input the relative location of the video camera with respect to the generating orifice. The **third and fourth input** will prompt for the input of the two locations of the core of the vortex ring in the video image. This is the end of this data acquisition sequence which is noticed by the cursor disappearing from the monitor. The above procedure can be repeated as many times as necessary. **When the measurements are finished,** simply press E and the program will save all the data in ASCII format onto a diskette in the file name specified at the beginning of this program. This data can be processed later in any spreadsheet program e.g. LOTUS 123.

**HINT: It is always a good practice to measure the location and size of the orifice at the beginning of the measurements. This will give a reference point on how far the ring has travel after it was generated, and will help to determine the ratio of Dv/D.**

## A.3 Analyzing the data stored in the data file:

The first column of data in the data file is the frame number of that particular frame. Since the video camera and/or the VCR both give 30 frames per second, the time difference between each frame is 1/30 sec. With the frame number of a particular frame, the time difference between this frame and the initial frame can be determined.

The second column is the vertical location of the vortex ring with respect to the scale show on the left hand side of the frame. By comparing the difference in the number of pixels between the inch mark and the location of the core of the ring in that frame, and knowing the number of pixels in one inch, the computer can calculate the vertical location of the core of the ring.

The third and fourth columns are the X and Y coordinates of the left centre of the core, or the left eye, of the ring. The final two, fifth and sixth, column are the X and Y coordinates of the right centre of the core of the ring.

Usually, the first row of this data file are the measurements of the location and diameter of the orifice tube. The location of this point is used as a reference for later calculations such as traverse distance of the ring and the diameter of the ring.

## Appendix B

Detail initial parameters of each of the experiments performed. This include:

$\rho_1$ - density of denser fluid,
$\rho_2$ - density of lighter fluid,
$V_{jtheo.}$ - theoretical jet velocity and
$V_{javg.}$ - averaged measured jet velocity.

| Filename | $\rho_H$ (kg/m^3) | $\rho_L$ (kg/m^3) | $V_{jheo.}$ (in/s) | $V_{javg.}$ (in/s) |
|---|---|---|---|---|
| EXPT2 | 1000 | 987 | 23.3 | 13.4 |
| EXPT4 | 999 | 985 | 8.0 | 5.7 |
| EXPT6-1 | 999 | 986 | 14.5 | 8.9 |
| EXPT7 | 998 | 988 | 8.1 | 5.7 |
| SEPT11-2 | 1048 | 997 | 20.0 | 11.7 |
| SEPT12-1 | 1008 | 997 | 9.8 | 6.6 |
| SEPT14-2 | 1042 | 997 | 19.0 | 11.2 |
| 2PDEC14 | 1050 | 999 | 12.1 | 11.1 |
| 2PDEC142 | 1050 | 999 | 12.1 | 11.1 |
| 4PDEC17 | 1018 | 999 | 12.1 | 11.1 |
| EXPT20 | 1055 | 1000 | 19.1 | 15.8 |
| EXPT21 | 1054 | 1000 | 25.3 | 18.8 |
| EXPT22 | 1051 | 1000 | 12.7 | 11.5 |
| EXPT24 | 1021 | 1000 | 12.5 | 11.4 |
| EXPT25 | 1022 | 1000 | 18.6 | 15.5 |
| EXPT26 | 1022 | 1000 | 7.3 | 6.9 |
| EXPT27 | 1020 | 999 | 19.6 | 16.1 |
| EXPT28 | 1020 | 1000 | 12.6 | 11.5 |
| EXPT29 | 1054 | 1000 | 18.6 | 15.5 |
| EXPT30 | 1023 | 1000 | 9.7 | 9.1 |

## Appendix C

```
'    PROGRAM "wall-3" ***** (Mar.4,91) *****
'    By: Siu Kin, HO.
'    Modified on March 4, 91.
'     This program will calculate the velocity induced at a
point
'     in the centre of the ring due to the present of the
primary
'    ring and the secondary or imaginary ring at 2L distance
away.

     DIM N AS INTEGER
     N = 1000
     DIM XP(N), YP(N), ZP(N), XP2(N), YP2(N), ZP2(N) AS SINGLE
     DIM X11(N), Y11(N), Z11(N), X21(N), Y21(N), Z21(N) AS
SINGLE
     DIM Q, L, PI, Q1, G  AS SINGLE
     DIM M, J1, J7, I6, J4  AS INTEGER
     DIM U11, UC AS SINGLE
     DIM V11, VC AS SINGLE
     DIM W11, WC AS SINGLE
     DIM DXS, DXS1 AS SINGLE
     DIM DXP1, DYP1, DZP1, DX11, DY11, DZ11 AS SINGLE

     OPEN "F:\MIKE\IMAGE\DATA1.dat" FOR INPUT AS #14

10   INPUT #14, FILN1$
     IF FILN1$ = "END" THEN
       GOTO 4400
     END IF
     OPEN FILN1$ FOR OUTPUT AS #16

'    Variable list:
'    Q -angle of one section of the core of the vortex ring
'     L -centre to centre distance between the primary and
imaginary
'       ring
     CLS
     INPUT #14, Q
     INPUT #14, L
     PRINT #16, "FILENAME:- "; FILN1$
     PRINT #16, "DeltaFeta= "; Q
     PRINT #16, "L/D ratio= "; L
```

```
     PI = 4# * ATN(1#)
     A$ = "          ": D$ = "  ": E$ = "      "
                                        C     $                  =
"-----------------------------------------------------------------
---------------------"
'
'   Calculate the number of sections the ring will be divided
into.
'
     M = 360 / Q
     N = M + 1
'
'    TO CALCULATE THE INITIAL POSITION  OF THE PRIMARY RING
'
     LOCATE 1, 1: PRINT "Calculating the initial position"

     FOR J1 = 1 TO N

'    CALCULATE THE ANGLE (IN RADIAN) FOR EACH SEGMENT

     Q1 = (J1 - 1) * Q * PI / 180
     G = (2 * J1 - 1) * Q * PI / (2 * 180)

'    CALCULATE THE INITIAL LOCATION OF THE PRIMARY RING

     XP(J1) = -L + COS(Q1)
     YP(J1) = SIN(Q1)
     XP2(J1) = -L + COS(G)
     YP2(J1) = SIN(G)
     ZP(J1) = 0
     ZP2(J1) = 0

'    CALCULATE THE INITIAL POSITION OF THE IMAGE RING

     X11(J1) = L - COS(Q1): Y11(J1) = SIN(Q1)
'     X21(J1) = L - COS(G): Y21(J1) = SIN(G)
     Z11(J1) = 0!: Z21(J1) = 0!
     NEXT J1

'     CALCULATE THE INDUCED VELOCITY AT THE CENTRE OF THE
PRIMARY RING

'     ZERO THE INDUCED VELOCITY AT THE CENTRE OF THE RING
BEFORE CALC.

     UC = 0: VC = 0: WC = 0

     FOR J7 = 1 TO M

        LOCATE 3, 1: PRINT "Calculating the induced velocity."
```

```
     Q1 = (J7 - 1) * Q * PI / 180
'     LOCATE 4, 1
'     PRINT "Q1="; Q1

'     LOCATE 5, 1: PRINT "Affected by section "; I8; " of the
other rings."

        DXP1 = -L - XP(J7)
        DYP1 = -YP(J7)
        DZP1 = -ZP(J7)
        DX11 = XP(J7 + 1) - XP(J7)
        DY11 = YP(J7 + 1) - YP(J7)
        DZ11 = ZP(J7 + 1) - ZP(J7)
        R11 = (DXP1 ^ 2 + DYP1 ^ 2 + DZP1 ^ 2) ^ .5
        K11 = R11 ^ 3 * 4 * PI


        UC = UC + (DZP1 * DY11 - DYP1 * DZ11) / K11
        VC = VC + (DXP1 * DZ11 - DZP1 * DX11) / K11
        WC = WC + (DYP1 * DX11 - DXP1 * DY11) / K11


'4000 UT(J7) = UI(J7) + US(J7)
'     VT(J7) = VI(J7) + VS(J7)
'     WT(J7) = WI(J7) + WS(J7)

     NEXT J7

     LOCATE 6, 1
     PRINT USING "###.#####  "; J7, UC; VC; WC
     PRINT #16, USING "###.##### "; J7, UC; UC; WC
     CLOSE #16
     GOTO 10
4400 CLOSE #14
     CLOSE #16
     END
     STOP
```